UNIVERSITÀ DEGLI STUDI DI NAPOLI FEDERICO II

DOTTORATO DI RICERCA IN INGEGNERIA DEI MATERIALI E DELLE STRUTTURE
COORDINATORE PROF. DOMENICO ACIERNO
XX CICLO

TESI DI DOTTORATO

Mechanical Behaviour of Traditional and Antivibration Railway Tracks with Recycled Rubber Materials

Ing. CONCETTA ONORII

A mio nonno Vittorio

ABSTRACT

The Environment and its safeguard are becoming more and more important for the social, economic and political system. In the first chapter data are given showing that the railway transportation system produce low levels of chemical pollution for this reason the demand of this transport system is rapidly increasing. However the problem of vibration emission remains and so the interest in new railway systems has been rapidly increasing to obtain a relevant vibration reduction. The problem becomes more important when a railway line have developed near urban areas where noise and vibration are a relevant impact factor and can produce complaints from people. The problem can be solved developing new antivibration systems with more elastic level respect to the traditional track. In this thesis the use of a new elastomeric composite material is proposed. This material derives from recycled rubber and it can be another important environmental aspect that has to be taken into account.

In the second chapter there is a brief description of the main components of the traditional track, then the most important innovative tracks are described to point out the elements that allow to obtain higher performances in terms of vibration reduction.

The following part of this thesis can be divided in two parts: the first one concerns the theoretical and experimental study of the new composite material for railway application and it is expanded in chapter 3, chapter 4 and chapter 5. The second one regards railway track modelling and the experimental validation of the studied theoretical model: this part is developed in chapter 6 and chapter 7.

In the third chapter the most important characteristics of elastomers are recalled: non linear mechanical behaviour, crystallization under stress and glass transition temperature. Two different approaches for the rubber behaviour study are described: hyperelastic approach that can represent the non-linear properties but not the time-depending properties that are considered through a viscoelastic approach.

In the forth chapter a particular type of composite recycled rubber material is considered, used to manufacture rubber mats and pads for innovative antivibration track systems. The material is composed by recycled rubber, an inert component, and by polyurethane that constitutes the binder. The recycled rubber is derived from used tyres and rubber factory leftovers. The process cycle is described. The main important properties of the inert are derived also considering experimental data. Composite materials are often non-homogeneous and anisotropic and require specific approaches to capture the main aspects of their static and dynamic behaviour. Starting from micro-scale in which inhomogeneities are visible, macro-scale behaviour is derived through homogenization techniques. Assuming an elastic and anisotropic material microstructure, Voigt and Reuss relations are considered in which global mechanical properties of the composite material are obtained from properties of its components and starting from the Reuss and Voigt models, the proper model for the considered material is discussed.. The main scope is to make predictions of material's behaviour from theoretical aspects with the possibility to reduce experimental tests and costs, i.e. to obtain criteria to design a material with desired mechanical characteristics.

Finally in the fifth chapter a comparison is made between the expected theoretic behaviour and the experimental results from tests performed on square specimens obtained from mats, classified according to compound type, form and dimension of the inert. Different densities are considered to show the effect of compactness on mechanical properties. Results of static and dynamic tests performed following UNI Italian standards are shown and discussed in the paper.

The previous considerations clear that it is important to conceive the track system considering the problem of the isolation of vibration from the beginning. The starting model is an Euler beam with distributed mass and flexural stiffness supported by a uniformly distributed spring bed representing an elastic foundation. The case of a constant force moving at constant speed is considered, the load is defined by means the Dirac function. The solution allows to understand the importance of the critical speed;

moreover it is showed how the damping can vary the amplification of displacement and the dynamical behaviour of the beam. The other load condition that has been studied consists of a fixed harmonic force. It has been solved considering that the solution is practically equal to the one for the Winkler beam in the static case. The results are expressed in terms of transfer function between load and displacement. New antivibration railway systems are often designed introducing one or more elastic levels in the track in order to modify its static and dynamic behaviour. To understand the effect of these additions, different models are considered able to explain the effect of added flexibilities at different positions. Lumped spring-mass models are studied first. The simplest is a mass-spring system characterized by a concentrated mass m and a constant stiffness k. Solving the problem, information is obtained regarding the behaviour in the static case, at resonance and at high frequencies. The behaviour of this model is compared with two other systems: a spring-mass-spring model in which another spring is added above the mass and a mass-spring-spring model in which a spring is added in series to the other one. The dimensionless dynamic flexibility and stiffness is determined and shown in the paper for each system. More refined models including a continuous bar of total length l, of axial stiffness EA and with mass per unit length $\mu_s A$, μ_s being the mass density are subsequently considered. The first of these model is a mass-bar system and its static and dynamic behaviour is described and shown. It is compared with the following further systems: a spring-mass-bar model in which another spring is added above the mass, a mass-spring-spring model in which a spring is added in series to the bar and a mass-spring-bar-spring model in which two springs are added, one spring is between the mass and the bar and the other one is in series to the bar. The results are still shown in terms of dimensionless dynamic flexibility and stiffness.

Finally, in the seventh chapter previous models are applied to a traditional and to its four varants studied within *AFERIA (Armamenti Ferrotranviari Ecocompatibili a Ridotto Impatto Ambientale,* environment friendly railway tracks with reduced environmental impact) funded

by MIUR (Italian Ministry for Education and Research). The results are given in terms of static displacement and characteristic length, moreover acceleration transfer functions in frequency domain is derived for each railway system. The traditional track consists of two rails and sleepers connected each other by fastenings and supported by a ballast layer. Two variants (1^{st} variant and 2^{nd} variant) of the previous system are both obtained adding an under ballast mat, but the first one is stiffer than the second one , the 3^{rd} variant is obtained including the effect of an elastic wrapping of the sleepers; finally the forth variant is a combination of the second variant and the third one. Full-scale prototypes have been developed for the traditional and innovative track systems. Static and dynamic tests have been performed and the results will be compared with analytical solutions.

TABLE OF CONTENTS

1 VIBRATION INDUCED BY RAILWAY TRAFFIC AND THE ENVIRONMENTAL SAFEGUARD PAG.1

1.1 Overview of Italian and international standards pag.5

1.2 Effects of vibrations on people pag.5

1.3 Effects of vibrations on structures pag.8

2. TRADITIONAL AND INNOVATIVE TRACK SYSTEMS PAG.9

2.1 Traditional track on a ballast layer pag.9

2.2 Overview of innovative railway track pag.11

2.2.1 Rheda 2000 pag.11

2.2.2 Japanese ballastless track system, Blog pag.12

2.2.3 Stedef, Sonneville Low vibration, Walo, Edilon Block System pag.13

2.2.4 Embedded Rail Construction pag.14

2.2.5 Vienna pag.17

2.2.6 Coopsette and IPA pag.18

2.2.7 Milano Massivo pag.19

3. AN OVERVIEW ON MODELS REGARDING ELASTOMERIC MATERIAL CHARACTERIZATION PAG.22

3.1 Elastomers: general characteristics pag.23

3.2 Mechanical behaviour modelling of rubber material pag.26

3.2.1 Hyperelastic models pag.26

3.2.2 Viscoelastic models pag.31

4. DESCRIPTION AND MODELING OF A NEW RUBBER MATERIAL PAG.38

4.1 Description of the material pag.39

4.1.1 Description of the production cycle pag.41

4.2 Tire composition pag.43

4.3 Properties of the rubber inert pag.44

4.4 Properties of the binder pag.49

4.5 Theoretical study of the composite material pag.50

4.5.1 Voigt and Reuss models pag.50

4.5.2 Model for the rubber-polyurethane material pag.54

5. EXPERIMENTAL ANALYSIS OF THE COMPOSITE MATERIAL PAG.63

5.1 Reference standards for the tests pag.64

5.1.1 UNI 10570: determination of mechanical characteristics of mats and pads pag.64

5.1.2 UNI 11059: elastomeric mats for railway tracks pag.69

5.2 Description of the testing equipment and machine pag.72

5.2.1 Software for the RPMTM use pag.76

5.3 Classification and properties of specimens pag.78

5.4 Results of static and dynamic tests pag.89

5.5 Experimental tests and theoretical results comparison pag.94

6. ANALYTICAL MODELS FOR TRADITIONAL AND INNOVATIVE RAILWAY TRACKS PAG.100

6.1 Single beam continuous model pag.101

6.1.1 General problem: concentrated harmonic load moving at constant speed pag.102

6.1.2 Vibration of the beam in the absence of damping pag.106

6.1.3 Vertical vibrations of the beam in damped case pag.115
6.1.3.1 The case of a constant force moving at constant speed pag.115
6.1.3.2 The case of a fixed harmonic load pag.129
6.1.4. Representation of rail defects pag.135
6.1.5 The effect of unsprung mass and rail defects pag.139
6.2 Double beam continuous model pag.141
6.2.1 The lower beam with zero bending stiffness pag.141
6.2.2 An “infinite” and flexible Floating slab pag.144
6.3 Single beam continuous model on a particular elastic foundation pag.147
6.3.1 Lumped spring-mass models pag.147
6.3.2 Continuous bar-spring-mass models pag.156

7. APPLICATION OF THE ANALYTICAL MODELS AND EXPERIENTAL VALIDATION PAG.172
7.1 Description of the railway track pag.174
7.2 Prototype models pag.179
7.2.1 Application of models for innovative railway tracks pag.182
7.3 Description of the static tests pag.187
7.3.1 Static test results pag.191
7.3.2 Elaboration of experimental results: static behaviour pag.202
7.4 Dynamic tests and theoretical results comparison pag.204

CONCLUSIONS PAG.213
ACKNOWLEDGEMENTS PAG.215
REFERENCES PAG.216

LIST OF FIGURES

CHAPTER 1 **PAGE**

figure 1 noise and vibration problem 4

figure 2 direction for level vibration evaluation 7

CHAPTER 2

PAGE

figure 1 traditional railway track 10

figure 2 rail profiles (Esveld, 2001) 10

figure 3 Rheda 2000 track system 12

figure 4 the Swiss Walo system 13

figure 5 Continuously Embededd Rail system 14

figure 6 the first variant of ERC system 15

figure 7 the Dutch innovative track with SA42 rail 16

figure 8 ERIA 16

figure 9 Vienna track system 17

figure 10 Coopsette track system 18

figure 11 IPA track system 19

figure 12 Milano Massivo track system 20

CHAPTER 3 **PAGE**

figure 1 experimental rubber stress-strain relation 24

figure 2 rubber stress-strain relation (Krevelen, 1990) 25

figure 3 glass transition temperature 26

figure 4 Maxwell and Voigt model 33

figure 5 typical relations between stress and strain
a) for a perfectly elastic solid subjected to an alternating stress;
b) for a simple viscous liquid; c) for a viscoelastic solid 35

CHAPTER 4 **PAGE**

figure 1 big granules of SBR 39

figure 2 big granules of grey EPDM 39

figure 3 small granules of SBR 40

figure 4 small granules of black EPDM 40

figure 5 small granules of grey EPDM 40

figure 6 big fibres of grey EPDM 41

figure 7 production cycle 42

figure 8 a) description of the experimental procedure; b) starting condition 45

figure 9 variation of the load during the tests 45

figure 10 a) compression condition 1; b) compression condition 2;
c) compression condition 3 46

figure 11 experimental cycles for big granules of grey EPDM: a) condition 1;

	b) condition 2; c) condition 3	47
figure 12	experimental cycles for big granules of SBR: a) condition 1; b) condition 2; c) condition 3	47
figure 13	experimental cycles for small granules of grey EPDM: a) condition 1; b) condition 2; c) condition 3	47
figure 14	experimental cycles for small granules of black EPDM: a) condition 1; b) condition 2; c) condition 3	47
figure 15	experimental cycles for small granules of SBR: a) condition 1; b) condition 2; c) condition 3	47
figure 16	chemical formulation of alcohol and alkyl group respectively	49
figure17	chemical formulation of ether and diethyl respectively	49
figure 18	Voigt model (Ward & Sweeney, 2004)	51
figure 19	Reuss model (Ward & Sweeney, 2004)	52
figure 20	Voigt and Reuss results	54
figure 21	Model for the new material	55
figure 22	equivalent elastic modulus for $\frac{v_2}{v_1}=1$	57
figure 23	equivalent elastic modulus for $\frac{v_2}{v_1}=\frac{1}{2}$	58
figure 24	equivalent elastic modulus for $\frac{v_2}{v_1}=2$	58
figure 25	equivalent elastic modulus for $\frac{v_2}{v_1}=\frac{1}{9}$	59

figure 26 equivalent elastic modulus for $\frac{v_2}{v_1} = 9$ 59

figure 27 Model for the new material (2) 60

CHAPTER 5 **PAGE**

figure 1 "elastic-viscous-isteretic" model (UNI 1997, UNI 2003) 67

figure 2 layout of testing machine 72

figure 3 cross-bar and handwheel 74

figure 4 hydraulic actuator and Moog valves 74

figure 5 displacement transducers 75

figure 6 the main panel of the software in labview language 77

figure 7 specimens 78

figure 8 load variation with the time for short fibres of SBR according to UNI 10570 90

figure 9 three cycles for static test of short fibres of SBR with density 600 kg/cm^3 91

figure 10 third cycle for specimens with different densities of short fibres of SBR 91

figure 11 real part of the inverse transfer function 92

figure 12 comparison between theoretical and experimental results for short fibres of SBR 95

figure 13 comparison between theoretical and experimental results for short granules of SBR 96

figure 14 comparison between theoretical and experimental results

for big granules of grey EPDM 96

figure 15 comparison between theoretical and experimental results for big granules of black EPDM 97

figure 16 comparison between theoretical and experimental results for short fibres of SBR (50%) and big granules of black EPDM (50%) 97

figure 17 comparison between theoretical and experimental results for short fibres of SBR (50%) and big granules of grey EPDM (50%) 98

figure 18 comparison between theoretical and experimental results for short fibres of SBR (50%) and small granules of SBR (50%) 98

figure 19 comparison between theoretical and experimental results for short fibres of SBR (90%) and big granules of black EPDM (10%) 99

figure 20 comparison theoretical and experimental results for short fibres of SBR (90%) and small granules of SBR (10%) 99

CHAPTER 6 **PAGE**

figure 1 simplified model for preliminary design 101

figure 2 relation between the values of α and W in instability conditions (Mathews, 1958) 112

figure 3 modulus of non-dimensional displacement Y for different values of α and W 114

figure 4 the critical damping β_{cr} 121

figure 5 poles in the complex plane 122

figure 6 displacement $y(R)$ in the absence of damping 126

figure 7 displacement $y(R)$ for the sub-critical damping 127

figure 8	displacement $y(R)$ for the critical damping	128
figure 9	displacement $y(R)$ for the super-critical damping	128
figure 10	modulus of the transfer function and amplification coefficient of SDF	134
figure 11	phase of the continuous beam and of SDF	135
figure 12	mediated power spectra of different Railway Institution	137
figure 13	Euler beam on elastic foundation with unsprung mass M_u and rail defects $r(x,t)$	140
figure 14	double beam model	142
figure 15	double beam model: flexible slab	144
figure 16	mass-spring system	147
figure 17	dimensionless dynamic flexibility of mass-spring system	149
figure 18	dimensionless dynamic stiffness of mass-spring system	150
figure 19	spring-mass-spring model	151
figure 20	dimensionless dynamic stiffness of the spring-mass-spring model	152
figure 21	mass-spring-spring model	153
figure 22	dimensionless dynamic stiffness of the mass-spring-spring model	155
figure 23	bar system	156
figure 24	mass-bar model	160
figure 25	dimensionless dynamic stiffness of the mass-bar model	161
figure 26	spring-mass-bar model	162
figure 27	dimensionless stiffness of the spring-mass-bar model (for $\zeta = 1$)	163

figure 28 mass-spring-bar model 164

figure 29 dimensionless stiffness of the mass-spring-bar model (for $\zeta = 1$) 166

figure30 mass-bar-spring model 167

figure 31 dimensionless stiffness of the mass-bar-spring model (for $\zeta = 1$) 168

figure 32 mass-spring-bar-spring model 160

figure 33 dimensionless stiffness of the mass-spring-bar-spring model (for $\zeta = 1$) 171

CHAPTER 7 **PAGE**

figure 1 Transverse section of the traditional system: reference track type 174

figure 2 Prototype on full scale of the reference track type 174

figure 3 UNI 60 rail 175

figure 4 concrete sleepers 175

figure 5 rigid and elastic fastenings 176

figure 6 transverse section of a traditional track with an exurban underballast mat: 1st variant 177

figure 7 transverse section of a traditional track with an urban underballast mat: 2nd variant 177

figure 8 transverse section of a traditional track with the sleepers wrapping: 3rd variant 178

figure 9 transverse section of a traditional track with an urban underballast mat: 4th variant 178

figure 10 model for the traditional track system 181

figure 11 model for the first variant 183

figure 12 model for the second variant 184
figure 13 model for the third variant 185
figure 14 model for the forth variant 186
figure 15 procedure scheme for the static test 187
figure 16 hydraulic actuators for the static tests 188
figure 17 position of displacement transducers on the prototype 189
figure 18 lay-out of the static tests 190
figure 19 details of the test equipment for the static tests 190
figure 20 phases of the railway track construction 191
figure 21 static tests on the traditional track 192
figure 22 static tests on the traditional track (2) 192
figure 23 static displacements for the reference track type 193
figure 24 concrete slab: the basement 194
figure 25 static test on the first variant 195
figure 26 static displacements for the first variant 195
figure 27 static test on the second variant 196
figure 28 static displacements for the second variant 197
figure 29 static test on the third variant 198
figure 30 static displacements for the third variant 199
figure 31 preparation of the forth variant 200
figure 32 static test on the forth variant 201

figure 33	static displacements for the forth variant	202
figure 34	dynamic load scheme	204
figure 35	scheme of the four helicoidal springs and of the vibrodyne	205
figure 36	four helicoidal springs	206
figure 37	vibrodyne VEM 20 kN 100Hz	206
figure 38	position of accelerometers	207
figure 39	accelerometers pos 1-5	208
figure 40	accelerometers pos 6-8 and pos 9-11	208
figure 41	theoretical and experimental modulus of the acceleration transfer function: reference track	209
figure 42	theoretical and experimental modulus of the acceleration transfer function: 1st variant	210
figure 43	theoretical and experimental modulus of the acceleration transfer function: 2nd variant	210
figure 44	theoretical and experimental modulus of the acceleration transfer function: 3rd variant	211
figure 45	theoretical and experimental modulus of the acceleration transfer function: 4th variant	211

LIST OF TABLES

CHAPTER 1 **PAGE**

table 1 CO_2 emission evolution (kt) (source: 5th "Earth friends" report in collaboration with Italian Railway Institution: Environmental and social transportation costs in Italy) 2

table 2 Emission and external cost of greenhouse gas in 2003 (source: 5th "Earth friends" report in collaboration with Italian Railway Institution: Environmental and social transportation costs in Italy) 2

table 3 total external costs of mobility in 2003 (millions of euro) (source: 5th "Earth friends" report in collaboration with Italian Railway Institution: Environmental and social transportation costs in Italy) 3

table 4 production, destination and recycling occasions of tyres in Europe in 2000 (t) (source: ETRA, European Tyre Recycling Association) 4

table 5 standards on the effect of vibration on people and structures 5

table 6 Limit levels of weighted acceleration [m/s^2] for continuous vibrations (Italian and international standard) 6

table 7 Limit levels of weighted acceleration [m/s^2] for impulsive vibrations (Italian and international standard) 6

CHAPTER 4 **PAGE**

table 1 tire composition 43

table 2 experimental results for inert component 48

CHAPTER 5 **PAGE**

table 1	description of the testing machine elements	73
table 2	short fibres of SBR	80
table 3	small granules of SBR	80
table 4	big granules of grey EPDM	80
table 5	big granules of black EPDM	81
table 6	50% short fibres of SBR and 50% big granules of black EPDM	81
table 7	50% short fibres of SBR and 50% big granules of grey EPDM	81
table 8	50% short fibres of SBR and 50% small granules of SBR	82
table 9	90% short fibres of SBR and 10% small granules of black EPDM	82
table 10	90% short fibres of SBR and 10% small granules of SBR	82
table 11	90% short fibres of SBR and 10% small granules of grey EPDM	82
table 12	volumes for short fibres of SBR	83
table 13	volumes for short granules of SBR	84
table 14	volumes for big granules of grey EPDM	84
table 15	volumes for big granules of black EPDM	85
table 16	volumes for 50% short fibres of SBR and 50% big granules of black EPDM	86
table 17	volumes for 50% short fibres of SBR and 50% big granules of grey EPDM	86
table 18	volumes for 50% short fibres of SBR and 50% small granules of SBR	87
table 19	volumes for 90% short fibres of SBR and	

	10% small granules of black EPDM	87
table 20	volumes for 90% short fibres of SBR and 10% small granules of SBR	88
table 21	volumes for 90% short fibres of SBR and 10% small granules of grey EPDM	88
table 22	results of static and dynamic tests	93
table 23	typical SBR and EPDM properties	94

CHAPTER 6 **PAGE**

table 1	A, C_1 e C_2 in function of non-dimensional parameters α e W (Mathews, 1958)	113
table 2	Integral transforms in the model	118

CHAPTER 7 **PAGE**

table 1	brief description of prototypes	173
table 2	Test load for the static test	189
table 3	maximum displacements: theoretical values and experimental results	202
table 4	theoretical characteristic length of the reference track and of its four variants	203
table 5	configuration of the system for dynamic tests	207
table 6	theoretical and experimental fundamental frequencies	212

CHAPTER 1
VIBRATION INDUCED BY RAILWAY TRAFFIC AND THE ENVIRONMENTAL SAFEGUARD

The environment and its safeguard are very important values for the social economic and political system. Pollution prevention and saving and re-cycling of resources are becoming more and more important. Today in the management of territory and natural resources, production of goods and services it is a must to take into account the environment and ecologic cycles. For this reason the demand of rail transport systems is rapidly increasing, as they produce much less chemical pollution greenhouse gas or atmospheric pollution) compared with road or air transportation.

In the following data of the 5th REPORT of the Italian association “Earth Friends” in collaboration with the Italian Railway Institution are shown. They consider the external costs (they load people in terms of greenhouse gas emission, accident and traffic) of the transportation system.

	1995	1997	1999	2001	2003	Variation (1995-2003)
ROAD	103573	105438	109574	113955	116171	12.2
RAIL	3034	3071	2953	2835	2796	-7.8
AIR	7047	7922	9640	10336	12181	72.9
TOTAL	113654	116431	122167	127126	131148	

table 1 CO_2 emission evolution (kt) (source: 5th "Earth friends" report in collaboration with Italian Railway Institution: Environmental and social transportation costs in Italy)

	Absolute emission CO_2 (kt)	Equivalent emission CO_2	Esternal Costs (10^6 euro)	Part of esternal costs divided for category (%)
ROAD	116,171	120,386	2,408	78.3
passenger transportation	76,787	80,319	1,606	52.2
private use	73,317	76,799	1,536	50.0
Cars	69,277	72,567	1,451	47.2
petrol	42,047	44,069	881	28.6
diesel	23,610	24,761	495	16.1
GPL	3,620	3,737	75	2.4
Motor-cycles	2,282	2,403	48	1.6
Motor-bicycles	1,758	1,829	37	1.2
bus	3,471	3,520	70	2.3
freight transportation	39,383	40,067	801	26.0
light vehicles	13,693	13,994	280	9.1
weight vehicles	25,690	26,073	521	16.9
RAIL	2,796	2,889	58	1.9
passenger transportation	1,944	2,012	40	1.3
freight transportation	852	877	18	0.6
AIR	12,181	*	609	19.8
passenger transportation	11,342	*	567	18.4
freight transportation	839	*	42	1.4
TOTAL	131,148	135,456	3,075	100.0

table 2 Emission and external cost of greenhouse gas in 2003 (source: 5th "Earth friends" report in collaboration with Italian Railway Institution: Environmental and social transportation costs in Italy)

	greenhouse gas	Atmosferic Pollution	Noise	Accident	traffic jam	TOTAL	(%)
ROAD	**2,408**	**7,277**	**5,224**	**3,941**	**19,435**	**38,285**	**94.4**
passenger transportation	**1,606**	**4,329**	**2,599**	**3,599**	**13,087**	**25,220**	**62.2**
private use	1,536	3,997	2,414	3,563	12,679	24,189	59.6
Cars	1,451	3,323	1,547	2,546	12,679	21,546	53.1
Motor-cycles	48	179	516	551	-	1,295	3.2
Motor-bicycles	37	495	350	466	-	1,348	3.3
bus	70	331	185	36	408	1,031	2.5
freigth transportation	**801**	**2,949**	**2,625**	**341**	**6,348**	**13,065**	**32.2**
ligth vehicles	280	948	1,108	40	2,647	5,023	12.4
weight vehicles	521	2,000	1,517	301	3,701	8,042	19.8
RAIL	**58**	**123**	**235**	**35**	**97**	**547**	**1.3**
passenger transportation	**40**	**94**	**140**	**31**	**97**	**402**	**1.0**
freight transportation	**18**	**29**	**95**	**3**	**-**	**145**	**0.4**
AIR	**609**	**581**	**440**	**29**	**74**	**1,734**	**4.3**
passenger transportation	**567**	**540**	**408**	**29**	**74**	**1,620**	**4.0**
freight transportation	**42**	**40**	**32**	-	-	**114**	**0.3**
TOTAL	**3,075**	**7,981**	**5,899**	**4,005**	**19,606**	**40,566**	**100.0**

table 3 total external costs of mobility in 2003 (millions of Euro) (source: 5th "Earth friends" report in collaboration with Italian Railway Institution: Environmental and social transportation costs in Italy)

These data clear the interest in the promotion of Railway transport systems, however, noise and vibration emission remains a relevant impact factor and they produce complaints from people living along lines and above underground lines (figure 1).

The main causes of vibration emissions are:

- Wheel rail irregularities
  - wheel wear;
  - rail corrugation;
  - displacement of the ballast and of the basement.
- The irregularities of vehicle motion
  - hunting;
  - sliding.

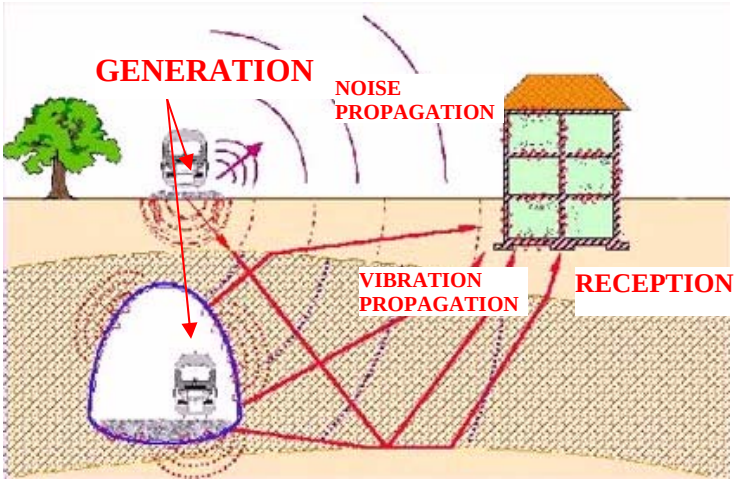

figure 1 noise and vibration problem

Nowadays a way to the problem of vibration is to develop new antivibration systems with more elastic levels that give upper performances in terms of vibration transmission.

In this thesis the use of new elastomeric material is proposed that can help to solve an other environmental aspect: the rubber recycling. Polymers need long time for the natural decomposition because of their chemical structures and their additives; for this reason the dump disposition is a serious Environmental problem (table 4).

COUNTRY	PRODUCTION	DUMP	EXPORT	RETREADING	RECYCLING	STOCKING	ENERGY RECOVERY	OTHER
Austria	50.000	20.000	5.000	4.500	500	0	20.000	0
Belgium	70.000	2.800	8.400	10.500	9.800	350	38.150	0
Denmark	37.500	0	4.500	1.125	26.250	0	5.625	0
Finland	30.000	0	3.000	1.800	24.000	1.200	0	0
France	370.000	74.000	18.500	74.000	55.500	92.500	29.600	25.900
Germany	650.000	32.500	110.500	117.000	78.000	0	279.500	32.500
Greece	58.500	48.065	0	1.755	4.585	0	4.095	0
Ireland	32.000	17.600	0	1.600	0	12.800	0	0
Italy	350.000	231.000	7.000	29.000	34.000	0	49.000	0
Luxembourg	2.750	0	2.612,5	137.5	0	0	0	0
Netherlands	67.000	0	12.060	1.340	20.100	0	33.500	0
Portugal	52.000	31.200	676	1.560	5.876	0	6.500	6.188
United Kingdom	435.000	117.450	8.700	73.590	113.100	19.575	69.600	32.625
Spain	244.000	195.200	3.660	30.744	7.076	0	7.320	0
Sweden	60.000	1.200	3.600	7.200	18.600	600	20.400	8.400
TOTAL	2.508.750	770.750	1.882.208	356.211,5	397.387	127.025	563.290	105.613
	100%	31%	8%	14%	16%	5%	22%	8%

table 4 production, destination and recycling occasions of tyres in Europe in 2000 (t) (source: ETRA, European Tyre Recycling Association)

1.1 OVERVIEW OF ITALIAN AND INTERNATIONAL STANDARDS

In this paper only vibration generated on the track line and transmitted through solid media are considered (no reference is made to noise problems). Present available standards regarding the effects of vibration can be divided in two groups: those which refer to annoyance produced on people during their activities and those which consider damage caused on buildings. The Italian *UNI 9614*, the German *DIN 4150* (parts 1 and 2) and the international *ISO 2631* belong to the first group; standards of the second group are*: UNI 9916, DIN 4150* (parts 1 and 3) and *ISO 4866,* as well as the Swiss standard *SN 640 312 a* (see table 5).

STANDARD	EFFECTS ON PEOPLE	EFFECTS ON STRUCTURES
ITALIAN	UNI 9614	UNI 9916
INTERNATIONAL	ISO 2631 (part 1 and 2)	ISO 4866
SWISS		Sn 640 312 a
GERMAN	DIN 4150 (part 1 and 2)	DIN 4150 (part 1 and 2)

table 5 standards on the effect of vibration on people and structures

A critical comparison among the above standards has been developed showing analogies and differences in the definition of levels of perception or limit levels for the effects on the human body, and of guideline values for effects on buildings.

1.2 EFFECTS OF VIBRATION ON PEOPLE

Standards concerning effects on people all consider a range of frequencies between 1-80 Hz. Vibrations are characterized through the root mean square of acceleration both in UNI 9614 (UNI, 1990) and in ISO 2631 (ISO, 1985-1989) . The effects of vibrations are different according to the frequency content: UNI 9614 supplies curves of perception limits that are equal to those reported in ISO 2631/2, there indicated as

base curves, but in the International Standard the same curves (or tables) are reported also for velocity. Limit levels (values that cause annoyance on people) are provided in a different form in the two standards: in terms of frequency weighted root mean square of acceleration in UNI 9614 and through a range multiplicative factor of base curves in the ISO 2631. However, as shown in tables 6 and 7, the corresponding values are very close when appropriately converted. In Both of theme three propagation directions are considered in a Cartesian reference with the origin point in the contact point of the man with the ground and the three axes correspond back-chest direction (X axis), left-right direction (Y axis), head feet direction (Z axis). The reference is shown in figure 2.

	Z axis		X and Y axes	
Location	**UNI 9614**	**ISO 2631**	**UNI 9614**	**ISO 2631**
critical areas	$5{,}0\cdot10^{-3}$	$5{,}0\cdot10^{-3}$	$3{,}6\cdot10^{-3}$	$3{,}6\cdot10^{-3}$
residential (night)	$7{,}0\cdot10^{-3}$	$7{,}0\cdot10^{-3}$	$5{,}0\cdot10^{-3}$	$5{,}04\cdot10^{-3}$
residential (day)	$10{,}0\cdot10^{-3}$	$10{,}0\text{-}20{,}0\cdot10^{-3}$	$7.2\cdot10^{-3}$	$7.2\text{-}14.4\cdot10^{-3}$
office	$20{,}0\cdot10^{-3}$	$20{,}0\cdot10^{-3}$	$14{,}4\cdot10^{-3}$	$14{,}4\cdot10^{-3}$
workshop	$40{,}0\cdot10^{-3}$	$40{,}0\cdot10^{-3}$	$28{,}8\cdot10^{-3}$	$28{,}8\cdot10^{-3}$

table 6 Limit levels of weighted acceleration [m/s^2] for continuous vibrations (Italian and international standard)

	Z axis		X and Y axes	
Place	**UNI 9614**	**ISO 2631**	**UNI 9614**	**ISO 2631**
critical areas	$5{,}0\cdot10^{-3}$	$5{,}0\cdot10^{-3}$	$3{,}6\cdot10^{-3}$	$3{,}6\cdot10^{-3}$
residential (night)	$7{,}0\cdot10^{-3}$	$7{,}0\cdot10^{-3}$-0,1	$5{,}0\cdot10^{-3}$	$5{,}0\cdot10^{-3}$-0,072
residential (day)	0,30	0.15-0.45	0,22	0,11-0,32
office	0,64	0,3-0,64	0,46	0,22-0,46
workshop	0,64	0,45-0,64	0,46	0,32-0,46

table 7 Limit levels of weighted acceleration [m/s^2] for impulsive vibrations (Italian and international standard).

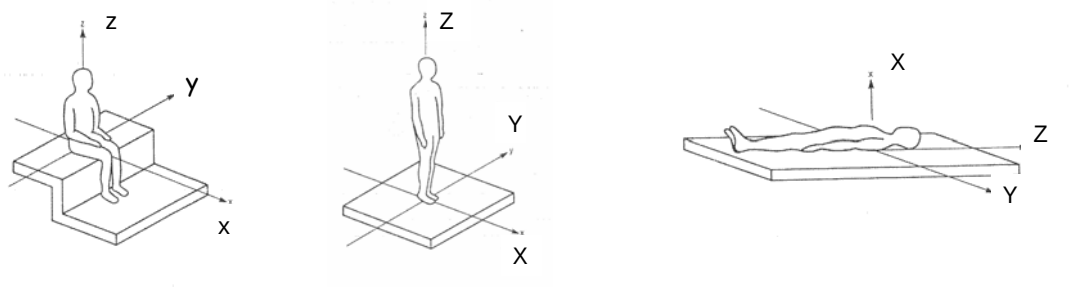

figure 2 direction for level vibration evaluation

ISO 2631 is much more detailed than the Italian standard fore some further aspects. In fact in the first part of ISO 2631 exposure limits (higher than the above threshold limit levels) are indicated which may be applied in the case of periodic vibrations and of random or non periodical vibrations. They are indicated with reference to three main human criteria: 1) the preservation of comfort ("reduced comfort limit"), 2) the preservation of working efficiency ("fatigue decreased proficiency boundary") and 3) the preservation of health or safety ("exposure limit"). In their definition, consideration is given to four physical factors that are considered very important in determining the human response to vibrations: the intensity the frequency, the direction and the duration.

A different approach is used in the German standard DIN 4150 (DIN, 1975), where vibrations are characterized by root mean square of velocity for frequencies higher than 8 Hz. Limit levels are given through an index, called KB, that depends on velocity, oscillation frequency, location and type of phenomenon:

$$\mathrm{KB} = \frac{1}{\sqrt{2}} \cdot \frac{v_{\max}}{\sqrt{1+(f_0/f)^2}} \tag{1.1}$$

In which $v_{\max}$ is the peak value of the speed; f is the vibration frequency and f_0 is a reference frequency of 5.6 Hz.

1.3 EFFECTS OF VIBRATION ON STRUCTURES

Standards concerning effects on buildings give guideline values of safety for which certainly serious damages do not occur on structures. ISO 4866 (ISO, 1990) and UNI 9916 (UNI, 1991) are very similar, as both consider a classification of buildings according to their presumed response to mechanical vibrations. The resistance of buildings depends on the characteristics of soil, type of foundation and superstructure. Explicit limit levels are not given, but in the appendix of Italian and international standards a table is provided which actually is taken from the German DIN 4150/3 (DIN, 1986) standard. These limits are in terms of peak value of velocity depend on the type of structure and range of frequency. The Swiss standard SN 640 312a (SN, 1992) is perhaps the most suitable for continuous and frequent vibrations, because limit levels depend on number of oscillations in a assigned time interval as well as on the frequency content and the type of structure.

CHAPTER 2
TRADITIONAL AND INNOVATIVE TRACK SYSTEMS

In the last years the need of reducing the emission of vibrations has significantly changed the design of track systems, as today they are designed considering the problem of the isolation of vibrations from the beginning.

A ballasted track with rigid fastenings gives low performances in terms of transmission of vibrations: this because in conventional track systems it is only possible to act on fastenings to obtain a relevant attenuation of vibrations.

New anti-vibration tracks are being designed, which are characterized by higher performances in vibration reduction. In this following the most important slab tracks are briefly described.

2.1 TRADITIONAL TRACK SYSTEM

The classical railway track consists of a flat framework made up of rails and sleepers connected to each other by fasteners; they are supported on ballast. The ballast bed sometimes rests on a sub-ballast layer (figure 1).

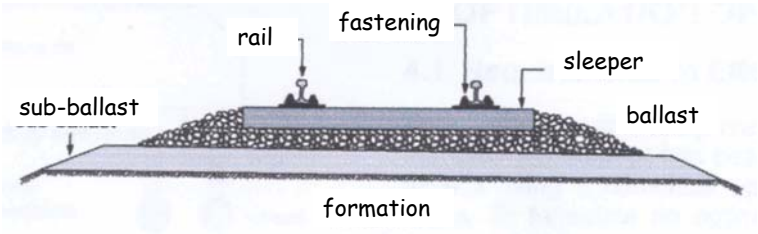

figure 1 traditional railway track

The *rail* is a steel element. There are three different types of rail profile: the flat-bottom rail, the non standard profile and the grooved rail. The last is used in enclosed track structures such us road ways, yards. The flat-bottom rail is always used in the conventional track. This rail profile is derived from the I-profile in which the upper flange is converted to form a rail head, because the rail is a support and a guidance for the vehicle. The flat-bottom rail can be divided in three parts: the rail head that is formed to ensure a good contact with the wheel tire profile, this upper part is the rolling plane; the rail web in which are made the holes for the joints in jointed rails, the thickness of the web can be different to obtain an adequate stiffness against bending and buckling; the rail foot serves to fasten rail either directly or indirectly to the sleeper and its width must be large to guarantee the stability of the rail profile, the load distribution to the sleepers and the required moment of inertia in the lateral direction. The non-standard profile is very similar to the flat-bottom rail but the web thickness is greater to provide for switch and crossing components. Rail profiles which are used in Europe include the 54 E1 (UIC 54) and the 60 E1 (UIC 60) that are shown in figure 2 (Esveld, 2001).

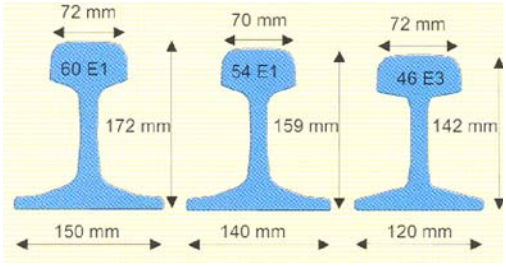

figure 2 rail profiles (Esveld, 2001)

The *sleepers* have to preserve track gauge and rail inclination; they support rail forces and transfer them to the ballast bed. Timber and concrete sleepers are usually used; the use of the steel sleepers is not very spread. The concrete sleepers are more resistant than timber or steel sleepers to the climatic effects. The timber sleeper is the rifest in the traditional track; it is prismatic in shape, 15 cm high and 25 cm wide; the length is 2.60-2.70 m. The distance between the sleepers depends on the track loads and on the type of the rail, it is usually 60 cm but in lightly loaded CWR (concrete welded rail) it can be increased and its value is 75 cm.

The *ballast bed* consists of a layer of loose, coarse grained material, which, as a result of internal friction between the grains, can adsorb considerable compressive stresses but not tensile stresses. The thickness is 35 cm for the secondary lines and 50 for the main lines measured from the lower side of the sleeper. The grading of the ballast bed elements is 25/70 mm, the best elements derive from broken, solid or sedimentary rock such us porphyry, basalt, granite.

The *sub-ballast* consists of a bituminous concrete layer that is sometimes present in the traditional track to reduce the displacement of the ballast, and it is always present in the high speed lines. Its thickness is about 12 cm (Esveld, 2001).

2.2 OVERVIEW OF INNOVATIVE TRACK SYSTEM

2.2.1 Rheda 2000

The ballastless track was undergoing rapid development in Germany thanks to the tests that the DB (The German railway institute) has been operating since 1996. The best-known designs are Rheda and Zublin, so called from the name of the place where they were made for the first time. There are numerous variants of the Rheda track system and the most developed one is Rheda 2000 (figure 3).

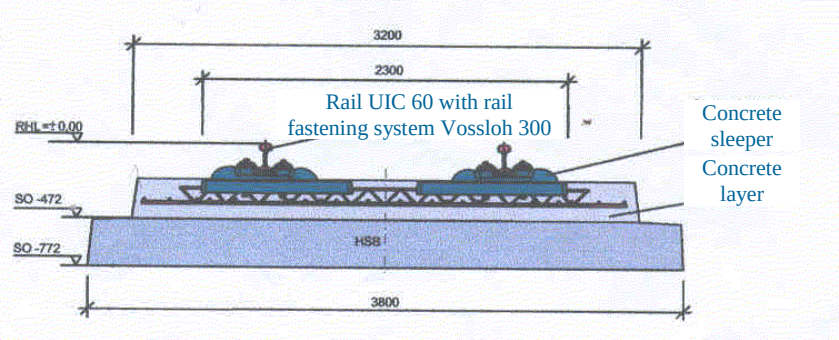

figure 3 Rheda 2000 track system

This track system has been used in high speed lines and in tunnel and the system was born to obtain an innovative system with low costs and this target is obtained with a continuous concrete cast. The conventional concrete trough was eliminated and so a simplification of the overall system configuration and a considerable reduction of the structural height were obtained and this reduction is very important in tunnel. Twin-block sleepers are used in Rheda 2000 with double elastic fastenings, and the sleepers are longitudinally connected with reinforcing steel to prevent them from loosening. They are fit in the concrete slab and so the whole cross section of the track becomes a monolithic component. The Rheda 2000 can give some maintenance problems because of the continuous concrete cast (Esveld, 2003).

2.2.2 Japanese ballastless track system, Blog

Japan was the birthplace of high speed rail and it was the first country that opened the first high speed line (between Tokyo and Osaka) in 1964, that was called Shinkansen network. The first Japanese ballastless track consists of a prefabricated slab on which the sleepers were fixed and it was used in high speed lines. Subsequently sub layer stabilized using cement was added to increase the elasticity of the system. Once the cast of the foundation has been made and the sub layer has been carried out the cylindrical stoppers are placed to prevent lateral and longitudinal movement; then the reinforced pressurised slab measuring 4.93m(2.39m(0.19m

(4.95m(2.34m(0.15m in tunnels) is built; eventually the fastenings and the rail are set (Crispino, 1996).

The innovative German Blog track is very similar to the Japanese one; Blog slabs are made of B55 steel fibre reinforced concrete and are 20 cm thick, 6.45 m long, and 2.55 or 2.80 m wide. The slabs are prestressed in the lateral direction, while in the longitudinal direction traditional reinforcement is applied. Spindles integrated in the slabs provide an easy and quick adjustment of the slabs. The slabs are connected longitudinally by post-tensioned steel rods in the neutral axis (Esveld, 2003).

2.2.3 Stedef, Sonneville Low vibration, Walo, Edilon Block System

These track systems fall in the same category. Both the French Stedef system and Sonneville Low Vibration track system use a rubber boot under the sleepers that gives a high degree of elasticity and ensures a good noise and vibration insulation.

The Swiss Walo system is related to the Stedef and Sonneville Low Vibration system, but it uses a twin block sleepers. A special slipform paver lays a concrete slab, the sleepers are fitted with the rubber boots and they are placed in the position and cast (figure 4)

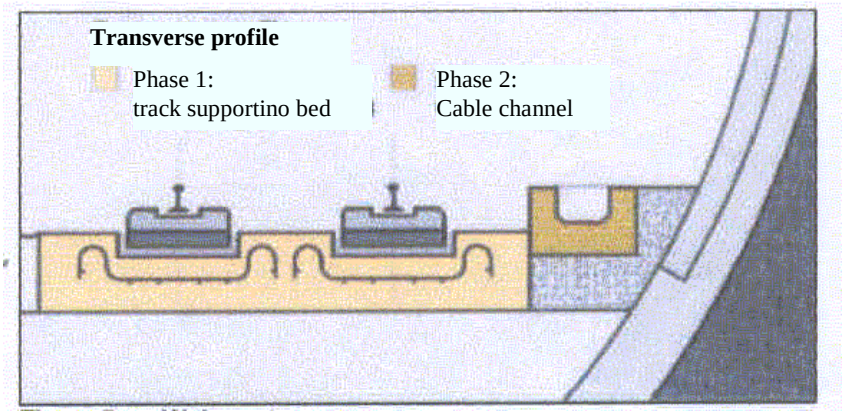

figure 4 the Swiss Walo system

The Edilon block track system is often used for bridges and tunnels. The first step is to place the rails and the block in the position. The blocks are then cast in using

corkelast (that is a cork/polyurethane mixture) to guarantee the necessary elastic support.

2.2.4 Embedded Rail Construction

All the designs mentioned so far were based on the rail being supported at discrete points. Since 1976 a continuously supported rail system has been in use in the Netherlands. The system is called Embedded Rail Construction (ERC) in which the continuous support for the rail is obtained by means of a compound consisting of corkelast. One of the most important advantages is that the wheel does not experience any difference in vertical stiffness like in the track systems with sleepers and it is known that this stiffness difference is one of the major sources for the development of the rail corrugation. The Dutch rail Institute has over 20 years experience with this system and it has proved to require little maintenance. The rail is placed in a longitudinal recess created in the base structure and pored out with elastic embedding material. This fastening system can be used only in the ballstless tracks (figure 5).

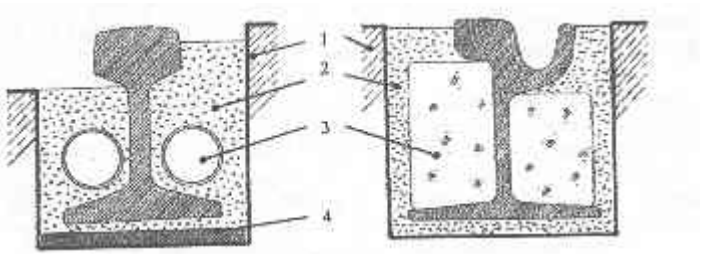

figure 5 Continuously Embededd Rail system

1	Longitudinal recess
2	Elastic embedding material
3	Space filling elements
4	Elastic base strip

The material of the recess can be reinforced concrete or steel, depending on the track structure. Fixing down of the rail is realized by the contact of the embedding

material with the rail and the recess surface. The systems can vary in the composition of the embedding materials, in most of the cases there is a two component elastomer occasionally with added cork. If a greater elasticity is necessary a cork base strip is placed under the rail. For reducing the amount of the embedding material space filling elements are placed on both sides of the rail, they can be PVC pipes or cement-based brick in the fish-plate pass (Ludvigh, 2002).

The first ERC system used the conventional UIC 54 rail (figure 6).

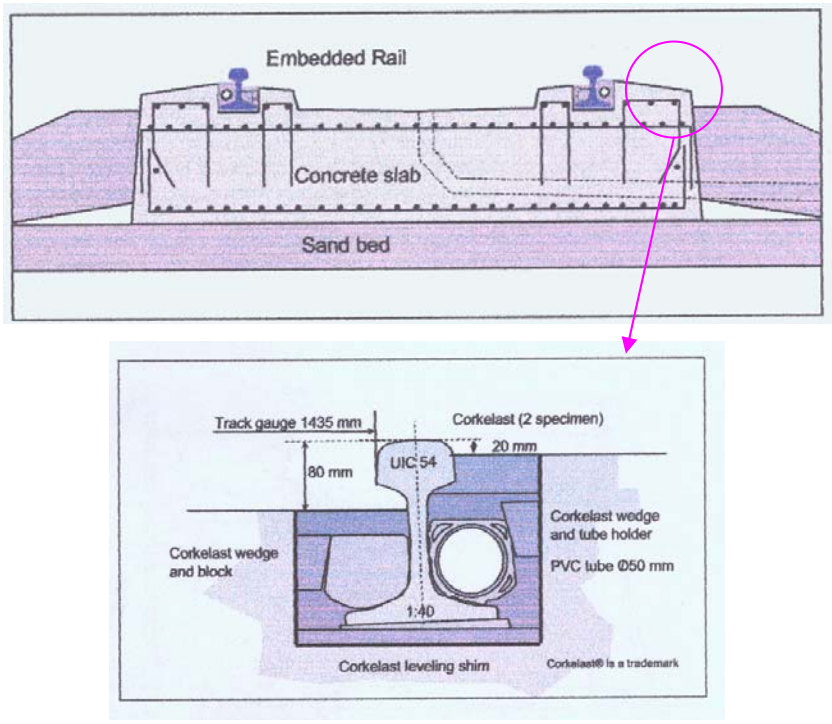

figure 6 the first variant of ERC system

The system has been developed in 1998 when the SA42 rail has been used which produces 5 dB(A) less noise. An additional advantage is the substantial reduction of polyurethane (figure 7).

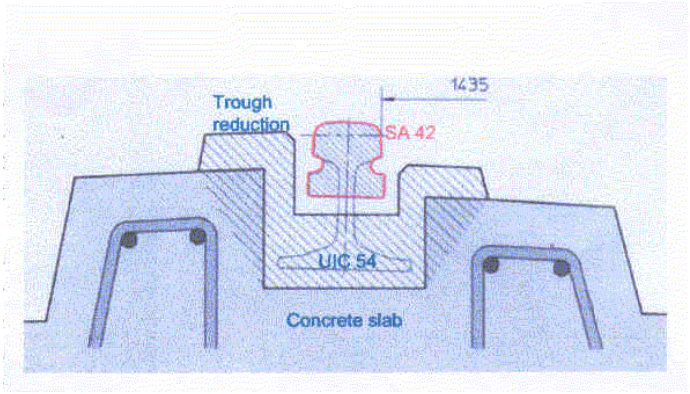

figure 7 the Dutch innovative track with SA42 rail

A new development is an embedded rail structure in asphalt pavement, this system is called ERIA (Embedded Rail In Asphalt). This is a special solution for trams and light rail in the urban areas (figure 8).

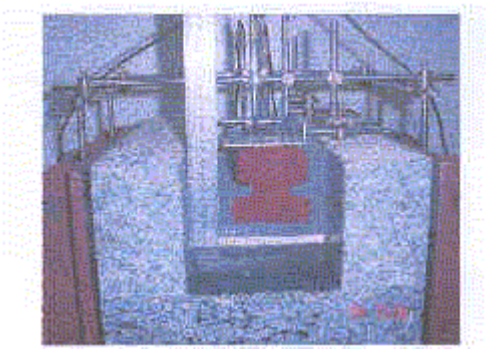

figure 8 ERIA

Two variants have been developed:

- The embedded rail prefabricated in a steel trough, which is fixed into a combi layer of very open asphalt concrete, filled up with a cement slurry.
- In the second variant the bitumen in the upper 10 cm has been replaced by the much stronger polyurethane to replace the steel trough (Esveld, 2003).

2.2.5 Vienna

Vienna is a floating mass track in which the mass consists of two independent concrete blocks and a little canal is between the two blocks (figure 9).

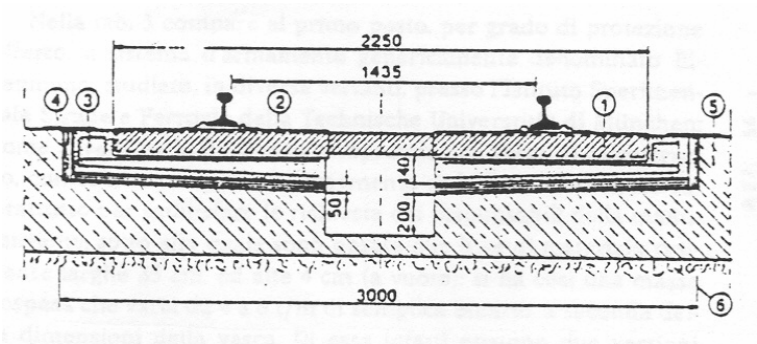

figure 9 Vienna track system

1	Poliurethane sleepers
2	Rubber covering
3	fiberglass
4	Levelling slab
5	slab

The adequate elasticity is obtained by means fibreglass mats on which the concrete castings rest. A dynamic mass-spring system is realized consisting of the concrete elements and of the elastic mats; good vibration isolation is obtained thanks to the floating concrete mass. The first vertical frequency of the system is 20Hz. Light weight sleepers that rest on the elastic elements are used to prevent the formation of “roaring rail” corrugations (Acquati, Cavagna, 2003). In spite of these important dynamic characteristics of the track, some aspects were not satisfactory:

- A reduced geometric stability because of the creep of fibreglass mats
- High flexural elasticity of the sleeper.

2.2.6 Coopsette e IPA

Coopsette track system consists of precast concrete elements that rest on elastomeric discrete bearings (figure 10).

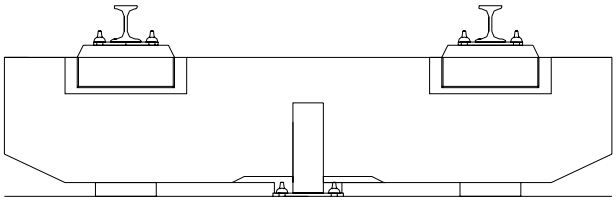

figure 10 Coopsette track system

The bearings underneath the slab are laid along a triangle to obtain an isostatic lying of the slab for which each bearing is load with the same load, therefore differential displacements are avoided, and they can reduce the useful life of the track.

There are six niches on the upper face to house the sleepers that are six concrete blocks fitted in rubber boots like in the Walo system. Separate sleepers give low performances in terms to preservation of the gauge; to overcome this disadvantage the stiffness of the rubber boots id increased, but it can make worse the problem of the rail corrugations. The elastomeric bearings do not resist to horizontal loads and a sufficient stability is not guaranteed; for this reason the ‘stoppers’ are used to face these loads with contained displacements. The stopper is a steel cylinder that is anchored in the slab. This cylinder can move in another cylinder and therefore a constraint is realized which allows vertical displacements but not horizontal ones. The stopper is in the centre of the slab and so it is difficult to notice feasible breakings. The first frequency of the track system is 18.5 Hz (Acquati, Cavagna, 2003).

The IPA track system consists of a concrete slab with a thickness of 40 cm; the sleepers are in the slab and they are not wrapped by any elastic element (figure 11).

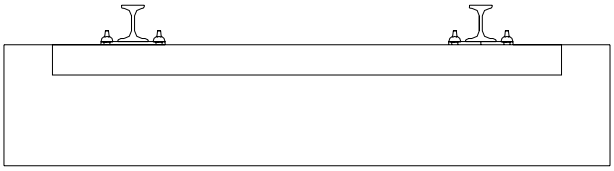

figure 11 IPA track system

The concrete casting rest on a continuous elastomeric mat with a small thickness that can control horizontal displacemets even if the stoppers are eliminated. This track system is cheaper than Coopsette because it has neither stoppers nor a second elastic level between the sleepers and the slab, but it has a good dynamic behaviour and its fundamental frequency is 19 Hz (Acquati, Cavagna, 2003).

2.2.7 Milano Massivo

Milano Massivo is an innovative track system that has been developed by Metropolitana Milanese S.p.A. with the cooperation of the polytechnic of Milan. It works as a floating slab system, which consists of a precast concrete slab resting on discrete elastomeric bearings. The slab weight is 4 t and the elastomeric bearings and it rests on four discrete elastomeric bearings. These elastic bearings and the high mass of the slab are very important to guarantee a good antivibration behaviour of the system. The slab has three niches on its upper side in which the sleepers are placed and their inter-axis is 75 cm. They are made of an African wood called “azobè” that offers a low weight and a very high strength. The sleepers are wrapped with elastomeric panels. Above each sleeper there are two steel plates that are used to fasten the rail by means the Vosshol elastic fastenings. The bearings underneath the slab are laid along a triangle like for the coopsette track system: two next to one vertex and each of other two next to the reaming two vertices (figure 1.12).

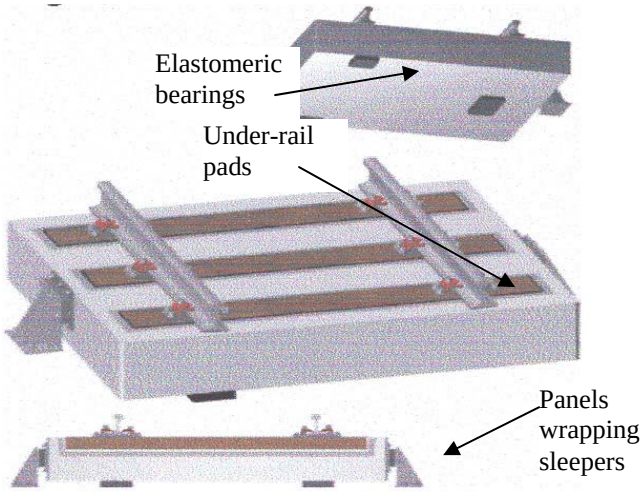

figure 12 Milano Massivo track system

At the middle of each of the two lateral faces of the slab there is a ‘stopper’ like in the Coopsette system but this one is different and is in a different position. The stopper of Milano Massivo is a rubber block (40×150×395mm) which is fixed at the middle of each of the two lateral faces of the slab; it is vulcanized to two steel plates that are used to bolt the block in the concrete slab. Its purpose is to control the horizontal movements, infact they have high stiffness in the horizzontal direction and low stiffness in the vertical direction.

Each slab is indirectly connected to the other ones infact the rail is welded and continuous and it is fastened to the sleepers which are fixed in the slab, but the slabs are completely independent.

It is clear that Milano Massivo has three elastic levels (Acquati, Cavagna, 2003):

- Under-rail pads;
- Panels wrapping the sleepers;
- Elastomeric bearings under the slab.

These three elastic levels can give high performances in terms of the reduction of the vibrations. To have a good antivibration behaviour, a track must be designed with a big

floating mass and an elastic element underneath the mass with a low stiffness; thus it is possible to make the fundamental frequency of the system as low as possible.

The first frequency of Milano Massivo is 18 Hz and it is obtained the right mediation between the the dimension of the floating mass (if it is too big it lead to a more difficult carrying of the slabs inside the small section of a urban metro tunnel) and the elasticity of the bearings (a reduction of their stiffness could involve higher deflections of the track and less safety of trains transit).

CHAPTER 3
AN OVERVIEW ON MODELS REGARDING ELASTOMERIC MATERIAL CHARACTERIZATION

Elastomers are substantially supercondensed gases because most of them derive from monomers that are gases; but their density is greater 3 orders of magnitude and viscosity 14 orders than gaseous state. They are polymer with the property of elasticity; the term is derived from elastic polymer and it is used interchangeably with the term rubber, actually this definition is preferred when vulcanized rubbers are considered. Elastomers are typically amorphous polymers having a random coil molecular arrangement.

Rubbers can be divided broadly in two categories: thermosets and thermoplastics. Thermosets are three-dimensional molecular networks with very long molecules that are held together by chemical bonds. They can adsorb solvent and swell without dissolving and it is impossible to reprocess them simply by heating. On the contrary thermoplastic molecules are not connected by primary chemical bonds and so they can dissolve in suitable solvents and soften on heating. There are some applications (such

us tires) in which some specific properties are necessary and thermosets are used for their better elasticity, resistance to set and durability.

Various ingredients can be added to raw rubber to obtained desired properties and this process is called “rubber compounding or formulation” (Gent, 2001).

3.1 ELASTOMERS: GENERAL CHARACTERISTICS

There are important general properties that have to be considered for a correct modelling. They are described in the following.

The most “famous” characteristics of natural rubber and other elastomers is the ability to undergo large and reversible deformation. It is necessary to clear that the native state of the natural rubber does not satisfy this property: its molecules tend to slide and can exist permanent deformations. Molecules have to be chemically crosslinked by sulphur bonds to prevent permanent flow.

Rubber materials have the ability to dissipate energy and consequently the mechanical behaviour depends on time and temperature.

Moreover the material can be considered incompressible, in other words deformations for the effect of a hydrostatic pressure can be disregarded and volume remains constant.

Other important property is the non linear mechanical behaviour. This is shown in figure 1 where tensile tests are performed on dumbbell specimens of natural rubber with additives.

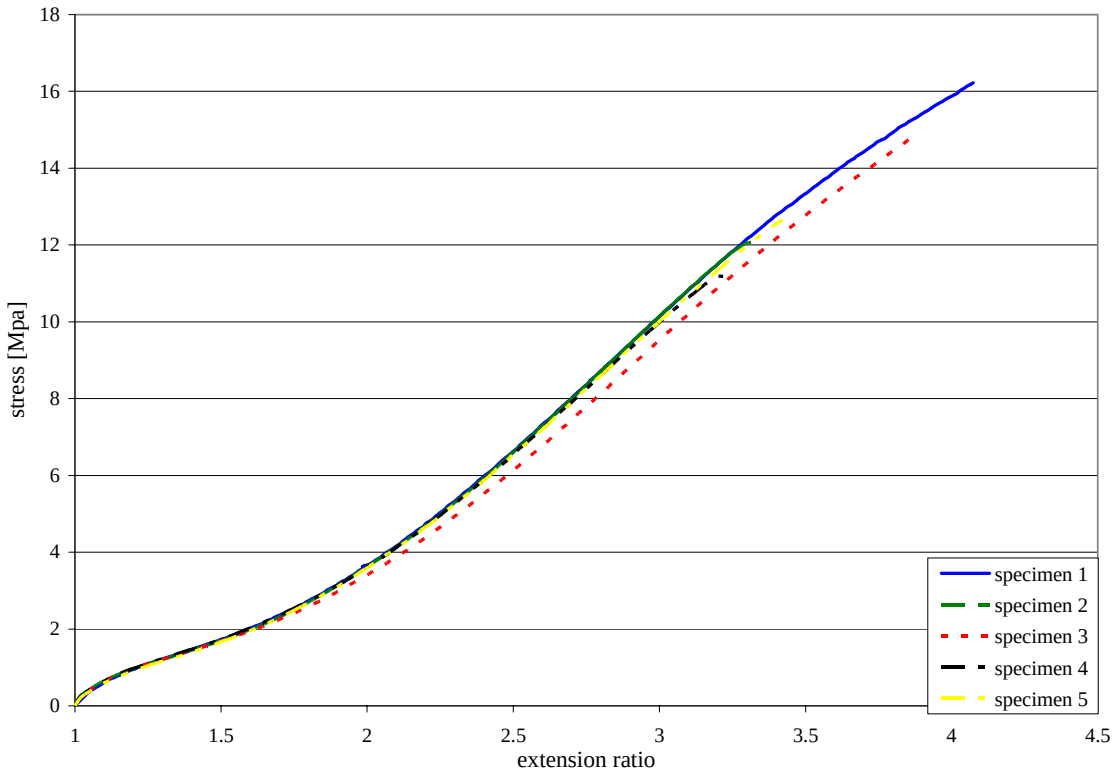

figure 1 experimental rubber stress-strain relation

These tests can determine the stress-strain relation and some considerations can be made:

- For lower deformation the rubber stiffness tends to decrease.
- When deformations reach higher levels (see in particular figure 2) the rubber stiffness goes up and this phenomenon is called “crystallization under stress” (Krevelen, 1990).

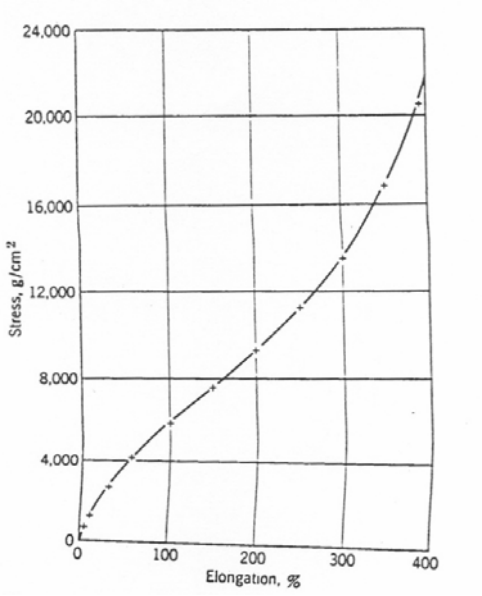

figure 2 rubber stress-strain relation (Krevelen, 1990)

Another type of crystallization can be caused by low temperature. There is a temperature, called the glass transition temperature, below which the physical properties of amorphous materials vary in a manner similar of a solid phase (glassy state) and above which amorphous materials behave like liquids (rubbery state). In other words a material's glass transition temperature is the temperature below which molecules have little relative mobility (figure 3).

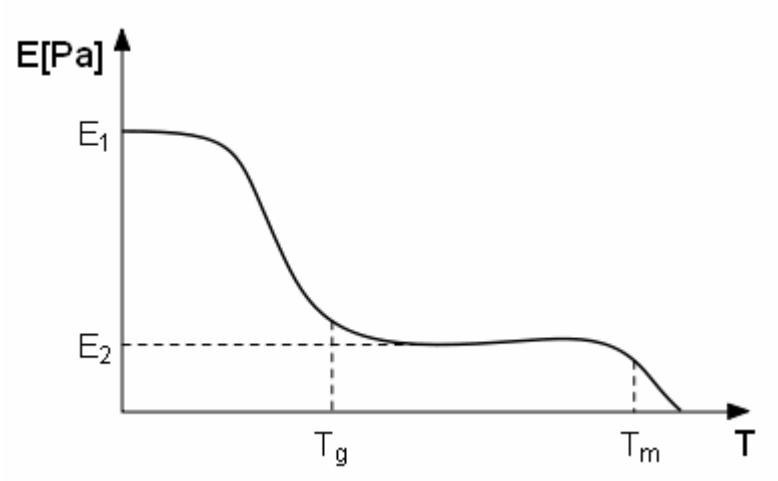

figure 3 glass transition temperature

3.2 MECHANICAL BEHAVIOUR MODELING OF RUBBER MATERIAL

Different models have been developed by different researchers to describe constitutive relations of rubber material.

There are two different approaches that can capture different aspects of the rubber behaviour:

1. Hyperelastic approach: hyperelastic models can represent the non-linear properties and the ability of the rubber to undergo large deformations. However they can not describe time-depending properties and so they do not describe damping aspects.
2. Viscoelastic approach: viscoelastic models can represent the damping properties of rubber materials and they take into account in the model the time variable.

3.2.1 Hyperelastic models

Rubber materials with hyperelastic behaviour can be described in terms of strain-energy function $U(\varepsilon)$, which defines the quantity of strain energy accumulated in the material per unit of reference volume.

There are different expressions of this function to model an elastomer considered isotropic and incompressible: the Arruda-Boyce form, the Marlow form, the Mooney-Rivlin form, the neo-Hookean form, the Ogden form, the polynomial form, the reduced polynomial form, the Yeoh form and the Van der Waals form.

It is noticed that the reduced polynomial and Mooney –Rivlin models can be considered as particular cases of the polynomial model; the Yeoh and neo-Hookean potentials can be viewed as special cases of the reduced polynomial model. For this reason they can be collectively called "polynomial models". They are easily applicable because they need limited test data for calibration; in particular when one set of test data is available (uniaxial, equibiaxial or planar test data) the Marlow form is recommended.

Generally, when it is possible to obtain data from multiply experimental tests (this requires at least uniaxial and equibiaxial test data) the Ogden and Van der Waals are more accurate in fitting experimental results.

The **form of Arruda-Boyce** strain energy is:

$$U = \mu\left\{\frac{1}{2}\cdot\left(\bar{I}_1-3\right)+\frac{1}{20\cdot\lambda_m^2}\cdot\left(\bar{I}_1^2-9\right)+\frac{11}{1050\cdot\lambda_m^4}\cdot\left(\bar{I}_1^3-27\right)+\right.$$
$$\left.+\frac{19}{7000\cdot\lambda_m^6}\cdot\left(\bar{I}_1^4-81\right)+\frac{519}{673750\cdot\lambda_m^8}\cdot\left(\bar{I}_1^5-243\right)\right\}+\frac{1}{D}\cdot\left(\frac{J_{el}^2-1}{2}-\ln J_{el}\right) \tag{3.1}$$

where U is the strain energy per unit of reference volume; μ, λ_m and D are temperature-depend material parameters; $\bar{I}_1$ is the first deviatoric strain invariant and J_{el} is the elastic volume ratio.

The initial shear modulus μ_0 is related to μ with the expression:

$$\mu_0 = \mu\cdot\left(1+\frac{3}{5\lambda_m^2}+\frac{99}{175\lambda_m^4}+\frac{513}{175\lambda_m^6}+\frac{42039}{67375\lambda_m^8}\right) \tag{3.2}$$

A typical value of λ_m is 7 for which $\mu_0 = 1.0125\cdot\mu$.

The initial bulk modulus is related to D:

$$K_0 = \frac{2}{D} \tag{3.3}$$

$\bar{I}_1$ is given by the following relation:

$$\bar{I}_1 = \bar{\lambda}_1^2 + \bar{\lambda}_2^2 + \bar{\lambda}_3^2 \tag{3.4}$$

In which the deviatoric stretches are:

$$\bar{\lambda}_i = J^{-1/3}\lambda_i \tag{3.5}$$

J is the total volume ratio:

$$J = \det(F)$$

The deformation gradient F expressed in the principal directions of stretch is:

$$F = \begin{bmatrix} \lambda_1 & 0 & 0 \\ 0 & \lambda_2 & 0 \\ 0 & 0 & \lambda_3 \end{bmatrix} \tag{3.6}$$

λ_i are the principal stretches: the ratios of current length to length in the original configuration in the principal directions. They are related to the principal nominal strains ε_i by:

$$\lambda_i = 1 + \varepsilon_i \tag{3.7}$$

In the case of isothermal response:

$$J = 1 \quad \lambda_1\lambda_2\lambda_3 = 1 \quad \bar{I}_1 = \lambda_1^2 + \lambda_2^2 + \lambda_3^2 \tag{3.8}$$

The elastic volume ratio J_{el} relates the total volume ratio and the thermal volume ratio J^{th}:

$$J_{el} = \frac{J}{J^{th}} = \frac{J}{\left(1 + \varepsilon^{th}\right)^3} \tag{3.9}$$

Where ε^{th} is the linear thermal expansion strain: it is obtained from the temperature and the isotropic thermal expansion coefficient.

The **form of Marlow** strain energy potential is:

$$U = U_{dev}\left(\bar{I}_1\right) + U_{vol}\left(J_{el}\right) \tag{3.10}$$

U is still the strain energy per unit of reference volume, U_{dev} is its deviatoric part and U_{vol} is its volumetric part. $\bar{I}_1$ is given by (3.4).

The **form of Mooney-Rivlin** strain energy potential is:

$$U = C_{10}\cdot\left(\bar{I}_1 - 3\right) + C_{01}\cdot\left(\bar{I}_2 - 3\right) + \frac{1}{D_1}\cdot\left(J_{el} - 1\right)^2 \tag{3.11}$$

U is the strain energy per unit of reference volume. C_{10}, C_{01} and D_1 are temperature-dependent material parameters, the initial shear modulus and the bulk modulus are given by:

$$\mu_0 = 2\left(C_{10} + C_{01}\right); \qquad K_0 = \frac{2}{D_1} \tag{3.12}$$

$\bar{I}_1$ and $\bar{I}_2$ are the first and second deviatoric strain invariants the first one is the defined by (3.4), the second one is:

$$\bar{I}_2 = \bar{\lambda}_1^{(-2)} + \bar{\lambda}_2^{(-2)} + \bar{\lambda}_3^{(-2)} \tag{3.13}$$

J_{el} is the elastic volume ratio defined by (3.9).

The **form of neo-Hookean** strain energy is:

$$U = C_{10}\cdot\left(\bar{I}_1 - 3\right) + \frac{1}{D_1}\cdot\left(J_{el} - 1\right)^2 \tag{3.14}$$

. C_{10} and D_1 are temperature-dependent material parameters, the initial shear modulus and the bulk modulus are given by:

$$\mu_0 = 2C_{10}; \qquad K_0 = \frac{2}{D_1} \tag{3.15}$$

$\bar{I}_1$ and J_{el} are still given by (3.4) and (3.8) respectively.

The **form of the Ogden** strain energy potential is:

$$U = \sum_{i=1}^{N}\frac{2\mu_i}{\alpha_i^2}\cdot\left(\bar{\lambda}_1^{\alpha_i} + \bar{\lambda}_2^{\alpha_i} + \bar{\lambda}_3^{\alpha_i} - 3\right) + \sum_{i=1}^{N}\frac{1}{D_i}\cdot\left(J^{el} - 1\right)^{2i} \tag{3.16}$$

$\bar{\lambda}_i$ are the deviatoric stretches defined in (3.5). N is a material parameter and μ_i, α_i and D_i are temperature-dependent material parameters. The initial shear modulus and bulk modulus for the Ogden form are given by:

$$\mu_0 = \sum_{i=1}^{N} \mu_i \qquad K_0 = \frac{2}{D_1} \tag{3.17}$$

It is important to point out that the Mooney-Rivlin and Neo-Hookean forms can be obtained from the general Ogden strain energy potential for special choices of μ_i and a_i.

The **form of the polynomial** strain energy potential is:

$$U = \sum_{i+j=1}^{N} C_{ij} \cdot \left(\bar{I}_1 - 3\right)^i \left(\bar{I}_2 - 3\right)^i + \sum_{i=1}^{N} \frac{1}{D_i} \cdot \left(J^{el} - 1\right)^{2i} \tag{3.18}$$

N is a material parameter and C_{ij} and D_i are temperature-dependent material parameters. The initial shear modulus and bulk modulus for the polynomial form are given by (3.12). $\bar{I}_1$ and $\bar{I}_2$ are the first and the second deviatoric strain invariants defined in (3.4) and (3.13).

When the nominal strains are small $(<100\%)$, the first terms in the polynomial series are usually sufficient to describe the material behaviour. Mooney-Rivlin, neo-Hookean and Yeoh forms can be obtained for special choices of C_{ij}.

The **form of reduced polynomial** strain energy potential is:

$$U = \sum_{i=1}^{N} C_{i0} \cdot \left(\bar{I}_1 - 3\right)^i + \sum_{i=1}^{N} \frac{1}{D_i} \cdot \left(J^{el} - 1\right)^{2i} \tag{3.19}$$

N is still a material parameter and C_{i0} and D_i are temperature-dependent material parameters. The initial shear modulus and bulk modulus for the polynomial form are given by (3.15). $\bar{I}_1$ is the first deviatoric strain invariants defined in (3.4).

The **Van der Waals form** strain energy potential is:

$$U = \mu\left\{-\left(\lambda_m^2 - 3\right)\cdot\left[\ln\left(1-\eta\right)+\eta\right] - \frac{2}{3}a\cdot\left(\frac{\tilde{I}-3}{2}\right)^{\frac{3}{2}}\right\} + \frac{1}{D}\cdot\left(\frac{J_{el}^2-1}{2} - \ln J_{el}\right) \tag{3.20}$$

In which $\tilde{I}$ and η are defined in the following:

$$\tilde{I} = \left(1-\beta\right)\cdot\bar{I}_1 + \beta\bar{I}_2 \qquad \eta = \sqrt{\frac{\tilde{I}-3}{\lambda_m^2-3}} \tag{3.21}$$

U is the strain energy per unit of reference volume; μ is the initial shear modulus; λ_m is the locking stretch; a is the global interaction parameter; β is an invariant mixture parameter; and D governs the compressibility. These parameters can be temperature-dependent. $\bar{I}_1$ and $\bar{I}_2$ are in (3.4) and (3.13) respectively.

Finally the **form of the Yeoh** strain energy potential is:

$$\begin{aligned} U = {} & C_{10}\cdot\left(\bar{I}_1-3\right) + C_{20}\cdot\left(\bar{I}_1-3\right)^2 + C_{30}\cdot\left(\bar{I}_1-3\right)^3 + \\ & + \frac{1}{D_1}\cdot\left(J_{el}-1\right)^2 + \frac{1}{D_2}\cdot\left(J_{el}-1\right)^4 + \frac{1}{D_3}\cdot\left(J_{el}-1\right)^6 \end{aligned} \tag{3.22}$$

U is the strain energy per unit of reference volume; C_{i0} and D_i are temperature-dependent material parameters. The initial shear modulus and bulk modulus for the polynomial form are given by (3.15) (ABAQUS manual).

3.2.2 Viscoelastic models

The ideal behaviour of elastomers assumes reversible relations between load and displacement. Actually, deviations from such ideal elastic behaviour are predictable. Elastomers combine both liquid and solid properties. They show viscous behaviour. There are some applications in which viscous properties are desired, but excessive viscous response can sometimes create problems.

An ideal linear solid is described by Hooke's law: stress is proportional to strain. An ideal viscous liquid obeys Newton's law: stress is proportional to rate of change of

strain with time. Elastomers have properties intermediate between these two cases and the response of these materials is called “viscoelastic” behaviour.

Hooke’s law can be written:

$$F = kx \tag{3.23}$$

where x is the deformation, F is the force and k is the spring constant.

Newton’s law is written in the following:

$$F = b \cdot \frac{dx}{dt} \tag{3.24}$$

in which b is a viscous damping coefficient. This behaviour is well represented by a viscous element called dashpot.

Previous relations can be written in terms of stress:

$$\sigma = E\varepsilon$$
$$\sigma = \eta_e \cdot \frac{d\varepsilon}{dt} \tag{3.25}$$

in which σ is the tensile stress, ε is the tensile strain, E is the elastic tensile modulus and η_e is the Newtonian viscosity coefficient in tension. For an incompressible fluid the tensile viscosity η_e is three times the shear viscosity η (the same relation between E and the shear modulus G for an incompressible solid). Traditionally Viscoelastic behaviour has been described by phenomenological approaches.

A Maxwell model consists on a spring and a dashpot placed in series (figure 4).

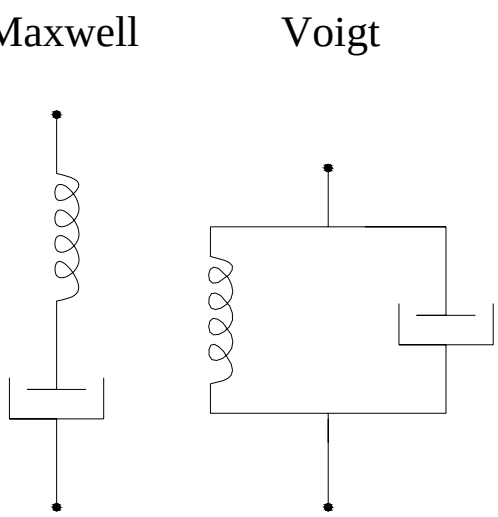

figure 4 Maxwell and Voigt model

In this case the equation of motion is written (equal terms being the forces, and the additive terms are the deformations):

$$\frac{dx}{dt} = \frac{1}{k} \cdot \left(\frac{dF}{dt} \right) + \frac{F}{b} \tag{3.26}$$

The stress relaxation is obtained considering that:

$$\frac{dx}{dt} = 0 \quad \left(\text{or} \quad x = a \text{ constant} \right) \tag{3.27}$$

Substituting (3.27) in(3.26):

$$F = F_0 \cdot e^{-t/\tau} \tag{3.28}$$

In which the relaxation time is defined:

$$\tau = \frac{b}{k} \tag{3.29}$$

The creep is represented by the following condition:

$$\frac{dF}{dt} = 0 \quad (\text{or} \quad F = a \ \text{ constant}) \tag{3.30}$$

Substituting in (3.26) it is obtained:

$$x = x_0 + \frac{Ft}{b} \tag{3.31}$$

Finally the case of a constant rate of deformation is considered:

$$\frac{dx}{dt} = R \tag{3.32}$$

Consequently the following relation is found:

$$F = bR \cdot \left(1 - e^{-t/\tau}\right) \tag{3.33}$$

Voigt model is obtained considering a spring and a dashpot in parallel (figure 4). In this case the equation of motion is given by (equal terms being the deformations and additive terms are the forces):

$$F = k \cdot x + b\frac{dx}{dt} \tag{3.34}$$

The stress relaxation, the creep and the constant rate deformation are still studied.
In the first case (stress relaxation) considering(3.27) is obtained:

$$F = kx \tag{3.35}$$

The creep is represented (applying (3.30)):

$$x = \frac{F_0}{k} \cdot \left(1 - e^{-t/\tau}\right) \tag{3.36}$$

In which τ is still given by (3.29) but it is now called retardation time.

A generalized Maxwell model consists of an infinite number of simple Maxwell elements in parallel and the distribution of elastic modulus $E(\tau)$ as a function of the relaxation time τ of the simple Maxwell model is obtained.

A generalized Voigt model consists of an infinite number of simple Voigt elements in series and the distribution of compliance $D(\tau)$ as a function of the retardation time τ of the simple Maxwell model is described.

Generally generalized Maxwell model is applied for stress-relaxation experiments while a generalized Voigt model describes well creep experiments.

The dynamic mechanical properties of elastomers can be important in several applications and they refers to the behaviour of these material subjected to stresses or strains changing with time. In the following the case of sinusoidally varying stresses and strains is discussed.

In the oscillatory dynamic experiment stress and strain are not in phase and there is not only the ratio of stress to strain but also the phase difference (or phase angle between them) is measured. The phase angle depends on the dynamic viscosity, being zero when the viscosity is zero.

Considering the phase angle three different behaviours can be considered. For a perfect spring the force and the deformation are in phase (figure 5a); in the case of dashpot the force leads the deformation by $\pi/2$ radians (figure 5b). Finally, a viscoelastic material has property both of a spring both of a dashpot then it has an intermediate phase angle (figure 5c).

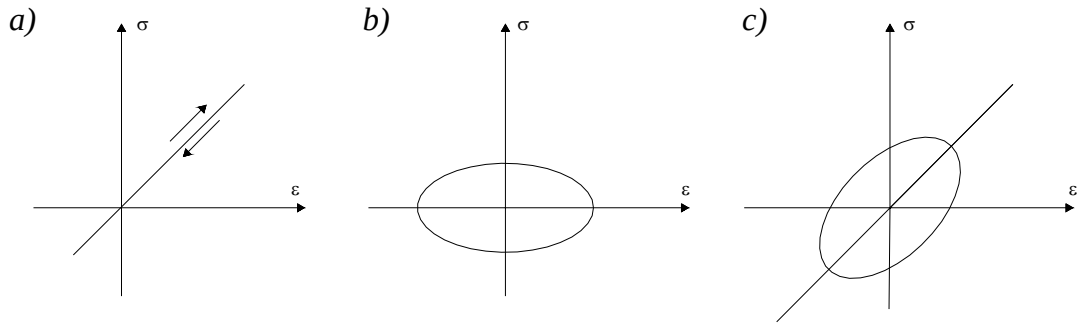

figure 5 typical relations between stress and strain a) for a perfectly elastic solid subjected to an alternating stress; b) for a simple viscous liquid; c) for a viscoelastic solid

A close parallel exists between dynamic mechanical theory and alternating current circuit. In a reactive circuit voltage and current are out of phase and electrical loss factor is given in terms of electrical loss tangent. For the same concept $\tan\delta$ represents mechanical energy losses and it is called mechanical loss tangent or factor (Gent, 2001).

The whole notation system for mechanical properties is also like that used in alternating current theory. For this reason some terms as complex and imaginary modulus are used and they hard to understand in a mechanical sense.

The Voigt element is considered in terms of stress σ and strain ε:

$$\sigma = E\varepsilon + \eta \cdot \left(\frac{d\varepsilon}{dt} \right) \tag{3.37}$$

In which η is the tensile viscosity.

A strain (varying with time in sinusoidal way) is applied:

$$\varepsilon = \varepsilon_0 \sin(\omega t) \tag{3.38}$$

In which ε_0 is the strain amplitude.

A complex relation is introduced for strain:

$$\varepsilon = \varepsilon_0 \exp(\omega t) = \varepsilon_0 (\cos \omega t + i \sin \omega t) \tag{3.39}$$

In this way both imaginary (3.38) and real part are considered.

The rate of change strain with time is given by:

$$\frac{d\varepsilon}{dt} = i\omega\varepsilon_0 \exp(i\omega t) = i\omega\varepsilon \tag{3.40}$$

This relation is substituted in (3.37):

$$\sigma = (E + i\omega\eta) \cdot \varepsilon \tag{3.41}$$

$E + i\omega\eta$ is a type of modulus because it is the ratio of a stress to a strain and it is called complex dynamic modulus E^*. $E_1 = E$ is the real part called real dynamic modulus and $E_2 = \omega\eta$ is the imaginary called imaginary dynamic modulus and the (3.41) can be written:

$$\sigma = (E_1 + iE_2) \cdot \varepsilon \tag{3.42}$$

The following definitions are considered:

$$E_1 = \frac{\text{component of stress in phase with strain}}{\text{strain}}$$

$$E_2 = \frac{\text{component of stress 90° out of phase with strain}}{\text{strain}}$$

The absolute value of complex modulus is expressed as a function of the loss factor:

$$E^* = \left(E_1^2 + E_2^2\right)^{1/2} = E_1\left[1+\left(\tan\delta\right)^2\right]^{1/2} \tag{3.43}$$

CHAPTER 4

DESCRIPTION AND MODELING OF A NEW RUBBER MATERIAL

Environmental and energy-saving issues are increasing the interest toward the use of recycled rubber for different applications in several industrial sectors. In this thesis a particular type of composite recycled rubber material is considered, it is used to manufacture rubber mats and pads for innovative antivibration track systems.

They are produced by ISOLGOMMA s.r.l. that is specialized in the production of anti-vibration mats of recycled rubber for railway applications, with manufacturing plant located in Albettone (Vicenza, Italy) and research centre in Pozzuoli (Napoli, Italy).

The use of new elastic element in railway track is becoming a very effective way to reduce vibrations induced by railway traffic. Elastomeric pads and mats can be included at different levels in a railway track and the importance to understand their effect is increasing together with the interest and the need to describe static and dynamic behaviour of the material.

4.1 DESCRIPTION OF THE MATERIAL

The material investigated is composed by recycled rubber and polyurethane; the recycled rubber is the inert component and it is derived from used tyres and rubber factory leftovers. The inert is in form of big (figure 1 and 2) or small (figures 3, 4, 5) granules (6 and 3 millimetres), while small or big (figure 6) fibres are obtained from the scraping of tyre external surface. Because of its origin the recycled rubber is SBR (Styrene Butadiene Rubber), that is the main component of tires together with the natural rubber, other products are in EPDM (Ethylene Propylene Dien Monomer) that can be grey or black (EPDMg, EPDMb). The binder is polyurethane, an urethane prepolymer with different aromatic poly-isocianates.

figure 1 big granules of SBR

figure 2 big granules of grey EPDM

figure 3 small granules of SBR

figure 4 small granules of black EPDM

figure 5 small granules of grey EPDM

figure 6 big fibres of grey EPDM

4.1.1 Description of the production cycle

The composite rubber material is used to manufacture mats and pads. The production cycle is composed by the four steps (figure 7):

1. **Material acceptance and accumulation**: in this phase the recycled rubber material is available but the production process starts with the following step.
2. **Rubber granulation:** the inert is put in the grinding chamber, where the rubber remains until granules or fibres get to stoker dimension under the grinding chamber.
3. **Binder-inert mixing**: the rubber compound, prepared in the previous step, is put in an automatic mixer, then the correct amount of binder is added to the rubber in the mixer and they are mixed together until becoming a homogeneous compound.
4. The last step is the **hot pressing** or the **cold forging**. In the first one the inert-binder compound is spread through a hopper on a paper support. While the compound goes on the belt, it is levelled and homogeneously put on the whole belt surface by means a levelling roller. During this phase the compound does the polymerization facilitated by the water presence (sprinkled when the compound enters in the press) and by the heat that is transferred by surfaces that are warmed until the temperature of the binder prescription is reached. This phase last until the polymerization is complete and the product is agglomerated maintaining desired

thickness, density and dimensions. Finally, the product undergoes a forced air cooling and it can be cut for different applications. In the cold forging Teflon-aluminium dies are applied and the hopper is used to fill them. The product is pressed for a fixed time at a defined pressure to obtain a desired compactness.

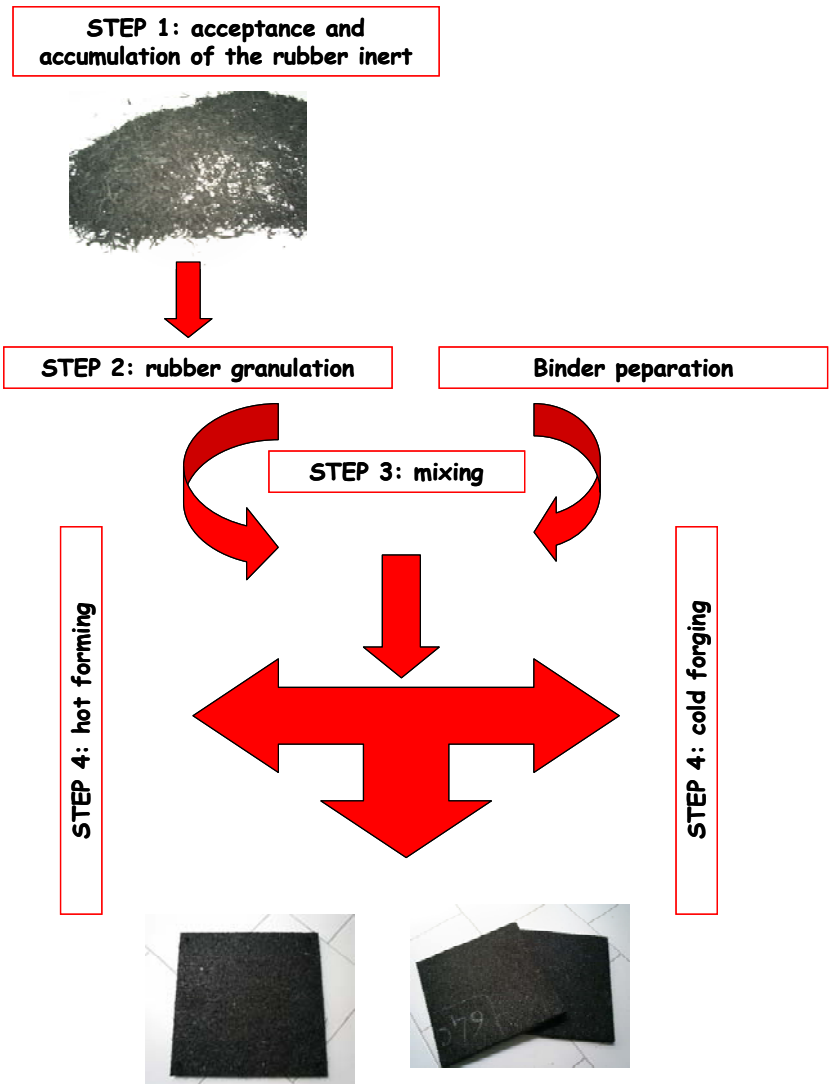

figure 7 production cycle

4.2 TIRE COMPOSITION

Tires consist of a rubber compound usually reinforced with steel and textile. They are composed by vulcanized rubber and different additives. SBR and polybutadiene are recently used because they improve their ultimate strength and wear proof. The natural rubber is added for adhesion problems and it carries out an improvement in the shock and tearing resistance, moreover it maintains constant the elastic modulus during the aging.

Tires also contain the following components:

- Black filler: it is used to increase the elastic modulus of the elastomer and to improve its abrasion resistance.
- Inert: they are used to control the viscosity and to decrease the internal friction during the production process; moreover they improve the rubber flexibility for lower temperatures.
- Curing agents: sulphur compounds are used as catalysts of the curing process and zinc oxide is used to start the curing.
- Reinforcing fibres: steel and textile fibres are used to increase the resistance. In the past inferior fibres were used (for example: synthetic fibres), but now it is spread the use of steel fibres.

The material composition of passenger car and truck tires from the European Union is in table 1.

table 1 tire composition

MATERIAL	CAR TIRES	TRUCK TIRES
Rubber/elastomers	47%	45%
Carbon black	21.5%	25%
Textile	5.5%	-
Zinc oxide	1%	2%
Sulphur	1%	1%
Additives	7.5%	5%

4.3 PROPERTIES OF THE RUBBER INERT

Previously the main components of the inert part had been described, now their most important characteristics are considered.

SBR denotes a copolymer of styrene and butadiene, typically containing about 23% styrene with a glass temperature transition of approximately $-55°C$. It is the most widely used synthetic elastomer with the largest volume production. It has good abrasion resistance and good aging stability. It is stable in mineral oils, fats, aliphatic, aromatic and chlorinated hydrocarbons. Its possible temperature range is -40 to $+100°C$ and its typical application is in the production of tyres (Gent, 2001).

EPDM is a synthetic elastomer, a terpolymer of ethylene, propylene and a diene-component which is characterized by wide range of applications. It has a small number of double bonds external to the backbone. The ratio ethylene to propylene in commercial grades can vary from 50/50 to 75/25. Its glass transition temperature is $-60°C$. It has excellent resistance to weathering a good heat stability. EPDM is applied for roofing, seals, gaskets and hose (Gent, 2001).

Some tests have been performed at research centre ISOLGOMMA on the inert component to show and classify different inert for their mechanical characteristics. Test instructions are in UNI 10570 standard that is described in the following.

A proper baseplate (1, in figure 8a) and load slab (2, in figure 8a) are designed. Inert granules or fibres (4, in figure 8a) are put in a tank (3, in figure 8a) without imparting pressure and the starting condition is obtained (figure 8b) for which the volume is given by:

$$V_0 = (390 - 2 \cdot 20) \cdot (390 - 2 \cdot 20) \cdot 80 \text{ mm}^3 = 9800 \cdot 10^3 \text{mm}^3 = 9800 \text{ cm}^3 \qquad (4.1)$$

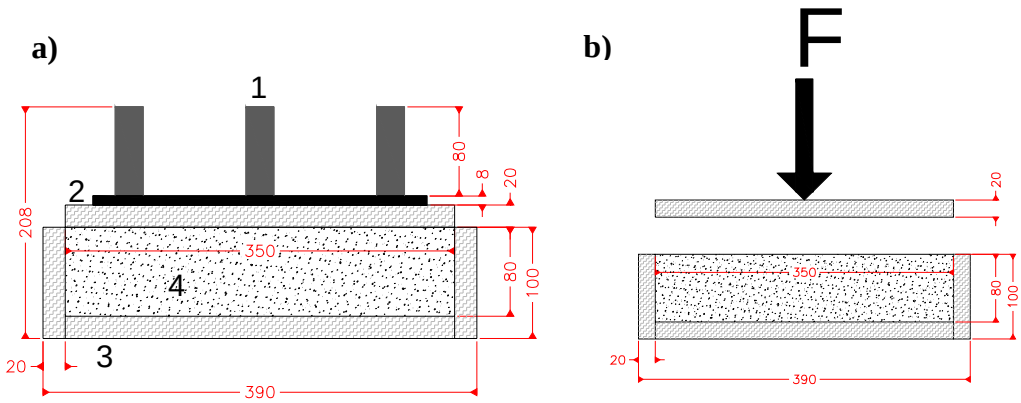

figure 8 a) description of the experimental procedure; b) starting condition

Static tests are performed considering the application of a load that linearly goes up with time, until the maximum value is reached and then it linearly goes down; three cycles are considered and the mechanical characteristics are derived by the third one. Test loads are:

$\sigma_0 = 1\ \text{N/cm}^2 \qquad \sigma_{ps} = 9\ \text{N/cm}^2 \qquad \sigma_{pd} = 2\ \text{N/cm}^2$

in which σ_0 is the initial load, σ_{ps} and σ_{pd} are the static and dynamic component respectively (figure 9).

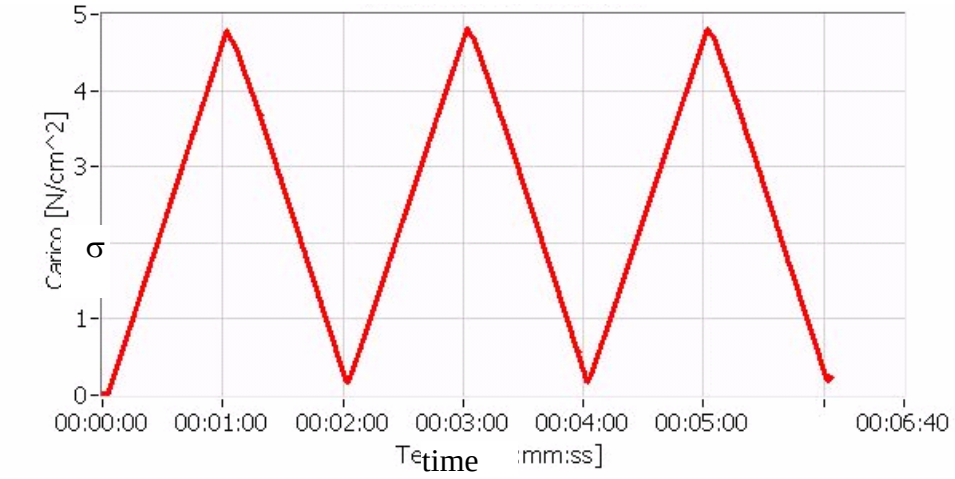

figure 9 variation of the load during the tests

Three different conditions for the inert are considered. The first one (condition 1) states an inert compression with the steel plate until it reaches the tank edge (figure 10a). This compression reduces the initial volume of 25% and the new value is:

$$V_1 = (390 - 2 \cdot 20) \cdot (390 - 2 \cdot 20) \cdot (80 - 20) \text{ mm}^3 = 7350 \cdot 10^3 \text{mm}^3 = 7350 \text{ cm}^3 \qquad (4.2)$$

The compression is greater in the second condition (condition 2) in which the steel plate is lowered of 5 mm from the tank edge (figure 10b). The volume is reduced of 31.25% for this compression:

$$V_2 = (390 - 2 \cdot 20) \cdot (390 - 2 \cdot 20) \cdot (80 - 25) \text{ mm}^3 = 6737,5 \cdot 10^3 \text{mm}^3 = 6737,5 \text{ cm}^3 \qquad (4.3)$$

The last condition (condition 3) is obtained lifting the steel plate as shown in figure 10c. The volume is greater than the other two conditions and it is given:

$$V_3 = (390 - 2 \cdot 20) \cdot (390 - 2 \cdot 20) \cdot (80 - 15) \text{ mm}^3 = 7962,5 \cdot 10^3 \text{mm}^3 = 7962,5 \text{ cm}^3 \qquad (4.4)$$

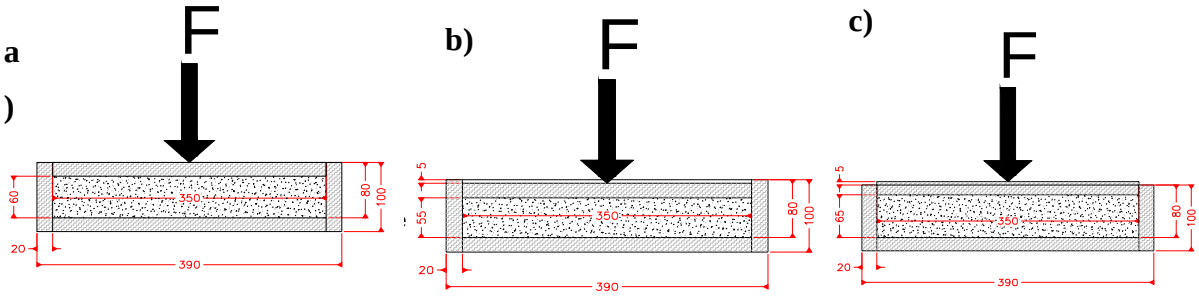

figure 10 a) compression condition 1; b) compression condition 2; c) compression condition 3

The following types of inert are considered: big granules of grey EPDM and SBR and small granules of grey and black EPDM and SBR. For each inert type the previous three compression conditions are considered. Figures from 11 to 15 show the experimental cycles: the mean displacement is on *x*-axis and the tension is on *y*-axis. The results in terms of static stiffness and loss factor are summarized in table 2.

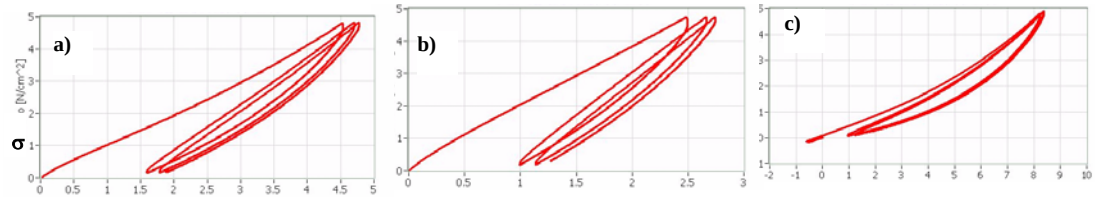

figure 11 experimental cycles for big granules of grey EPDM: a) condition 1; b) condition 2; c) condition 3

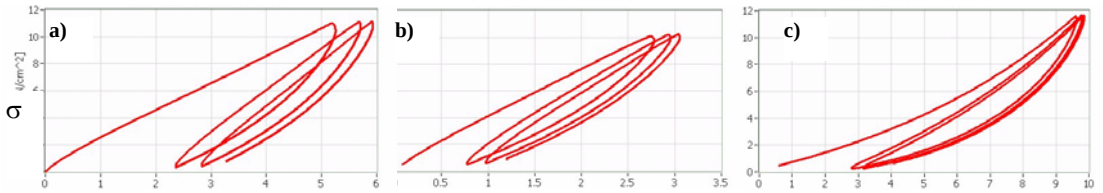

figure 12 experimental cycles for big granules of SBR: a) condition 1; b) condition 2; c) condition 3

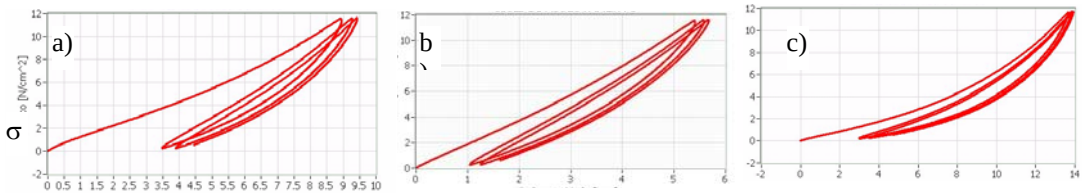

figure 13 experimental cycles for small granules of grey EPDM: a) condition 1; b) condition 2; c) condition 3

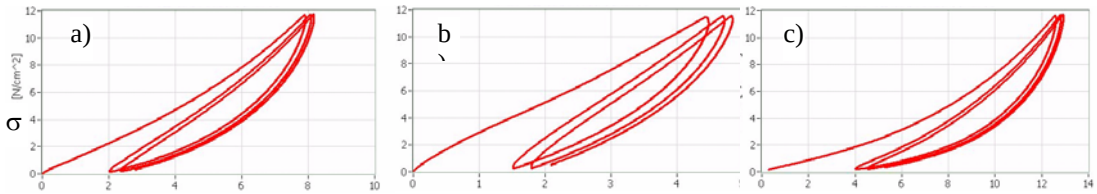

figure 14 experimental cycles for small granules of black EPDM: a) condition 1; b) condition 2; c) condition 3

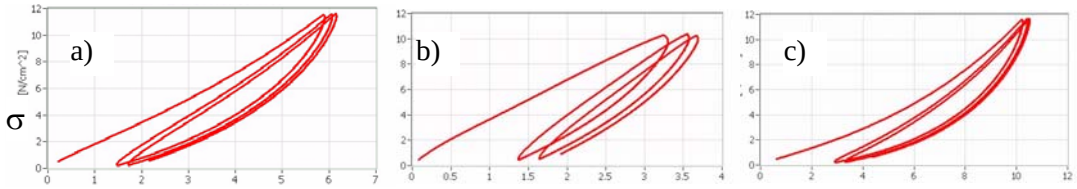

figure 15 experimental cycles for small granules of SBR: a) condition 1; b) condition 2; c) condition 3

table 2 experimental results for inert component

INERT TYPE	CONDITION	STATIC STIFFNESS k_s[N/cm^3]	LOSS FACTOR [%]
Grey EPDM (BG)	1	14.93	31.52
	2	27.25	17.79
	3	6.79	29.24
Grey EPDM (SG)	1	19.81	19.18
	2	24.66	17.02
	3	10.81	32.23
Black EPDM (SG)	1	18.90	30.38
	2	35.46	30.45
	3	13.29	31.57
SBR (BG)	1	33.94	48.25
	2	45.70	25.33
	3	16.34	25.61
SBR (SG)	1	24.40	25.40
	2	47.08	27.86
	3	15.25	27.70

It is evident that the second condition gives stiffness values greater caused by a greater material compression. The grey EPDM compound has the lowest stiffness values and the stiffest compound is the SBR one.

4.4 PROPERTIES OF THE BINDER

The binder is a polyurethane resin. The polyurethane is a polymer consisting of a chain of organic units joined by urethane links. Generally polyurethane polymers are formed by reacting a monomer containing at least two isocyanate functional groups ($-N=C=O$; when an isocyanate has two isocyanate group is called diisocyanate) with another monomer containing at least two alcohol groups in the presence of catalyst (the acceleration of a chemical reaction). The alcohol is an organic compound in which a hydroxyl group (OH) is bound to carbon atom of an alkyl, that is an equivalent radical containing only carbon and hydrogen atoms arranged in a chain.

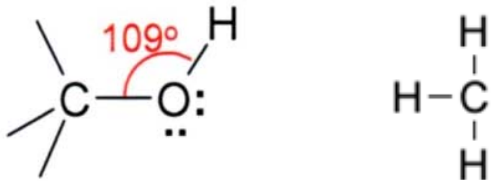

figure 16 chemical formulation of alcohol and alkyl group respectively

Polyurethane formulations cover an extremely wide range of stiffness, hardness and densities.

The binder in the described material is a polyether that consists of more than one ether group (an oxygen atom and two alkyl groups). The diethyl ether is CH_3-CH_2-O-CH_2-CH_3.

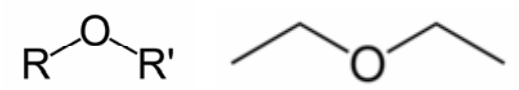

figure 17 chemical formulation of ether and diethyl respectively

The binder is provided by a French society called SNAD POLYURETANE and it is the commercial name Stobicoll R389.00.The chemical description is a pre-polymer of urethane with different aromatic poly-isocyanates.

4.5 THEORETHICAL STUDY OF THE COMPOSITE MATERIAL

In the mechanical approach of composite materials three size scales can be considered: micro-scale, meso-scale and macro-scale.

The first one considers matrix-fibre heterogeneities, it consists of the study of composite material behaviour where the interaction of constituent material is examined in detail and used to predict and define the behaviour of the heterogeneous material.

The meso-scale is an intermediate scale useful to understand the nature of fibres disposition (orderly or random).

The last one is the scale of the global structure. It consists of the study of composite material behaviour where the material is presumed homogeneous and the effects of constituent material are detected only as averaged 'apparent' properties of the composite. Considering the macromechanics, composite properties can be obtained from single component properties, i.e. the microscopic nature of the structure can be disregarded and considered as a homogeneous material.

4.5.1 Voigt and Reuss models

Regarding polymer composites in literature (Ward & Sweeney, 2004) an idealized lamellar composite that consists of high modulus layer and a more compliant matrix layer is modelled. It is assumed that the bond between layers remains intact and the volume fraction of each component is an important parameter, but not the thickness of the individual layer. Both Voigt and Reuss models are considered in the following.

In the first one an uniaxial stress is applied parallel to the layers direction orientation (figure 18).

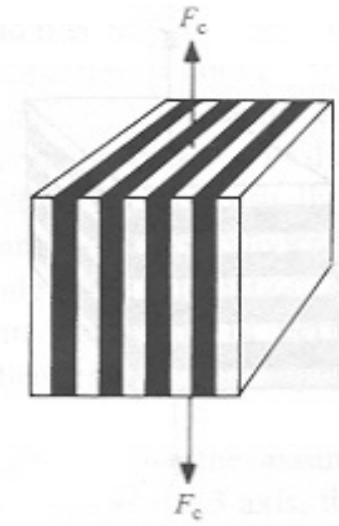

figure 18 Voigt model (Ward & Sweeney, 2004)

The strain is the same in all layers (isostrain condition) and the force F_c acting on the composite is equal to the sum of the forces acting on the fibre F_f and matrix F_m layers:

$$F_c = F_f + F_m \tag{4.5}$$

Considering the relation between the force and the tension each addendum can be written:

$$F_f = \sigma_f \cdot A = \sigma_f \cdot h_f \cdot 1 \qquad F_m = \sigma_m \cdot A = \sigma_m \cdot h_m \cdot 1 \tag{4.6}$$

The total stress σ is given by:

$$\sigma = \frac{F_c}{A} = \frac{F_c}{h \cdot 1} = E_f \cdot \varepsilon \cdot \frac{h_f}{h} + E_m \cdot \varepsilon \cdot \frac{h_m}{h} = \left(E_f \cdot V_f + E_m \cdot V_m\right) \cdot \varepsilon \tag{4.7}$$

The equivalent modulus of the composite material, called Voigt average modulus, is given by:

$$E_{eq,Voigt} = E_f V_f + E_m V_m \tag{4.8}$$

where E_f and E_m are the fibre and the matrix elastic modulus respectively; V_f is the volume fraction of fibres and V_m is the volume fraction of the matrix (such that: $V_f + V_m = 1$).

In the Reuss model the uniaxial stress is applied in transverse direction with respect to the layers direction orientation (figure 19).

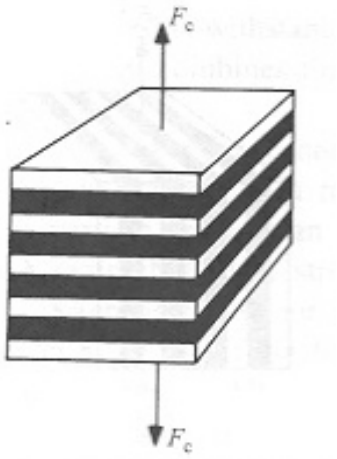

figure 19 Reuss model (Ward & Sweeney, 2004)

Each layer is subjected to the same force and hence to the same stress (isostress condition) whereas the total deformation s_c is equal to the sum of the deformations of each component:

$$s_c = s_f + s_m . \tag{4.9}$$

The displacement of the fibre part is:

$$s_f = \frac{F_c \cdot h_f}{E_f \cdot A} \tag{4.10}$$

The displacement of the matrix part is given by:

$$s_m = \frac{F_c \cdot h_m}{E_m \cdot A} \tag{4.11}$$

The total displacement is expressed as a function of an equivalent modulus E_{eq}:

$$s = \frac{F_c \cdot h}{E_{eq} \cdot A} \tag{4.12}$$

Considering the relation (4.9):

$$s = \frac{F_c \cdot h}{E_{eq} \cdot A} = \frac{F_c \cdot h_f}{E_f \cdot A} + \frac{F_c \cdot h_m}{E_m \cdot A} \quad \Rightarrow \quad \frac{h}{E_{eq}} = \frac{h_f}{E_f} + \frac{h_m}{E_m} \tag{4.13}$$

$$E_{eq} = \frac{E_f \cdot E_m}{E_m h_f + E_f h_m} \cdot h$$

In this case the equivalent modulus of the composite, called Reuss average modulus is given:

$$E_{eq,\mathrm{Re}uss} = \frac{E_f E_m}{E_m V_f + E_f V_m} \tag{4.14}$$

In figure 20 the ratio between the equivalent Voigt and Reuss elastic modulus and the fibres one is represented as a function of the fibres fraction volume for different ratios between the fibres elastic modulus and the matrix one:

$$\frac{E_{eq,Voigt}}{E_f} = V_f + \frac{E_m}{E_f} V_m \qquad \frac{E_{eq,\mathrm{Re}uss}}{E_f} = \frac{1}{V_f + \frac{E_f}{E_m} V_m} \tag{4.15}$$

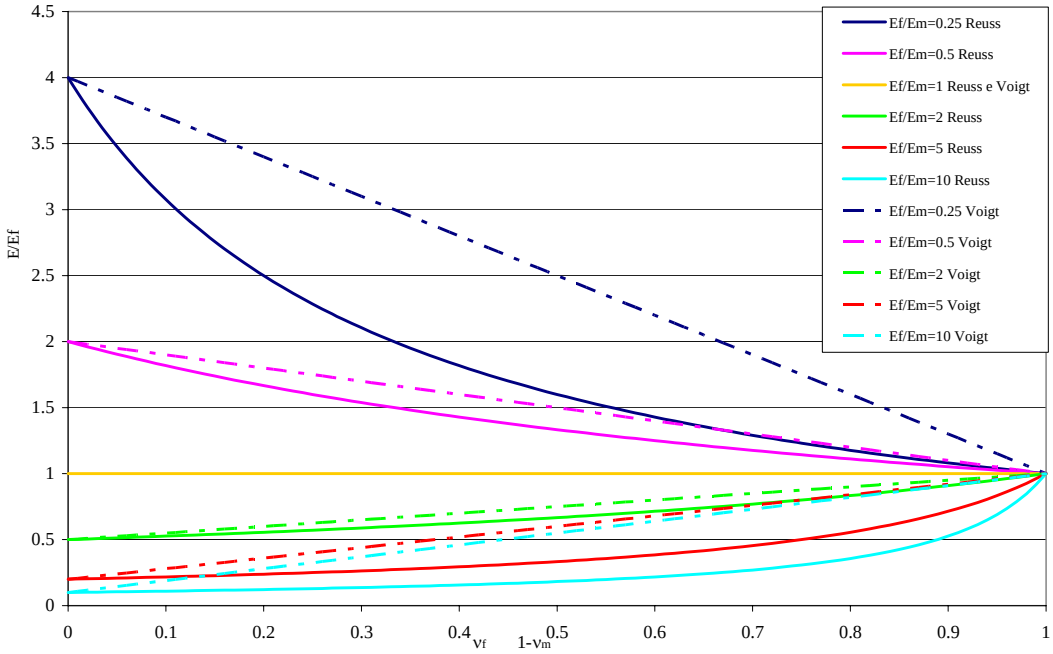

figure 20 Voigt and Reuss results

Considering the same type of matrix and fibre and the same material composition the Voigt equivalent elastic modulus is greater than the Reuss one. When the matrix has a greater elastic modulus than the fibre one $\left(\frac{E_f}{E_m}=0.25;\ \frac{E_f}{E_m}=0.5\right)$, the equivalent elastic modulus is always greater than the elastic modulus of the fibre and it increases with the matrix volume fraction.

4.5.2 Model for the rubber-polyurethane material

Starting from the Reuss and Voigt models, the proper model for the considered material is now discussed.

The material consists of two components: binder (1) and inert (2) although the presence of voids (v) can not be disregarded. A combination of Voigt and Reuss model is considered which includes rubber and polyurethane through a Reuss model; the

equivalent modulus is then obtained if the presence of voids is assumed as a new material combined with the inert and the binder through a Voigt model (figure 21).

Rubber and polyurethane volumes are respectively:

$$V_1 = (1-h_v)\cdot 1\cdot h_1 \qquad V_2 = (1-h_v)\cdot 1\cdot h_2 \tag{4.16}$$

The total force F_c is taken by rubber and polyurethane part.

The relation between the stress and force is still considered:

$$\sigma = \frac{F_c}{A} = \frac{F_c}{(1-h_v)\cdot 1} \tag{4.17}$$

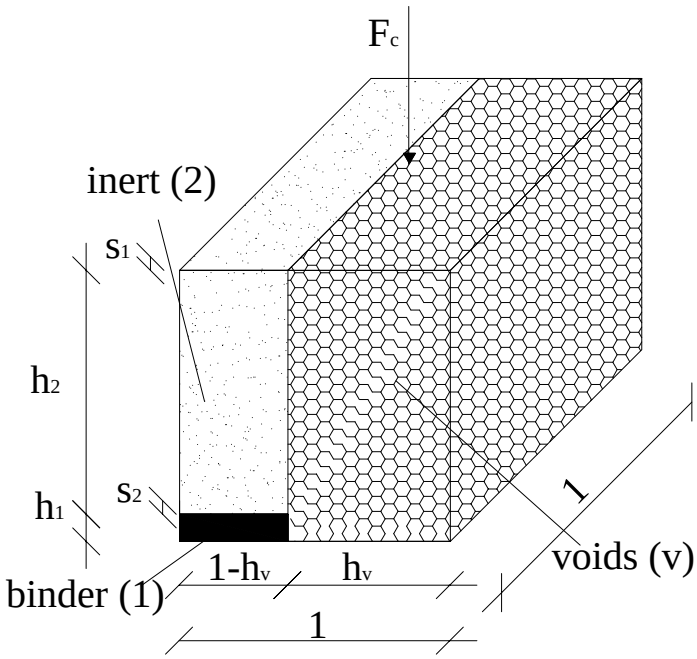

figure 21 Model for the new material

The total displacement in the force direction is:

$$s = \frac{F_c}{A_{tot}\cdot E_{eq}}\cdot(h_1+h_2) = s_1+s_2 = \frac{F_c}{E_1\cdot(1-h_v)\cdot 1}\cdot h_1 + \frac{F_c}{E_2\cdot(1-h_v)\cdot 1}\cdot h_2 \tag{4.18}$$

where $A_{tot} = 1\cdot 1$.

hence:

$$s = \frac{(h_1+h_2)}{1\cdot E_{eq}} = \frac{h_1}{(1-h_v)\cdot E_1} + \frac{h_2}{(1-h_v)\cdot E_2} \tag{4.19}$$

The voids volume is given by:

$$V_v = h_v \cdot 1 \cdot (h_1 + h_2) \tag{4.20}$$

h_v can be calculated:

$$h_v = \frac{V_v}{1 \cdot (h_1 + h_2)} = \frac{1 \cdot V_v}{1 \cdot 1 \cdot (h_1 + h_2)} \tag{4.21}$$

The dominator represents the total volume and h_v can be written as a function of voids volume fraction v_v:

$$h_v = \frac{1 \cdot V_v}{V_{tot}} = 1 \cdot v_v \tag{4.22}$$

Moreover, h_1 and h_2 can be written:

$$h_1 = \frac{V_1}{(1 - h_v) \cdot 1} = \frac{V_1}{(1 - 1 \cdot v_v) \cdot 1} = \frac{V_1}{(1 - v_v) \cdot 1 \cdot 1} \tag{4.23}$$

$$h_2 = \frac{V_2}{(1 - h_v) \cdot 1} = \frac{V_2}{(1 - 1 \cdot v_v) \cdot 1} = \frac{V_2}{(1 - v_v) \cdot 1 \cdot 1} \tag{4.24}$$

(4.22), (4.23) and (4.24) is substituted in (4.19):

$$\frac{1}{E_{eq}} = \frac{V_1}{(1 - v_v)^2 \cdot 1 \cdot 1 \cdot (h_1 + h_2) E_1} + \frac{V_2}{(1 - v_v)^2 \cdot 1 \cdot 1 \cdot (h_1 + h_2) E_2} \tag{4.25}$$

Considering that $V_{tot} = 1 \cdot 1 \cdot (h_1 + h_2)$ the relation (4.25) is written as a function of the volume fractions of the binder and the inert v_1 and v_2 respectively:

$$v_1 = \frac{V_1}{1 \cdot 1 \cdot (h_1 + h_2)} \qquad v_2 = \frac{V_2}{1 \cdot 1 \cdot (h_1 + h_2)} \tag{4.26}$$

Hence:

$$\frac{1}{E_{eq}} = \frac{v_1}{(1 - v_v)^2 \cdot E_1} + \frac{v_2}{(1 - v_v)^2 \cdot E_2} \tag{4.27}$$

The equivalent elastic modulus of the composite material ca be expressed as:

$$E_{eq} = \frac{E_1 \cdot E_2}{\frac{\nu_1}{(1-\nu_v)^2} \cdot E_2 + \frac{\nu_2}{(1-\nu_v)^2} \cdot E_1} \tag{4.28}$$

The ratio between the equivalent elastic modulus and the inert modulus is given by:

$$\frac{E_{eq}}{E_2} = \frac{1}{\frac{\nu_1}{(1-\nu_v)^2} \cdot \frac{E_2}{E_1} + \frac{\nu_2}{(1-\nu_v)^2}} \tag{4.29}$$

This ratio is plotted in the following figures as a function of volume fraction of voids and for different values of ratio $\frac{E_2}{E_1}$ and for different values of ratio $\frac{\nu_2}{\nu_1}$ (figures 22-26).

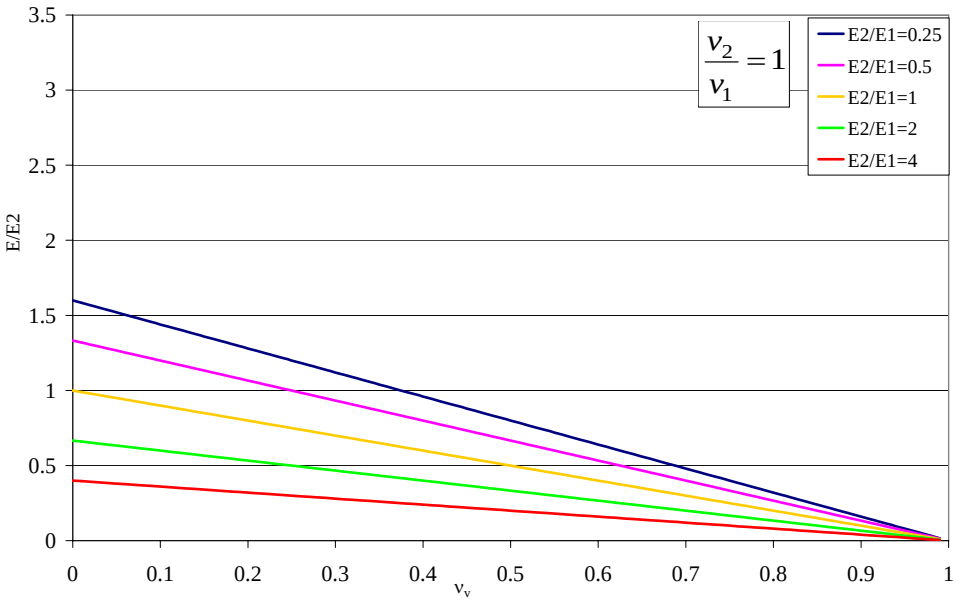

figure 22 equivalent elastic modulus for $\frac{\nu_2}{\nu_1}$ =1

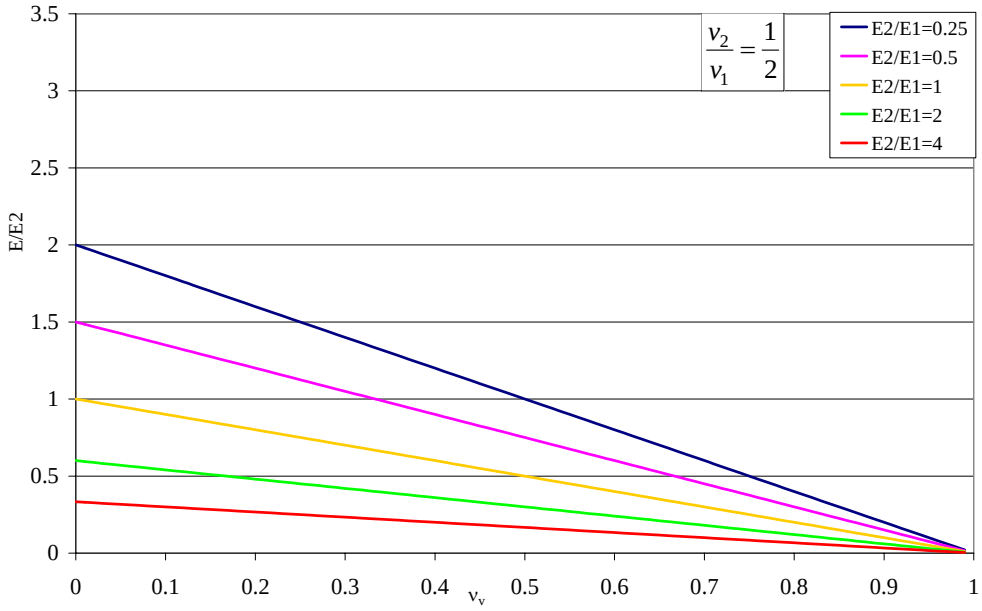

figure 23 equivalent elastic modulus for $\frac{v_2}{v_1} = \frac{1}{2}$

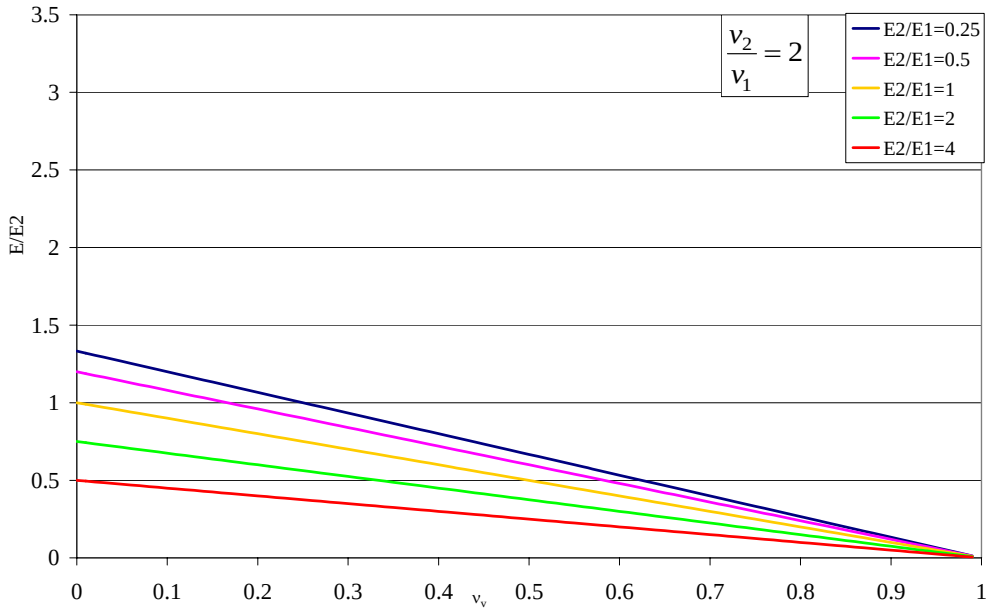

figure 24 equivalent elastic modulus for $\frac{v_2}{v_1} = 2$

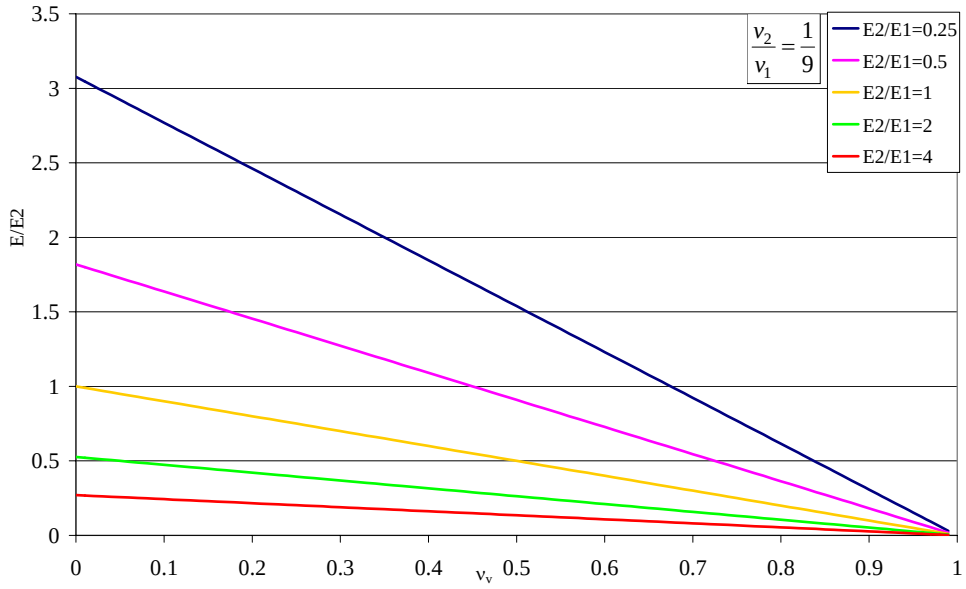

figure 25 equivalent elastic modulus for $\frac{\nu_2}{\nu_1}=\frac{1}{9}$

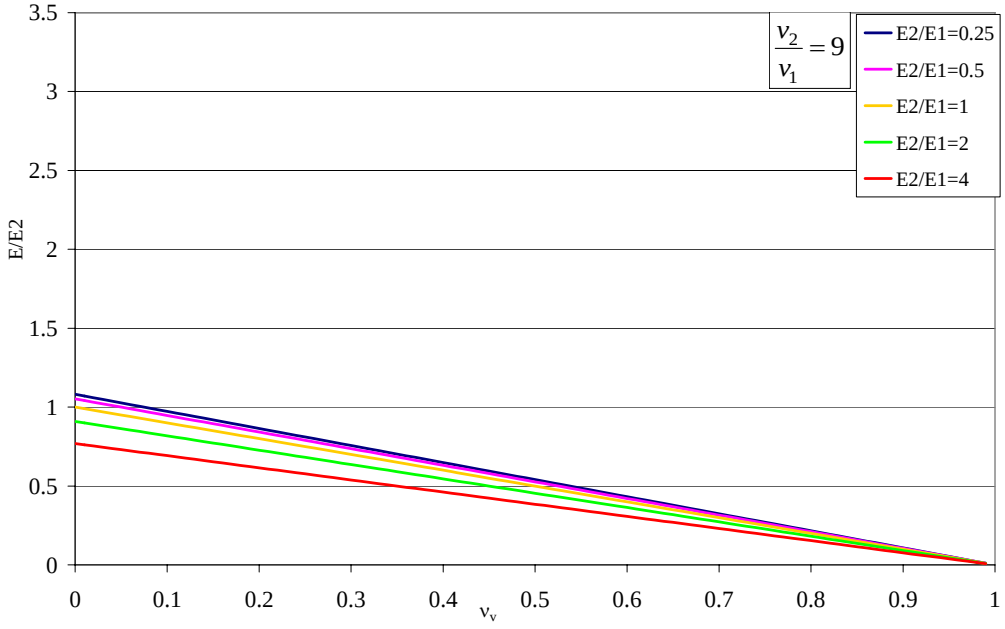

figure 26 equivalent elastic modulus for $\frac{\nu_2}{\nu_1}=9$

When the material consists of polyurethane and two rubber component a variant of this model can be considered. A combination of Voigt and Reuss model is still considered which includes two rubber components and polyurethane through a Reuss model; the equivalent modulus is then obtained assuming voids as a new material combined with the two inert components and the binder through a Voigt model (figure 27).

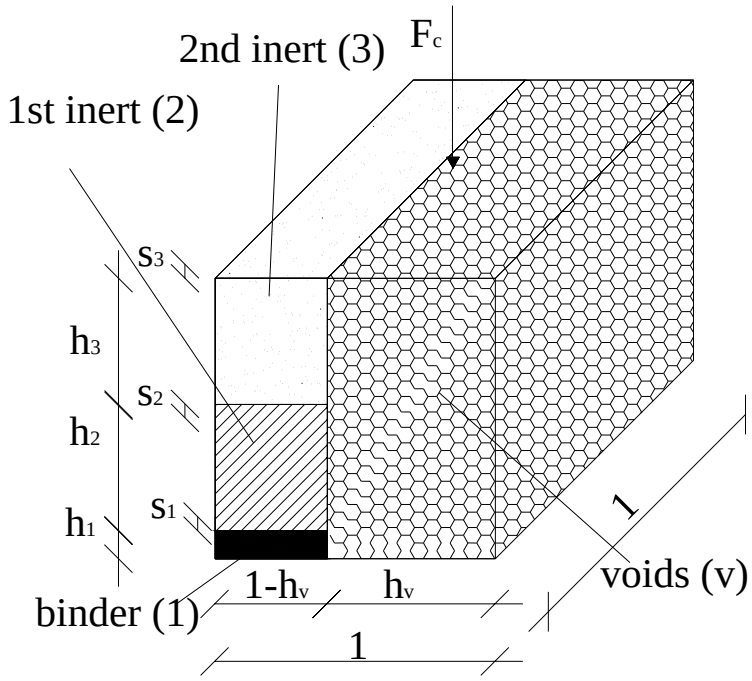

figure 27 Model for the new material (2)

The total displacement in the force direction is:

$$s = \frac{F_c \cdot (h_1 + h_2 + h_3)}{A_{tot} \cdot E_{eq}} = s_1 + s_2 + s_3 = \frac{F_c \cdot h_1}{E_1 \cdot (1 - h_v) \cdot 1} + \frac{F_c \cdot h_2}{E_2 \cdot (1 - h_v) \cdot 1} + \frac{F_c \cdot h_3}{E_3 \cdot (1 - h_v) \cdot 1} \qquad (4.30)$$

In which $A_{tot} = 1 \cdot 1$; the total is written as in the following:

$$s = \frac{(h_1 + h_2 + h_3)}{1 \cdot E_{eq}} = \frac{h_1}{(1 - h_v) \cdot E_1} + \frac{h_2}{(1 - h_v) \cdot E_2} + \frac{h_3}{(1 - h_v) \cdot E_3} \qquad (4.31)$$

The voids volume is given by: $V_v = h_v \cdot 1 \cdot (h_1 + h_2 + h_3)$ (4.32)

h_v can be calculated:

$$h_v = \frac{V_v}{1\cdot\left(h_1+h_2+h_3\right)} = \frac{1\cdot V_v}{1\cdot 1\cdot\left(h_1+h_2+h_3\right)} \tag{4.33}$$

The dominator still represents the total volume and h_v can still be written as a function of voids volume fraction v_v.

Moreover, h_1, h_2 and h_3 can be written:

$$h_1 = \frac{V_1}{\left(1-h_v\right)\cdot 1} = \frac{V_1}{\left(1-1\cdot v_v\right)\cdot 1} = \frac{V_1}{\left(1-v_v\right)\cdot 1\cdot 1} \tag{4.34}$$

$$h_2 = \frac{V_2}{\left(1-h_v\right)\cdot 1} = \frac{V_2}{\left(1-1\cdot v_v\right)\cdot 1} = \frac{V_2}{\left(1-v_v\right)\cdot 1\cdot 1} \tag{4.35}$$

$$h_3 = \frac{V_3}{\left(1-h_v\right)\cdot 1} = \frac{V_3}{\left(1-1\cdot v_v\right)\cdot 1} = \frac{V_3}{\left(1-v_v\right)\cdot 1\cdot 1} \tag{4.36}$$

(4.34), (4.35) and (4.36) are substituted in(4.31):

$$\frac{1}{E_{eq}} = \frac{V_1}{(1-v_v)^2\cdot 1\cdot 1\cdot(h_1+h_2+h_3)E_1} + \frac{V_2}{(1-v_v)^2\cdot 1\cdot 1\cdot(h_1+h_2+h_3)E_2} + \\ + \frac{V_3}{(1-v_v)^2\cdot 1\cdot 1\cdot(h_1+h_2+h_3)E_3} \tag{4.37}$$

Considering that $V_{tot} = 1\cdot 1\cdot(h_1+h_2+h_3)$ the relation (4.37) is written as a function of the volume fractions of the binder v_1 and the two inert component v_2 and v_3:

$$v_1 = \frac{V_1}{1\cdot 1\cdot\left(h_1+h_2+h_3\right)} \qquad v_2 = \frac{V_2}{1\cdot 1\cdot\left(h_1+h_2+h_3\right)} \qquad v_3 = \frac{V_3}{1\cdot 1\cdot\left(h_1+h_2+h_3\right)} \tag{4.38}$$

Hence: $$\frac{1}{E_{eq}} = \frac{v_1}{(1-v_v)^2\cdot E_1} + \frac{v_2}{(1-v_v)^2\cdot E_2} + \frac{v_3}{(1-v_v)^2\cdot E_3} \tag{4.39}$$

Consequently, the equivalent elastic modulus of the composite material can be expressed as:

$$E_{eq} = \frac{E_1 \cdot E_2 \cdot E_3}{\frac{\nu_1}{(1-\nu_v)^2} \cdot E_2 \cdot E_3 + \frac{\nu_2}{(1-\nu_v)^2} \cdot E_1 \cdot E_3 + \frac{\nu_3}{(1-\nu_v)^2} \cdot E_1 \cdot E_2} \tag{4.40}$$

CHAPTER 5

EXPERIMENTAL ANALYSIS OF THE COMPOSITE MATERIAL

The application of new systems to attenuate disturbance in residential area located along underground lines increases the interest in using of new elastomeric materials.

Castellani et al. (1998) have already studied an elastomeric material used for vibration isolation of railway lines comparing the theoretical and the experimental behaviour: they performed both static and dynamic tests on specimens characterized by different densities. Pichler and Zindler (1999) considered a cellular polyurethane (PUR) material to develop artificial elastomers for railway applications.

In this thesis the experimental tests on the composite material (previously described) are performed at research centre ISOLGOMMA. They have three main purposes:

- evaluate elastic and damping properties of the studied composite material;
- compare different types of rubber compound;
- verify the effect of different densities.

5.1 REFERENCE STANDARDS FOR THE TESTS

The first standard regarding rubber material used for railway applications is UNI 5572/72. It deals in rubber under-rail grooved pads for railway and tramway lines, but it does not mention the problem of vibration reduction. In 1980 applications of antivibration systems started. Most of them have introduced elastic elements at different levels in the track (under rail, sleeper, ballast or slab). The need of specific standards regarding antivibration elements was born together with the evolution in the railway field.

In particular two Italian standards are considered:

- UNI 10570: it was issued in 1997 and regards pads and mats in railway tracks.
- UNI11059: it substituted the previous one for the part on mats in 2003.

5.1.1 UNI 10570: determination of mechanical characteristics of mats and pads

The UNI 10570 (UNI, 1997) defines and describes procedures to determine elastic and damping mechanical properties of the product; moreover the aging test is considered (it represents the ability of the product to maintain its properties for permanent load).

This standard gives prescriptions to test and check pad and mat that are applied in railway field. In the standard the pad is a “discrete” product with defined geometrical dimensions and the mat is a “continuous” product given in form of rolls or big sheets.

Tests for mechanical characterization are:

- Static tests;
- Forced dynamic test,
- Dynamic test of free oscillations.

Tests of mechanical aging are:

- Tests of permanent deformation;
- Fatigue tests.

In the standards the following test loads are considered:

- Initial load $\left(F_0 \text{ [N] or } \sigma_0 \text{ [N/mm}^2\text{]}\right)$: it always acts on the railway line and it is produced by clips and by gravitation loads.
- Design static load $\left(F_{ps} \text{ [N] or } \sigma_{ps} \text{ [N/mm}^2\text{]}\right)$: it consists of the accidental load that acts during the useful life of the railway line.
- Design dynamic load $\left(F_{pd} \text{ [N] or } \sigma_{pd} \text{ [N/mm}^2\text{]}\right)$: it consists of the dynamic component of the exercise loads.

In the following details are only given for the tests that are of interesting in the considered application.

Static tests are performed with the application of a slow load. It starts to zero value and increases with linear pattern until its maximum value: three cycles are considered. Each cycle last two minutes: the first cycle and the second one help to arrange the specimen, while the mechanical parameters are derived by the third one. The maximum test load is given:

$$F_{\max} = F_0 + F_{PS} + F_{Pd} \quad (\text{for pads}) \tag{5.1}$$

$$\sigma_{\max} = \sigma_0 + \sigma_{PS} + \sigma_{Pd} \quad (\text{for mats}) \tag{5.2}$$

The terms are previously defined.

Other prescriptions regard the following test parameters

- the geometrical dimensions of specimens: they must not be smaller than $30 \text{ cm} \times 30 \text{ cm}$;
- the test temperature: 15-20 °C.

The static stiffness is obtained considering the following relations:

$$K_S = \frac{F_{\text{PS}}}{\delta_{\text{PS}} - \delta_0} \quad (\text{for pads}) \tag{5.3}$$

$$k_S = \frac{\sigma_{\text{PS}}}{\delta_{\text{PS}} - \delta_0} \quad (\text{for mats}) \tag{5.4}$$

in which δ_{PS} is the displacement for $(F_{PS}+F_0)$ or $(\sigma_{PS}+\sigma_0)$ and δ_0 is the displacement for the initial load.

The loss factor is given by:

$$\tan(\theta)=\frac{G_s}{K_s} \quad (\text{for pads}) \tag{5.5}$$

$$\tan(\theta)=\frac{g_s}{k_s} \quad (\text{for mats}) \tag{5.6}$$

In which G_S and g_S are the static damping for pads and slabs respectively and given by:

$$G_S=2\cdot K_S\cdot \nu_S \qquad g_S=2\cdot k_S\cdot \nu_S \tag{5.7}$$

ν_s is the damping static factor:

$$\nu_S=\frac{1}{\pi}\cdot\frac{E_{ciclo}}{E_{carico}-\frac{E_{ciclo}}{2}} \tag{5.8}$$

where E_{ciclo} represents the energy that is dissipated in a cycle, while E_{carico} is the energy that is stored during the loading phase.

The forced dynamic tests are performed to determine how the mechanical parameters vary for different values of frequency. The applied force $F(t)$ (or stress $\sigma(t)$) is composed by a static component $F_s\,(\sigma_s)$ and a dynamic component $F_d\,(\sigma_d)$ varying sinusoidally with the time:

$$F(t)=F_S+F_d\cdot\sin\left[(2\cdot\pi\cdot f)\cdot t\right]=F_0+F_{ps}+F_d\cdot\sin\left[(2\cdot\pi\cdot f)\cdot t\right](\text{for pads}) \tag{5.9}$$

$$\sigma(t)=\sigma_S+\sigma_d\cdot\sin\left[(2\cdot\pi\cdot f)\cdot t\right]=\sigma_0+\sigma_{pd}+\sigma_d\cdot\sin\left[(2\cdot\pi\cdot f)\cdot t\right]\ (\text{for mats}) \tag{5.10}$$

The dynamic load is given by:

$$F_d=\pm F_{Pd} \qquad \sigma_d=\pm\sigma_{Pd} \tag{5.11}$$

The frequency varies from the initial value f_i to the final one f_f with discrete step of Δf :

$$f = f_i, \left(f_i + \Delta f \right),\ \left(f_i + 2\Delta f \right),\ \ldots \left(f_f - \Delta f \right),\ f_f \tag{5.12}$$

In the standard the elastic-viscous-hysteretic model is assumed as the ideal behaviour of the material to evaluate elastic and damping dynamic parameters (figure1).

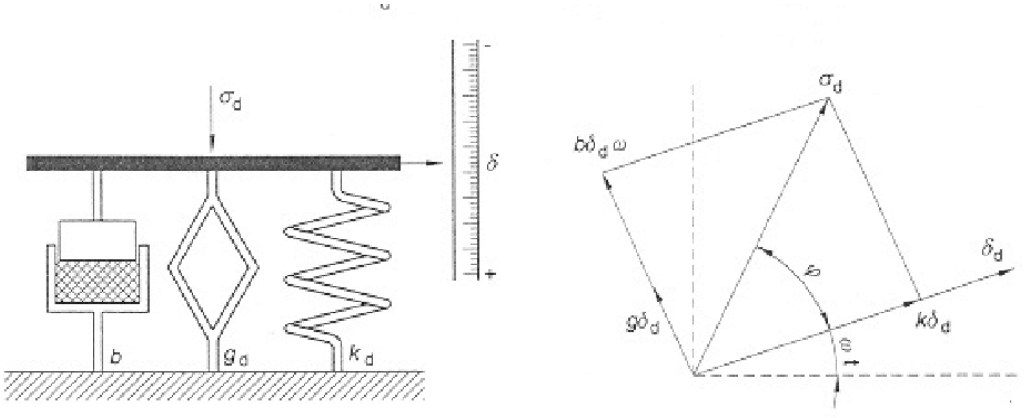

figure 1 "elastic-viscous-isteretic" model (UNI 1997, UNI 2003)

The elaboration starts from the displacement analysis for each test frequency, it is evaluated considering the mean value of the four transducers and it will be sinusoidal form:

$$\delta(t) = \delta_S + \delta_d \cdot \sin\left[\left(2 \cdot \pi \cdot f\right) \cdot t + \varphi\right] + \delta^0(t) \tag{5.13}$$

In which δ_S and δ_d are obtained from static and dynamic load respectively while $\delta^0(t)$ is the signal distortion that must be negligible as shown in the following condition:

$$\frac{\sqrt{\frac{1}{T} \cdot \int_0^T \delta^o(t)^2 \cdot dt}}{\sqrt{\frac{1}{T} \cdot \int_0^T \delta(t)^2 \cdot dt}} \leq 10\% \tag{5.14}$$

The spectral transfer functions of the specimen for pads and mats are given by:

$$H(f)^{-1} = \frac{F_d(f)}{\delta_d(f)} \times e^{j\times\varphi(f)} \qquad h(f)^{-1} = \frac{\sigma_d(f)}{\delta_d(f)} \times e^{j\times\varphi(f)} \tag{5.15}$$

Considering the model in figure 1 they can be written in the form:

$$H(f)^{-1} = [K_d] + j\times[G_d + B\times(2\times\pi\times f)] \quad h(f)^{-1} = [k_d] + j\times[g_d + b\times(2\times\pi\times f)] \tag{5.16}$$

The real part is the dynamic stiffness and it is constant for different values of frequency, while the imaginary part varies linearly with the frequency in which g_d represents the hysteretic dissipation and b is the viscous dissipation.

Materials can show a bit different behaviour for which they has an intermediate phase where there is a gradual transition from static to dynamic behaviour. The extension of this phase is given by the transition frequency.

The analytical expressions for the calculation of dynamic parameters are given

$$K_d \cong \frac{\sum_{i=1}^{N}\left[H(f_n)^{-1}\right]_{Re}}{N} \tag{5.17}$$

$$\begin{bmatrix} G_d \\ B \end{bmatrix} \cong \begin{bmatrix} N & \sum_{n=1}^{N}(2\pi f_n) \\ \sum_{n=1}^{N}(2\pi f_n) & \sum_{n=1}^{N}(2\pi f_n)^2 \end{bmatrix}^{-1} \times \begin{bmatrix} \sum_{n=1}^{N}\left[H(f_n)^{-1}\right]_{Im} \\ \sum_{n=1}^{N}\left\{\left[H(f_n)^{-1}\right]_{Im}\times(2\pi f_n)\right\} \end{bmatrix} \tag{5.18}$$

$$k_d \cong \frac{\sum_{i=1}^{N}\left[h(f_n)^{-1}\right]_{Re}}{N} \tag{5.19}$$

$$\begin{bmatrix} g_d \\ b \end{bmatrix} \cong \begin{bmatrix} N & \sum_{n=1}^{N}(2\pi f_n) \\ \sum_{n=1}^{N}(2\pi f_n) & \sum_{n=1}^{N}(2\pi f_n)^2 \end{bmatrix}^{-1} \times \begin{bmatrix} \sum_{n=1}^{N}\left[h(f_n)^{-1}\right]_{Im} \\ \sum_{n=1}^{N}\left\{\left[h(f_n)^{-1}\right]_{Im}\times(2\pi f_n)\right\} \end{bmatrix} \tag{5.20}$$

relation (5.17) and (5.18) are applied for pads ; relations (5.19)and (5.20) are applied for mats.

For other specific considerations the reference is the standard test.

5.1.2 UNI 11059: elastomeric mats for railway tracks

UNI 11059 (UNI, 2003) is applied for elastic mats in new railway tracks or as an underballast element or as an under concrete slab element. Some experimental tests in 11059 are mentioned in 10570, in the following innovations of UNI 11059 (respect to UNI 10570) will be considered.

The elastomeric mat is designed to reduce vibration induced by railway traffic, it has constant thickness and it has the following characteristics:

- One dimension (the thickness h) is significantly smaller than the other two dimensions (the longitudinal one d_l and the transverse one d_t):

$$\frac{\sqrt{\frac{d_l \cdot d_t}{\pi}}}{h} \geq 10 \tag{5.21}$$

- During the useful life of the railway line loads are orthogonally applied on the mat surface.

Two categories of tests are considered.

1. Characterization tests that include:
   - Static tests;
   - Simulation tests (as a function of train speed);
   - Forced dynamic tests;
   - Dynamic tests of free oscillations
2. Performance tests that include:
   - Permanent load tests;
   - fatigue tests;
   - frost strength tests with water;
   - atmospheric conditions strength tests;
   - adequacy of mats to be put along lines;
   - geometric stability of mats.

In the standards the following test loads are considered:

- Nominal initial load $\left(\sigma_0\ [\text{N/mm}^2]\right)$: it always constantly acts on the railway line and it is produced by the weight of the rack on the elastomeric mat. It approximately assumes values $\sigma_0 = 0.7 - 1.0\ \text{N/cm}^2$ for ballasted systems and values $\sigma_0 = 0.4 - 2.0\ \text{N/cm}^2$ for slab track systems.
- Nominal railway load $\left(\sigma_f\ [\text{N/mm}^2]\right)$: it consists of the accidental load and corresponds to the weight of the train that runs on the line. The standard gives this component as a function of the railway track and of the vehicle.
- Nominal dynamic railway factor $\left(\gamma_d\right)$: it is an amplification factor of the nominal railway load and depends on the railway track type and conditions, on train and on dynamic interaction track-train. It varies from 20% to 50%.

The procedure of the load application does not change respect to the UNI 10570.

The maximum test load is given:

$$\sigma_{\max} = \sigma_0 + \left(1 + \gamma_d\right) \cdot \sigma_f \tag{5.22}$$

In the UNI 11059 specimen dimensions are indicated with more details: for thickness smaller than $50\ \text{mm}$ the dimensions of specimens must to be greater than $30\ \text{cm} \times 30\ \text{cm}$ and for thickness greater than $50\ \text{mm}$ their dimensions depend on the thickness and they must to be greater than $\left(6h\right) \times \left(6h\right)$ in which h is the nominal thickness.

This standard only refers to mat that are “continuous” element and so it accurately describes the procedure to obtain specimens considering the possible heterogeneity of rolls or sheets.

The evaluation of the static stiffness is obtained by the following relation:

$$k_{qs} = \frac{\sigma_1 - \sigma_0}{\delta_1 - \delta_0} = \frac{\sigma_{\text{f}}}{\delta_1 - \delta_0} \tag{5.23}$$

In which $\sigma_1 = \sigma_0 + \sigma_f$ and δ_1 is the correspondent displacement and δ_0 is the displacement for the nominal initial load σ_0.

The procedure to determine the damping static factor and the loss factor has already described for UNI 10570.

Regarding forced dynamic tests they involve the application of a load $\sigma(t)$ that consists of a static component σ_S and of a dynamic component σ_d that varies sinusoidally with the time:

$$\sigma(t) = \sigma_S + \sigma_d \cdot \sin\left[\left(2 \cdot \pi \cdot f\right) \cdot t\right] \tag{5.24}$$

Tests have to be performed with two different static and dynamic test load components, in particular the static component is:

$$\sigma_{S1} = 100\% \times \left[\sigma_0 + (1+\gamma_d) \times \sigma_{\mathrm{f}}\right] \quad \sigma_{S2} = 60\% \times \left[\sigma_0 + (1+\gamma_d) \times \sigma_{\mathrm{f}}\right] \tag{5.25}$$

the dynamic one is:

$$\pm\sigma_{d1} = \pm\left(5-10\right)\% \times \sigma_{S1} \quad \pm\sigma_{d2} = \pm\left(5-10\right)\% \times \sigma_{S2} \tag{5.26}$$

The frequency still varies from the initial value f_i to the final one f_f with discrete step of Δf.

The following parameters are determined: dynamic stiffness k_d, dynamic hysteretic damping g_d, viscous damping b, dynamic hysteretic and viscous damping factor $\nu_{i,d}$ and $\nu_{v,d}$ respectively, dynamic loss factor $\tan(\theta_d)$ and the transition frequency. These parameters are determined considering the "elastic-viscous-hysteretic" model that has been previously described. k_d, g_d and b are determined using (5.19) and (5.20). Finally other parameters are given by the following relations:

$$\nu_{i,d} = \frac{g_d}{2 \times k_d} \qquad \tan\left(\theta_d\right) = \frac{g_d}{k_d} \qquad \nu_{v,d} = \frac{b}{2 \times \sqrt{k_d \times m}} \tag{5.27}$$

In which m is the mat mass per unit of area and it is given by:

$$m_{f1} = 100\% \cdot \frac{\left[\sigma_0 + (1+\gamma_d)\cdot\sigma_f\right]}{a_g} \tag{5.28}$$

For other specific considerations the reference is the standard test.

5.2 DESCRIPTION OF THE TESTING EQUIPMENT AND MACHINE

The testing machine is called Resilient Pad and Mat Testing Machine (RPMTM). It has been design to perform static and dynamic tests according to standards UNI 10570 and UNI 11059 that are described previously.

There is a frame that supports and contains the working equipment rest on a steel plate (figure 2).

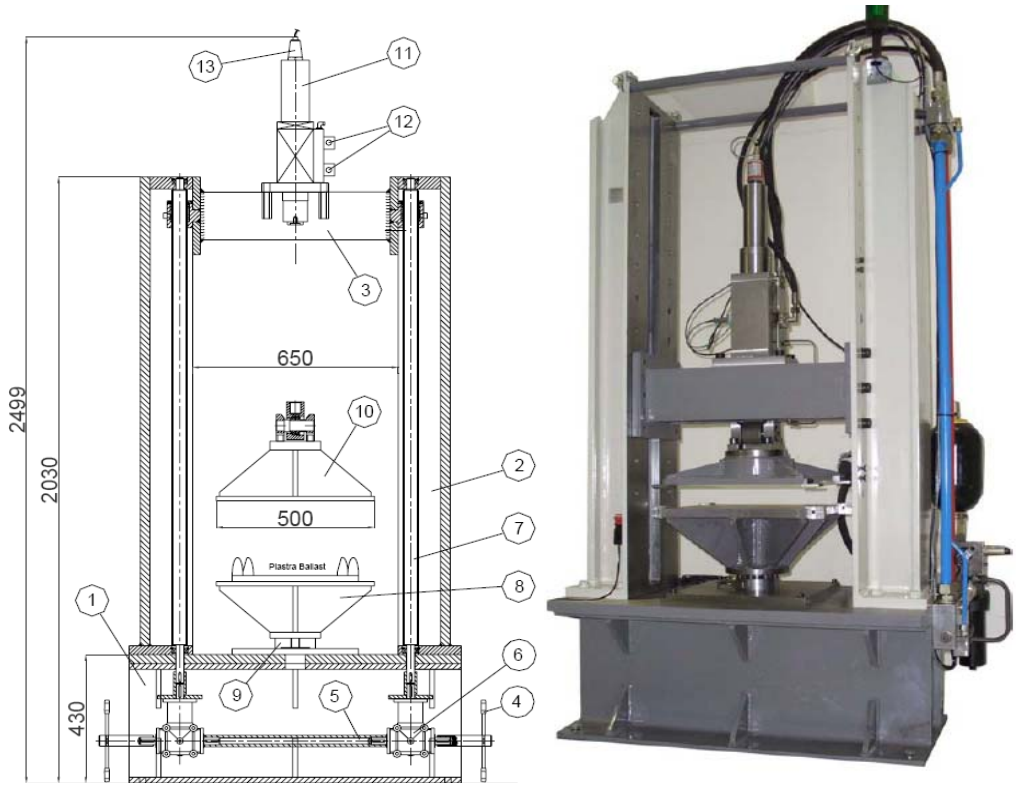

figure 2 layout of testing machine

Every element in figure 2 is described in the following table 1.

table 1 description of the testing machine elements

1	press basement
2	press columns
3	movable upper cross-bar
4	handwheel
5	connection bar
6	angular transmission
7	screw
8	lower plate
9	load cell
10	upper plate
11	hydraulic actuator 15 kN
12	Moog valves and differential pressure cell
13	dispacement transducer

This system is on four dampers. In the following the main components of the testing machine are described.

The load frame is designed for a maximum force of 100 kN in the dynamic condition. The upper cross-bar is moved by two worm-screws placed in the lateral columns of the press. The cross-bar can be placed in the vertical direction at regular distance of 100 mm and it can contain both an actuator of 15 kN and of 100 kN. The displacement of the cross-bar is obtained thanks to a handwheel that puts on (through a worm-screw and two angular transmissions) two thread shafts with bronze bush anchored on the cross-bar (figure 3).

The actuator has transverse section $A_a = 10.54 \text{ cm}^2$, it has a device that prevents the rotation, it is equipped of Moog valves (each is 38 lpm) that are calculated for a maximum frequency of 100 Hz with 50 lit/min. The actuator has also a linear displacement sensor “MTS Temposonics” and a differential pressure transducer “Paine” (figure 4).

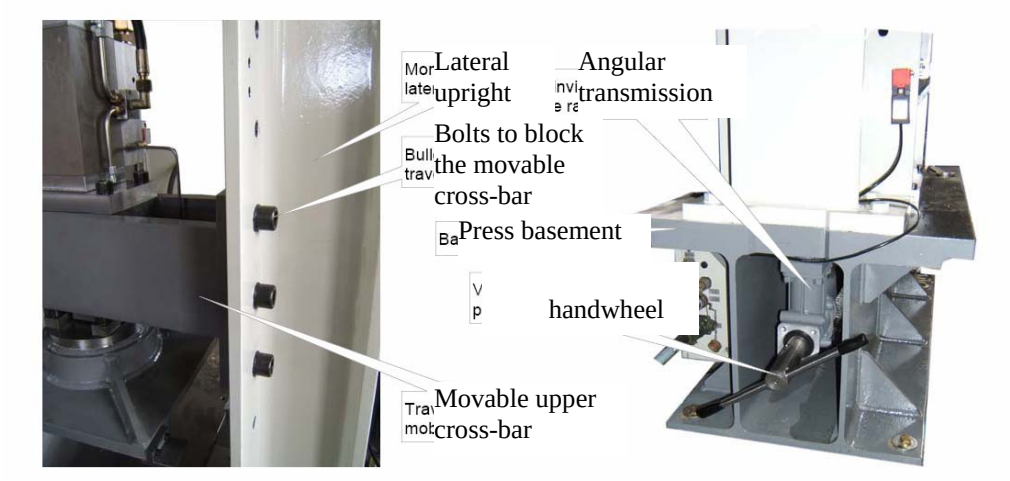

figure 3 cross-bar and handwheel

figure 4 hydraulic actuator and Moog valves

The oleo dynamic junction box works at variable capacity and at a pressure of 210 bar. The maximum capacity of the tank is 250 l. There is an air-oil heat and a control thermostat.

The testing machine includes the following measure sensors:

- four inductive displacement transducers HBM WA-T-50mm and four inductive HBM WA-T-100mm. They can be placed on four corners of the load plate (figure 5);
- two inductive accelerometers HBM B12-200;

- a load cell is installed between the press basement and the lower plate;
- a displacement transducer is installed on the hydraulic actuator and a differential pressure transducer is installed in the lateral part of the actuator.

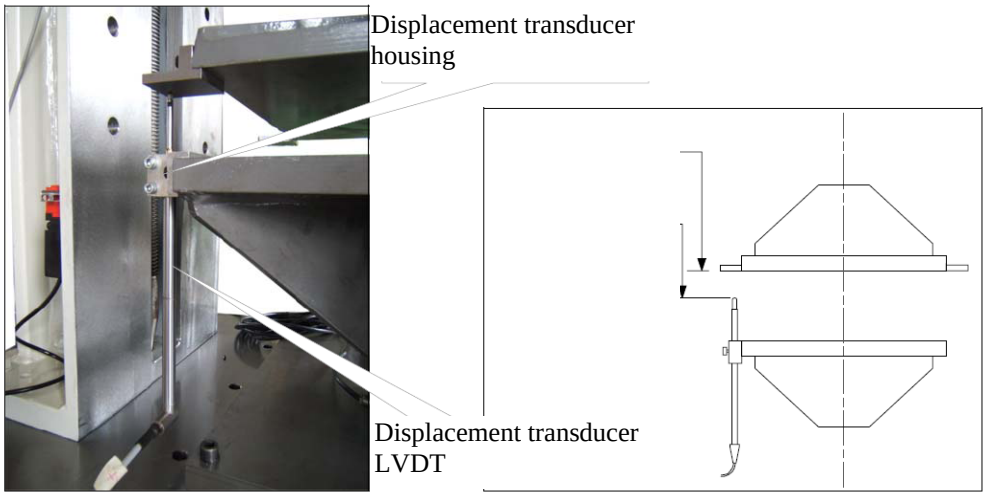

figure 5 displacement transducers

Finally, the main components of the digital control system are:

- Control and data acquisition unit is based on PXI platform of the National Instruments with multifunction card with eight differential analogical input channels and an analogical output to command the valves; the resolution is 16 bit and his maximum sampling frequency is 250.000 sps. The digital control system permits to condition load, displacement and differential pressure transducers, moreover it controls the load and the limit of the actuator, and it communicates with the hydraulic junction box to start the test or interrupt it. Another important characteristic is the saving on file of test data, test parameters and transducers configuration.
- Data logger HBM mod. Spider 8 is the data acquisition unit connected to personal computer, it permits to acquire signals of measure sensors concerning the test specimen (typically vertical deformations or acceleration). The system has eight differential analogical input channels.

5.2.1 Software for the RPMTM use

A software has been developed in labview language that permits to perform tests on mats and pads (Indapro, RPMTM, 2005). This software is a graphic interface with the user and helps to use correctly the testing machine.

Some of its functions are listed in the following:

- ignition and shutdown of the system;
- visualization of the alarm signal that can be present during the execution of the test;
- configuration of measurement chains of the control unit and of the acquisition unit given by the Spider 8;
- controlled management of the hydraulic actuator by means the control panel;
- visualization in real time of the acquired data in graphic and numerical form;
- rescue of data in Ascii form;
- database management of the performed tests.

The main panel is in figure 6: it can be divided in different parts. The central part is given to the visualization of graphs of the test progress. In the upper part the measure indicators are visualized during the test progress, moreover there is the possibility to enter in the configuration of measurement chains by means the push-button “configurazione (the first button on the left in the upper part)”. The push-button “pannello di controllo (the second button in the upper part)” permits to enter in the actuator control panel and the last button in this part “giornale di prove” permits the visualization of the list of performed tests. The lower part is given to the visualization of alarm signals. On the left initial data of the product to test are given. In this panel the type of the test is chosen.

For other information the reference is the manual document ((Indapro, RPMTM, 2005).

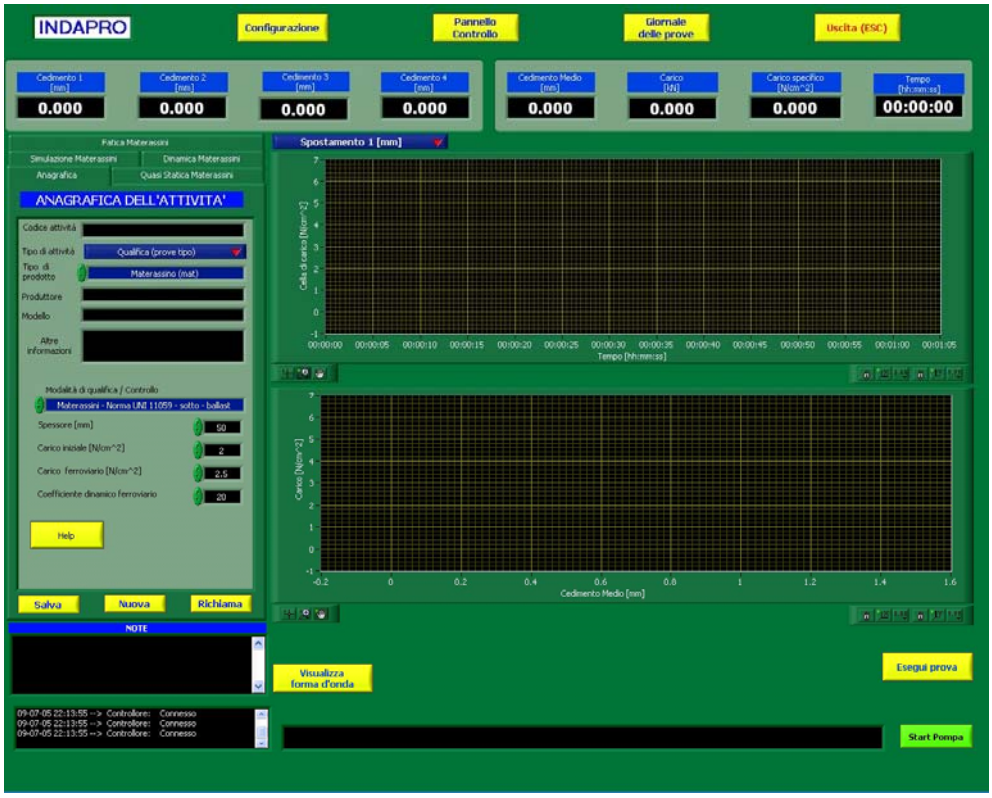

figure 6 the main panel of the software in labview language

5.3 CLASSIFICATION AND PROPERTIES OF SPECIMENS

Square specimen dimensions are approximately 345mm×345mm and the thickness is 20 mm (figure 7).

figure 7 specimens

The specimens can vary with the type or dimension of the inert component, while the binder is always polyurethane (polyether).

Four specimens consist of a single inert component:

- short fibres (sf) of SBR;
- small granules (sg) of SBR;
- big granules (bg) of grey EPDM:
- big granules (bg) of black EPDM.

Three specimens are composed by two types of the inert component in which the first one always consists of short fibres of SBR and the amount of each one is the same:

- short fibres (sf) of SBR (50%) and big granules (bg) of black EPDM (50%);
- short fibres (sf) of SBR (50%) and big granules (bg) of grey EPDM (50%);
- short fibres (sf) of SBR (50%) and small granules (sg) of SBR (50%).

Three specimens are still composed by two types of the inert component and the first one still consists of short fibres of SBR but its amount is greater than the second component as shown in the following:

- short fibres (sf) of SBR (90%) and small granules (sg) of black EPDM(10%);
- short fibres (sf) of SBR (90%) and small granules (sg) of grey EPDM (10%);
- short fibres (sf) of SBR (90%) and small granules (sg) of SBR (10%).

Different densities are obtained to verify its importance in the determination of material mechanical parameters. Four classes of density are considered (500; 600; 700; 900 kg/m^3).The binder amount in the composite material is 8% in weight, but it can decrease (6%) to obtain higher densities (i.e. 900 kg/m^3).

The main specimen characteristics are in tables from 1 to 11.

table 2 Short fibres of SBR

composite			binder			inert 1			inert 2		
weight [Kg]	total volume [m^3]	density [Kg/m^3]	weight [Kg]	specific weight [Kg/m^3]	volume Vb [m^3]	weight [Kg]	specific weight [Kg/m^3]	volume Vi1 [m^3]	weight [Kg]	specific weight [Kg/m^3]	volume Vi2 [m^3]
1.005	2.261E-03	444	0.080	1070	7.514E-05	0.925	1100	8.405E-04	0	0	0
1.005	2.261E-03	444	0.080	1070	7.514E-05	0.925	1100	8.405E-04	0	0	0
1.015	2.261E-03	449	0.081	1070	7.589E-05	0.934	1100	8.489E-04	0	0	0
1.525	2.514E-03	607	0.122	1070	1.140E-04	1.403	1100	1.275E-03	0	0	0
1.555	2.529E-03	615	0.124	1070	1.163E-04	1.431	1100	1.301E-03	0	0	0
1.490	2.543E-03	586	0.119	1070	1.114E-04	1.371	1100	1.246E-03	0	0	0
1.710	2.415E-03	708	0.137	1070	1.279E-04	1.573	1100	1.430E-03	0	0	0
1.730	2.394E-03	723	0.138	1070	1.293E-04	1.592	1100	1.447E-03	0	0	0
1.720	2.394E-03	718	0.138	1070	1.286E-04	1.582	1100	1.439E-03	0	0	0
2.295	2.436E-03	942	0.184	1070	1.716E-04	2.111	1100	1.919E-03	0	0	0
2.390	2.450E-03	976	0.191	1070	1.787E-04	2.199	1100	1.999E-03	0	0	0
2.170	2.450E-03	886	0.174	1070	1.622E-04	1.996	1100	1.815E-03	0	0	0

table 3 small granules of SBR

composite			binder			inert 1			inert 2		
weight [Kg]	total volume [m^3]	density [Kg/m^3]	weight [Kg]	specific weight [Kg/m^3]	volume Vb [m^3]	weight [Kg]	specific weight [Kg/m^3]	volume Vi1 [m^3]	weight [Kg]	specific weight [Kg/m^3]	volume Vi2 [m^3]
1.515	2.381E-03	636	0.121	1070	1.133E-04	1.394	1200	1.162E-03	0	0	0
1.505	2.394E-03	629	0.120	1070	1.125E-04	1.385	1200	1.154E-03	0	0	0
1.520	2.394E-03	635	0.122	1070	1.136E-04	1.398	1200	1.165E-03	0	0	0
1.710	2.536E-03	674	0.137	1070	1.279E-04	1.573	1200	1.311E-03	0	0	0
1.700	2.394E-03	710	0.136	1070	1.271E-04	1.564	1200	1.303E-03	0	0	0
1.720	2.401E-03	716	0.138	1070	1.286E-04	1.582	1200	1.319E-03	0	0	0
2.155	2.415E-03	892	0.129	1070	1.208E-04	2.026	1200	1.688E-03	0	0	0
2.180	2.401E-03	908	0.131	1070	1.222E-04	2.049	1200	1.708E-03	0	0	0
2.165	2.401E-03	902	0.130	1070	1.214E-04	2.035	1200	1.696E-03	0	0	0

table 4 big granules of grey EPDM

composite			binder			inert 1			inert 2		
weight [Kg]	total volume [m^3]	density [Kg/m^3]	weight [Kg]	specific weight [Kg/m^3]	volume Vb [m^3]	weight [Kg]	specific weight [Kg/m^3]	volume Vi1 [m^3]	weight [Kg]	specific weight [Kg/m^3]	volume Vi2 [m^3]
1.550	2.353E-03	659	0.124	1070	1.159E-04	1.426	1400	1.019E-03	0	0	0
1.500	2.381E-03	630	0.120	1070	1.121E-04	1.380	1400	9.857E-04	0	0	0
1.525	2.374E-03	642	0.122	1070	1.140E-04	1.403	1400	1.002E-03	0	0	0
1.735	2.381E-03	729	0.139	1070	1.297E-04	1.596	1400	1.140E-03	0	0	0
1.720	2.381E-03	723	0.138	1070	1.286E-04	1.582	1400	1.130E-03	0	0	0
1.760	2.394E-03	735	0.141	1070	1.316E-04	1.619	1400	1.157E-03	0	0	0
2.180	2.381E-03	916	0.131	1070	1.222E-04	2.049	1400	1.464E-03	0	0	0
2.180	2.387E-03	913	0.131	1070	1.222E-04	2.049	1400	1.464E-03	0	0	0
2.190	2.381E-03	920	0.131	1070	1.228E-04	2.059	1400	1.470E-03	0	0	0

table 5 big granules of black EPDM

composite			binder			inert 1			inert 2		
weight [Kg]	total volume [m^3]	density [Kg/m^3]	weight [Kg]	specific weight [Kg/m^3]	volume Vb [m^3]	weight [Kg]	specific weight [Kg/m^3]	volume Vi1 [m^3]	weight [Kg]	specific weight [Kg/m^3]	volume Vi2 [m^3]
1.525	2.381E-03	641	0.122	1070	1.140E-04	1.403	1250	1.122E-03	0	0	0
1.505	2.394E-03	629	0.120	1070	1.125E-04	1.385	1250	1.108E-03	0	0	0
1.510	2.394E-03	631	0.121	1070	1.129E-04	1.389	1250	1.111E-03	0	0	0
1.690	2.394E-03	706	0.135	1070	1.264E-04	1.555	1250	1.244E-03	0	0	0
1.710	2.387E-03	716	0.137	1070	1.279E-04	1.573	1250	1.259E-03	0	0	0
1.695	2.381E-03	712	0.136	1070	1.267E-04	1.559	1250	1.248E-03	0	0	0
2.175	2.381E-03	914	0.174	1070	1.626E-04	2.001	1250	1.601E-03	0	0	0
2.190	2.381E-03	920	0.175	1070	1.637E-04	2.015	1250	1.612E-03	0	0	0
2.190	2.381E-03	920	0.175	1070	1.637E-04	2.015	1250	1.612E-03	0	0	0

table 6 50% short fibres of SBR and 50% big granules of black EPDM

composite			binder			inert 1			inert 2		
weight [Kg]	total volume [m^3]	density [Kg/m^3]	weight [Kg]	specific weight [Kg/m^3]	volume Vb [m^3]	weight [Kg]	specific weight [Kg/m^3]	volume Vi1 [m^3]	weight [Kg]	specific weight [Kg/m^3]	volume Vi2 [m^3]
1.530	2.492E-03	614	0.122	1070	1.144E-04	0.704	1100	6.398E-04	0.704	1250	5.630E-04
1.525	2.514E-03	607	0.122	1070	1.140E-04	0.702	1100	6.377E-04	0.702	1250	5.612E-04
1.325	2.360E-03	561	0.106	1070	9.907E-05	0.610	1100	5.541E-04	0.610	1250	4.876E-04
1.740	2.401E-03	725	0.139	1070	1.301E-04	0.800	1100	7.276E-04	0.800	1250	6.422E-04
1.745	2.543E-03	686	0.140	1070	1.305E-04	0.803	1100	7.297E-04	0.803	1250	6.440E-04
1.755	2.422E-03	725	0.140	1070	1.312E-04	0.807	1100	7.339E-04	0.805	1250	6.458E-04
2.205	2.381E-03	926	0.176	1070	1.649E-04	1.014	1100	9.221E-04	1.014	1250	8.114E-04
2.200	2.381E-03	924	0.176	1070	1.645E-04	1.012	1100	9.200E-04	1.012	1250	8.096E-04
2.195	2.381E-03	922	0.176	1070	1.641E-04	1.010	1100	9.179E-04	1.010	1250	8.078E-04

table 7 50% short fibres of SBR and 50% big granules of grey EPDM

composite			binder			inert 1			inert 2		
weight [Kg]	total volume [m^3]	density [Kg/m^3]	weight [Kg]	specific weight [Kg/m^3]	volume Vb [m^3]	weight [Kg]	specific weight [Kg/m^3]	volume Vi1 [m^3]	weight [Kg]	specific weight [Kg/m^3]	volume Vi2 [m^3]
1.505	2.401E-03	627	0.120	1070	1.125E-04	0.692	1100	6.294E-04	0.692	1400	4.945E-04
1.370	2.387E-03	574	0.110	1070	1.024E-04	0.630	1100	5.729E-04	0.630	1400	4.501E-04
1.370	2.394E-03	572	0.110	1070	1.024E-04	0.630	1100	5.729E-04	0.630	1400	4.501E-04
1.715	2.450E-03	700	0.137	1070	1.282E-04	0.789	1100	7.172E-04	0.789	1400	5.635E-04
1.710	2.415E-03	708	0.137	1070	1.279E-04	0.787	1100	7.151E-04	0.787	1400	5.619E-04
1.725	2.408E-03	716	0.138	1070	1.290E-04	0.794	1100	7.214E-04	0.794	1400	5.668E-04
2.200	2.422E-03	908	0.176	1070	1.645E-04	1.012	1100	9.200E-04	1.012	1400	7.229E-04
2.200	2.443E-03	901	0.176	1070	1.645E-04	1.012	1100	9.200E-04	1.012	1400	7.229E-04
2.180	2.436E-03	895	0.174	1070	1.630E-04	1.003	1100	9.116E-04	1.003	1400	7.163E-04

table 8 50% short fibres of SBR and 50% small granules of SBR

composite			binder			inert 1			inert 2		
weight [Kg]	total volume [m^3]	density [Kg/m^3]	weight [Kg]	specific weight [Kg/m^3]	volume Vb [m^3]	weight [Kg]	specific weight [Kg/m^3]	volume Vi1 [m^3]	weight [Kg]	specific weight [Kg/m^3]	volume Vi2 [m^3]
1.530	2.401E-03	637	0.122	1070	1.144E-04	0.704	1100	6.398E-04	0.704	1200	5.865E-04
1.510	2.450E-03	616	0.121	1070	1.129E-04	0.695	1100	6.315E-04	0.695	1200	5.788E-04
1.535	2.450E-03	627	0.123	1070	1.148E-04	0.706	1100	6.419E-04	0.706	1200	5.884E-04
1.735	2.422E-03	716	0.139	1070	1.297E-04	0.798	1100	7.255E-04	0.787	1200	6.651E-04
1.745	2.422E-03	720	0.140	1070	1.305E-04	0.803	1100	7.297E-04	0.798	1200	6.689E-04
1.790	2.401E-03	745	0.143	1070	1.338E-04	0.823	1100	7.485E-04	0.803	1200	6.862E-04
2.625	2.680E-03	980	0.210	1070	1.963E-04	1.208	1100	1.098E-03	1.208	1200	1.006E-03
2.625	2.703E-03	971	0.210	1070	1.963E-04	1.208	1100	1.098E-03	1.208	1200	1.006E-03
2.715	2.703E-03	1005	0.217	1070	2.030E-04	1.249	1100	1.135E-03	1.249	1200	1.041E-03

table 9 90% short fibres of SBR and 10% small granules of black EPDM

composite			binder			inert 1			inert 2		
weight [Kg]	total volume [m^3]	density [Kg/m^3]	weight [Kg]	specific weight [Kg/m^3]	volume Vb [m^3]	weight [Kg]	specific weight [Kg/m^3]	volume Vi1 [m^3]	weight [Kg]	specific weight [Kg/m^3]	volume Vi2 [m^3]
1.100	2.268E-03	485	0.088	1070	8.224E-05	0.913	1100	8.300E-04	0.099	1250	7.920E-05
1.110	2.261E-03	491	0.089	1070	8.299E-05	0.9213	1100	8.375E-04	0.100	1250	7.992E-05
1.115	2.261E-03	493	0.089	1070	8.336E-05	0.92545	1100	8.413E-04	0.100	1250	8.028E-05
1.525	2.514E-03	607	0.122	1070	1.140E-04	1.26575	1100	1.151E-03	0.137	1250	1.098E-04
1.515	2.657E-03	570	0.121	1070	1.133E-04	1.25745	1100	1.143E-03	0.136	1250	1.091E-04
1.390	2.422E-03	574	0.111	1070	1.039E-04	1.1537	1100	1.049E-03	0.125	1250	1.001E-04
1.745	2.436E-03	716	0.140	1070	1.305E-04	1.44835	1100	1.317E-03	0.157	1250	1.256E-04
1.720	2.429E-03	708	0.138	1070	1.286E-04	1.4276	1100	1.298E-03	0.155	1250	1.238E-04
1.720	2.436E-03	706	0.138	1070	1.286E-04	1.4276	1100	1.298E-03	0.155	1250	1.238E-04

table 10 90% short fibres of SBR and 10% small granules of SBR

composite			binder			inert 1			inert 2		
weight [Kg]	total volume [m^3]	density [Kg/m^3]	weight [Kg]	specific weight [Kg/m^3]	volume Vb [m^3]	weight [Kg]	specific weight [Kg/m^3]	volume Vi1 [m^3]	weight [Kg]	specific weight [Kg/m^3]	volume Vi2 [m^3]
1.120	2.261E-03	495	0.090	1070	8.374E-05	0.930	1100	8.451E-04	0.101	1200	8.400E-05
1.105	2.261E-03	489	0.088	1070	8.262E-05	0.917	1100	8.338E-04	0.099	1200	8.288E-05
1.105	2.261E-03	489	0.088	1070	8.262E-05	0.917	1100	8.338E-04	0.099	1200	8.288E-05
1.525	2.657E-03	574	0.122	1070	1.140E-04	1.266	1100	1.151E-03	0.137	1200	1.144E-04
1.515	2.565E-03	591	0.121	1070	1.133E-04	1.257	1100	1.143E-03	0.136	1200	1.136E-04
1.495	2.565E-03	583	0.120	1070	1.118E-04	1.241	1100	1.128E-03	0.135	1200	1.121E-04
1.720	2.422E-03	710	0.138	1070	1.286E-04	1.428	1100	1.298E-03	0.155	1200	1.290E-04
1.720	2.408E-03	714	0.138	1070	1.286E-04	1.428	1100	1.298E-03	0.155	1200	1.290E-04
1.730	2.408E-03	718	0.138	1070	1.293E-04	1.436	1100	1.305E-03	0.156	1200	1.298E-04

table 11 90% short fibres of SBR and 10% small granules of grey EPDM

composite			binder			inert 1			inert 2		
weight [Kg]	total volume [m^3]	density [Kg/m^3]	weight [Kg]	specific weight [Kg/m^3]	volume Vb [m^3]	weight [Kg]	specific weight [Kg/m^3]	volume Vi1 [m^3]	weight [Kg]	specific weight [Kg/m^3]	volume Vi2 [m^3]
1.115	2.142E-03	520	0.0892	1070	8.34E-05	0.925	1100	8.413E-04	0.100	1400	7.168E-05
1.11	2.261E-03	491	0.0888	1070	8.30E-05	0.921	1100	8.375E-04	0.100	1400	7.136E-05
1.105	2.142E-03	516	0.0884	1070	8.26E-05	0.917	1100	8.338E-04	0.099	1400	7.104E-05

For each type of material composition and density volumes of the inert (V_{in1}, V_{in2}), binder (V_b) and voids (V_v) are obtained. The volumes for specimens are shown in tables from 12 to 21.

table 12 volumes for short fibres of SBR

short fibres of SBR				
Vt m^3	**Vb m^3**	**V_{in1} m^3**	**V_{in2} m^3**	**Vv m^3**
2.261E-03	**7.514E-05**	**8.405E-04**	**0**	**1.346E-03**
2.261E-03	**7.514E-05**	**8.405E-04**	**0**	**1.346E-03**
2.261E-03	**7.589E-05**	**8.489E-04**	**0**	**1.337E-03**
2.415E-03	**1.279E-04**	**1.430E-03**	**0**	**8.571E-04**
2.394E-03	**1.293E-04**	**1.447E-03**	**0**	**8.181E-04**
2.394E-03	**1.286E-04**	**1.439E-03**	**0**	**8.272E-04**
2.514E-03	**1.140E-04**	**1.275E-03**	**0**	**1.125E-03**
2.529E-03	**1.163E-04**	**1.301E-03**	**0**	**1.112E-03**
2.543E-03	**1.114E-04**	**1.246E-03**	**0**	**1.186E-03**
2.436E-03	**1.716E-04**	**1.919E-03**	**0**	**3.450E-04**
2.450E-03	**1.787E-04**	**1.999E-03**	**0**	**2.724E-04**
2.450E-03	**1.622E-04**	**1.815E-03**	**0**	**4.728E-04**

table 13 volumes for short granules of SBR

small granules of SBR				
Vt m^3	**Vb** m^3	**V_{in1}** m^3	**V_{in2}** m^3	**Vv** m^3
2.381E-03	1.133E-04	1.162E-03	0	1.106E-03
2.394E-03	1.125E-04	1.154E-03	0	1.128E-03
2.394E-03	1.136E-04	1.165E-03	0	1.115E-03
2.536E-03	1.279E-04	1.311E-03	0	1.097E-03
2.394E-03	1.271E-04	1.303E-03	0	9.639E-04
2.401E-03	1.286E-04	1.319E-03	0	9.540E-04
2.415E-03	1.208E-04	1.688E-03	0	6.062E-04
2.401E-03	1.222E-04	1.708E-03	0	5.713E-04
2.401E-03	1.214E-04	1.696E-03	0	5.839E-04

table 14 volumes for big granules of grey EPDM

big granules of grey EPDM				
Vt m^3	**Vb** m^3	**V_{in1}** m^3	**V_{in2}** m^3	**Vv** m^3
2.353E-03	1.159E-04	1.019E-03	0	1.219E-03
2.381E-03	1.121E-04	9.857E-04	0	1.283E-03
2.374E-03	1.140E-04	1.002E-03	0	1.257E-03
2.381E-03	1.297E-04	1.140E-03	0	1.111E-03
2.381E-03	1.286E-04	1.130E-03	0	1.122E-03
2.394E-03	1.316E-04	1.157E-03	0	1.106E-03
2.381E-03	1.222E-04	1.464E-03	0	7.945E-04
2.387E-03	1.222E-04	1.464E-03	0	8.014E-04
2.381E-03	1.228E-04	1.470E-03	0	7.873E-04

table 15 volumes for big granules of black EPDM

big granules of black EPDM				
Vt m^3	**Vb** m^3	V_{in1} m^3	V_{in2} m^3	**Vv** m^3
2.381E-03	1.140E-04	1.122E-03	0	1.144E-03
2.394E-03	1.125E-04	1.108E-03	0	1.174E-03
2.394E-03	1.129E-04	1.111E-03	0	1.170E-03
2.394E-03	1.264E-04	1.244E-03	0	1.024E-03
2.387E-03	1.279E-04	1.259E-03	0	1.001E-03
2.381E-03	1.267E-04	1.248E-03	0	1.006E-03
2.381E-03	1.626E-04	1.601E-03	0	6.171E-04
2.381E-03	1.637E-04	1.612E-03	0	6.049E-04
2.381E-03	1.637E-04	1.612E-03	0	6.049E-04

table 16 volumes for 50% short fibres of SBR and 50% big granules of black EPDM

50 % short fibres of SBR 50% big granules of black EPDM				
Vt m^3	**Vb** m^3	**V_{in1}** m^3	**V_{in2}** m^3	**Vv** m^3
2.492E-03	1.144E-04	6.398E-04	5.630E-04	1.175E-03
2.514E-03	1.140E-04	6.377E-04	5.612E-04	1.201E-03
2.360E-03	9.907E-05	5.541E-04	4.876E-04	1.219E-03
2.543E-03	1.305E-04	7.297E-04	6.422E-04	1.041E-03
2.450E-03	1.308E-04	7.318E-04	6.440E-04	9.433E-04
2.422E-03	1.312E-04	7.339E-04	6.458E-04	9.111E-04
2.381E-03	1.649E-04	9.221E-04	8.114E-04	4.821E-04
2.381E-03	1.645E-04	9.200E-04	8.096E-04	4.864E-04
2.381E-03	1.641E-04	9.179E-04	8.078E-04	4.907E-04

table 17 volumes for 50% short fibres of SBR and 50% big granules of grey EPDM

50 % short fibres of SBR 50% big granules of grey EPDM				
Vt m^3	**Vb** m^3	**V_{in1}** m^3	**V_{in2}** m^3	**Vv** m^3
2.401E-03	1.125E-04	6.294E-04	4.945E-04	1.165E-03
2.387E-03	1.024E-04	5.729E-04	4.501E-04	1.262E-03
2.394E-03	1.024E-04	5.729E-04	4.501E-04	1.269E-03
2.450E-03	1.282E-04	7.172E-04	5.635E-04	1.041E-03
2.415E-03	1.279E-04	7.151E-04	5.619E-04	1.010E-03
2.408E-03	1.290E-04	7.214E-04	5.668E-04	9.911E-04
2.422E-03	1.645E-04	9.200E-04	7.229E-04	6.147E-04
2.443E-03	1.645E-04	9.200E-04	7.229E-04	6.357E-04
2.436E-03	1.630E-04	9.116E-04	7.163E-04	6.451E-04

table 18 volumes for 50% short fibres of SBR and 50% small granules of SBR

50 % short fibres of SBR 50% small granules of SBR				
Vt m^3	**Vb** m^3	V_{in1} m^3	V_{in2} m^3	**Vv** m^3
2.401E-03	1.144E-04	6.398E-04	5.865E-04	1.061E-03
2.450E-03	1.129E-04	6.315E-04	5.788E-04	1.127E-03
2.450E-03	1.148E-04	6.419E-04	5.884E-04	1.105E-03
2.422E-03	1.297E-04	7.255E-04	6.651E-04	9.017E-04
2.422E-03	1.305E-04	7.297E-04	6.689E-04	8.929E-04
2.401E-03	1.338E-04	7.485E-04	6.862E-04	8.327E-04
2.680E-03	1.963E-04	1.098E-03	1.006E-03	3.794E-04
2.703E-03	1.963E-04	1.098E-03	1.006E-03	4.025E-04
2.703E-03	2.030E-04	1.135E-03	1.041E-03	3.236E-04

table 19 volumes for 90% short fibres of SBR and 10% small granules of black EPDM

90 % short fibres of SBR 10% small granules of black EPDM				
Vt m^3	**Vb** m^3	V_{in1} m^3	V_{in2} m^3	**Vv** m^3
2.268E-03	8.224E-05	8.300E-04	7.920E-05	1.277E-03
2.261E-03	8.299E-05	8.375E-04	7.992E-05	1.261E-03
2.261E-03	8.336E-05	8.413E-04	8.028E-05	1.257E-03
2.514E-03	1.140E-04	1.151E-03	1.098E-04	1.140E-03
2.657E-03	1.133E-04	1.143E-03	1.091E-04	1.291E-03
2.422E-03	1.039E-04	1.049E-03	1.001E-04	1.169E-03
2.436E-03	1.305E-04	1.317E-03	1.256E-04	8.632E-04
2.429E-03	1.286E-04	1.298E-03	1.238E-04	8.787E-04
2.436E-03	1.286E-04	1.298E-03	1.238E-04	8.858E-04

table 20 volumes for 90% short fibres of SBR and 10% small granules of SBR

90 % short fibres of SBR 10% small granules of SBR				
Vt m^3	**Vb** m^3	**V_{in1}** m^3	**V_{in2}** m^3	**Vv** m^3
2.261E-03	8.374E-05	8.451E-04	8.400E-05	1.249E-03
2.261E-03	8.262E-05	8.338E-04	8.288E-05	1.262E-03
2.261E-03	8.262E-05	8.338E-04	8.288E-05	1.262E-03
2.657E-03	1.140E-04	1.151E-03	1.144E-04	1.278E-03
2.565E-03	1.133E-04	1.143E-03	1.136E-04	1.195E-03
2.565E-03	1.118E-04	1.128E-03	1.121E-04	1.213E-03
2.422E-03	1.286E-04	1.298E-03	1.290E-04	8.666E-04
2.408E-03	1.286E-04	1.298E-03	1.290E-04	8.528E-04
2.408E-03	1.293E-04	1.305E-03	1.298E-04	8.437E-04

table 21 volumes for 90% short fibres of SBR and 10% small granules of grey EPDM

90 % short fibres of SBR 10% small granules of SBR				
Vt m^3	**Vb** m^3	**V_{in1}** m^3	**V_{in2}** m^3	**Vv** m^3
2.142E-03	8.336E-05	8.413E-04	7.168E-05	1.146E-03
2.261E-03	8.299E-05	8.375E-04	7.136E-05	1.270E-03
2.142E-03	8.262E-05	8.338E-04	7.104E-05	1.155E-03

It is clear that the specimen weight increases considering greater densities and consequently the voids volume decreases. This aspect is shown by previous tables.

5.4 RESULTS OF STATIC AND DYNAMIC TESTS

Static and dynamic tests on the material are performed according to the following Italian standards (previously they have been described):

- UNI 10570, which rules “the determination of mechanical characteristics of mats and pads”;
- UNI 11059, ruling “elastomeric mats for railway tramway tracks”.

Loads for static tests are indicated in the standards and previously they are defined. For tests according to UNI 10570 it is assumed:

$$\sigma_{\max} = \sigma_0 + \sigma_{ps} + \sigma_{pd} = (0.01 + 0.07 + 0.04)\,\text{Mpa} = 0.12\ \text{Mpa} \tag{5.29}$$

Remembering that σ_0 is the initial load, σ_{ps} is the static component and σ_{pd} is the dynamic component.

For tests according to UNI 11059, it is assumed:

$$\sigma_{\max} = \sigma_0 + \sigma_f (1 + \gamma_d) = 0.01 + (0.4 + 1) \cdot 0.03\ \text{Mpa} = 0.052\ \text{Mpa} \tag{5.30}$$

Considering that σ_0 is the initial load, σ_f is the maximum value of the “variable” load and γ_d is the amplification parameter of the nominal railway track, it has been chosen considering good geometrical conditions of the railway track (it is obviously greater for old railway line) and for a running speed of about 200 km/h.

Previously the procedure for the load application had been described; an example of the load variation with time is in figure 8 for test of short fibres of SBR according to UNI 10570.

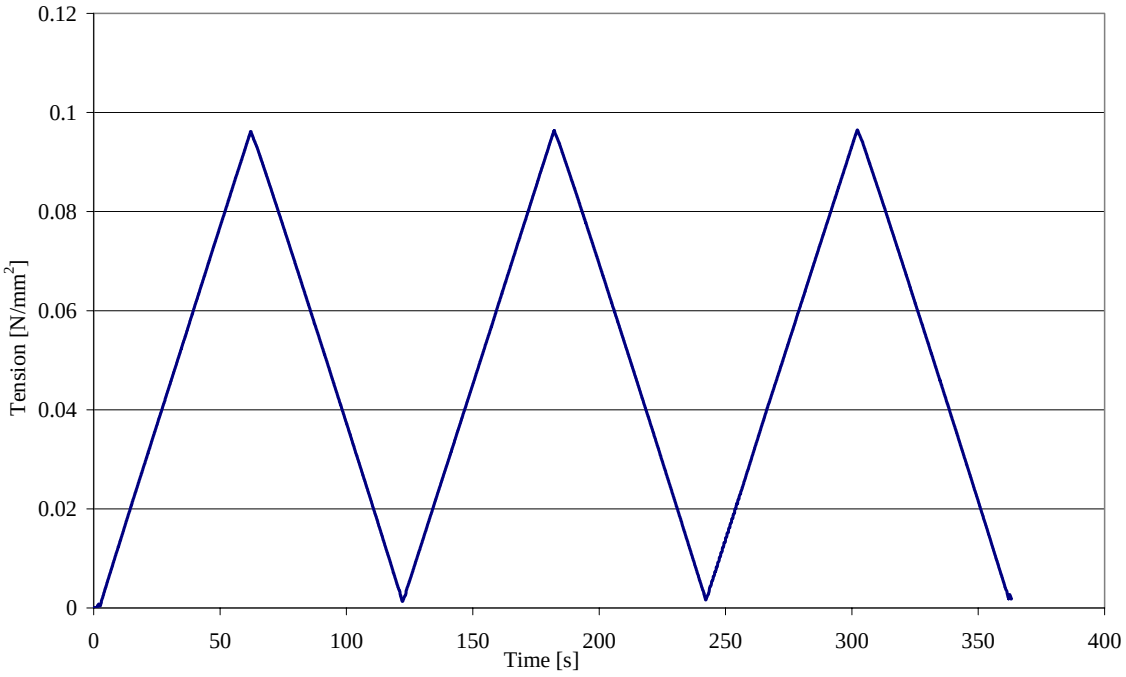

figure 8 load variation with the time for short fibres of SBR according to UNI 10570

For each type of material composition and density, three specimens are considered. The results are given by the third cycle for each specimen. For an example three cycles for the specimen consisting of short fibres of SBR with density 600 kg/cm^3 is in figure 9 and in figure 10 the third cycle for four values of density of specimen composed by short fibres of SBR.

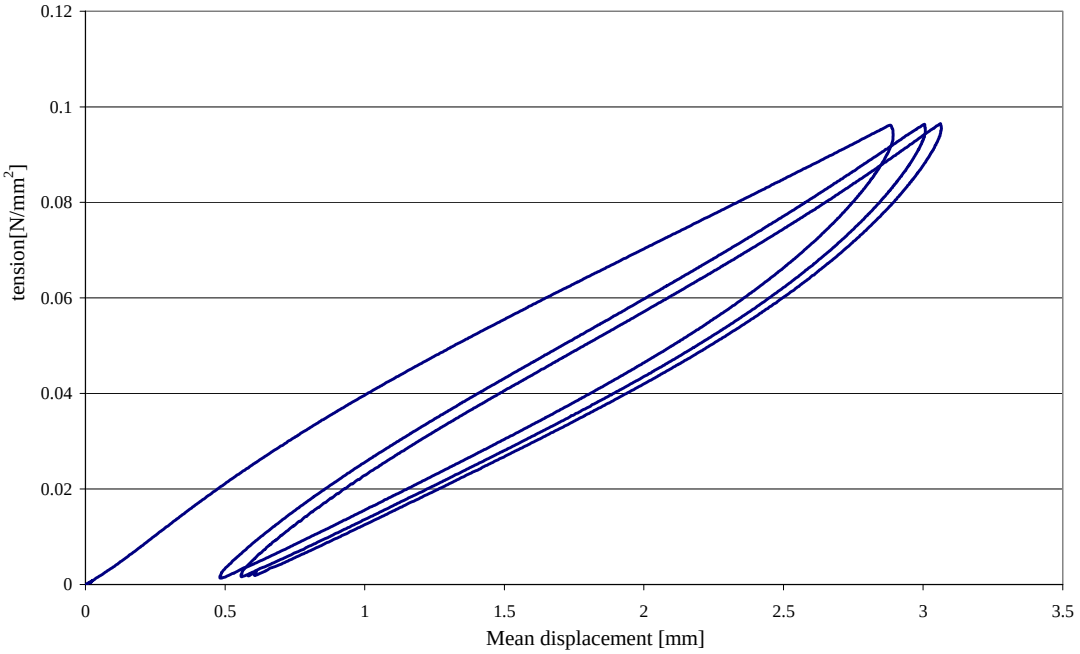

figure 9 three cycles for static test of short fibres of SBR with density 600 kg/cm^3

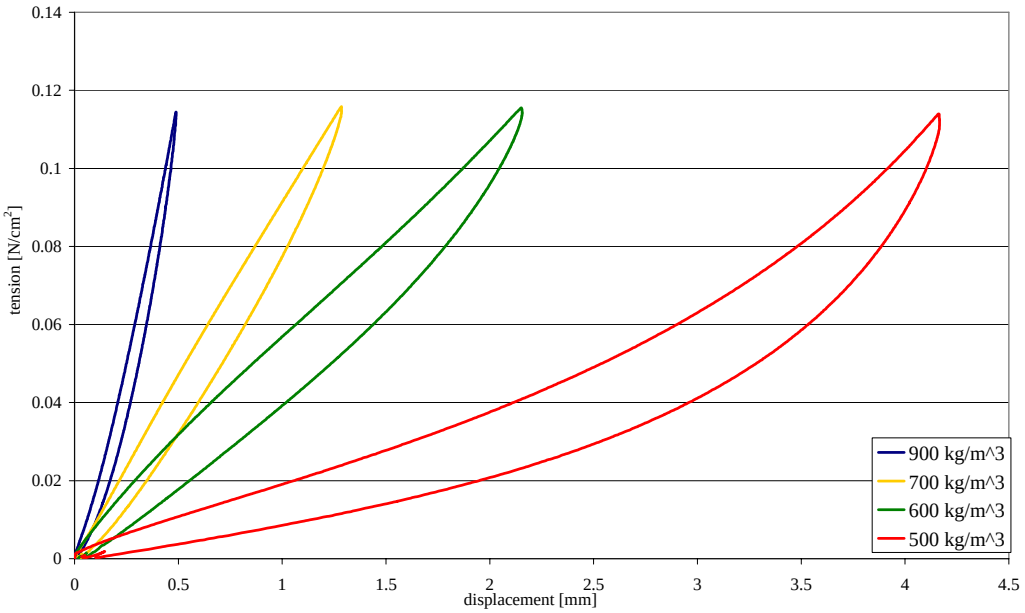

figure 10 third cycle for specimens with different densities of short fibres of SBR

The results discussed in the following are in terms of mean value of the static stiffness (table 22).

Loads for the dynamic tests are indicated in the standards. For tests according to UNI 10570 it is assumed the following static component:

$$\sigma_s = \sigma_0 + \sigma_{qs} = 0.01\frac{\mathrm{N}}{\mathrm{mm}^2} + 0.07\frac{\mathrm{N}}{\mathrm{mm}^2} = 0.08\frac{\mathrm{N}}{\mathrm{mm}^2} \tag{5.31}$$

The dynamic component is given by:

$$\sigma_d = \pm\sigma_{pd} = \pm 0.04\ \frac{\mathrm{N}}{\mathrm{mm}^2} \tag{5.32}$$

During the test the frequency starts from the initial value $f_i = 2$ Hz and reaches the last value

$f_f = 100$ Hz considering step of 2 Hz.

In the following the real part of the inverse transfer function (5.15) for the specimen composed by short fibres of SBR is shown as an example (figure 11).

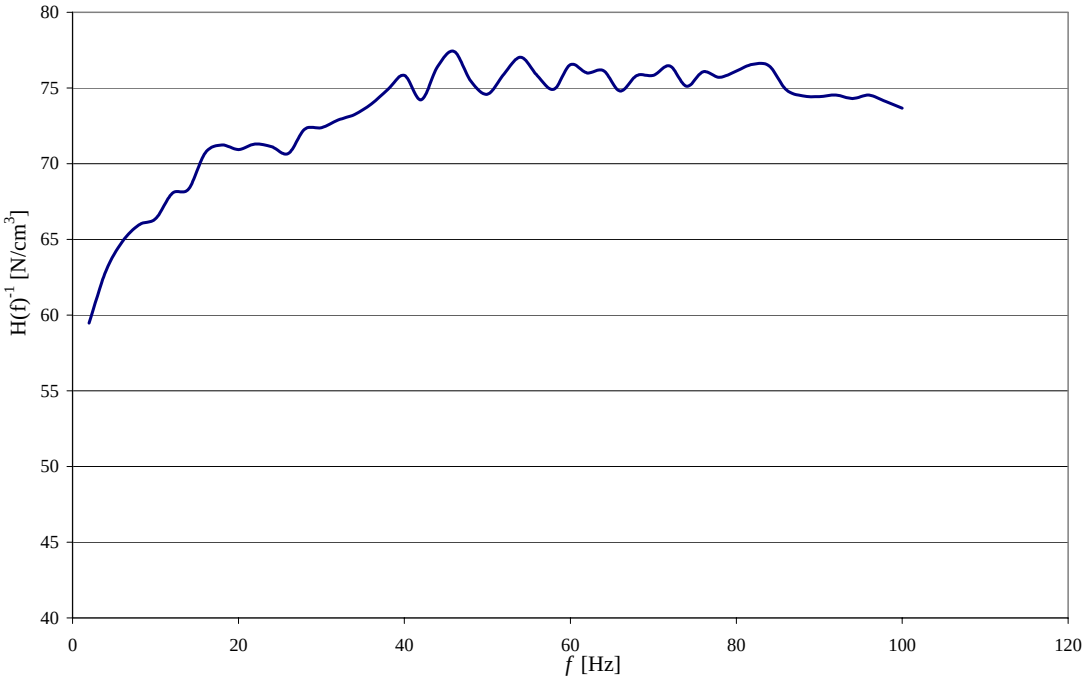

figure 11 real part of the inverse transfer function

For tests according to UNI 11059 it is assumed the following static component:

$$\sigma_s = \sigma_0 + \sigma_f \cdot (1+\gamma_d) = 0.01\frac{\mathrm{N}}{\mathrm{mm}^2} + (1+0.4)\cdot 0.03\frac{\mathrm{N}}{\mathrm{mm}^2} = 0.052\frac{\mathrm{N}}{\mathrm{mm}^2} \tag{5.33}$$

And the dynamic one is given by:

$$\sigma_d = 10\% \cdot \sigma_s = 0.0052\frac{\mathrm{N}}{\mathrm{mm}^2} \tag{5.34}$$

The initial frequency is still 2 Hz, the final one 100 Hz and the step is 2 Hz.

The results discussed in the following are in terms of mean value of the dynamic stiffness and of dynamic loss factor (table 22).

table 22 results of static and dynamic tests

TYPE	density [kg/m^3]	Ks [N/cm^3]		Kd [N/cm^3]		Dynamic stiffening		Dynamic loss factor [%]
		UNI 10570	UNI 11059	UNI 10570	UNI 11059	UNI 10570	UNI 11059	
SF SBR	500	23	25	91	102	3.96	4.08	
	600	50	59	82	123	1.64	2.08	16.9
	700	97	96	145	187	1.49	1.95	13.9
	900	242	227	537	503	2.22	2.22	
SG SBR	600	48	48	90	96	1.88	2.00	15.4
	700	60	67	112	148	1.87	2.21	18.2
	900	153	153	354	355	2.31	2.32	
BG grey EPDM	600	28	26	59	63	2.11	2.42	14.3
	700	32	33	59	65	1.84	1.97	13.4
	900	59	58	114	112	1.93	1.93	
BG black EPDM	600	31	28	91	102	2.94	3.64	18.9
	700	57	61	115	152	2.02	2.49	20.0
	900	281	276	851	835	3.03	3.03	
50% SF SBR 50% BG black EPDM	600	39	43	79	102	2.03	2.37	17.0
	700	76	84	137	198	1.80	2.36	18.7
	900	296	288	776	755	2.62	2.62	
50% SF SBR 50% BG grey EPDM	600	27	26	58	64	2.15	2.46	15.4
	700	49	50	81	107	1.65	2.14	14.4
	900	103	104	202	202	1.96	1.94	
50% SF SBR 50% SG SBR	600	44	50	82	112	1.86	2.24	17.1
	700	131	127	215	261	1.64	2.06	15.3
	900	287	265	723	667	2.52	2.52	
90% SF SBR 10% SG black EPDM	500	21	21	90	92	4.29	4.38	
	600	43	49	76	105	1.77	2.14	17.2
	700	85	94	142	210	1.67	2.23	16.6
90% SF SBR 10% SG SBR	500	21	22	88	90	4.19	4.09	
	600	41	46	90	97	2.20	2.11	17.8
	700	134	127	230	270	1.72	2.13	15.2
90% SF SBR 10% SG grey EPDM	500	22	21	83	82	3.77	3.90	
	600	41	47	78	93	1.90	1.98	16.5
	700	72	76	113	157	1.57	2.07	15.0

Experimental results confirm that the lowest values of stiffness are obtained by specimens composed by grey EPDM. The product becomes stiffer if the density goes up but there is not a significant changing in the loss factor. The standard model

explains the presence of a dynamic stiffening of the material for higher frequencies and it is confirmed by experimental data and the stiffening factor varies by about 1.5 to 4.5 and it is important to take into account this phenomenon during the railway track design.

5.5 EXPERIMENTAL TESTS AND THEORETICAL RESULTS COMPARISON

The theoretical value of the equivalent elastic modulus is obtained considering the model described in the previous chapter (chapter 4).

The elastic modulus of the polyether is assumed equal to 0.35 Mpa. Regarding the rubber component, proper values found in literature (Gent, 2001) are summarized in table 23.

table 23 Typical SBR and EPDM properties

Property	SBR	EPDM
Shore A hardness	65	64
300% modulus (Mpa)	13.5	6.8
Tensile strength (Mpa	25	15.5
Breaking elongation (%)	500	410

The equivalent elastic modulus for each material composition and density is evaluated as mean value on the three specimens.

Tests results are in terms of static stiffness, whereas the experimental elastic modulus for each specimen is obtained considering its thickness. Again for each material composition and density the static stiffness is the mean value computed on the three specimens. Two different elastic modules are obtained because tests are performed considering two different standards.

The theoretical model explained in this thesis is a very simplified model which assumes the material elastic and homogeneous, but it allows obtaining equivalent elastic modulus values of the composite material close to the experimental test results. Significant differences do not occur if test results obtained with the UNI 10570 and UNI 11059 loads are compared. Some problems can occur when very big density ($900\ kg/m^3$) is considered. Moreover the agreement between tests and theoretical results is greater if the inert component is SBR and if it is the prevalent one. These aspects are shown in the following figures (figures 12-20). The fitting curves of the experimental data are evaluated for each type of specimen.

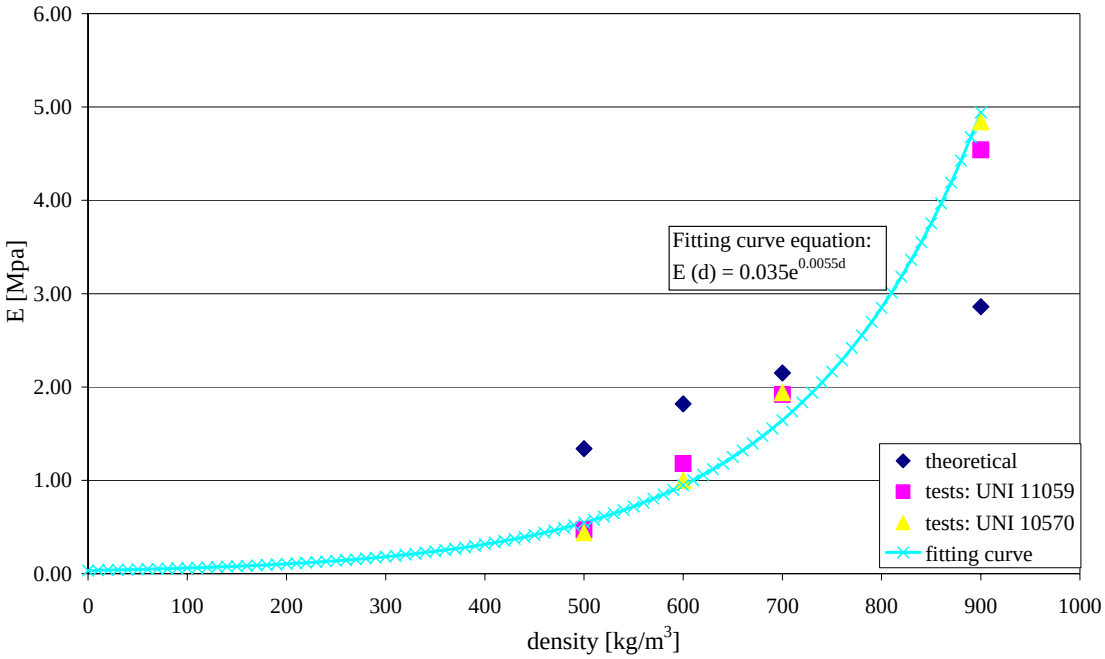

figure 12 comparison between theoretical and experimental results for short fibres of SBR

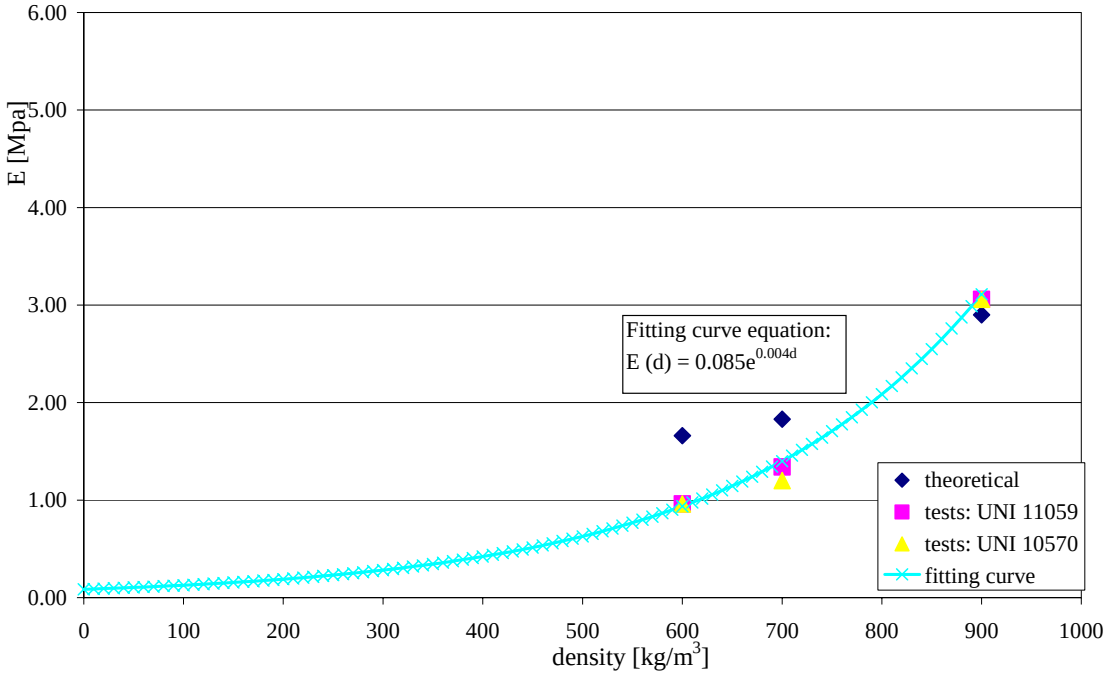

figure 13 comparison between theoretical and experimental results for short granules of SBR

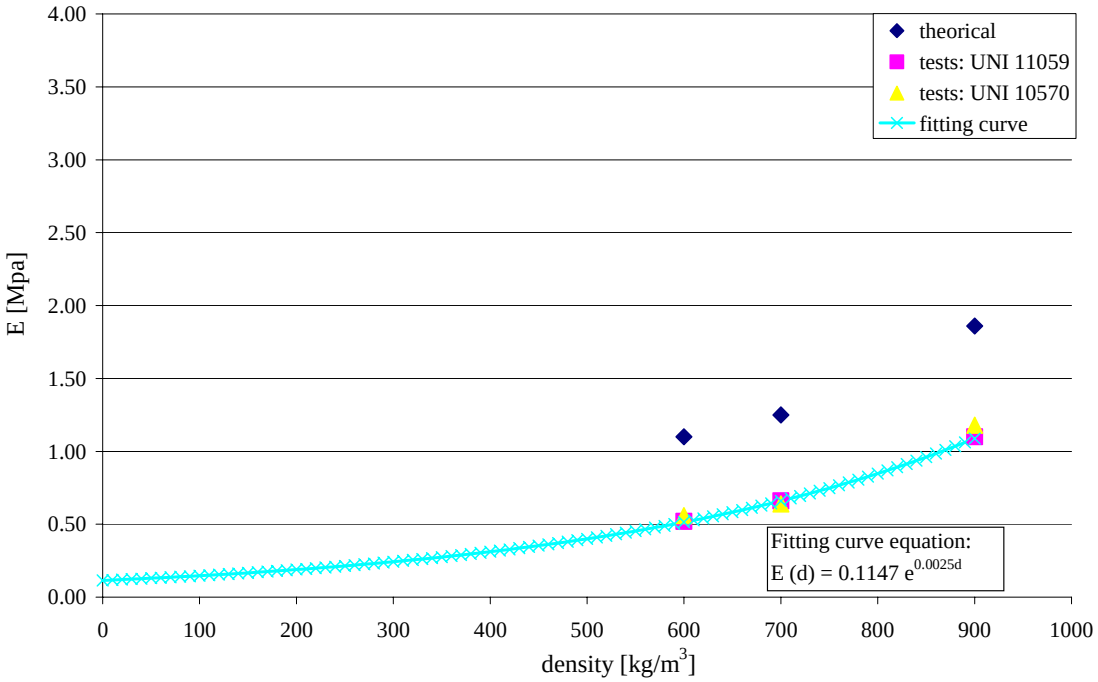

figure 14 comparison between theoretical and experimental results for big granules of grey EPDM

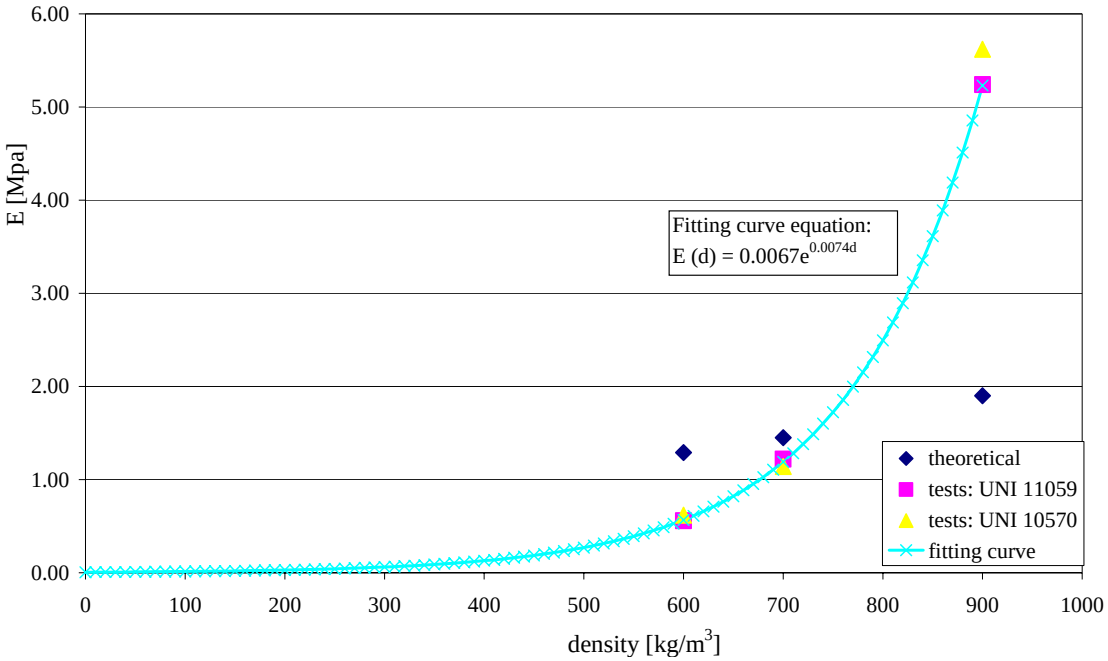

figure 15 comparison between theoretical and experimental results for big granules of black EPDM

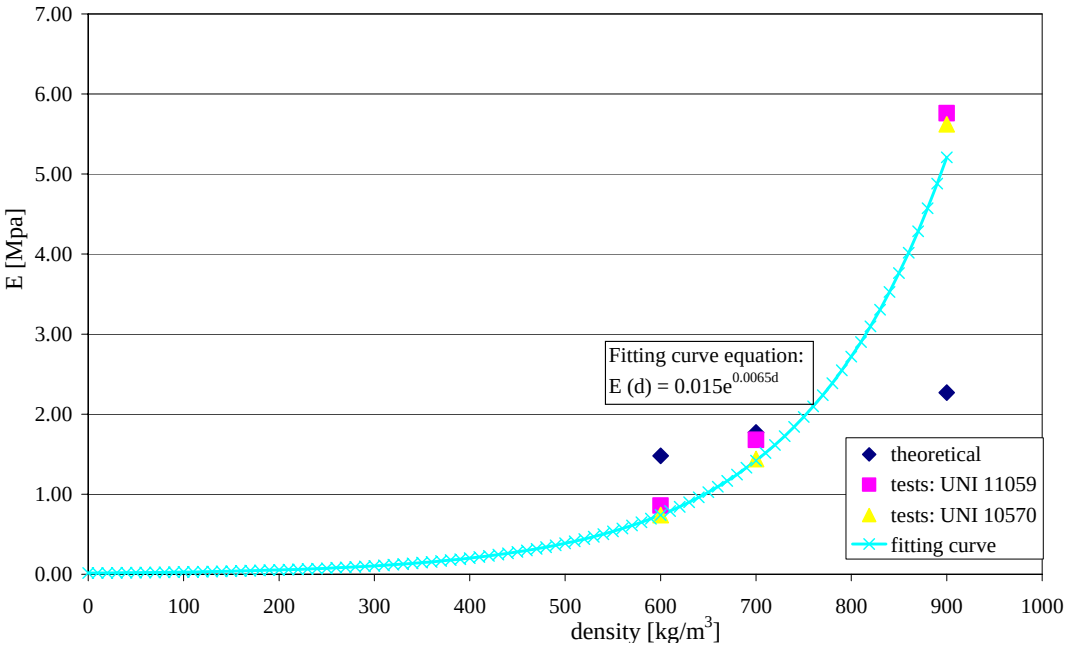

figure 16 comparison between theoretical and experimental results for short fibres of SBR (50%) and big granules of black EPDM (50%)

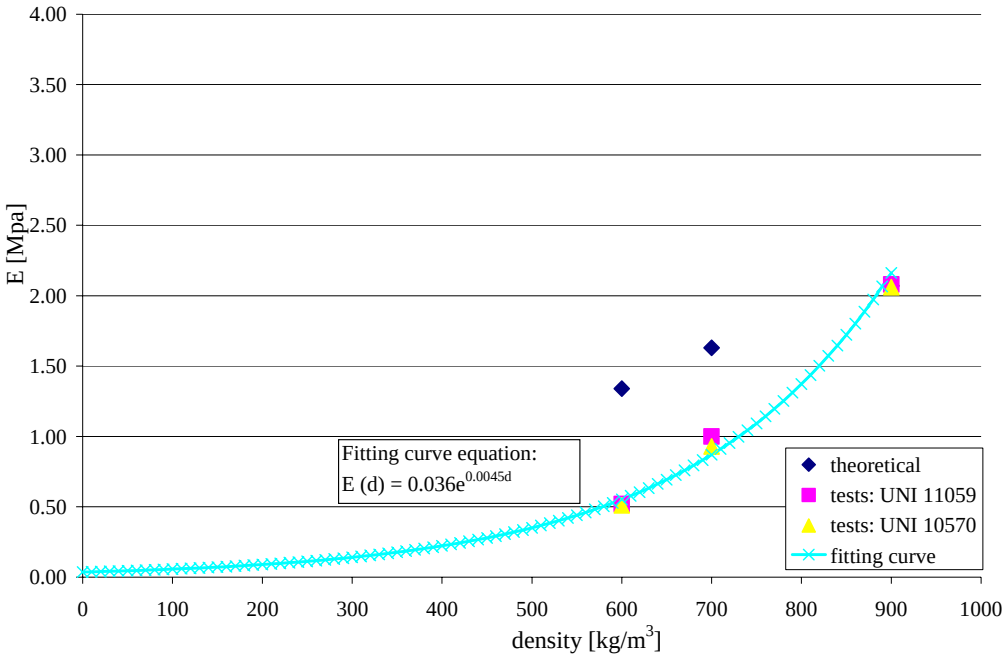

figure 17 comparison between theoretical and experimental results for short fibres of SBR (50%) and big granules of grey EPDM (50%)

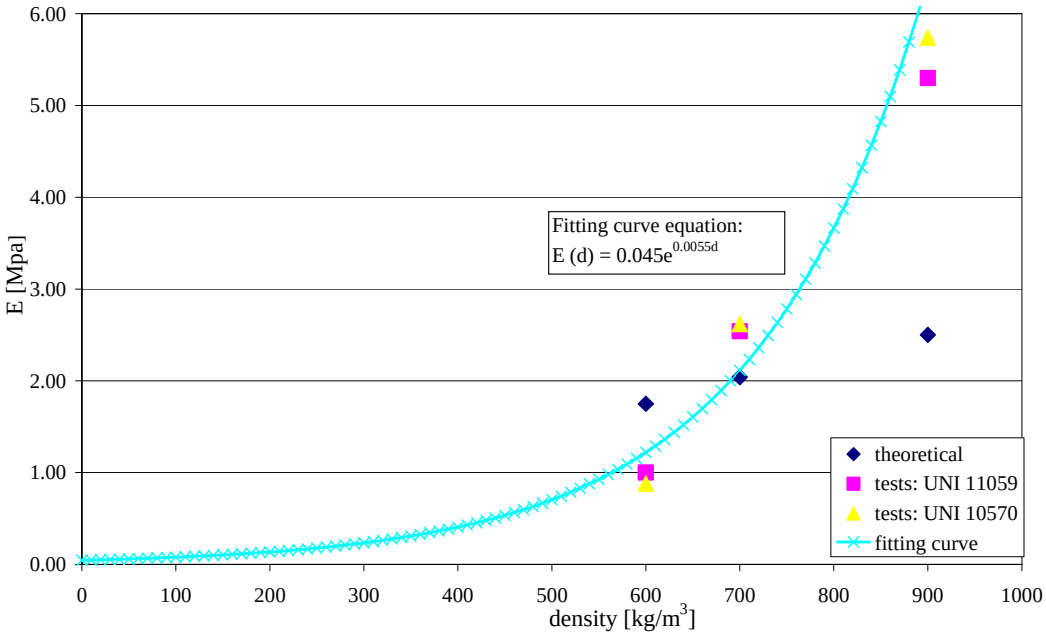

figure 18 comparison between theoretical and experimental results for short fibres of SBR (50%) and small granules of SBR (50%)

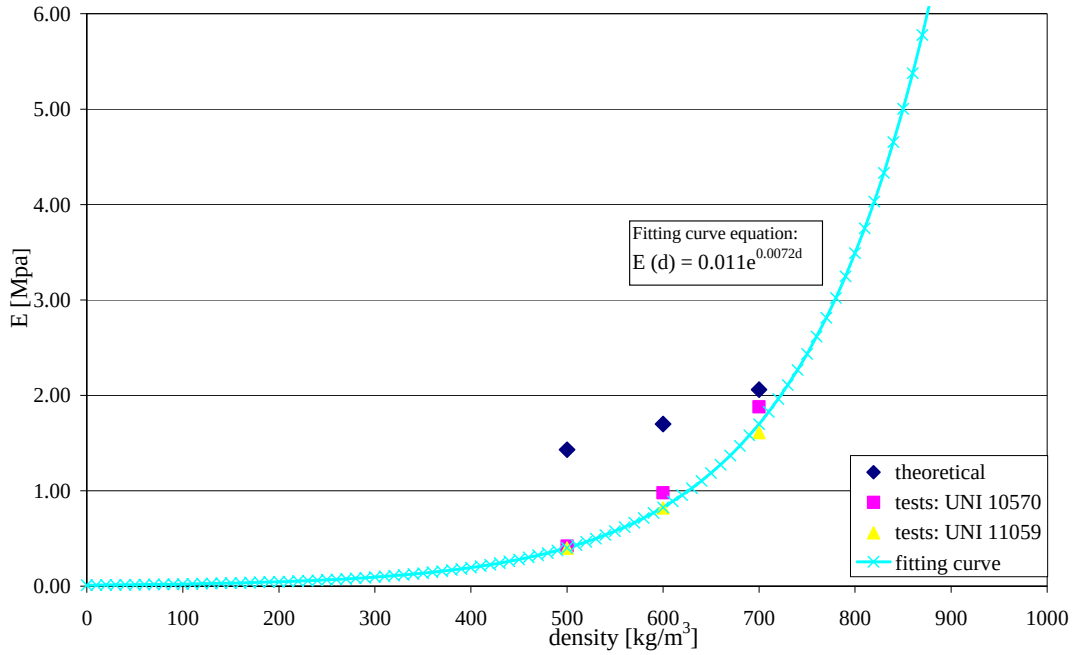

figure 19 comparison between theoretical and experimental results for short fibres of SBR (90%) and big granules of black EPDM (10%)

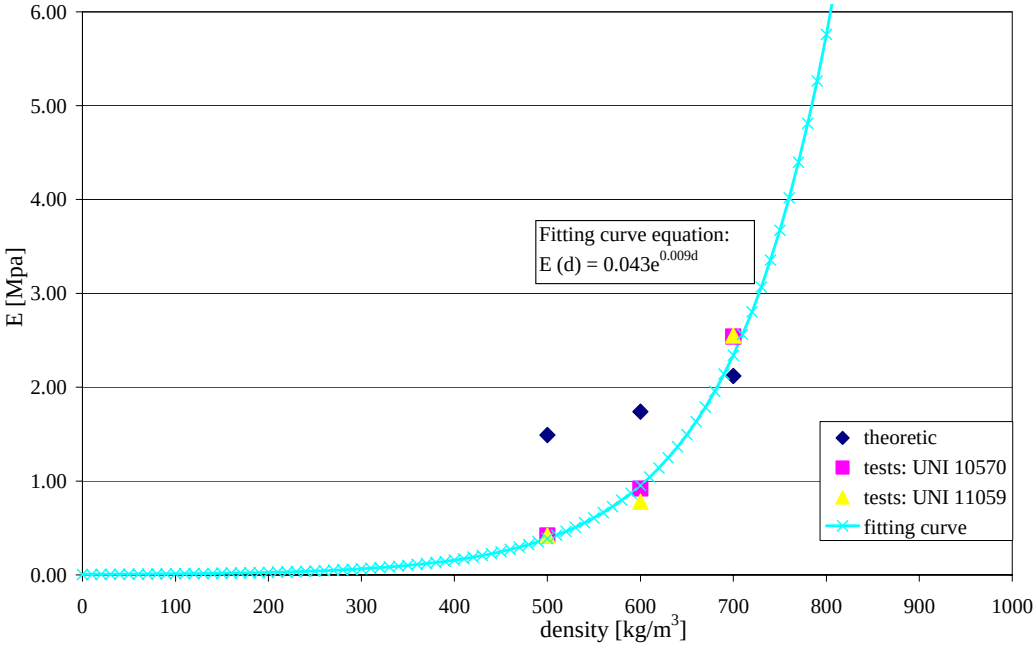

figure 20 comparison theoretical and experimental results for short fibres of SBR (90%) and small granules of SBR (10%)

CHAPTER 6

ANALYTICAL MODELS FOR TRADITIONAL AND INNOVATIVE RAILWAY TRACK

In the past the design of new track system was often guided by experience only, while the previous study of their static and dynamic behaviour can give good suggestions to improve the performances of the system. In the mathematical modelling of railway tracks, three-dimensional models are obviously the most complete but in the study of longitudinal and vertical problems two-dimensional ore one-dimensional models are often sufficient.

Simple analytical models can capture the main aspects of the problem and guide the development of more detailed model. One of the simplest of these models consists of a single beam on elastic or visco-elastic foundation and it will be discussed in the following.

6.1 SINGLE BEAM CONTINUOUS MODEL

Considering the classical railway track described in the third chapter, it can be represented as a beam resting on visco-elastic foundation modeled by a continuously distributed stiffness and damping (figure1).

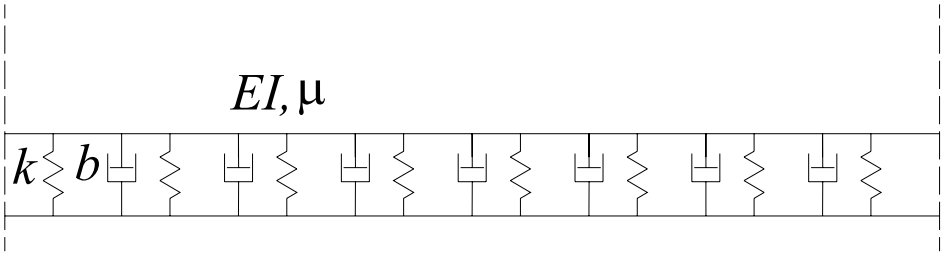

figure 1 simplified model for preliminary design

The axes of coordinates are chosen in such a manner that the *x*-axis coincides with the beam and the direction in which the beam has elastic support from the foundation is perpendicular to the *x*-direction and the *y*-direction is parallel to it.

E	young modulus of the beam
I	moment of inertia of the beam cross section (constant)
EI	flexural stiffness
k	railway track stiffness
μ	mass for unit length of the beam (constant)
b	viscous damping parameter

The viscous damping parameter includes all possible forms of the dissipation energy.

The beam is modelled as an Euler beam characterized only by its mass and flexural stiffness, while the rotational inertia and shear force deformation are disregarded. The aim is the study of vertical deformations of the beam, therefore the displacements in *y*-direction are considered.

The equation that governs the problem is obtained by means dynamical equilibrium of the beam element:

$$EI \cdot \frac{\partial^4 y(x,t)}{\partial x^4} + \mu \cdot \frac{\partial^2 y(x,t)}{\partial t^2} + b \cdot \frac{\partial y(x,t)}{\partial t} + k \cdot y(x,t) = 0 \tag{6.1}$$

In which $y(x,t)$ is the vertical displacement of the point of the beam whose coordinate is x at time t.

This is a differential equation with partial derivates, in fact the flexural term is a spatial derivate, while the damping and inertial terms are temporal derivates.

6.1.1 General problem: concentrated harmonic load moving at constant speed

In this general case a concentrated load is considered varying sinusoidally with time, whose point of application moves with constant speed v in the positive direction; in this way it is possible to consider both the effect of the train that run and the effect of the rail irregularities causing dynamic overloads. It can be mathematically represented as:

$$F(x,t) = F_0 \cdot \cos \omega t \cdot \delta(x - vt) \tag{6.2}$$

in which F_0 is the constant concentrated force, $\delta(x - vt)$ is the Dirac delta function (or impulsive function) and v represents the train speed.

The Dirac function is not a function in the conventional sense. It is a so-called generalized function and it can be defined as the distributional derivate of the Heaviside function $H(x)$:

$$\delta(x) = \frac{dH(x)}{dx} \tag{6.3}$$

For the Dirac function the following relations can be considered (a, b, ξ are constant and $f(x)$ is a continuous function in the interval < a,b>):

$$\int_{-\infty}^{+\infty} \delta(x)dx = 1 \tag{6.4}$$

$$\int_{-\infty}^{+\infty} \delta(x-a) f(x)dx = f(a) \tag{6.5}$$

$$\int_b^a \delta(x-\xi) f(x) dx = \begin{cases} 0 & \text{per } \xi < a < b \\ f(\xi) & \text{per } a < \xi < b \\ 0 & \text{per } a < b < \xi \end{cases} \tag{6.6}$$

$$\int_b^a \delta^{(n)}(x-\xi) f(x) dx = \begin{cases} 0 & \text{per } \xi < a < b \\ (-1)^n f^{(n)}(\xi) & \text{per } a < \xi < b \\ 0 & \text{per } a < b < \xi \end{cases} \tag{6.7}$$

The substitution of $\varphi(x)$ having zero value at some (single) point ξ $\left[\varphi(\xi) = 0\right]$ gives:

$$\delta\left[\varphi(x)\right] = \frac{1}{\left|\varphi'(x)\right|} \cdot \delta(x-\xi) \tag{6.8}$$

If $\varphi(x) = ax$ then:

$$\delta(ax) = \frac{1}{a} \cdot \delta(x) \tag{6.9}$$

The equation that governs the problem is:

$$EI \cdot \frac{\partial^4 y(x,t)}{\partial x^4} + \mu \cdot \frac{\partial^2 y(x,t)}{\partial t^2} + b \cdot \frac{\partial y(x,t)}{\partial t} + k \cdot y(x,t) = F_0 \cdot \cos \omega t \cdot \delta(x - vt) \tag{6.10}$$

A new variable is introduced which expresses the fact that its origin moves together the load with constant speed v:

$$r = x - vt \tag{6.11}$$

The displacement $y(r,t)$ is periodic in t, the period being $2\pi/\omega$. The displacement can be expressed in the form (Mathews, 1958):

$$y(r,t) = y_1(r) \cdot \cos(\omega t) + y_2(r) \cdot \sin(\omega t) \tag{6.12}$$

Considering the total derivative definition the equation is written in terms of the two variables r and t:

$$EI \cdot \frac{\partial^4 y}{\partial r^4} + \mu \cdot \left(v^2 \cdot \frac{\partial^2 y}{\partial r^2} - 2v \cdot \frac{\partial^2 y}{\partial r \cdot \partial t} + \frac{\partial^2 y}{\partial t^2} \right) + b \cdot \left(-v \cdot \frac{\partial y}{\partial r} + \frac{\partial y}{\partial t} \right) + ky = \tag{6.13}$$
$$= F_0 \cdot \cos \omega t \cdot \delta(x - vt)$$

The y expression (6.12) is substituted in (6.13); the two sides of the equation are compared considering separately the terms containing $\cos(\omega t)$ and $\sin(\omega t)$ and the equation is written trough two simultaneous equations:

$$\begin{aligned} EI\cdot\frac{\partial^4 y_1}{\partial r^4}+\mu\cdot v^2\cdot\frac{\partial^2 y_1}{\partial r^2}-vb\cdot\frac{\partial^2 y_1}{\partial r^2}-2v\omega\mu\cdot\frac{\partial y_2}{\partial r}+b\omega\cdot y_2+\left(k-\mu\omega^2\right)\cdot y_1=F_0\delta(r)\\ EI\cdot\frac{\partial^4 y_2}{\partial r^4}+\mu\cdot v^2\cdot\frac{\partial^2 y_2}{\partial r^2}-vb\cdot\frac{\partial^2 y_2}{\partial r^2}+2v\omega\mu\cdot\frac{\partial y_1}{\partial r}-b\omega\cdot y_1+\left(k-\mu\omega^2\right)\cdot y_2=0 \end{aligned} \tag{6.14}$$

Regarding boundary conditions, at infinite distance the deflection, the slope of the deflection line, the bending moment and the shear force all vanish; and the solution can be obtained by the method of Fourier integral transformations using the following fundamental relations:

$$y(r)=\frac{1}{2\pi}\int_{-\infty}^{+\infty}P(s)\cdot e^{isr}ds \tag{6.15}$$

$$P(s)=P(s)=\int_{-\infty}^{+\infty}y(r)\cdot e^{-isr}dr \tag{6.16}$$

where s is a variable in the complex plane. And $P(s)$ is the transform of $y(s)$.

The two equation of (6.14) are rewritten in the following form:

$$\begin{aligned} \left(EIs^4-\mu v^2s^2-bvis+k-\mu\omega^2\right)\cdot p_1-\left(2v\omega\mu is-b\omega\right)\cdot p_2=F_0\\ \left(2v\omega\mu is-b\omega\right)\cdot p_1-\left(EIs^4-\mu v^2s^2-bvis+k-\mu\omega^2\right)\cdot p_2=0 \end{aligned} \tag{6.17}$$

The (6.17) equations form an algebraic system in p_1 and p_2, that can be easily solved:

$$p_1=F_0\cdot\frac{EIs^4-\mu v^2s^2-bvis+k-\mu\omega^2}{\left(EIs^4-\mu v^2s^2-bvis+k-\mu\omega^2\right)^2+\left(2v\omega\mu is-b\omega\right)^2} \tag{6.18}$$

$$p_2=F_0\cdot\frac{-\left(2v\omega\mu is-b\omega\right)}{\left(EIs^4-\mu v^2s^2-bvis+k-\mu\omega^2\right)^2+\left(2v\omega\mu is-b\omega\right)^2} \tag{6.19}$$

The solution in terms of the vertical displacement $y(r,t)$ is obtained inverting (6.18) and (6.19) considering (6.15). The inversion can be carried out through the

Cauchy's residue theorem, if p_1 and p_2 can be split up into partial fractions. For this aim the denominator has to be expressed through linear factors:

$$(EIs^4 - \mu v^2 s^2 - bvis + k - \mu\omega^2)^2 + (2v\omega\mu \cdot is - b\omega)^2 \tag{6.20}$$

The results can be expressed in non-dimensional form introducing proper parameters that consider the frequency, speed and damping effect. Thus, the following parameters are defined:

$$\omega_0 = \sqrt{\frac{k}{\mu}} \qquad \text{fundamental frequency of the system} \tag{6.21}$$

$$v_0 = \sqrt[4]{\frac{4EIk}{\mu^2}} = 2\theta\sqrt{\frac{EI}{k}} \qquad \text{critical speed in which } \theta = \sqrt[4]{\frac{k}{4EI}} \tag{6.22}$$

$$b_0 = 2 \cdot \sqrt{\mu k} \qquad \text{critical damping} \tag{6.23}$$

The three non-dimensional parameters are:

$$W = \frac{\omega}{\omega_0}, \quad \alpha = \frac{v}{v_0}, \quad \beta = \frac{b}{b_0} \tag{6.24}$$

Moreover a non dimensional variable is considered obtained by the variable r:

$$R = \theta \cdot (x - vt) \tag{6.25}$$

Regarding the displacement, the non-dimensional parameter is:

$$Y = \frac{y}{y_0} \qquad \text{in which} \qquad y_0 = \frac{F_0}{8EI\theta^3} = \left(\frac{4EI}{k}\right)^{3/4} \frac{F_0}{8EI} \tag{6.26}$$

The Laplace transform is written:

$$P_j(S) \int_{-\infty}^{+\infty} Y_j(r) \cdot e^{-iSR} dR = \frac{2k}{F_0} p_j(s) \quad \text{with} \quad j = 1, 2 \tag{6.27}$$

The solution in terms of non-dimensional parameters is:

$$Y(R,t) = Y_1(r) \cdot \cos(\omega \cdot t) + Y_2(r) \sin(\omega \cdot t) \tag{6.28}$$

in which $Y_1(R)$ and $Y_2(R)$ are Fourier inverses with respect to S of $P_1(S)$ and $P_2(S)$, that are expressed:

$$P_1(S)=\frac{8\cdot\left[S^4-4\cdot\alpha^2S^2-8\cdot\beta\cdot\alpha\cdot iS+4\left(1-W^2\right)\right]}{\left[S^4-4\cdot\alpha^2S^2-8\cdot\beta\cdot\alpha\cdot iS+4\left(1-W^2\right)\right]^2+64\cdot\left[\alpha WiS-\beta W\right]^2} \tag{6.29}$$

$$P_2(S)=\frac{-64\cdot\left(\alpha WiS-\beta W\right)}{\left[S^4-4\cdot\alpha^2S^2-8\cdot\beta\cdot\alpha\cdot iS+4\left(1-W^2\right)\right]^2+64\cdot\left[\alpha WiS-\beta W\right]^2} \tag{6.30}$$

The solution is obtained when the denominator is factorized, or equivalently, the following equation is solved:

$$\left[S^4-4\cdot\alpha^2S^2-8\cdot\beta\cdot\alpha\cdot iS+4\left(1-W^2\right)\right]^2+64\cdot\left[\alpha WiS-\beta W\right]^2=0 \tag{6.31}$$

The general solution is quite difficult to obtain but the salient aspects of the railway track dynamical behaviour can be obtained considering less complex particular cases.

6.1.2 Vibration of the beam in the absence of damping

The absence of damping can simplify the previous relations and facilitate the consequently solution. In (6.18) and (6.19) the damping parameter b disappears:

$$p_1=F_0\cdot\frac{EIs^4-\mu v^2s^2+k-\mu\omega^2}{\left(EIs^4-\mu v^2s^2+k-\mu\omega^2\right)^2+\left(2v\omega\mu is\right)^2} \tag{6.32}$$

$$p_2=F_0\cdot\frac{-2v\omega\mu is}{\left(EIs^4-\mu v^2s^2+k-\mu\omega^2\right)^2+\left(2v\omega\mu is\right)^2} \tag{6.33}$$

The denominator can be split up in two fourth degree factors:

$$\begin{aligned} &EIs^4-\mu v^2s^2+k-\mu\omega^2+2v\omega\mu s=0\\ &EIs^4-\mu v^2s^2+k-\mu\omega^2-2v\omega\mu s=0 \end{aligned} \tag{6.34}$$

Solving the first equation of (6.34) all roots are obtained because if $s-a$ is a solution of the first one, then $s-a$ is a root of the second one. The following equation is solved:

$$EIs^4-\mu v^2s^2+2v\omega\mu\cdot s+k-\mu\omega^2=0 \tag{6.35}$$

Depending on equation coefficients the roots may be all real or all complex or two may be real and two complex.

When the roots are real p_1, p_2 and their transform function $y_1(r), y_2(r)$ lead to a solution for y which includes terms representing an undamped sinusoidal wave existing over the whole length of the beam and moving in the positive x direction with velocity v. This situation is never realized physically and so the roots are all complex.

As all the coefficients are real, the roots must occur in conjugated pairs. Moreover the sum of the four roots must be zero because the coefficient of s^3 is zero. In order to satisfy these requirements, the four roots must be expressed in the form:

$a + ic_1 \qquad a - ic_1 \qquad -a + ic_2 \qquad -a - ic_2$

hence:

$$EIs^4 - \mu v^2 s^2 + k - \mu\omega^2 + 2v\omega\mu s = (s - a - ic_1)\cdot(s - a + ic_1)\cdot(s + a - ic_2)\cdot(s + a + ic_2)$$

The three unknown values a, c_1 and c_2 can be obtained through the following equation, applying the identity principle of the polynomials:

$$2a^2 - c_1^2 - c_2^2 = \frac{\mu \cdot v^2}{EI} \tag{6.36}$$

$$2a \cdot (c_1^2 - c_2^2) = \frac{2v\omega\mu}{EI} \tag{6.37}$$

$$(a^2 + c_1^2)\cdot(a^2 + c_2^2) = \frac{k - \mu\omega^2}{EI} \tag{6.38}$$

When a, c_1 and c_2 are obtained the four roots are known and the process of expanding of p_1 and p_2 into partial fractions is carried out:

$$\frac{(EI)^2}{F_0}p_1(s)=\frac{v\omega\mu}{4a\cdot\left(c_1^2-c_2^2\right)}\left\{\frac{1}{ic_1\left(2a+ic_1-ic_2\right)\cdot\left(2a+ic_1+ic_2\right)}\cdot\left[\frac{1}{s-a-ic_1}-\frac{1}{s+a+ic_1}\right]+\right.$$
$$-\frac{1}{ic_1\left(2a-ic_1-ic_2\right)\cdot\left(2a-ic_1+ic_2\right)}\cdot\left[\frac{1}{s-a+ic_1}-\frac{1}{s+a-ic_1}\right]+$$
$$+\frac{1}{ic_2\left(2a+ic_1-ic_2\right)\cdot\left(2a-ic_1-ic_2\right)}\cdot\left[\frac{1}{s+a-ic_2}-\frac{1}{s-a+ic_2}\right]+$$
$$\left.-\frac{1}{ib_2\left(2a+ic_1+ic_2\right)\cdot\left(2a-ic_1+ic_2\right)}\cdot\left[\frac{1}{s+a+ic_2}-\frac{1}{s-a-ic_2}\right]\right\}$$

Considering that:

the inverse of $\frac{1}{s-a-ic}$ is $ie^{-(c-ia)r}H(r)$

the inverse of $\frac{1}{s-a+ic}$ is $-ie^{(c+ia)r}H(-r)$

the inverse of $\frac{1}{s+a-ic}$ is $ie^{-(c+ia)r}H(r)$

the inverse $\frac{1}{s+a+ic}$ is $-ie^{(c-ia)r}H(-r)$

where a and c are positive and $H(r)$ is the Heaviside unit function for which $H(r)=1$ if $r>0$ and $H(r)=0$ if $r<0$ (Mathews, 1958).

Hence the $p_1(s)$ function can be easily inverted obtaining $y_1(r)$; $p_2(s)$ and $y_2(r)$ are found using the same procedure outlined above and so the following expression is obtained:

$$
\begin{aligned}
y &= y_1(r)\cdot\cos\omega t + y_2(r)\cdot\sin\omega t = \\
&= \frac{F_0}{2EI}\cdot\cos\omega t\cdot\left[\frac{1}{c_1}\cdot\frac{\left(4\cdot a^2 - c_1^2 + c_2^2\right)\cdot e^{-c_1|r|}\cos a|r| + 4ac_1 e^{-c_1|r|}\sin a|r|}{\left(4\cdot a^2 - c_1^2 + c_2^2\right)^2 + 16a^2c_1^2} + \right. \\
&\left. + \frac{1}{c_2}\cdot\frac{\left(4\cdot a^2 - c_2^2 + c_1^2\right)\cdot e^{-c_1|r|}\cos a|r| + 4ac_2 e^{-c_2|r|}\sin a|r|}{\left(4\cdot a^2 - c_2^2 + c_1^2\right)^2 + 16a^2c_2^2}\right] + \\
&\mp \frac{F_0}{2EI}\sin\omega t\cdot\left[\frac{1}{b_1}\cdot\frac{\left(4\cdot a^2 - c_1^2 + c_2^2\right)\cdot e^{-c_1|r|}\sin a|r| - 4ab_1 e^{-c_1|r|}\cos a|r|}{\left(4\cdot a^2 - c_1^2 + c_2^2\right)^2 + 16a^2c_1^2} + \right. \\
&\left. - \frac{1}{c_2}\cdot\frac{\left(4\cdot a^2 - c_2^2 + c_1^2\right)\cdot e^{-c_2|r|}\sin a|r| - 4ac_2 e^{-c_2|r|}\cos a|r|}{\left(4\cdot a^2 - c_2^2 + c_1^2\right)^2 + 16a^2c_2^2}\right]
\end{aligned}
\tag{6.39}
$$

In (6.39) the negative sign holds when $r > 0$ and the positive sign for $r < 0$.

This is the formal solution, which describes the vibrations of the beam under the action of a concentrated force varying sinusoidally with time and whose point of the application on the beam moves with speed v in the positive x direction when the damping is absent. The values of a, c_1 and c_2 are evaluated as a function of the inertial, elastic and damping parameters for the different cases.

If the force is fixed $(v = 0)$ and varies sinusoidally with the time:

$$a = c_1 = c_2 = \sqrt[4]{\frac{k - \mu\omega^2}{4EI}} \tag{6.40}$$

therefore the deflection of the beam is written:

$$y(x,t) = \frac{F_0}{8EIa^3}e^{-a|x|}\left(\cos a|x| + \sin a|x|\right)\cdot\cos\omega t \tag{6.41}$$

The maximum amplitude of the vibration is at the point of application of the load and its value is:

$$y_{\max} = \frac{F_0}{8EIa^3} = \frac{F_0}{8EI}\left(\frac{4EI}{k - \mu\omega^2}\right)^{3\backslash 4} \tag{6.42}$$

The maximum amplitude (6.42) tends to infinity when the frequency of the load is near the fundamental frequency of the beam:

$$\omega^2 = \frac{k}{\mu} = \omega_0^2 \tag{6.43}$$

this fact reveals the existence of a resonance phenomenon.

A force constant and moving with constant speed is now considered, the values of a, c_1 and c_2 are obtained from the following relations:

$$c_1 = c_2 \qquad\qquad c_1 = a^2 - \frac{\mu v^2}{2EI} \tag{6.44}$$

Substituting in (6.38):

$$2a^2 - \frac{\mu v^2}{2EI} = \sqrt{\frac{k}{EI}} \tag{6.45}$$

hence:

$$a = \left\{ \sqrt{\frac{k}{4EI}} + \frac{\mu v^2}{4EI} \right\}^{1/2} \qquad\qquad c_1 = c_2 = c = \left\{ \sqrt{\frac{k}{4EI}} - \frac{\mu v^2}{4EI} \right\}^{1/2} \tag{6.46}$$

The vertical displacements of the beam are given by:

$$y = \frac{F_0}{2EI} \frac{e^{-c|x-vt|}}{2ac\left(a^2 + c^2\right)} \cdot \left\{ a \cos a|x - vt| + c \sin a|x - vt| \right\} \tag{6.47}$$

The deflection at the point where the moving load is applied $\left(r = x - vt\right)$ is:

$$y_{\max} = \frac{F_0}{2EI} \cdot \frac{e^{-c|x-vt|}}{2ac \cdot (a^2 + c^2)} = \frac{F_0}{8EI} \cdot \left(\frac{4EI}{k} \right)^{1/2} \left\{ \sqrt{\frac{k}{4EI}} - \frac{\mu v^2}{4EI} \right\}^{-1/2} \tag{6.48}$$

this displacement is compared with the static one given by (6.26):

$$\frac{y_{\max}}{y_0} = \frac{(k / 4EI)^{1/4}}{\left\{ \sqrt{\frac{k}{4EI}} - \frac{\mu v^2}{4EI} \right\}^{1/2}} \tag{6.49}$$

If the critical speed v_0 is considered, (6.49) can be written:

$$\frac{y_{\max}}{y_0} = \left(1 - \frac{v^2}{v_0^2}\right)^{-1/2} \tag{6.50}$$

The effect of the speed can cause instability if the train speed is near the value of the critical one.

It is of interest to enquire as to how the resonance frequency is modified when the speed v has a finite value. A relationship between the values of v and ω that correspond to instability conditions is found. The (6.39) shows that y tends to infinite if one of the following conditions is satisfied:

$c_1 = 0$ or $c_2 = 0$ or $a = 0$ and $c_1 = c_2$

However, from (6.37) when $v \neq 0$ and $\omega \neq 0$, it must be $c_1 > c_2$; this condition considering that a, c_1 and c_2 are non-negative by definition, rules out the first and the third of the above alternatives and leaves the first the condition $c_2 = 0$.

The introduction of this condition into (6.36), (6.37) and (6.38) gives:

$$-2a^2 + b_1^2 = -\frac{\mu \cdot v^2}{EI} \tag{6.51}$$

$$2ab_1^2 = \frac{2v\omega\mu}{EI} \tag{6.52}$$

$$(a^2 + b_1^2) \cdot a^2 = \frac{k - \mu\omega^2}{EI} \tag{6.53}$$

Eliminating a and c_1 from the three equations, it is found that y tends to infinite if v and ω are such that:

$$\frac{1}{\sqrt{6}}\left\{\frac{\mu v^2}{EI} + \left[\left(\frac{\mu v^2}{EI}\right)^2 + 12\frac{k - \mu\omega^2}{EI}\right]^{1/2}\right\}^{1/2} \cdot \left\{\frac{1}{3}\left[\left(\frac{\mu\omega^2}{EI}\right)^2 + 12\frac{k - \mu\omega^2}{EI}\right]^{1/2} - \frac{2}{3}\frac{\mu v^2}{EI}\right\} = \frac{v\omega\mu}{EI}$$

this relation (figure 2) can be expressed in terms of the non-dimensional parameters α and W:

$$\alpha^4\left\{27 - 18\cdot(1 - W^2) - (1 - W^2)^2 - 4\alpha^4\right\} = 4\cdot(1 - W^2)^3 \tag{6.54}$$

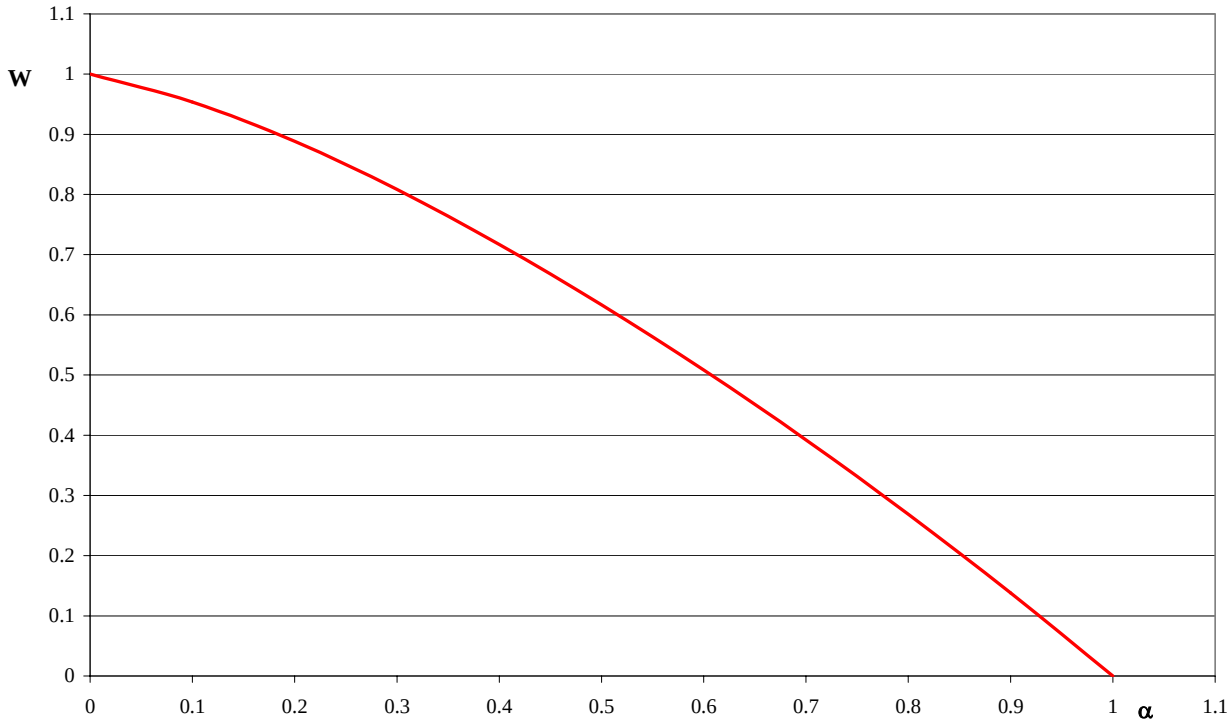

figure 2 relation between the values of α and W in instability conditions (Mathews, 1958):

(6.36), (6.37) and (6.38) can be expressed in a non-dimensional form as a function of α and W an of the non-dimensional variable R. Moreover A, C_1 and C_2 are defined:

$$A = \frac{a}{\theta} \qquad C_1 = \frac{c_1}{\theta} \qquad C_2 = \frac{c_2}{\theta} \tag{6.55}$$

Hence:

$$2A^2 - C_1^2 - C_2^2 = 4 \cdot V^2 \tag{6.56}$$

$$A \cdot \left(C_1^2 - C_2^2\right) = 4 \cdot V \cdot W \tag{6.57}$$

$$\left(A^2 + C_1^2\right) \cdot \left(A^2 + C_2^2\right) = 4 \cdot \left(1 - W^2\right) \tag{6.58}$$

The values of A, C_1 and C_2 for the different values of V and W are obtained solving the three equations (6.56), (6.57) and (6.58); they are in table 1.

table 1 A, C_1 e C_2 in function of non-dimensional parameters α e W (Mathews, 1958)

W / α		0	0.1	0.2	0.3	0.4	0.5	0.6	0.7	0.8	0.9
0	$A=C_1=C_2$	1.000	0.997	0.990	0.977	0.957	0.931	0.894	0.845	0.775	0.660
	A	1.005	1.002	0.995	0.982	0.963	0.937	0.902	0.854	0.787	0.682
0.1	C_1	0.995	1.002	1.005	1.003	0.995	0.982	0.962	0.934	0.896	0.842
	C_2	0.995	0.982	0.964	0.940	0.908	0.867	0.812	0.738	0.629	0.426
	A	1.020	1.017	1.010	0.998	0.980	0.955	0.922	0.879	0.819	
0.2	C_1	0.980	0.997	1.010	1.018	1.022	1.021	1.015	1.005	0.991	
	C_2	0.980	0.957	0.928	0.892	0.847	0.783	0.714	0.611	0.448	
	A	1.044	1.042	1.035	1.024	1.007	0.985	0.955	0.917	0.867	
0.3	C_1	0.954	0.981	1.004	1.022	1.036	1.046	1.053	1.057	1.061	
	C_2	0.954	0.921	0.881	0.832	0.772	0.696	0.596	0.449	0.130	
	A	1.077	1.075	1.069	1.059	1.044	1.024	0.998	0.965		
0.4	C_1	0.917	0.954	0.986	1.014	1.036	1.036	1.075	1.092		
	C_2	0.917	0.873	0.820	0.758	0.680	0.680	0.441	0.175		
	A	1.118	1.116	1.111	1.102	1.089	1.071	1.049			
0.5	C_1	0.866	0.914	0.956	0.993	1.026	1.055	1.083			
	C_2	0.866	0.810	0.744	0.664	0.563	0.424	0.166			
	A	1.166	1.165	1.160	1.152	1.140	1.125				
0.6	C_1	0.800	0.860	0.912	0.959	1.001	1.039				
	C_2	0.800	0.730	0.647	0.542	0.399	0.114				
	A	1.221	1.219	1.215	1.208						
0.7	C_1	0.714	0.788	0.853	0.910						
	C_2	0.714	0.626	0.516	0.363						
	A	1.281	1.279	1.276							
0.8	C_1	0.600	0.694	0.774							
	C_2	0.600	0.482	0.311							
	A	1.345									
0.9	C_1	0.436									
	C_2	0.436									

The non-dimensional displacement (6.26) is written in the form:

$$
\begin{aligned}
Y = Y_1(R)\cdot\cos\omega\cdot t + Y_2(R)\cdot\sin\omega\cdot t = \\
4\cdot\cos\omega\cdot t\cdot\left[\frac{1}{C_1}\cdot\frac{\left(4A^2-C_1^2+C_2^2\right)\cdot e^{-C_1|R|}\cdot\cos A\,|R|+4AC_1e^{-C_1|R|}\sin A\,|R|}{(4A^2-C_1^2+C_2^2)^2+16A^2C_1^2}+\right. \\
\left.+\frac{1}{C_2}\cdot\frac{\left(4A^2-C_2^2+C_1^2\right)\cdot e^{-C_2|R|}\cdot\cos A\,|R|+4AC_2e^{-C_2|R|}\sin A\,|R|}{(4A^2-C_2^2+C_1^2)^2+16A^2C_2^2}\right]+ \\
\mp 4\cdot\sin\omega\cdot t\cdot\left[\frac{1}{C_1}\cdot\frac{\left(4A^2-C_1^2+C_2^2\right)\cdot e^{-C_1|R|}\cdot\sin A\,|R|-4AC_1e^{-C_1|R|}\cos A\,|R|}{(4A^2-C_1^2+C_2^2)^2+16A^2C_1^2}+\right. \\
\left.-\frac{1}{C_2}\cdot\frac{\left(4A^2-C_2^2+C_1^2\right)\cdot e^{-C_2|R|}\cdot\sin A\,|R|+4AC_2e^{-C_2|R|}\cos A\,|R|}{(4A^2-C_2^2+C_1^2)^2+16A^2C_2^2}\right]
\end{aligned}
\qquad (6.59)
$$

If $R>0$ the second term assumes negative sign; if $R<0$ the second term assumes positive sign.

The modulus of Y as a function of R is shown for different values of non-dimensional parameters α and W in figure 3.

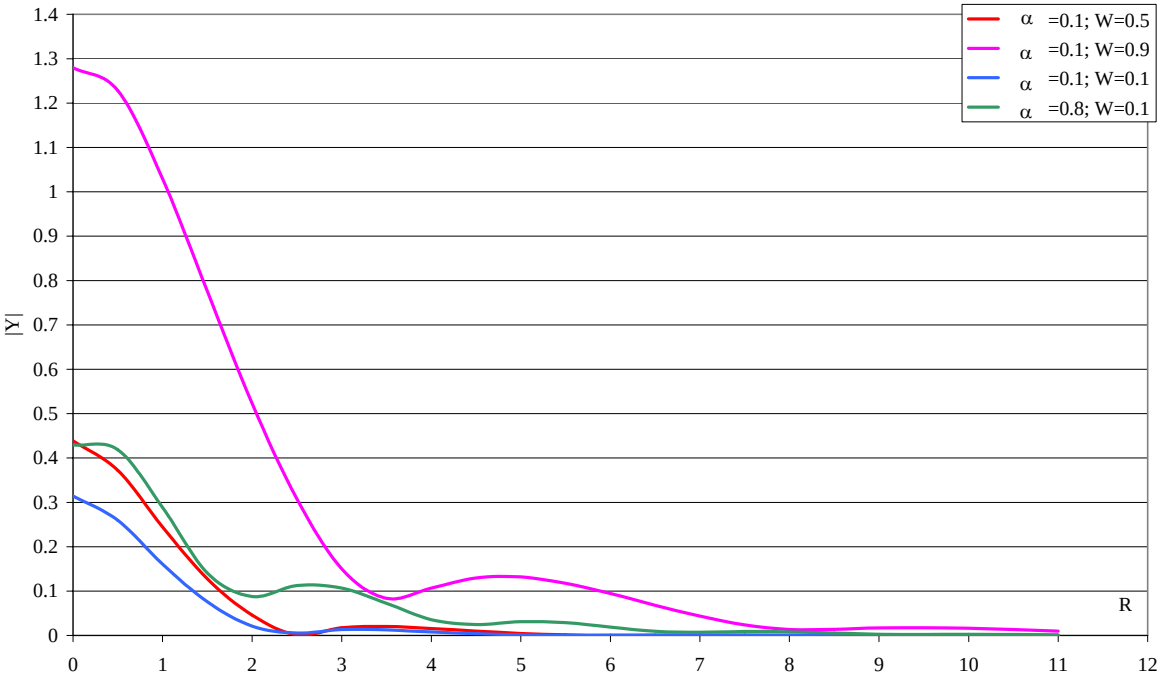

figure 3 Modulus of non-dimensional displacement Y for different values of α and W

6.1.3 Vertical vibrations of the beam in damped case

The general analytical solution in which the harmonic force moves on the beam with constant speed is quite difficult to determine in damped case. The equation (6.31) has to be solved; it is a polynomial of the eighth degree and its eight roots can be written in the following form (Mathews, 1959):

$$S_i = \begin{cases} A_1 + iB_1, & A_2 - iB_2, & -A_3 + iB_3, & -A_4 - iB_4 \\ -A_1 + iB_1, & -A_2 - iB_2, & A_3 + iB_3, & A_4 - iB_4 \end{cases} \text{ with } i = 1...8$$

Two simpler cases are studied from which some important results concerning the dynamical behaviour of the track system can be derived.

6.1.3.1 The case of a constant force moving at constant speed

The track model is in figure 1 still consists of a beam with infinite length on viscoelastic foundation. It is loaded by a constant force F_0 moving at constant speed v.

Vertical vibrations of the beam are described by the following differential equation:

$$EI \cdot \frac{\partial^4 y(x,t)}{\partial x^4} + \mu \cdot \frac{\partial^2 y(x,t)}{\partial t^2} + b \cdot \frac{\partial y(x,t)}{\partial t} + k \cdot y(x,t) = F_0 \cdot \delta(x) \tag{6.60}$$

The first member of the equation is that of equation(6.1), the second one describes the load acting on the beam, which represents the train running on the track. F_0 is constant and $\delta(x)$ is still the Dirac function.

The damping coefficient b can be expressed as shown in the following:

$$b = 2\mu\omega_b \tag{6.61}$$

In which μ is the beam mass per unit length and ω_b is a circular frequency of damping.

The problem is solved using the method of Fourier integral transformations very effective in the study of moving loads.

Regarding the boundary conditions the slope of the deflection line, the bending moment and the shear force are zero at an infinite distance on the right as well as on the left of the force F_0.

The dimensionless variable R is considered again: the coordinate system origin moves together with the load at a uniform speed v (Fryba, 1999).

Moreover the hypothesis of quasi-stationary state is introduced, in which the beam is at rest with respect to the moving coordinate system and so the solution in terms of displacement can be written in the form:

$$y(x,t) = y_0 \cdot y(R) \tag{6.62}$$

in which y_0 is the static displacement defined in (6.26) and $y(R)$ is the non-dimensional displacement.

The partial derivates of R defined in (6.25) are:

$$\frac{\partial R}{\partial x} = \theta \qquad \frac{\partial R}{\partial t} = -\theta v \tag{6.63}$$

Considering the (6.63) and the quasi-stationary state the partial derivates of the rail displacement $y(x,t)$ can be written:

$$\frac{\partial^4 y(x,t)}{\partial x^4} = \theta^4 y_0 \cdot \frac{d^4 y(R)}{dR^4} \tag{6.64}$$

$$\frac{\partial^2 y(x,t)}{\partial t^2} = \theta^2 v^2 y_0 \cdot \frac{d^2 y(R)}{dR^2} \tag{6.65}$$

$$\frac{\partial y(x,t)}{\partial t} = -\theta v y_0 \cdot \frac{dy(R)}{dR} \tag{6.66}$$

According to the properties of the Dirac function, expressed by (6.8) and (6.9), the non-dimensional form of the function is written as:

$$\delta(R) = \frac{1}{\theta} \cdot \delta(x) \tag{6.67}$$

considering that:

$$\int_{-\infty}^{+\infty} \delta(R)dR = \int_{-\infty}^{+\infty} \frac{1}{\theta}\delta(x)\lambda dx = 1 \tag{6.68}$$

(6.67), (6.66), (6.65) and (6.64) are substituted in (6.60):

$$\frac{EIy_0\theta^4}{EIy_0\theta^4}\cdot\frac{d^4y(R)}{dR^4} + \frac{\mu y_0\theta^2 v^2}{EIy_0\theta^4}\cdot\frac{d^2y(R)}{dR^2} + \frac{y_0\theta v}{EIy_0\theta^4}\cdot\frac{dy(R)}{dR} + \frac{ky_0}{EIy_0\theta^4}\cdot y(R) = \frac{F_0\theta\delta(R)}{EIy_0\theta^4} \tag{6.69}$$

If the two non-dimensional parameters α and β (defined in previous paragraph) are considered the differential equation coefficients can be written:

$$\begin{aligned}
&\frac{\mu y_0\theta^2 v^2}{EIy_0\theta^4} = \frac{\mu v^2}{EI\theta^2}\cdot\frac{4}{4} = 4\alpha^2 \\
&\frac{y_0\theta v}{EIy_0\theta^4} = \frac{by_0\theta\ v}{EIy_0\theta^4}\cdot\frac{4}{4} = 8\cdot\frac{b\theta}{k}\cdot\frac{\sqrt{\mu}}{2\theta\sqrt{EI}}\cdot\frac{v\cdot 2\theta\cdot\sqrt{EI}}{\sqrt{\mu}} = \frac{8\alpha b}{2\cdot\sqrt{\mu}\cdot\sqrt{k}} = 8\alpha\beta \\
&\frac{ky_0}{EIy_0\theta^4} = \frac{\theta^4 4EI}{EI\theta^4} = 4 \\
&\frac{F_0\theta}{EIy_0\theta^4} = \frac{F_0\theta 2k}{F_0\theta EI\theta^4} = \frac{8\theta^4 EI}{EI\theta^4} = 8
\end{aligned} \tag{6.70}$$

Substituting (6.70) in (6.69):

$$\frac{d^4v(R)}{dR^4} + 4\alpha^2\cdot\frac{d^2v(R)}{dR^2} - 8\alpha\beta\cdot\frac{dv(R)}{dR} + 4v(R) = 8\delta(R) \tag{6.71}$$

The boundary conditions are:

for $R\to+\infty$ and for $R\to-\infty$ $v(R) = v'(R) = v''(R) = v'''(R) = 0$

The method of Fourier integral transformations is used. The following fundamental relations have to be remembered:

$$y(R) = \frac{1}{2\pi}\cdot\int_{-\infty}^{+\infty} P(S)\cdot e^{iSR}dS \tag{6.72}$$

$$P(S) = \int_{-\infty}^{+\infty} y(R)\cdot e^{-iSR}dR \tag{6.73}$$

in which S is a variable in the complex plane, and $P(S)$ is the transform of the function $y(R)$. The integral transforms applied in the model are in table 2.

table 2 Integral transforms in the model

FUNCTION	TRANSFORM
$\frac{dy}{dR}$ for $y(\pm\infty)=0$	$iSP(S)$
$\frac{d^2y}{dR^2}$ for $y(\pm\infty)=y'(\pm\infty)=0$	$-S^2P(S)$
$\frac{d^3y}{dR^3}$ for $y(\pm\infty)=y'(\pm\infty)=y''(\pm\infty)=0$	$-iS^3P(S)$
$\frac{d^4y}{dR^4}$ for $y(\pm\infty)=y'(\pm\infty)=y''(\pm\infty)=y'''(\pm\infty)=0$	$S^4P(S)$
$a\cdot y(R)$ (a=constant)	$a\cdot P(S)$
$\delta(R)$ (Dirac function)	1

The integral transforms are substituted in (6.71) and the non-dimensional parameters of the speed and damping (α and β respectively) are considered:

$$S^4\cdot P(S)-4\alpha^2S^2\cdot P(S)-i8\alpha\beta S\cdot P(S)+4\cdot P(S)=8 \tag{6.74}$$

An algebraic equation is obtained and the single unknown function is $P(S)$:

$$P(S)=\frac{8}{S^4-4\alpha^2S^2-i\alpha\beta S+4} \tag{6.75}$$

hence:

$$y(R)=\frac{4}{\pi}\cdot\int_{-\infty}^{+\infty}\frac{e^{iRS}}{S^4-4\alpha^2S^2-i\alpha\beta S+4}dS \tag{6.76}$$

The residue theory is applied to obtain the solution in closed form, therefore the integrand denominator has to be factorized, in other words the integrand poles have to be found. They are derived from the roots of the denominator $Q(S)$ in (6.76):

$$Q(S) = S^4 - 4\alpha^2 S^2 - 8\alpha\beta S + 4 = 0 \tag{6.77}$$

The particular form of the equation and the hypothesis of light damping $(\beta < \beta_{cr})$ makes possible to write the roots in the following way:

$$A_1 = a_1 + ic \qquad A_2 = -a_1 + ic \qquad A_3 = a_2 - ic \qquad A_4 = -a_2 - ic$$

Hence:

$$S^4 - 4\alpha^2 S^2 - 8\alpha\beta S + 4 = (S - A_1)\cdot(S - A_2)\cdot(S - A_3)\cdot(S - A_4) = (S - a_1 - ic)\cdot(S + a_1 - ic)\cdot$$
$$\cdot(S - a_2 + ic)\cdot(S + a_2 + ic) = \left(S^2 - 2icS - a_1^2 + i^2c^2\right)\cdot\left(S^2 + 2icS - a_2^2 + i^2c^2\right)$$

Applying the identity principle of polynomials:

$$a_2^2 = 2\alpha^2 + c^2 - \frac{2\alpha\beta}{c} \tag{6.78}$$

$$a_1^2 = 2\alpha^2 + c^2 + \frac{2\alpha\beta}{c} \tag{6.79}$$

$$c^6 + 2\alpha^2 c^4 + \left(\alpha^4 - 1\right)\cdot c^2 - \alpha^2\beta^2 = 0 \tag{6.80}$$

The roots of the equation (6.80) are six, but only the positive ones are taken into account; in fact, according to Descartes' rule of signs, the equation has a positive root when $\alpha \geq 0$ and $\beta \geq 0$. The equation (6.80) is solved as a third degree equation in c^2.

In the following solutions in terms of a_1, a_2, c are carried out for different values of the two non-dimensional parameters α and β.

In the static case $(\alpha = 0)$:

$$b = 1 \qquad a_1 = 1 \qquad a_2 = 1 \tag{6.81}$$

In the case of the absence of damping $(\beta = 0)$:

$$\text{for } \alpha < 1 \Rightarrow c = \sqrt{1-\alpha^2} \quad a = a_1 = a_2 = \sqrt{1+\alpha^2} \tag{6.82}$$

$$\text{for } \alpha = 1 \Rightarrow c = 1 \quad a = a_1 = a_2 = \sqrt{2} \tag{6.83}$$

$$\text{for } \alpha > 1 \Rightarrow c = 0 \quad a_1 = \sqrt{1+\alpha^2} + \sqrt{1-\alpha^2} \quad a_2 = \sqrt{1+\alpha^2} - \sqrt{1-\alpha^2} \tag{6.84}$$

When the damping is considered an approximate solution is obtained and there are different solution depending on the ratio between the damping parameter β and the critical damping β_{cr}. The first case is given by $\beta < 1$ and the solution is obtained:

$$\text{for } \alpha < 1 \Rightarrow c \approx \sqrt{1-\alpha^2} \quad a_1 \approx \left(1+\alpha^2+\frac{2\alpha\beta}{\sqrt{1+\alpha^2}}\right)^{1/2} \quad a_2 \approx \left(1+\alpha^2-\frac{2\alpha\beta}{\sqrt{1+\alpha^2}}\right)^{1/2} \tag{6.85}$$

$$\text{for } \alpha = 1 \Rightarrow c \approx 2^{-1/4}\cdot\beta^{1/2} \quad a \approx a_1 \approx a_2 \approx 2^{1/2}\cdot\left(1+2^{-3/4}\cdot\beta^{1/2}\right) \tag{6.86}$$

$$\text{for } \alpha > 1 \Rightarrow c \approx \frac{\alpha\beta}{\sqrt{\alpha^4-1}} \quad a_1 \approx \sqrt{1+\alpha^2}+\sqrt{1-\alpha^2} \quad a_2 \approx \sqrt{1+\alpha^2}-\sqrt{1-\alpha^2} \tag{6.87}$$

When the damping parameter reaches its critical value the value of a_2 always assumes zero value, considering (6.78):

$$2\alpha^2+c^2 = \frac{2\alpha\beta_{cr}}{c} \Rightarrow \alpha\beta_{cr} = \frac{1}{2}c\cdot\left(2\alpha^2+c^2\right) \tag{6.88}$$

(6.88) is substituted in (6.80) and finally the expression of the critical damping is obtained:

$$\beta_{cr} = \frac{2^{1/2}}{3^{3/2}}\cdot\left(-\alpha^2+\left(\alpha^4+3\right)^{1/2}\right)^{1/2}\cdot\left(2\alpha+\frac{1}{\alpha}\cdot\left(\alpha^4+3\right)^{1/2}\right)^{1/2} \tag{6.89}$$

It depends on the load speed, since depends on the non dimensional α; on the contrary if a single degree of freedom system is considered the critical damping does not depend on the speed, but it is an intrinsic characteristic of the system. However the critical damping becomes constant when the non dimensional parameter α reaches higher values and it is shown in figure 4.

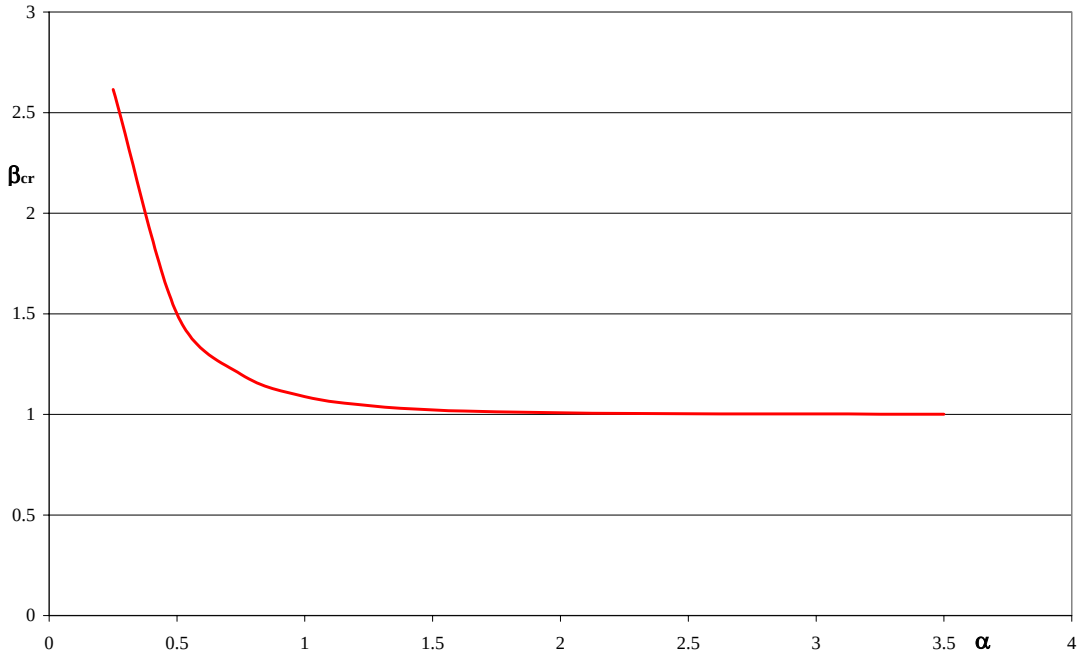

figure 4 the critical damping β_{cr}

In this case a_1 and c are given by:

$$a_1^2 = \frac{4}{3}\cdot\left(2\alpha^2 + \sqrt{\alpha^4 + 3}\right) \tag{6.90}$$

$$c = \frac{2}{3}\cdot\left(-\alpha^2 + \sqrt{\alpha^4 + 3}\right) \tag{6.91}$$

When the damping parameter is higher than the critical one the equation (6.78) becomes negative and the poles have to be expressed in a different way:

$$A_1 = a_1 + ic \qquad A_2 = -a_1 + ic \qquad A_3 = -\left(c - a_2\right)\cdot i \qquad A_4 = -\left(c + a_2\right)\cdot i$$

Again the identity principle of polynomials is applied:

$$S^4 - 4\alpha^2 S^2 - 8\alpha\beta S + 4 = \left(S - A_1\right)\cdot\left(S - A_2\right)\cdot\left(S - A_3\right)\cdot\left(S - A_4\right)$$

a_1 and c are still defined by equation (6.79) and (6.80), while a_2 is given by:

$$a_2^2 = -2\alpha^2 - c^2 + \frac{2\alpha\beta}{c} \qquad a_2 > 0 \qquad a_2 > b \tag{6.92}$$

When the integrand poles are known, the integral (6.76) can be solved:

$$y(R) = \frac{4}{\pi} \cdot \int_{-\infty}^{+\infty} F(S) dS$$

It represents the solution of the differential equation.

The integral can be expressed as a limit in the following way:

$$\int_{-\infty}^{+\infty} \frac{e^{iRS}}{Q(S)} dS = \lim_{R_1 \to \infty} \int_{-R_1}^{R_1} \frac{e^{iRS}}{Q(S)} dS \tag{6.93}$$

in which R_1 is the radius of the semicircle C_{R_1} which passes around all the poles in a half-plane (for an example see figure 5).

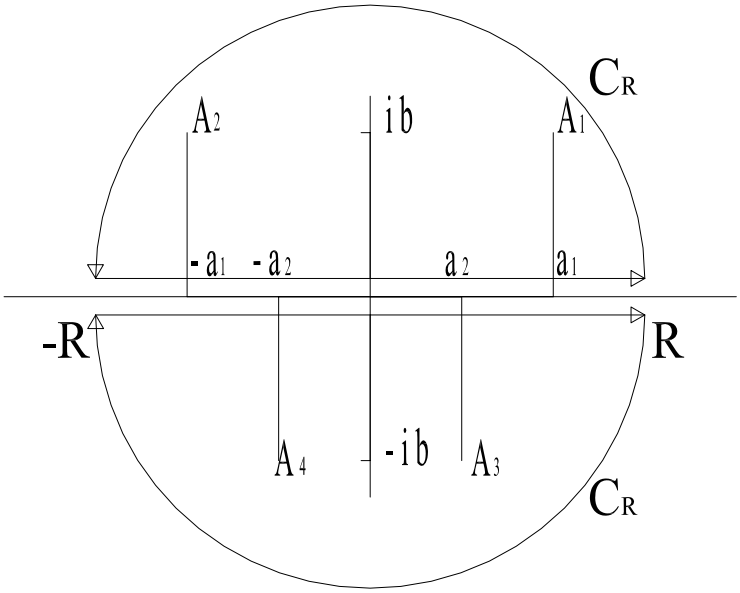

figure 5 poles in the complex plane

According to the Cauchy's residue theorem, the integral in the counter-clockwise direction around the close curve C (consisting of segments $-R$, $+R$, and semicircle C_R

and a point in which the function is not analytical) does not depend on the particular curve. The integral only depends on the value of the function *F(s)* residue:

$$\oint_{C_{R_1}} F(S)dS = \oint_{C_{R_1}} \frac{e^{iSR}}{Q(S)} dS = \lim_{R_1\to\infty}\left[\int_{-R_1}^{+R_1} \frac{e^{iSR}}{Q(S)} dS + \oint_{C_{R1}} \frac{e^{iSR}}{Q(S)} dS\right] = 2\pi i \mathrm{Res} F(S)|_{S=A_i} \quad (6.94)$$

In (6.94) $\mathrm{Res}F(S)|_{S=A_i}$ is the residue of the function $F(S)$ in the pole A_j.

These results can be extended in the case the poles are more than one:

$$\oint_{C_R} \frac{e^{iSR}}{Q(S)} dS = 2\pi i \sum_{j=1}^{n} \mathrm{Res}\, F(S)|_{S=A_j} \quad (6.95)$$

The integral (6.94) converges because $F(S)$ is a regular function if the upper half-plane is considered and along the real axis except for a finite number of poles which lie in the upper half-plane. Moreover for $S\to\infty$, $SF(S)$ uniformly tends to zero in fact $Q(S)$ is a fourth degree polynomial and the following relations are derived if $S=\xi+i\eta$ is the complex variable:

$$\begin{aligned} &\text{For} \quad R>0 \quad \left|e^{iSR}\right| = \left|e^{iR(\xi+i\eta)}\right| = \left|e^{iR\xi-\eta R)}\right| = e^{-R\eta} \le 1 \\ &\text{For} \quad R<0 \quad \left|e^{iS(-R)}\right| = \left|e^{i(-R)(\xi+i\eta)}\right| = \left|e^{-i(-R)\xi+\eta(-R)}\right| = e^{(-R)\eta} \le 1 \end{aligned} \quad (6.96)$$

For this reason in the evaluation of integrals the semicircle C_R is drawn in the upper half-plane $(\eta>0 \text{ for } R>0)$, and in the lower half-plane $(\eta>0 \text{ for } R>0)$.

The second integral in the square brackets of (6.94) is zero: $Q(S)$ is a fourth degree polynomial, therefore $|Q(S)| \ge R_1^n$ on semicircle C_{R_1} and considering that:

$$|F(S)| = \left|\frac{e^{iRS}}{Q(S)}\right| \le \frac{1}{R_1^n}$$

applying the Jordan's lemma the integral around C_{R_1} is:

$$\lim_{R_1\to\infty}\left|\oint_{C_{R1}} F(S)dS\right| \le \frac{\pi R_1}{R_1^n} = \frac{\pi}{R_1^{n-1}} = 0 = \quad (6.97)$$

Therefore the solution is derived from (6.95) and (6.97):

$$\int_{-\infty}^{+\infty} \frac{e^{iSR}}{Q(S)} = \begin{cases} +2\pi i \sum_{j=1}^{n} \mathrm{Res} F(S)|_{S=A_j} & \mathrm{s} > 0 \\ -2\pi \mathrm{i} \sum_{i=1}^{n} \mathrm{Res} F(S)|_{S=A_j} & \mathrm{s} < 0 \end{cases} \tag{6.98}$$

In the following the relations to compute the residue of a function are reported. For a pole of the first order:

$$\mathrm{Res}\ F(S)|_{S=A_j} = F(S) \cdot \left(S - A_j\right)|_{S=A_j} \tag{6.99}$$

For an example the case of poles of the second order is considered $\left(j = 2\right)$:

$$\mathrm{Res}\ F(S)\big|_{S=A_j} = \frac{e^{iRS}}{(A_2 - A_1)(A_2 - A_3)(A_2 - A_4)} \tag{6.100}$$

Finally the general case is derived:

$$\mathrm{Res}\ F(S)\big|_{S=A_j} = \frac{1}{(k-1)!} \lim_{S \to A_j} \left(\frac{d^{(k-1)}[(S - A_j)^k F(S)]}{dS^{(k-1)}} \right) \tag{6.101}$$

In which *k* is the order of the pole.

These relations allow to solve the integral in closed form for different values of the two non-dimensional parameters α and β.

The static solution $\left(\alpha = 0\right)$ is quickly obtained:

$$y(R) = e^{-|R|} \cdot \left(\cos R + \sin |R|\right) \tag{6.102}$$

In the absence of camping $\left(\beta = 0\right)$ three different ranges of the speed parameter are considered. The first one is the case of $\alpha < 1$:

$$y(R) = \frac{1}{ab} e^{-c|R|} \cdot \left(a \cos\left(aR\right) + b \sin\left(a|R|\right)\right) \tag{6.103}$$

When $\alpha = 1$ the load speed reaches its critical value v_{cr}. In this case the solution is not defined and the beam will lose its stability. This condition is very important and in the following other consideration will be made.

For $\alpha > 1$

$$y(R) = \begin{cases} -\dfrac{2}{a_1\sqrt{\alpha^4 - 1}} \cdot \sin a_1 R & \text{for } R > 0 \\ -\dfrac{2}{a_2\sqrt{\alpha^4 - 1}} \cdot \sin a_2 R & \text{for } R < 0 \end{cases} \tag{6.104}$$

In the case of light damping $(\beta << 1)$ the solution can be written in the form:

$$y(R) = \begin{cases} \dfrac{2}{a_1(D_1^2 + D_2^2)} \cdot e^{-cR} \cdot \left(D_1 \cos a_1 R + D_2 \sin a_2 R\right) & \text{for } R > 0 \\ \dfrac{2}{a_1(D_3^2 + D_4^2)} \cdot e^{-cR} \cdot \left(D_3 \cos a_1 R + D_4 \sin a_2 R\right) & \text{for } R < 0 \end{cases} \tag{6.105}$$

In which:

$$\begin{aligned} D_1 &= a_1 c \qquad D_2 = c^2 - \frac{1}{4} \cdot \left(a_1^2 - a_2^2\right) \\ D_3 &= a_2 c \qquad D_4 = c^2 - \frac{1}{4} \cdot \left(a_1^2 - a_2^2\right) \end{aligned} \tag{6.106}$$

The solutions is obtained for different values of the speed parameter α substituting the proper expressions of a_1, a_2 and c (see (6.85), (6.86) and (6.87)).

The light damping solution is still fit in the condition of critical damping for positive values of the variable R substituting the proper values of a_1, a_2 and c (see (6.90) and (6.91)); when R assumes negative values there is the double pole $A_3 = A_4$ and the integral in (6.98) is computed using (6.100). In this case the solution is:

$$y(R) = \frac{2}{\alpha^4 + 3} \cdot e^{cR} \cdot \left(c - \sqrt{\alpha^4 + 3} \cdot R\right) \tag{6.107}$$

At supercritical damping $(\beta > \beta_{cr})$ the poles change. The solution (6.105) is still fit for positive values of R but with different values of coefficients:

$$D_2 = c^2 - \frac{1}{4}\left(a_1^2 + a_2^2\right)$$

$$D_4 = c^2 + \frac{1}{4}\left(a_1^2 + a_2^2\right)$$

while for $R < 0$ the solution is:

$$y(R) = \frac{1}{a_2(D_4^2 - D_3^2)} \cdot \left[\left(D_3 + D_4\right) \cdot e^{(c-a_2)\cdot R} - \left(D_4 - D_3\right) \cdot e^{(c+a_2)\cdot R} \right] \tag{6.108}$$

The plots of the non-dimensional displacement are shown as a function of the non-dimensional variable R and for different values of the speed and damping parameters α and β . In the absence of damping $(\beta = 0)$ or in the condition of sub-critical damping $(\beta < 1)$ when the load speed is smaller than the critical value $(\alpha < 1)$, the diagram of the displacement is almost symmetric about the load position (perfectly symmetric only for $\alpha = 0$) and the maximum displacement occurs where the load is applied (see figure 6 and 7); when the parameter α is greater than one the diagram of the displacement is not symmetric and the maximum occurs in a previous section respect to the section where the load is applied.

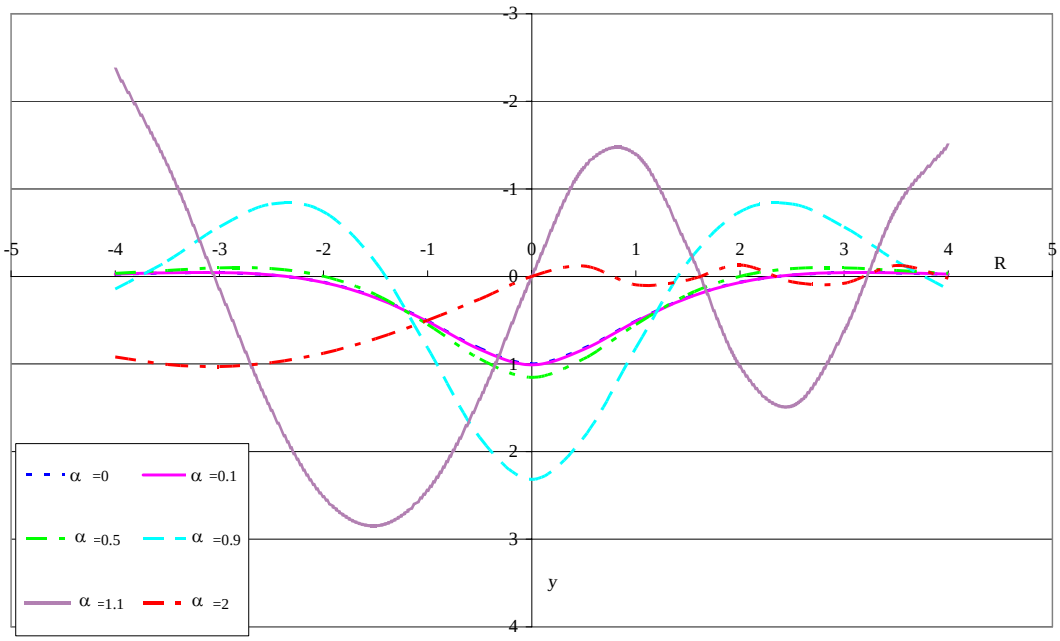

figure 6 displacement $y(R)$ in the absence of damping

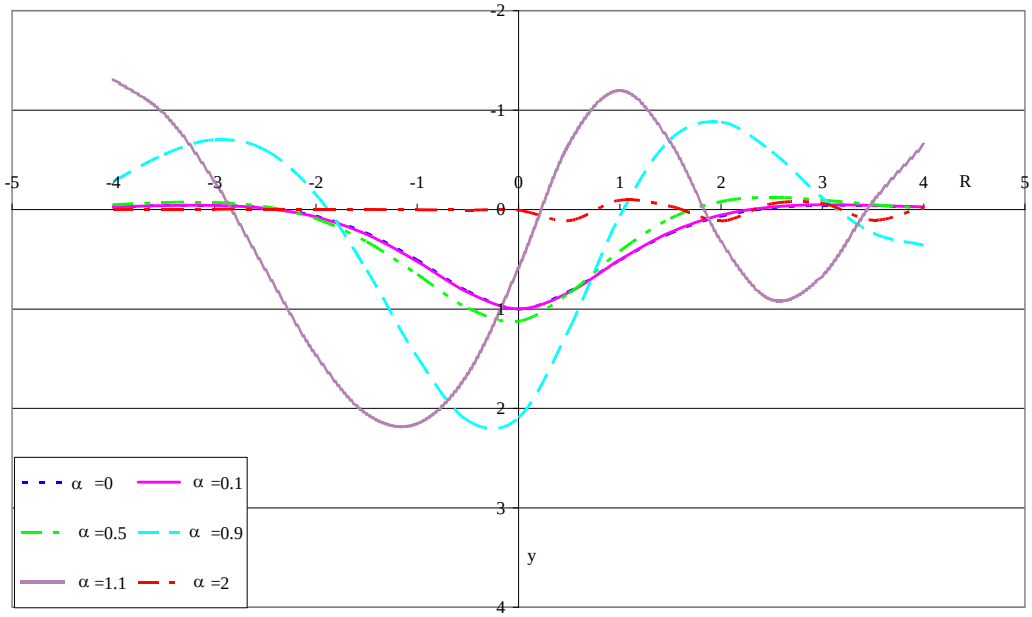

figure 7 displacement $y(R)$ for the sub-critical damping

In the super-critical damping condition $(\beta > \beta_{cr})$ the diagram is never symmetric (see figure 8 and 9), even if the load speed is smaller than the critical one.

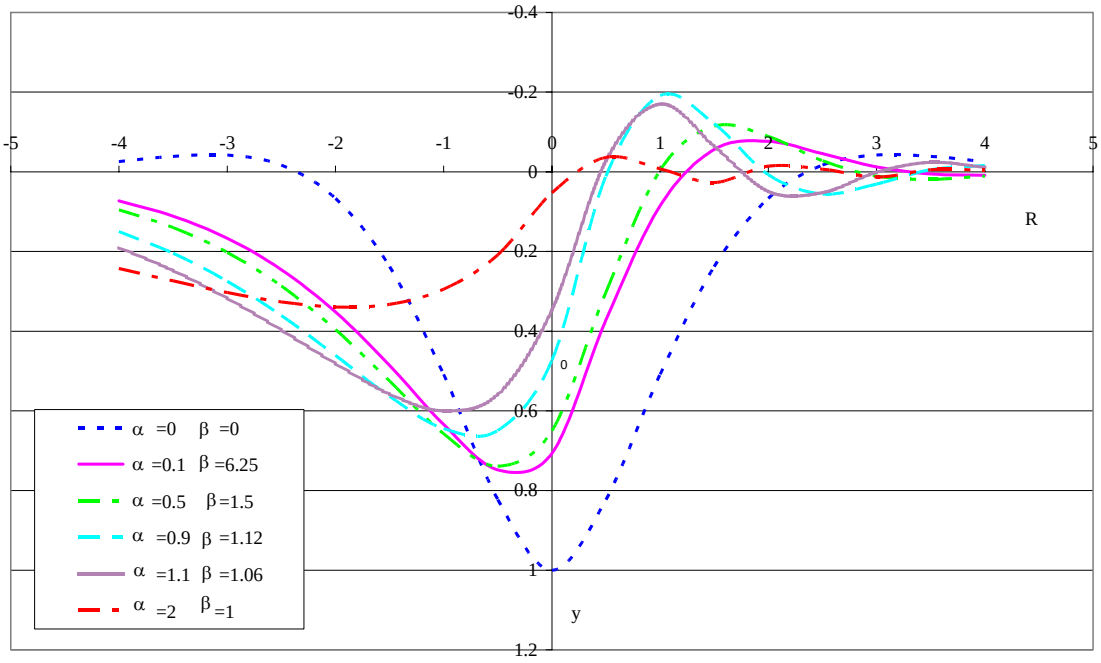

figure 8 displacement $y(R)$ for the critical damping

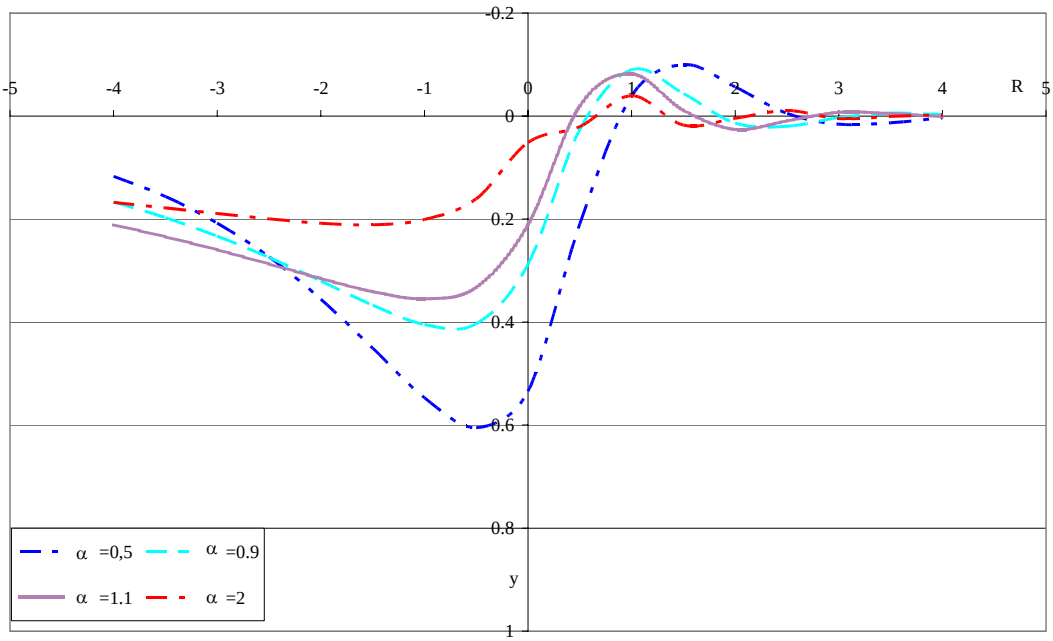

figure 9 displacement $y(R)$ for the super-critical damping

Regarding maximum amplifications it is possible to affirm that high amplifications occur when the load speed is near the value of the critical one (α = 0.9, α=1.1), while the dynamic displacement is almost equal to the static one when the load speed is far from the critical one (α = 0.1, α = 0.5, α = 2).

The solution of this load condition allows to introduce the concept of critical speed which is the value for which, if a train rides with slower speed, static displacement is not amplified by the dynamic effect; if the speed of train is near the value of critical speed there is a strong amplification of static displacements. One of the main results of this load condition is that it is possible to study the problem as though the train were at a stop, if the critical speed is rather high compared to the speed of the train.

6.1.3.2 The case of a fixed harmonic load

The dynamic track model is in figure 1. The load consists of a fixed harmonic concentrated force at $x = 0$; this load can be written by the complex form that is very rife in structural dynamics (Clough, Penzien, 1982):

$$F(t) = F_0 \cdot e^{i\omega t} \tag{6.109}$$

The boundary conditions are:

$$\lim_{x \to +\infty} y(x,t) = 0 \tag{6.110}$$

$$\lim_{x \to -\infty} y(x,t) = 0 \tag{6.111}$$

$$\frac{\partial y(0,t)}{\partial x} = 0 \tag{6.112}$$

$$EI \frac{\partial^3 y(0,t)}{\partial x^3} = 0.5 \cdot F_0 e^{i\omega t} \tag{6.113}$$

At the quasi-stationary state the solution of the differential equation (6.1) can be written in the form:

$$y(x,t) = w(x) \cdot e^{i\omega t} \tag{6.114}$$

the partial derivatives are obtained:

$$\frac{\partial^4 y(x,t)}{\partial x^4} = w^{IV}(x)\cdot e^{i\omega t} \tag{6.115}$$

$$\frac{\partial y(x,t)}{\partial t} = i\omega w(x)\cdot e^{i\omega t} \tag{6.116}$$

$$\frac{\partial^2 y(x,t)}{\partial t^2} = (i\omega)^2 \cdot w(x)\cdot e^{i\omega t} = -\omega^2 \cdot w(x)\cdot e^{i\omega t} \tag{6.117}$$

Substituting the partial derivates in (6.1):

$$EI\cdot w^{IV}(x) + \left[-\omega^2\mu + i\omega b + k\right]\cdot w(x) = 0 \tag{6.118}$$

The solution of the differential equation is practically equal to the one for the Winkler beam in the static case if the foundation coefficient k is replaced by the complex coefficient $k*$ (Esveld 1997, 2001):

$$k* = k - \omega^2\cdot\mu + i\omega b \tag{6.119}$$

It is easy to identify the modulus and the phase of the complex expression, if the complex stiffness is written in the following form:

$$k* = \sqrt{[(k-\omega^2\mu)^2 + \omega^2 b^2}\cdot e^{i\cdot\arctan\left[\frac{\omega b}{k-\omega^2 b}\right]} \tag{6.120}$$

The dynamic problem can be solved considering the solution of the static case $(\mu = b = 0)$:

$$w^{IV}(x) + 4\vartheta^4\cdot w(x) = 0 \tag{6.121}$$

The parameter ϑ is defined by (6.22) and here recalled:

$$\vartheta = \sqrt[4]{\frac{k}{4EI}}$$

Moreover the characteristic length and the wavelength can be defined:

$$L = \frac{1}{\vartheta} \qquad (6.122);\ \lambda = 2\pi L \tag{6.123}$$

The solution is in the form:

$$w(x) = e^{\vartheta x}\cdot\left(c_1\cos(\vartheta x) + c_2\sin(\vartheta x)\right) + e^{-\vartheta x}\cdot\left(c_3\cos(\vartheta x) + c_4\sin(\vartheta x)\right) \tag{6.124}$$

The constants are found out by the boundary conditions; the first one (6.110) and the second one (6.111) give:

$$c_1 = c_2 = 0 \tag{6.125}$$

the condition (6.112) gives:

$$c_3 = c_4 \tag{6.126}$$

The value of the constant is deduced by the fourth boundary condition (6.113):

$$EI \cdot w^{III}(x) \cdot e^{i\omega t} = 0.5 \cdot F_0 \cdot e^{i\omega t} \tag{6.127}$$

The derivates of the displacement function $w(x)$ are:

$$\begin{aligned} w(x) &= e^{-\vartheta x} \cdot c_3 \cdot \left(\cos(\vartheta x) + \sin(\vartheta x)\right) \\ w^{I}(x) &= -2\vartheta e^{-\vartheta x} \cdot c_3 \cdot \sin(\vartheta x) \\ w^{II}(x) &= 2\vartheta^2 e^{-\vartheta x} \cdot c_3 \cdot \left(-\cos(\vartheta x) + \sin(\vartheta x)\right) \\ w^{III}(x) &= 4\vartheta^3 e^{-\vartheta x} \cdot c_3 \cdot \cos(\vartheta x) \end{aligned} \tag{6.128}$$

The constant value is:

$$4EI\vartheta^3 c_3 = 0.5F_0 \qquad \Rightarrow \qquad c_3 = c_4 = \frac{F_0}{8EI\vartheta^3} = \frac{F_0\vartheta}{2k} = \frac{F_0}{2kL} \tag{6.129}$$

The expression of the static displacement is:

$$w(x) = \frac{F_0}{2kL} e^{-\frac{|x|}{L}} \cdot \left(\cos\left(\frac{x}{L}\right) + \sin\left(\frac{|x|}{L}\right)\right) \tag{6.130}$$

The solution of the dynamic problem is the same if the complex stiffness k^* and the complex characteristic length L^* are substituted for k and L:

$$w(x) = \frac{F_0}{2k^*L^*} e^{-\frac{|x|}{L^*}} \cdot \left(\cos\left(\frac{x}{L^*}\right) + \sin\left(\frac{|x|}{L^*}\right)\right) \tag{6.131}$$

k^* is given by (6.120).

Previously two non dimensional parameters have been defined: W and β. The first one is the ratio between the load frequency ω and the fundamental frequency of the

system ω_0; β is the ratio between the damping parameter b and the critical damping b_{cr}. The complex stiffness is written as a function of the two dimensionless parameters:

$$k^* = k \cdot \sqrt{\left(1-\frac{\omega^2}{\omega_0^2}\right)^2 + 4 \cdot \frac{\omega^2}{\omega_0^2} \cdot \beta} \cdot e^{i \cdot \arctan\left[\frac{2 \cdot \frac{\omega}{\omega_0} \cdot \beta}{1-\frac{\omega^2}{\omega_0^2}}\right]} \tag{6.132}$$

In the static case the characteristic length depends on the static stiffness by the equation (6.122), the same relation is still valid in the dynamic case but the complex stiffness k^* is substituted for k:

$$L^* = \frac{1}{\vartheta^*} = \frac{\sqrt[4]{4EI}}{\sqrt[4]{k*}} \tag{6.133}$$

Placed that:

$$\Gamma = \left(1-W^2\right)^2 + 4\beta^2 W^2 \qquad (6.134); \quad \Omega = \arctan\left[\frac{2 \cdot W \cdot \beta}{1-W^2}\right] \tag{6.135}$$

Hence:

$$\begin{aligned} k^* &= k \cdot \Gamma^{1/2} \cdot e^{\frac{i\Omega}{4}} \\ L^* &= \frac{\sqrt[4]{EI4}}{k^{1/4}\Gamma^{1/8}e^{i\Omega/4}} = L \cdot \Gamma^{-1/8} \cdot e^{-i\Omega/4} \end{aligned} \tag{6.136}$$

In which L is the static characteristic length.

k^* and L^* are substituted in the expression of the static displacement to obtain the dynamic one:

$$\begin{aligned} w(x) = \frac{F_0}{2kL} \cdot \Gamma^{-3/8} \cdot e^{-(i3\Omega)/4} \cdot e^{-\frac{|x|}{L}} \cdot \Gamma^{-1/8} \cdot e^{(i\Omega)/4} \cdot \\ \cdot \left(\cos\left(\frac{x}{L}\Gamma^{1/8}e^{i\Omega/4}\right) + \operatorname{sen}\left(\frac{|x|}{L}\Gamma^{1/8}e^{i\Omega/4}\right)\right) \end{aligned} \tag{6.137}$$

It is of interest to know the transfer function $H_w(\omega)$ between the load and the displacement at $x = 0$:

$$H_w(\omega) = \frac{w(0)}{F_0}$$

$$w(0) = \frac{F_0}{2k^* L^*} = \frac{F_0}{8EI\vartheta^{*3}} \tag{6.138}$$

hence:

$$H_w(\omega) = \frac{1}{8EI\theta^{*3}} \tag{6.139}$$

(6.139) is written as a function of W and β substituting (6.136) for k^* and L^* :

$$H_w(W) = \frac{1}{2k\Gamma^{1/2}e^{i\Omega}L\Gamma^{-1/8}e^{-i\Omega/4}} \tag{6.140}$$

Substituting (6.134) and (6.135):

$$H_w(\omega/\omega_0) = \frac{1}{2kL}\cdot\left(\left(1-\frac{\omega^2}{\omega_0^2}\right)^2 + 4\beta^2\frac{\omega^2}{\omega_0^2}\right)^{-3/8} \cdot e^{-i\frac{3}{4}\cdot\arctan\left[\frac{\frac{2\omega}{\omega_0}\cdot\beta}{1-\frac{\omega^2}{\omega_0^2}}\right]} \tag{6.141}$$

The modulus of the transfer function is given by the term preceding the exponential function in (6.141):

$$\left|H_w(\omega/\omega_0)\right| = \frac{1}{2kL}\cdot\left(\left(1-\frac{\omega^2}{\omega_0^2}\right)^2 + 4\beta^2\frac{\omega^2}{\omega_0^2}\right)^{-3/8} \tag{6.142}$$

whereas the phase is:

$$\varphi = \frac{3}{4}\arctan\left(\frac{2\frac{\omega}{\omega_n}\beta}{1-\frac{\omega^2}{\omega_0^2}}\right) \tag{6.143}$$

The modulus and the phase are showed in figure 10 and 11.

The transfer function has been compared with that is obtained by the study of a further simplified model with a single degree of freedom (SDF). The track system is modeled as a concentrated mass while a spring and a damper give elastic and viscous properties

respectively. Proper correlations have been found to make a direct comparison between the two models. The transfer function module and phase of a single degree of freedom system are:

$$N = \left(\left(1 - \frac{f^2}{f_n^2} \right)^2 + 4\xi^2 \frac{f^2}{f_n^2} \right)^{-1/2} \qquad (6.144) \varphi = \arctan \left(\frac{2 \frac{f}{f_n} \xi}{1 - \frac{f^2}{f_n^2}} \right) \qquad (6.145)$$

The module of the transfer function is practically equal except for the exponent. The plot of the module of the two transfer functions (figure 10) is analogue, it is observed a peak value when the load frequency is near the frequency of system; the peak is equal if the dimensionless damping parameter is chosen adequately.

The plots of phase of two transfer functions are very much alike, but the phase of the discrete system approaches -π for high frequencies, instead that of the continuous model approaches –3/4π.

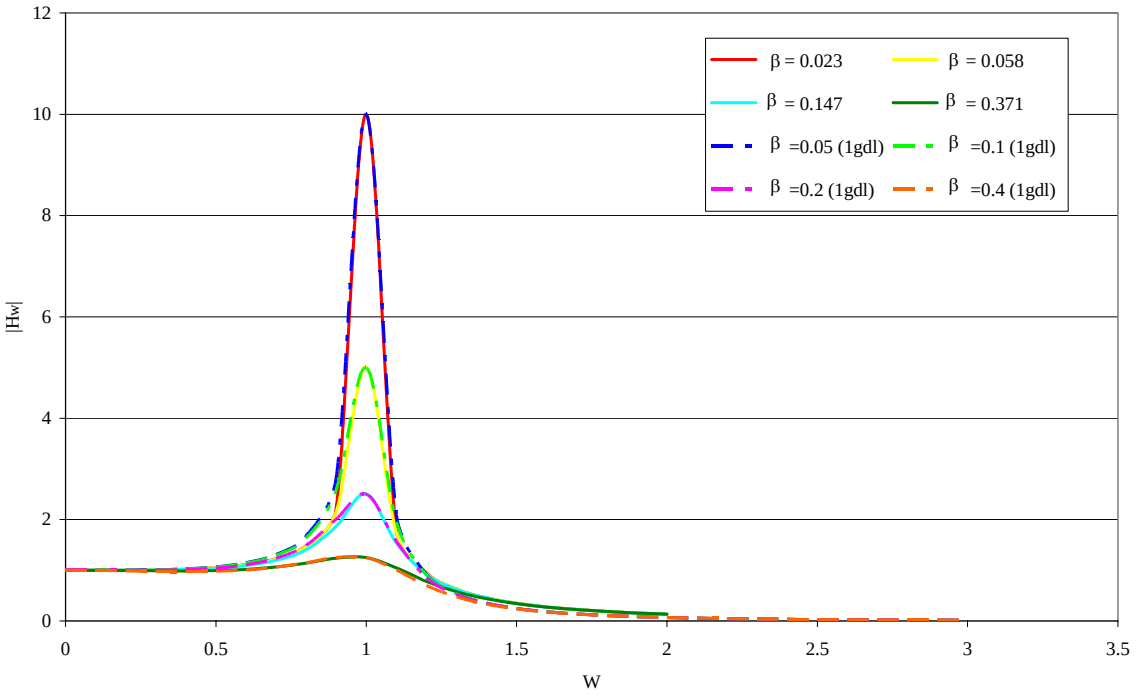

figure 10 Modulus of the transfer function and amplification coefficient of SDF

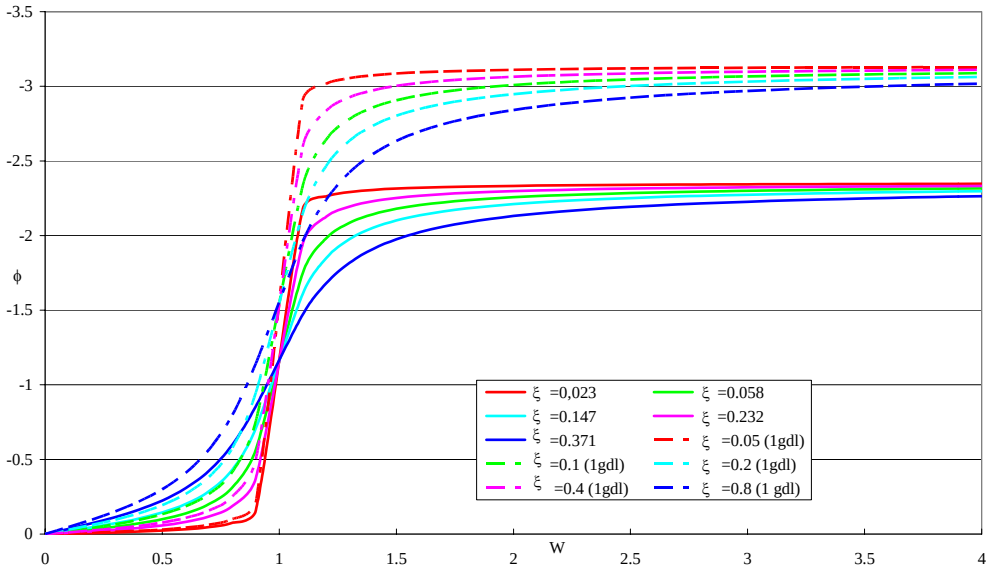

figure 11 Phase of the continuous beam and of SDF

6.1.4. Representation of rail defects

The rail profile can be described as a stochastic process that can be assumed stationary and ergodic and so it is synthetically represented by means of a power spectral density (PSD) function of the vertical defects. Rail defects are measured by some Railway Institutions and are represented in terms of power spectral density, which describes the frequency content of the mean square value of the signal (rail profile defects), if the random process has a mean value of zero (Crispino, 1996).

The power spectral density function S_p can be given as a function of the spatial frequency $F\left(\text{cycles/m}\right)$ in which case it is expressed in $\text{m}^2/\left(\text{cycles/m}\right)$, or as a function of the temporal frequency $F\left(\text{cycles/s} = f\right)$ then expressed in $\text{m}^2/\left(\text{cycles/s}\right)$. If the spatial power spectrum is known, the temporal one is easily obtained when the train speed is known. The temporal frequency written as a function of the spatial one is:

$$f_{Hz} = \frac{V_{km/h}}{3.6} \cdot F_{cycles/m} = V_{m/s} \cdot F_{cycles/m} \tag{6.146}$$

The relationship between the spatial power spectrum and the temporal one is then obtained as:

$$S(f) = \left[\frac{\mathrm{m}^2}{\mathrm{cycles/s}} \right] = \frac{S(F) \left[\frac{\mathrm{m}^2}{\mathrm{cycles/m}} \right]}{V \left[\mathrm{m/s} \right]} \tag{6.147}$$

Finally, if the temporal frequency is expressed in rad/s the following relations are considered:

$$\omega_{rad/s} = 2\pi \cdot \frac{V_{km/h}}{3.6} \cdot F_{cycles/m} = 2 \cdot \pi \cdot V_{m/s} F_{cycles/m} \tag{6.148}$$

$$S(\omega) \left[\frac{\mathrm{m}^2}{\mathrm{rad/s}} \right] = 2\pi \cdot \frac{S(F) \left[\frac{\mathrm{m}^2}{\mathrm{cycles/m}} \right]}{V \left[\mathrm{m/s} \right]} \tag{6.149}$$

In the railway field the following four mediated power spectra are commonly used (see figure 12):

- the basic spectrum: for the Swedish (SAB Swedel) and German (DB) Railway Institutions;
- the bilinear British Railways spectrum;
- the curvilinear French Railway Institutions (SNCF) spectrum;
- the power spectrum of the American Railway Standard.

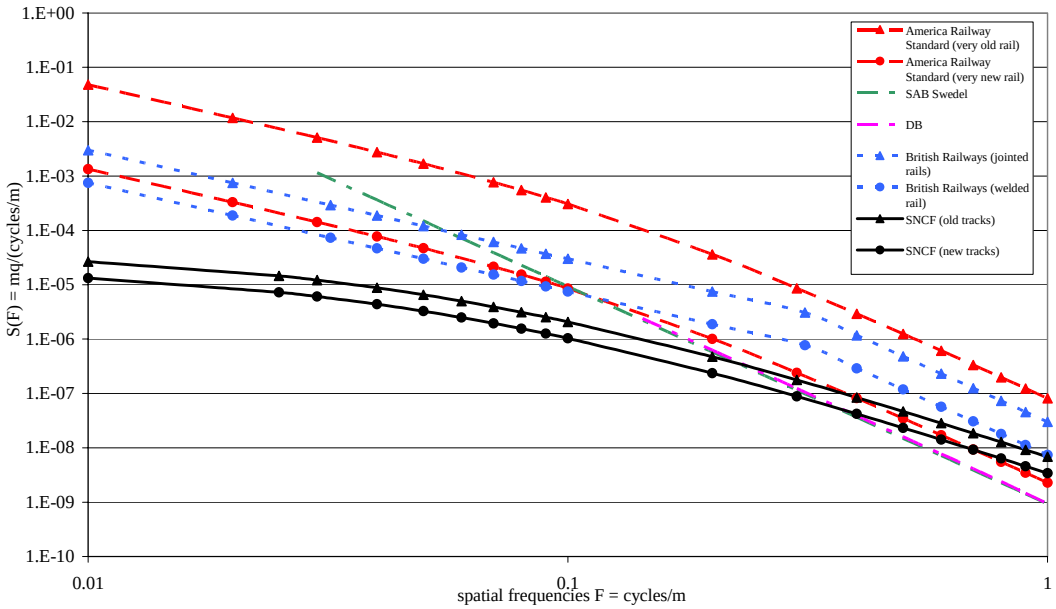

figure 12 mediated power spectra of different Railway Institution

The analytical expressions of the basic spectra of the Swedish and German Railway Institutions are slightly different, but they are represented by means a straight line in a logarithmic plot. The expression of the spatial power spectrum for the Swedish Railway Institution is (Panagin, 1990):

$$S(F) = CF^{-N}\left(\mathrm{m}^2 / Cycles / m\right) \tag{6.150}$$

For the spatial vertical spectrum C and N assume the following values:

$C = 0.928 \cdot 10^{-9}$ (it represents the vertical coordinates when the horizontal one F is zero)

$N = 4$ (It gives the slope of the straight line representing the power spectrum)

Hence:

$$S(F) = 0.928 \cdot 10^{-9} \cdot F^{-4}\left(\mathrm{m}^2 / Cycles / m\right)$$

The German railway institution has a spatial power spectrum for high speed lines when the spatial frequencies are such as $F > 0.143$ and it is written (Panagin, 1990):

$$S(F)=\frac{10^{-9}F^{-4}}{1+\left(\frac{2\pi F}{10}\right)^{6}}\left(\mathrm{m}^2/\mathrm{cycle/m}\right) \tag{6.151}$$

Two straight lines representing (6.150) and (6.151) are practically coincident.

The bilinear British Railways spectrum has the analytical expression of the basic spectrum, but for smaller spatial frequencies the slope of the line (expressed by the parameter N) is smaller than the slope of the second one. The British Railway has spatial spectra both for good railway lines with welded rails and for bad lines with joined rails. For welded rails the spectrum is (Panagin, 1990):

$$S(F)=\begin{cases}\dfrac{7.5\cdot10^{-8}}{F^2}\ (m^2/cycles/m) & \text{for} \quad 3.2\cdot10^{-2}V<F<3.12\cdot10^{-1}V\\ \dfrac{7.5\cdot10^{-9}}{F^4}(m^2/cycles/m) & \text{for} \quad 3.10\cdot10^{-1}V<F<6.24\cdot10^{-1}V\end{cases} \tag{6.152}$$

and for joined rails is:

$$S(F)=\begin{cases}\dfrac{3\cdot10^{-7}}{F^2}\ (m^2/cycles/m) & \text{for} \quad 3.2\cdot10^{-2}<F<3.12\cdot10^{-1}\\ \dfrac{3\cdot10^{-8}}{F^4}(m^2/cycles/m) & \text{for} \quad 3.10\cdot10^{-1}<F<6.24\cdot10^{-1}\end{cases} \tag{6.153}$$

The French Railway Institution (SNCF) has defined the power spectrum of the rail profile considering both vertical and horizontal defects. The data are obtained by tests along the Paris-Toulose line between the 136th and 137th kilometre considering a part of the line that is representative of the whole line. Tests are made by means the Mauzin carriage in the space of spatial frequencies between 0.025 and 0.5 cycles/m. It is important to underline that the precision of the measurements is insufficient when the frequencies outside this space are considered (Panagin, 1990).

The power spectral density function as a function of spatial frequency which is adopted by the French Railway Institution is (Panagin, 1990):

$$S(F)=\frac{C}{(a+2\pi F)^N}\qquad\left(\mathrm{m}^2/\mathrm{cycles/m}\right) \tag{6.154}$$

In which N is equal to 3; F is the spatial frequency; C is a parameter depending on the age of the railway track, in particular: $C = 10^{-6}$ or $2 \cdot 10^{-6}$ for new and old tracks respectively; a is equal to 0.36.
The lateral power spectrum is:

$$S(F) = \frac{0.368 \cdot 10^{-6}}{(0.136 + 2\pi F)^3} \quad \left(\text{m}^2/\text{cycles/m}\right) \tag{6.155}$$

Finally the power spectrum of the America Railway Standard is considered given for six line grades (line grade one is the worst line and six is the best line). The analytical expression is in cm^2/rad/m as a function of the spatial frequency in rad/m (X. Lei, N.A. Noda, 2002):

$$S(\omega) = \frac{kA_v\omega_c^2}{(\omega^2 + \omega_c^2) \cdot \omega^2} \quad \left[\text{cm}^2/\text{rad/m}\right] \tag{6.156}$$

Where A_v and ω_c are coefficients associated with the line grade (see table 3) and k is a constant normally equal to 0.25.

6.1.5 The effect of unsprung mass and rail defects

The railway model in figure 13 is now applied for a different load condition. The Euler beam is solved considering the effect of rail defects that are represented by a dynamic overload:

$$Q = -M_u\left[\ddot{y}(x,t) + \ddot{r}(x,t)\right] \tag{6.157}$$

M_u is the unsprung mass of the vehicle that is the axle weight with the wheels, $w(x,t)$ is the rail displacement function and $r(x,t)$ is the rail defect function that can be expressed as:

$$r(x,t) = R \cdot e^{i\omega t} \tag{6.158}$$

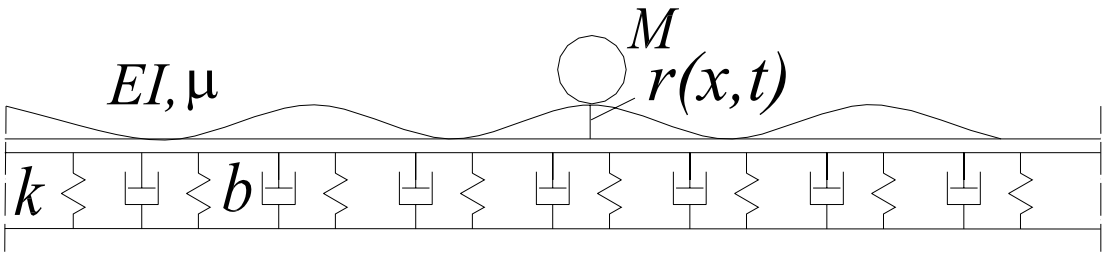

figure 13 Euler beam on elastic foundation with unsprung mass M_u and rail defects $r(x,t)$

Three boundary condition are given by (6.110), (6.111) and (6.112), while the forth is now different and given by:

$$EI\frac{\partial^3 y(x,t)}{\partial x^3} = -0.5M_u \cdot \left(\frac{\partial^2 v(0,t)}{\partial t^2} + \ddot{r}\right) \tag{6.159}$$

The state stationary is still considered and the solution is in the form (6.114). Substituting the proper derivates the equation is (6.118). The solution is obtained if the static case is solved and it is still in the following form:

$$w(x) = e^{\vartheta x}\cdot\left(c_1\cos(\vartheta x) + c_2\sin(\vartheta x)\right) + e^{-\vartheta x}\cdot\left(c_3\cos(\vartheta x) + c_4\sin(\vartheta x)\right)$$

In which ϑ is still given by (6.22) and the constants values are found out considering the boundary conditions. Three conditions still give:

$$c_1 = c_2 = 0 \qquad c_3 = c_4$$

The shear condition gives:

$$EIw'''(0) = -0.5\omega^2 M_u \cdot \left(w(0) + R\right) \tag{6.160}$$

Remembering the derivates of the function $w(x)$(6.128), the following relation is obtained:

$$4\vartheta^3 c_3 = 0.5\cdot\omega^2\cdot M_u\cdot\left(R + c_3\right) \tag{6.161}$$

The constant c_3 is found:

$$c_3 = \frac{M_u\cdot\omega^2}{8EI\vartheta^3 - \omega^2\cdot M_u} \tag{6.162}$$

The static displacement is:

$$w(x) = \frac{M_u \cdot \omega^2}{8EI\vartheta^3 - \omega^2 \cdot M_u} \cdot e^{-\vartheta x} \cdot \left(\cos\left(\vartheta x\right) + \sin\left(\vartheta x\right)\right) \tag{6.163}$$

Substituting the complex equivalent stiffness k^* and the complex characteristic length L^* the dynamic displacement is given by:

$$w(x) = \frac{M_u \cdot \omega^2}{8EI\vartheta^{*3} - \omega^2 \cdot M_u} \cdot e^{-\vartheta^* x} \cdot \left(\cos\left(\vartheta^* x\right) + \sin\left(\vartheta^* x\right)\right) \tag{6.164}$$

The transfer function of the displacement is:

$$H\left(\omega\right) = w(0) = \frac{M_u \cdot \omega^2}{8EI\vartheta^{*3} - \omega^2 \cdot M_u} \tag{6.165}$$

6.2 DOUBLE BEAM CONTINUOUS MODEL

If an innovative antivibration track has to be studied, it can be convenient to model the track as a double beam, in which the upper beam generally represents the rail and it is characterized by its distributed mass and its flexural stiffness, while the lower beam can represent the sleepers or a concrete floating slab. This model is very proper to study the static and dynamic behaviour of innovative tracks because they often have two or more elastic levels. The dynamic effects of the wheel-rail irregularities are considered but the effect of the movement of the train is disregarded; in other words the load consists of a harmonic fixed force and so it is considered that the train speed is far from the critical one.

6.2.1 The lower beam with zero bending stiffness

The upper beam represents the rail that is characterized by its mass for unit of length μ_1 and its flexural stiffness EI. The lower beam represents the sleepers with their distributed mass μ_2 and it has a zero bending stiffness. The first viscoelastic level is between the two beams and it can represent the under-rail pads, it is characterized by

an elastic parameter k_1 and an equivalent viscous damping coefficient b_1. The second level gives the viscoelastic contribution of the ballast through the coefficients k_2 and b_2 (figure 14).

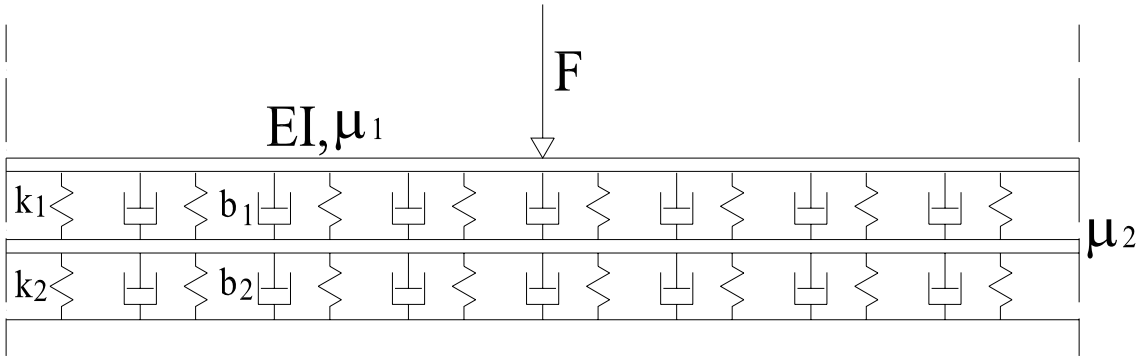

figure 14 double beam model

The solution of the dynamic problem is obtained considering the solution of the Winkler beam in the static case (Esveld, 2001). The load is expressed:

$$F(t) = F_0 \cdot e^{i\omega t} \tag{6.166}$$

The equation of the dynamic equilibrium is written for each beam:

$$\begin{cases} EI \cdot \dfrac{\partial^4 y_1(x,t)}{\partial x^4} + \mu_1 \cdot \dfrac{\partial^2 y_1(x,t)}{\partial t^2} + b_1\left(\dfrac{\partial y_1(x,t)}{\partial t} - \dfrac{\partial y_2(x,t)}{\partial t}\right) + k_1\left(y_1(x,t) - y_2(x,t)\right) = 0 \\ \mu_2 \cdot \dfrac{\partial^2 y_2(x,t)}{\partial t^2} + b_2 \dfrac{\partial y_2(x,t)}{\partial t} + b_1\left(\dfrac{\partial y_2(x,t)}{\partial t} - \dfrac{\partial y_1(x,t)}{\partial t}\right) + k_1\left(y_2(x,t) - y_1(x,t)\right) + k_2 \cdot y_2(x,t) = 0 \end{cases}$$

The displacements of the two beams have the following expressions:

$$y_1(x) = w_1(x) \cdot e^{i\omega t} \qquad y_2(x) = w_2(x) \cdot e^{i\omega t}$$

The equations of the dynamic equilibrium are written considering (6.115),(6.116) and (6.117):

$$\begin{cases} EIw^{IV}(x) - \omega^2 \mu_1 w_1 + \omega\, b_1 i \cdot (w_1 - w_2) + k_1 \cdot (w_1 - w_2) = 0 \\ -\omega^2 \mu_2 w_2 + \omega\, b_1 i \cdot (w_2 - w_1) + i\omega\, b_2 w_2 + k_1 \cdot (w_2 - w_1) + k_2 w_2 = 0 \end{cases} \tag{6.167}$$

Two complex stiffness are defined:

$$k_1^* = k_1 - \omega^2 \mu_1 + i\omega b_1 \qquad k_2^* = k_2 - \omega^2 \mu_2 + i\omega b_2$$

The displacement of the second beam w_2 is obtained from the second equation of the system (6.167) :

$$w_2(-\omega^2 \mu_2 + i\omega\, b_2 + k_2) + w_2(i\omega\, b_1 + k_1) - w_1(i\omega\, b_1 + k_1) = 0 \tag{6.168}$$

Set that:

$$A = k_1 + i\omega\, b_1 \qquad\qquad B = -\omega^2 \mu_2 + i\omega\, b_2 + k_2 \tag{6.169}$$

hence:

$$w_2 = \frac{A}{A+B} \cdot w_1 \tag{6.170}$$

w_2 , given by (6.170), is substituted in the first equation of the system (6.167):

$$EI\, w_1^{IV} - \omega^2 \mu_1 w_1 + A w_1 - \frac{A^2}{A+B} w_1 = 0 \tag{6.171}$$

$$EI\, w_1^{IV} - \omega^2 \mu_1 w_1 + \frac{AB}{A+B} w_1 = 0 \tag{6.172}$$

A new equivalent stiffness is defined:

$$k_t = \frac{AB}{A+B} \tag{6.173}$$

Hence:

$$EI\, w_1^{IV} + (-\omega^2 \mu_1 + k_t) \cdot w_1 = 0 \tag{6.174}$$

The following transfer function is obtained:

$$H_r(\omega) = \frac{w(0)}{F_0} = \frac{1}{8EI\beta^3} \tag{6.175}$$

in which:

$$\beta^4 = \frac{k_t^2 - \omega^2 \mu_1}{16EI} \tag{6.176}$$

6.2.2 An "infinite" and flexible Floating slab

Both upper and lower beam are characterized by their mass for unit of length μ_1 and μ_2 and their bending stiffness E_1I_1 and E_2I_2. The two elastic levels are represented by the elastic coefficients: k_1 and k_2 (figure 15).

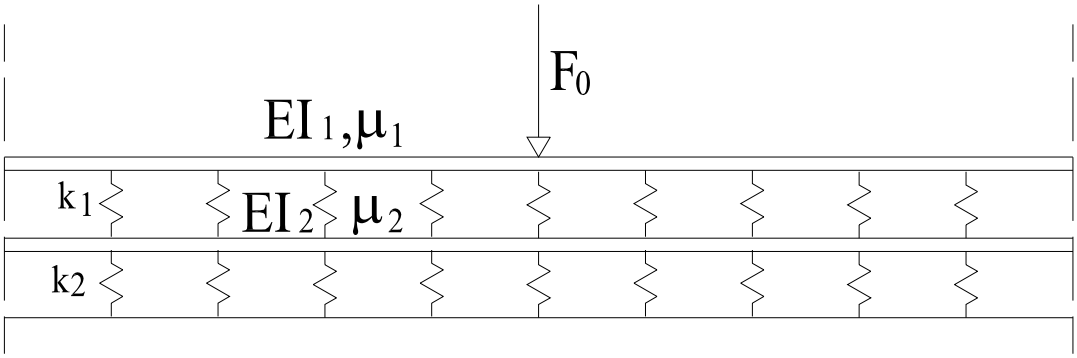

figure 15 double beam model: flexible slab

The problem is studied in the absence of damping and a constant concentrated load F_0 is considered (Acquati, 2003).

The equations that govern the problem are:

$$\begin{cases} E_1 I_1 w_1^{IV} + k_1(w_1 - w_2) = 0 \\ E_2 I_2 w_2^{IV} + k_2 w_2 + k_1(w_2 - w_1) = 0 \end{cases} \tag{6.177}$$

The solution is written in the form:

$$y_1 = A_1 e^{s_1 \cdot x} \qquad y_2 = A_2 e^{s_2 \cdot x} \tag{6.178}$$

$$\begin{cases} k_1(w_2 - w_1) = E_1 I_1 w_1^{IV} \\ E_2 I_2 w_2^{IV} + k_2 w_2 + E_1 I_1 w_1^{IV} = 0 \end{cases} \tag{6.179}$$

Substituting (6.178) in the second equation of the system (6.179):

$$E_2 I_2 A_2 s_2^4 e^{s_2 x} + k_2 A_2 e^{s_2 x} + E_1 I_1 A_1 s_1^4 e^{s_1 x} = 0 \tag{6.180}$$

hence: $s_1 = s_2$

The solutions are written:

$$y_1 = A_1 e^{s \cdot x} \qquad y_2 = A_2 e^{s \cdot x} \tag{6.181}$$

The first equation of the system becomes:

$$(E_1 I_1 s^4 + k_1) \cdot A_1 = k_1 A_2 \tag{6.182}$$

Hence:

$$A_1 = \frac{k_1}{E_1 I_1 s^4 + k_1} \cdot A_2 \tag{6.183}$$

(6.183) is substituted in the second equation of the system (6.177):

$$E_2 I_2 A_2 s^4 + k_2 A_2 + k_1 A_2 = k_1 A_1$$

$$E_2 I_2 A_2 s^4 + k_2 A_2 + k_1 A_2 = \frac{k_1^2}{E_1 I_1 s^4 + k_1} A_2 \tag{6.184}$$

the following equation of the eighth degree in s is obtained:

$$E_2 I_2 E_1 I_1 s^8 + [E_2 I_2 k_1 + E_1 I_1 \cdot (k_2 + k_1)] \cdot s^4 + k_1 k_2 = 0 \tag{6.185}$$

it is solved as an equation of the second degree in s^4:

$$s^4 = \frac{-[E_2 I_2 k_1 + E_1 I_1 (k_2 + k_1)] \pm \sqrt{[E_2 I_2 k_1 + E_1 I_1 (k_2 + k_1)]^2 - 4 k_1 k_2 E_1 I_1 E_2 I_2}}{2 E_1 I_1 E_2 I_2} \tag{6.186}$$

$s_1^4 \langle 0$ $\qquad s_{1,j}^2 = \pm i \sqrt{|\, s_1^4 \,|}$ $\qquad$ 4 solutions

$s_2^4 \langle 0$ $\qquad s_{2,j}^2 = \pm i \sqrt{|\, s_2^4 \,|}$ $\qquad$ 4 solutions

the eight roots of the equation are written in the form:

$s_{1,1} = \alpha \cdot (1 + i)$ $\qquad s_{2,1} = \beta \cdot (1 + i)$

$s_{1,2} = \alpha \cdot (1 - i)$ $\qquad s_{2,2} = \beta \cdot (1 - i)$

$s_{1,3} = \alpha \cdot (-1 - i)$ $\qquad s_{2,3} = \beta \cdot (-1 - i)$

$s_{1,4} = \alpha \cdot (-1 + i)$ $\qquad s_{2,4} = \beta \cdot (-1 + i)$

in which:

$$\alpha = \sqrt[4]{|\, s_1^4 \,|} \cdot \frac{\sqrt{2}}{2} \qquad \beta = \sqrt[4]{|\, s_2^4 \,|} \cdot \frac{\sqrt{2}}{2} \tag{6.187}$$

For the boundary conditions it is possible to disregard the growing terms and only the real terms are considered:

$$\begin{cases} y_1(x) = e^{-\alpha x}\left(A_{\alpha 1}^{(1)}\cos\alpha x + A_{\alpha 2}^{(1)}\sin\alpha x\right) + e^{-\beta x}\left(A_{\beta 1}^{(1)}\cos\beta x + A_{\beta 2}^{(1)}\sin\beta x\right) \\ y_2(x) = e^{-\alpha x}\left(A_{\alpha 1}^{(2)}\cos\alpha x + A_{\alpha 2}^{(2)}\sin\beta x\right) + e^{-\beta x}\left(A_{\beta 1}^{(2)}\cos\alpha x + A_{\beta 2}^{(2)}\sin\beta x\right) \end{cases} \quad (6.188)$$

The eight constants in the expression are determined through eight equations. Four equations derive from relations between the coefficients that are given by (6.183):

$$A_{\alpha 1}^{(1)} = \frac{k_1 \cdot A_{\alpha 1}^{(2)}}{k_1 - 4\alpha^4 E_1 I_1} \quad (6.189) \qquad A_{\alpha 2}^{(1)} = \frac{k_1 \cdot A_{\alpha 2}^{(2)}}{k_1 - 4\alpha^4 E_1 I_1} \quad (6.190)$$

$$A_{\beta 1}^{(1)} = \frac{k_1 \cdot A_{\beta 1}^{(2)}}{k_1 - 4\beta^4 E_1 I_1} \quad (6.191) \qquad A_{\beta 2}^{(1)} = \frac{k_1 \cdot A_{\beta 2}^{(2)}}{k_1 - 4\beta^4 E_1 I_1} \quad (6.192)$$

Four equations derive from boundary conditions: the slope of the rail and the slab deflection line at $x = 0$ is zero; while the shear on the rail at $x = 0$ is $F_0 / 2$, and on the slab is zero.

The derivate of the first order of the rail deflection line is:

$$\begin{aligned} y_1^{'}(x) = &-\alpha \cdot e^{-\alpha x}\left(A_{\alpha 1}^{(1)}\cos\alpha x + A_{\alpha 2}^{(1)}\sin\alpha x\right) + \alpha \cdot e^{-\alpha x}\left(-A_{\alpha 1}^{(1)}\sin\alpha x + A_{\alpha 2}^{(1)}\cos\alpha x\right) + \\ &-\beta \cdot e^{-\beta x}\left(A_{\beta 1}^{(1)}\cos\beta x + A_{\beta 2}^{(1)}\sin\beta x\right) + \beta \cdot e^{-\beta x}\left(-A_{\beta 1}^{(1)}\sin\beta x + A_{\beta 2}^{(1)}\cos\beta x\right) \end{aligned} \quad (6.193)$$

it is calculated at $x = 0$:

$$y_1^{'}(0) = -\alpha \cdot A_{\alpha 1}^{(1)} + \alpha \cdot A_{\alpha 2}^{(1)} - \beta \cdot A_{\beta 1}^{(1)} + \beta \cdot A_{\beta 2}^{(1)} = 0 \quad (6.194)$$

an analogous expression is valid for the slab deflection line:

$$y_2^{'}(0) = -\alpha \cdot A_{\alpha 1}^{(2)} + \alpha \cdot A_{\alpha 2}^{(2)} - \beta \cdot A_{\beta 1}^{(2)} + \beta \cdot A_{\beta 2}^{(2)} = 0 \quad (6.195)$$

Regarding on the shear condition the derivate of the third order of the rail deflection line is:

$$\begin{aligned} y_1^{III}(x) = &\left[2\alpha^3 e^{-\alpha x}\cdot(-\sin\alpha x + \cos\alpha x)\right]A_{\alpha 1}^{(1)} + \left[2\alpha^3 e^{-\alpha x}\cdot(\cos\alpha + \sin\alpha x)\right]A_{\alpha 2}^{(1)} + \\ &+\left[2\beta^3 e^{-\beta x}\cdot(-\sin\beta x + \cos\beta x)\right]A_{\beta 1}^{(1)} + \left[2\beta^3 e^{-\beta x}\cdot(\cos\beta x + \sin\beta x)\right]A_{\beta 2}^{(1)} \end{aligned} \quad (6.196)$$

it is calculated at $x = 0$:

$$y_1^{III}(0^+) = 2\alpha^3 A_{\alpha 1}^{(1)} + 2\alpha^3 A_{\alpha 2}^{(1)} + 2\beta^3 A_{\beta 1}^{(1)} + 2\beta^3 A_{\beta 2}^{(1)} = \frac{F_0}{2} \tag{6.197}$$

for the slab deflection line:

$$y_2^{III}(0^+) = 2\alpha^3 A_{\alpha 1}^{(1)} + 2\alpha^3 A_{\alpha 2}^{(1)} + 2\beta^3 A_{\beta 1}^{(1)} + 2\beta^3 A_{\beta 2}^{(1)} = 0 \tag{6.198}$$

It is obtained a system of eight equations.

6.3 SINGLE BEAM ON A PARTICULAR ELASTIC FOUNDATION

The model consists of the Euler beam described in the previous part and now the most important results are recalled. New antivibration railway systems are often designed introducing one or most elastic levels in the track to modify its static and dynamic behaviour. To understand the effect of these additions, different models are considered in the paper able to explain the effect of added flexibilities at different positions.

6.3.1 Lumped spring-mass models

The first model is a very simple mass-spring system characterized by a concentrated mass m, and a constant stiffness k (figure 16).

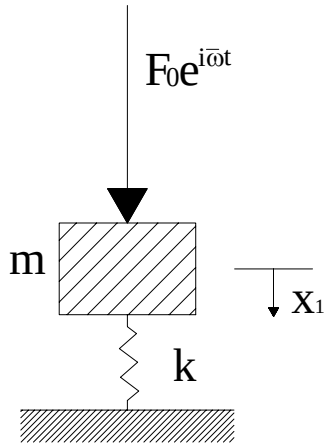

figure 16 Mass-spring system

This may very approximately represent the inertia and flexibility present under the rail.

The equation that governs the problem is:

$$m\ddot{x}_1 + kx_1 = F_0 e^{i\bar{\omega}t} \tag{6.199}$$

Dividing for the mass m:

$$\ddot{x}_1 + \frac{k}{m}x_1 = \frac{F_0}{m}\cdot\frac{k}{k}e^{i\bar{\omega}t} \tag{6.200}$$

The static displacement and the first system frequency are defined:

$$x_{st} = \frac{F_0}{k} \qquad \omega^2 = \frac{k}{m} \tag{6.201}$$

The solution can be written in the form:

$$x_1 = x_0 \cdot e^{i\bar{\omega}t} \qquad \Rightarrow \qquad \dot{x}_1 = i\bar{\omega}\cdot x_0 \cdot e^{i\bar{\omega}t} \qquad \ddot{x}_1 = -\bar{\omega}^2 \cdot x_0 \cdot e^{i\bar{\omega}t} \tag{6.202}$$

$$x_1 = \frac{F}{k}\cdot\frac{\omega^2}{\omega^2 - \bar{\omega}^2} = x_{st}\cdot\left(1-\frac{\bar{\omega}^2}{\omega^2}\right)^{-1} \tag{6.203}$$

The dynamic flexibility d_1 of the mass-spring system is given by:

$$d_1\left(\bar{\omega}/\omega\right) = \frac{x_1}{F} = \frac{1}{k}\cdot\left(1-\frac{\bar{\omega}^2}{\omega^2}\right)^{-1} \tag{6.204}$$

Consequently the dynamic stiffness is written as:

$$k_1\left(\bar{\omega}/\omega\right) = \frac{F}{x_1} = k\cdot\left(1-\frac{\bar{\omega}^2}{\omega^2}\right) \tag{6.205}$$

The dimensionless dynamic flexibility and stiffness are represented in figure 17 and 18 respectively.

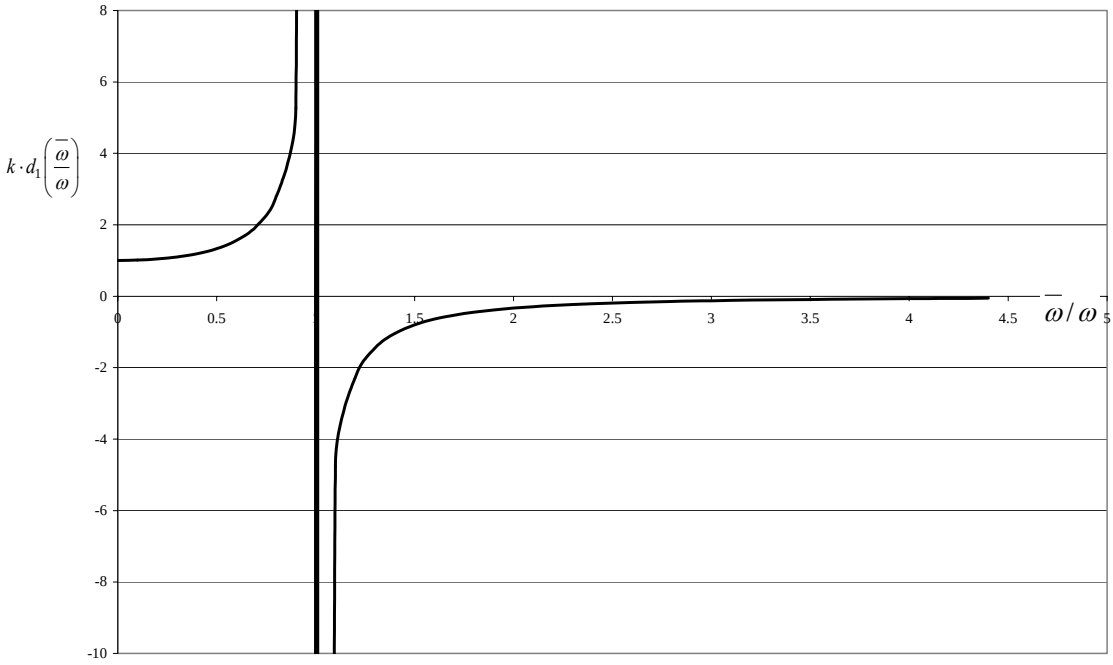

figure 17 dimensionless dynamic flexibility of mass-spring system

figure 18 dimensionless dynamic stiffness of mass-spring system

The point at $\overline{\omega}/\omega = 0$ in the figures above describes the static behaviour; when the resonance frequency is reached the stiffness assumes the value $k_1 = 0$ and the flexibility tends to infinite; at high frequencies $\left(\overline{\omega}/\omega \to \infty\right)$ the stiffness tends to infinite and so the flexibility tends to zero.

A spring-mass-spring model (figure 19) is now considered in which another spring is added at the top of the mass (representing as an example the flexibility of rail-sleepers fastenings), its stiffness being: $k_{fas} = \alpha \cdot k$ with $\alpha \geq 0$

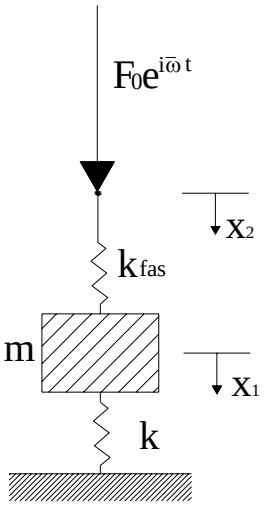

figure 19 spring-mass-spring model

The equations of motion are:

$$\begin{cases} m\ddot{x}_1 + kx_1 = F_0 e^{i\bar{\omega}t} \\ k_{fas}\cdot\left(x_2 - x_1\right) = F_0 e^{i\bar{\omega}t} \end{cases} \Rightarrow \begin{cases} m\ddot{x}_1 + kx_1 = F_0 e^{i\bar{\omega}t} \\ x_2 = \dfrac{F_0 e^{i\bar{\omega}t} + k_{fas}\cdot x_1}{k_{fas}} \end{cases} \tag{6.206}$$

Substituting x_1 still given by (6.203) in the second equation of (6.206), the displacement at the point of load application is given by:

$$x_2 = \frac{F}{k_{fas}} + \frac{F}{k}\cdot\frac{1}{1-\dfrac{\bar{\omega}^2}{\omega^2}} = \frac{F}{\alpha k} + \frac{F}{k}\cdot\frac{1}{1-\dfrac{\bar{\omega}^2}{\omega^2}} = \frac{F}{k}\cdot\left(\frac{1}{\alpha} + \frac{1}{1-\dfrac{\bar{\omega}^2}{\omega^2}}\right) \tag{6.207}$$

The dynamic flexibility is d_2:

$$d_2\left(\bar{\omega}/\omega\right) = \frac{x_2}{F} = \frac{1}{k}\cdot\frac{\alpha + \left(1-\dfrac{\bar{\omega}^2}{\omega^2}\right)}{\alpha\cdot\left(1-\dfrac{\bar{\omega}^2}{\omega^2}\right)} \tag{6.208}$$

The dynamic stiffness k_2 is still obtained as the inverse function of the flexibility:

$$k_2\left(\bar{\omega}/\omega\right) = k \cdot \frac{\alpha \cdot \left(1 - \frac{\bar{\omega}^2}{\omega^2}\right)}{\alpha + \left(1 - \frac{\bar{\omega}^2}{\omega^2}\right)} \tag{6.209}$$

The dimensionless dynamic stiffness is represented in figure 20.

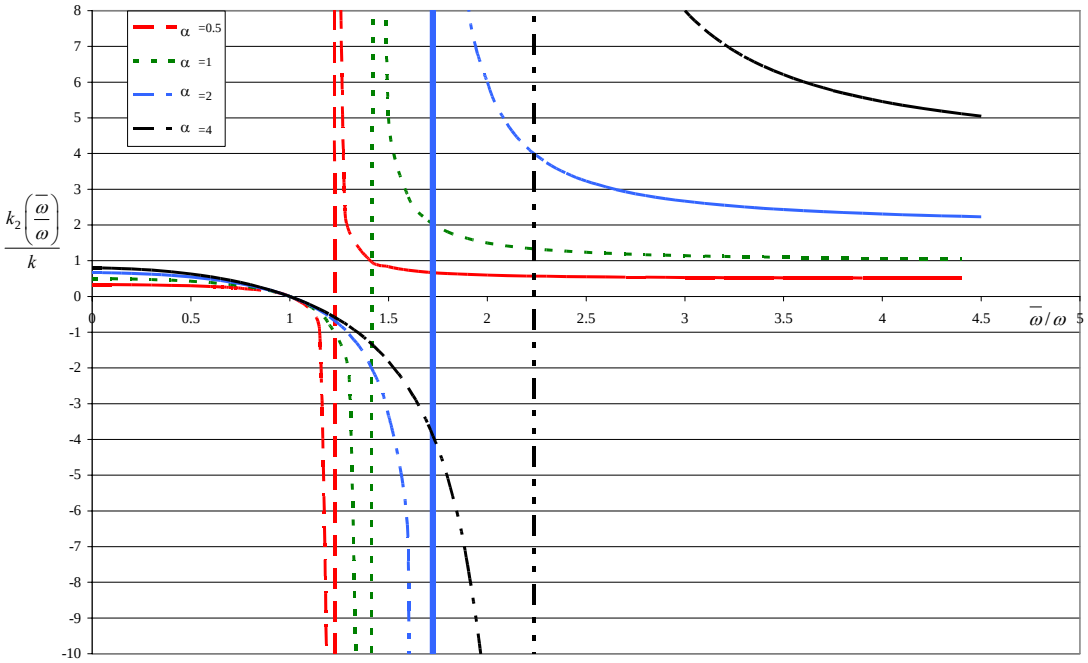

figure 20 dimensionless dynamic stiffness of the spring-mass-spring model

Different curves are obtained for different values of the α parameter; it is clear that the presence of the added spring modifies the shape of the stiffness function and consequently of the flexibility one. For $\bar{\omega}/\omega = 0$ (static behaviour) the total stiffness is given by the stiffness of two springs in series and so the static flexibility increases and the static stiffness decreases:

for $\bar{\omega}/\omega = 0 \quad \Rightarrow \quad d_2\left(\bar{\omega}/\omega\right) = \frac{1}{\alpha} + 1$ and $k_2\left(\bar{\omega}/\omega\right) = \frac{\alpha}{\alpha + 1}$

The resonance frequency does not change. At high frequencies the stiffness does not tend to infinite but to the k_{fas} value:

$$\lim_{\bar{\omega}/\omega\to\infty} d_2\left(\bar{\omega}/\omega\right) = \frac{1}{\alpha} \qquad \lim_{\bar{\omega}/\omega\to\infty} k_2\left(\bar{\omega}/\omega\right) = \alpha$$

A different case is obtained considering a mass-spring-spring model (figure 21) in which a spring is in series to the first one (representing as an example the flexibility of an underballast mat), its stiffness being: $k_{mat} = \beta \cdot k$ con $\beta \geq 0$

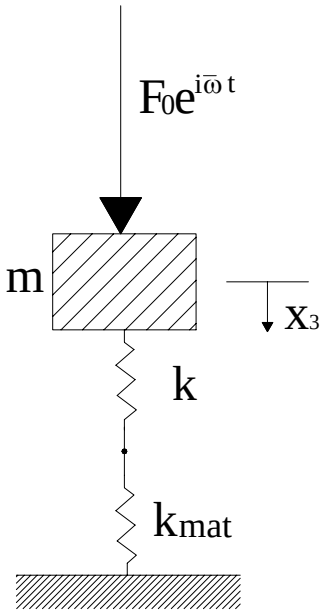

figure 21 mass-spring-spring model

This system is studied considering that two springs placed in series have the total stiffness:

$$k_{tot} = \frac{1}{\frac{1}{\beta k} + \frac{1}{k}} \tag{6.210}$$

Reconsidering the (6.199) equation with the proper k expression:

$$m\ddot{x}_3 + k_{tot}x_3 = F_0 e^{i\bar{\omega}t} \tag{6.211}$$

The following solution is obtained:

$$x_3 = \frac{F}{k_{tot}} \cdot \frac{1}{1-\frac{\overline{\omega}^2}{k_{tot}/m}} = F \cdot \left(\frac{1}{\beta k}+\frac{1}{k}\right) \cdot \frac{1}{1-\frac{\overline{\omega}^2}{1/\left[m \cdot \left(\frac{1}{\beta k}+\frac{1}{k}\right)\right]}} = \frac{F}{k} \cdot \left(\frac{1}{\beta}+1\right) \cdot \frac{1}{1-\frac{\overline{\omega}^2}{\frac{k}{\left(\frac{1}{\beta}+1\right) \cdot m}}}$$

Hence:

$$x_3 = x_{st} \cdot \left(\frac{\beta+1}{\beta}\right) \cdot \frac{1}{1-\frac{\overline{\omega}^2}{\left(\frac{\beta}{\beta+1}\right) \cdot \omega^2}} = x_3 = x_{st} \cdot \left(\frac{\beta+1}{\beta}\right) \cdot \frac{1}{1-\left(\frac{\beta+1}{\beta}\right) \cdot \frac{\overline{\omega}^2}{\omega^2}} \tag{6.212}$$

The dynamic flexibility is d_3:

$$x_3 = \frac{1}{k} \cdot \frac{\beta+1}{\beta} \frac{1}{1-\left(\frac{\beta+1}{\beta}\right) \cdot \frac{\overline{\omega}^2}{\omega^2}} \tag{6.213}$$

Consequently the dynamic stiffness is:

$$x_3 = k \cdot \frac{\beta}{\beta+1} \cdot \left[1-\left(\frac{\beta+1}{\beta}\right) \cdot \frac{\overline{\omega}^2}{\omega^2}\right] \tag{6.214}$$

The dimensionless dynamic flexibility curves are plotted in figure 22 for different values of the β parameter.

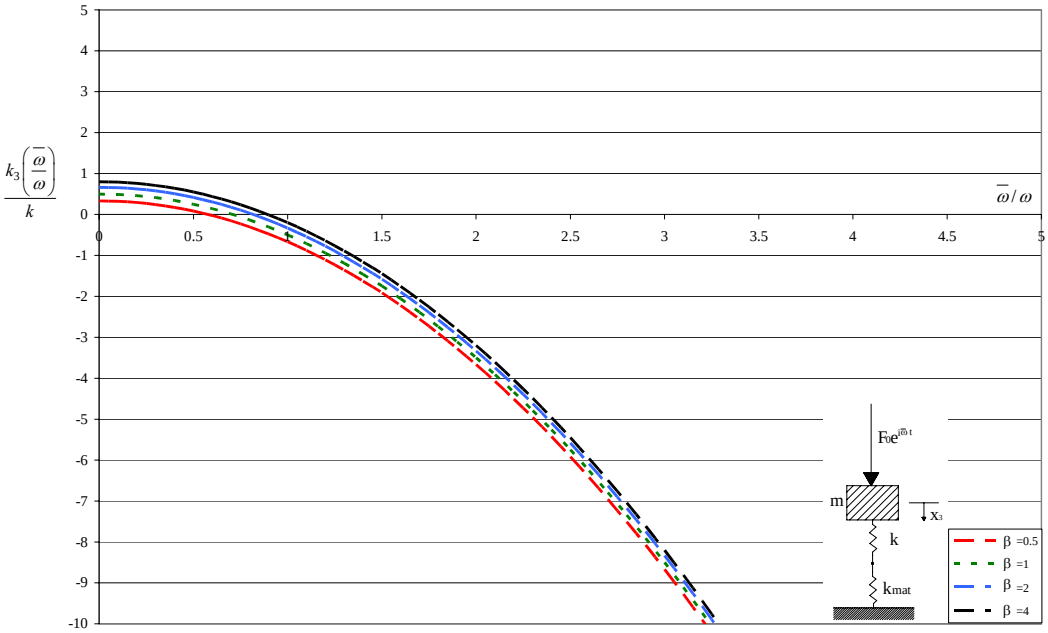

figure 22 dimensionless dynamic stiffness of the mass-spring-spring model

For $\overline{\omega}/\omega = 0$ (static behaviour) the total stiffness is still given by the stiffness of two springs in series:

$$d_3\left(\overline{\omega}/\omega = 0\right) = \frac{\beta+1}{\beta} \quad \text{and} \quad k_3\left(\overline{\omega}/\omega = 0\right) = \frac{\beta}{\beta+1} \tag{6.215}$$

The resonance frequency is modified by the presence of the added spring and it assumes the value:

$$\frac{\overline{\omega}}{\omega} = \sqrt{\frac{\beta}{\beta+1}} \tag{6.216}$$

The high frequency behaviour does not change in fact it is evident that the flexibility tends to zero and the stiffness tends to infinity.

6.3.2 Continuous bar-spring-mass models

More refined models including a continuous bar of total length l, of axial stiffness EA and with mass per unit length ρA, ρ being the mass density, are now considered. The bar may synthetically represent the distributed ballast flexibility and inertia.

First of all it is necessary to consider the stationary state stiffness matrix of a bar with distributed mass and flexibility under harmonic motion of circular frequency $\bar{\omega}$.
Considering the bar in figure 23 the equilibrium equation is:

$$dN - \rho A dy \cdot \frac{\partial^2 v(y,t)}{\partial t^2} = 0 \tag{6.217}$$

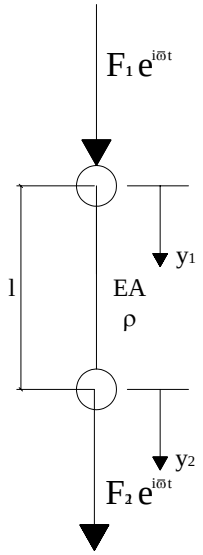

figure 23 bar system

In the following $\dot{v}$ and $\ddot{v}$ represent the first and the second temporal derivate of $v(y,t)$ function respectively; v' and v'' represent the first and the second spatial derivate of $v(y,t)$ function respectively.
Applying equation of continuous mechanics:

$$\varepsilon = v' \quad \Rightarrow \quad \sigma = E\varepsilon = Ev' \tag{6.218}$$

In which ε is the non-dimensional axial deformation, σ is the corresponding stress and E is the material young modulus.

Axial force N and its spatial derivate are given by:

$$N = \sigma \cdot A = EA \cdot v' \qquad \frac{dN}{dy} = EAv'' \Rightarrow dN = EAv''dy \tag{6.219}$$

Substituting (6.219) in (6.217):

$$EAv''dy - \rho A dy \cdot \ddot{v} = 0 \tag{6.220}$$

$$\frac{E}{\rho} v'' - \ddot{v} = 0 \tag{6.221}$$

Propagation speed of compressive bar waves is defined:

$$\frac{E}{\rho} = \tau^2 \tag{6.222}$$

For stationary state hypothesis the solution can be written:

$$v(y,t) = \Psi(y) \cdot e^{i\bar{\omega}t} \tag{6.223}$$

And the following derivates are obtained:

$$\begin{aligned} v'(y,t) &= \Psi'(y) \cdot e^{i\bar{\omega}t} \\ v''(y,t) &= \Psi''(y) \cdot e^{i\bar{\omega}t} \\ \ddot{v}(y,t) &= -\bar{\omega}^2 \Psi(y) \cdot e^{i\bar{\omega}t} \end{aligned} \tag{6.224}$$

Substituting the third and the forth relation of (6.224) and (6.222) in (6.221) the following equation is obtained:

$$\tau^2 \Psi'' + \omega^2 \Psi = 0 \tag{6.225}$$

$$\Psi'' + \frac{\omega^2}{\tau^2} \Psi = 0 \tag{6.226}$$

The (6.226) is a differential equation with a characteristic polynomial with two complex conjugate roots and the equation solution can be written:

$$\Psi(y) = c_1 \sin\left(\frac{\omega}{\tau} y\right) + c_2 \cos\left(\frac{\omega}{\tau} y\right) \tag{6.227}$$

Boundary conditions are written to find the constant c_1 and c_2:

$$\begin{aligned} v(0,t) &= y_1 e^{i\bar{\omega}t} = \Psi(0)\cdot e^{i\bar{\omega}t} \Rightarrow y_1 = \Psi(0) \\ v(l,t) &= y_2 e^{i\bar{\omega}t} = \Psi(l)\cdot e^{i\bar{\omega}t} \Rightarrow y_2 = \Psi(l) \end{aligned} \tag{6.228}$$

Considering (6.227):

$$\Psi(0) = c_2 = y_1$$

$$\Psi(l) = c_1 \sin\left(\frac{\bar{\omega}}{\tau} l\right) + y_1 \cos\left(\frac{\bar{\omega}}{\tau} l\right) = y_2$$

Hence:

$$c_1 = \frac{y_2 - y_1 \cos\left(\frac{\bar{\omega}}{\tau} y\right)}{\sin\left(\frac{\bar{\omega}}{\tau} y\right)} \qquad c_2 = y_1 \tag{6.229}$$

The solution is:

$$\Psi(y) = \left[\frac{y_2}{\sin\left(\frac{\omega}{\tau} l\right)} - \frac{y_1}{\tan\left(\frac{\omega}{\tau} l\right)}\right] \cdot \sin\left(\frac{\omega}{\tau} y\right) + y_1 \cos\left(\frac{\omega}{\tau} y\right) \tag{6.230}$$

Its first derivate is:

$$\Psi'(y) = c_1 \cdot \frac{\omega}{\tau} \cdot \cos\left(\frac{\omega}{\tau} y\right) - c_2 \cdot \frac{\omega}{\tau} \cdot \sin\left(\frac{\omega}{\tau} y\right) \tag{6.231}$$

The axial stresses acting at two ends of the bar are obtained:

$$\begin{aligned} N(0,t) &= EAv'(0,t) = EA\Psi'(0)\cdot e^{i\bar{\omega}t} = -F_1 e^{i\bar{\omega}t} \\ N(l,t) &= EAv'(l,t) = EA\Psi'(l)\cdot e^{i\bar{\omega}t} = F_2 e^{i\bar{\omega}t} \end{aligned} \tag{6.232}$$

Hence:

$$F_1 = -EA\Psi'(0) = -EA\left[\frac{y_2}{\sin\left(\frac{\bar{\omega}}{\tau}l\right)} - \frac{y_1}{\tan\left(\frac{\bar{\omega}}{\tau}l\right)}\right]\cdot\frac{\bar{\omega}}{\tau}$$
$$F_2 = EA\Psi'(l) = EA\cdot\left\{\left[\frac{y_2}{\sin\left(\frac{\bar{\omega}}{\tau}l\right)} - \frac{y_1}{\tan\left(\frac{\bar{\omega}}{\tau}l\right)}\right]\cdot\frac{\bar{\omega}}{\tau}\cdot\cos\left(\frac{\bar{\omega}}{\tau}l\right) - y_1\cdot\frac{\bar{\omega}}{\tau}\cdot\sin\left(\frac{\bar{\omega}}{\tau}l\right)\right\} \quad (6.233)$$

Finally the stationary state stiffness matrix of the bar with distributed mass and flexibility is obtained:

$$\begin{Bmatrix}F_1\\F_2\end{Bmatrix} = EA\cdot\begin{bmatrix}\frac{\bar{\omega}/\tau}{\tan\left(\bar{\omega}l/\tau\right)} & -\frac{\bar{\omega}/\tau}{\sin\left(\bar{\omega}l/\tau\right)}\\ -\frac{\bar{\omega}/\tau}{\sin\left(\bar{\omega}l/\tau\right)} & \frac{\bar{\omega}/\tau}{\tan\left(\bar{\omega}l/\tau\right)}\end{bmatrix}\cdot\begin{Bmatrix}y_1\\y_2\end{Bmatrix} \quad (6.234)$$

The first model case is a mass-bar system (figure 24). The relation (6.234) is applied considering that $F_1 = F_0\cdot e^{i\bar{\omega}t}$ and $y_2 = 0$ and the dynamic stiffness K_{bar} of the bar with one fixed end is obtained:

$$K_{bar} = \frac{EA}{l}\cdot\frac{\frac{l}{\tau}\cdot\bar{\omega}}{\tan\left(\frac{l}{\tau}\cdot\bar{\omega}\right)} \quad (6.235)$$

Indicating with:

$$k_{bar} = \frac{EA}{l} \qquad \omega = \sqrt{\frac{k_{bar}}{m}} \qquad \tau = \sqrt{\frac{E}{\rho}} \qquad \zeta = \frac{\rho Al}{m} \qquad f_1\left(\frac{\bar{\omega}}{\omega},\zeta\right) = \frac{\bar{\omega}/\omega\cdot\sqrt{\zeta}}{\tan\left(\bar{\omega}/\omega\cdot\sqrt{\zeta}\right)} \quad (6.236)$$

Then:

$$K_{bar}\left(\bar{\omega}/\omega\right)=\frac{\frac{EA}{l}\cdot\frac{l\cdot\sqrt{\rho}\cdot\sqrt{A}\cdot\sqrt{l}\cdot\sqrt{m}}{\sqrt{E}\cdot\sqrt{A}\cdot\sqrt{l}\cdot\sqrt{m}}\cdot\bar{\omega}}{\tan\left(\frac{l\cdot\sqrt{\rho}\cdot\sqrt{A}\cdot\sqrt{l}\cdot\sqrt{m}}{\sqrt{E}\cdot\sqrt{A}\cdot\sqrt{l}\cdot\sqrt{m}}\cdot\bar{\omega}\right)}=k_{bar}\cdot\frac{\sqrt{\zeta}\cdot\bar{\omega}/\omega}{\tan\left(\sqrt{\zeta}\cdot\bar{\omega}/\omega\right)}=k_{bar}\cdot f_1\left(\zeta,\frac{\bar{\omega}}{\omega}\right) \quad (6.237)$$

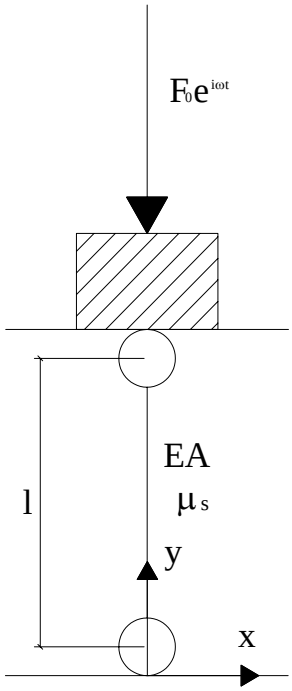

figure 24 mass-bar model

The mass-bar system is studied as the simple mass-spring model. The equation of the problem is:

$$m\ddot{x}_{1c}+K_{bar}x_{1c}=F_0e^{i\bar{\omega}t} \quad (6.238)$$

Substituting (6.237):

$$\ddot{x}_{1c}+\frac{k_{bar}}{m}\cdot\frac{\sqrt{\zeta}\cdot\bar{\omega}/\omega}{\tan\left(\sqrt{\zeta}\cdot\bar{\omega}/\omega\right)}x_{1c}=\frac{F_0}{m}\cdot\frac{k_{bar}}{k_{bar}}e^{i\bar{\omega}t} \quad (6.239)$$

Hence:

$$\ddot{x}_{1c} + \omega^2 \cdot f_1\left(\bar{\omega}/\omega, \zeta\right) x_{1c} = x_{st} \cdot \omega^2 \cdot e^{i\bar{\omega}t} \tag{6.240}$$

Again the solution can be written in the form:

$$x_{1c} = x_0 \cdot e^{i\bar{\omega}t} \qquad \Rightarrow \qquad \dot{x}_{1c} = i\bar{\omega} \cdot x_0 \cdot e^{i\bar{\omega}t} \qquad \ddot{x}_{1c} = -\bar{\omega}^2 \cdot x_0 \cdot e^{i\bar{\omega}t} \tag{6.241}$$

The solution is:

$$x_{1c} = x_{st} \cdot \frac{1}{f_1\left(\bar{\omega}/\omega, \zeta\right) - \left(\frac{\bar{\omega}}{\omega}\right)^2} \tag{6.242}$$

The results are still expressed in terms of flexibility and stiffness given by:

$$d_{1c}\left(\bar{\omega}/\omega\right) = \frac{x_{1c}}{F} = \frac{1}{k_{bar}} \cdot \left[f_1\left(\frac{\bar{\omega}}{\omega}, \zeta\right) - \left(\frac{\bar{\omega}}{\omega}\right)^2 \right]^{-1} \tag{6.243}$$

$$k_{1c}\left(\bar{\omega}/\omega\right) = k_{bar}\left[f_1\left(\frac{\bar{\omega}}{\omega}, \zeta\right) - \left(\frac{\bar{\omega}}{\omega}\right)^2 \right] \tag{6.244}$$

The dimensionless stiffness is represented in figure 25.

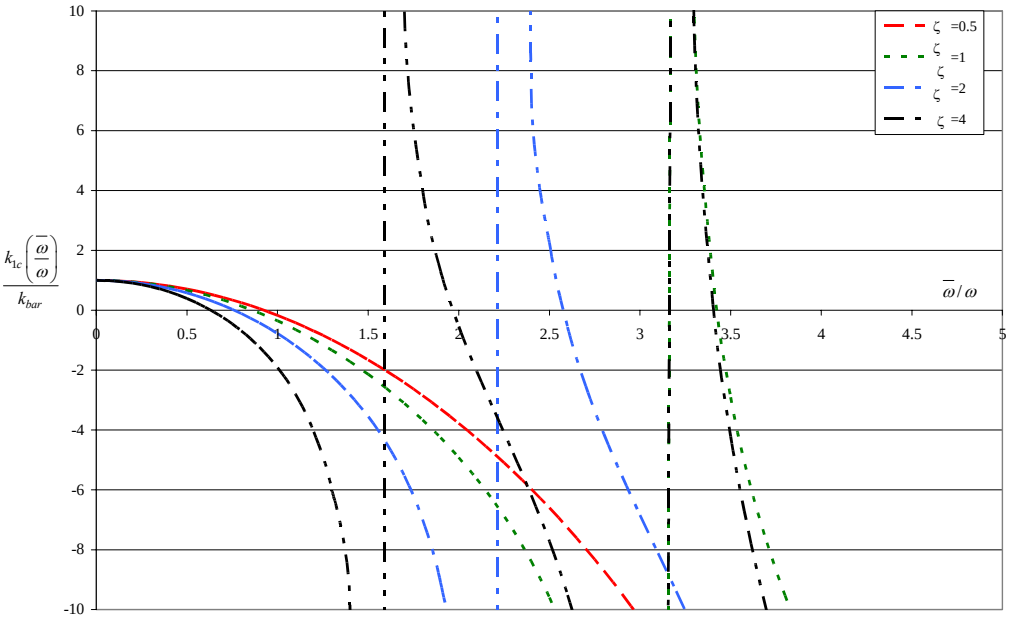

figure 25 dimensionless dynamic stiffness of the mass-bar model

For $\bar{\omega}/\omega = 0$ (static behaviour) $d_{1c} = 1/k_{bar}$ and therefore $k_{1c} = k_{bar}$. Being the bar a continuous model an infinite number of resonance frequencies occurs their values depending on the dimensionless mass parameter ζ.

A spring of stiffness $k_{fas} = \alpha k_{bar}$ is now added above the mass to obtain a spring-mass-bar system (figure 26).

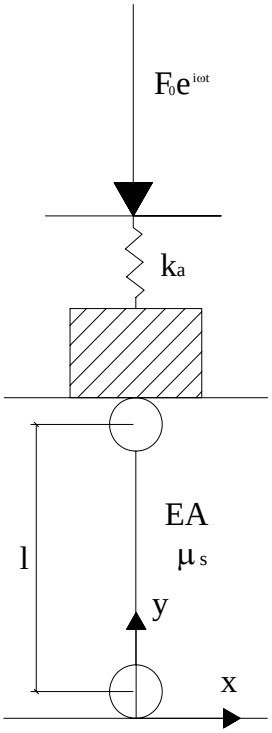

figure 26 spring-mass-bar model

Solving the following system:

$$\begin{cases} m\ddot{x}_{1c} + K_{bar}x_{1c} = F_0 e^{i\bar{\omega}t} \\ k_{fas} \cdot \left(x_{2c} - x_{1c}\right) = F_0 e^{i\bar{\omega}t} \end{cases} \tag{6.245}$$

Proceeding as in the corresponding discrete case, is obtained:

$$x_{2c} = \frac{F}{\alpha k_{bar}} + \frac{F}{k_{bar}} \cdot \frac{1}{f_1\left(\frac{\overline{\omega}}{\omega}, \zeta\right) - \frac{\overline{\omega}^2}{\omega^2}} = \frac{F}{k_{bar}} \cdot \left[\frac{1}{\alpha} + \frac{1}{f_1\left(\frac{\overline{\omega}}{\omega}, \zeta\right) - \frac{\overline{\omega}^2}{\omega^2}} \right] \tag{6.246}$$

The dynamic flexibility and stiffness are:

$$d_{2c}\left(\overline{\omega}/\omega\right) = \frac{x_{2c}}{F} = \frac{1}{k_{bar}} \cdot \left\{ \frac{\alpha \cdot \left[f_1\left(\frac{\overline{\omega}}{\omega}, \zeta\right) - \frac{\overline{\omega}^2}{\omega^2} \right]}{f_1\left(\frac{\overline{\omega}}{\omega}, \zeta\right) - \frac{\overline{\omega}^2}{\omega^2} + \alpha} \right\}^{-1} \tag{6.247}$$

$$k_{2c}\left(\overline{\omega}/\omega\right) = \frac{k_{bar} \cdot \alpha \cdot \left[f_1\left(\frac{\overline{\omega}}{\omega}, \zeta\right) - \frac{\overline{\omega}^2}{\omega^2} \right]}{f_1\left(\frac{\overline{\omega}}{\omega}, \zeta\right) - \frac{\overline{\omega}^2}{\omega^2} + \alpha} \tag{6.248}$$

Dimensionless stiffness is represented in figure 27.

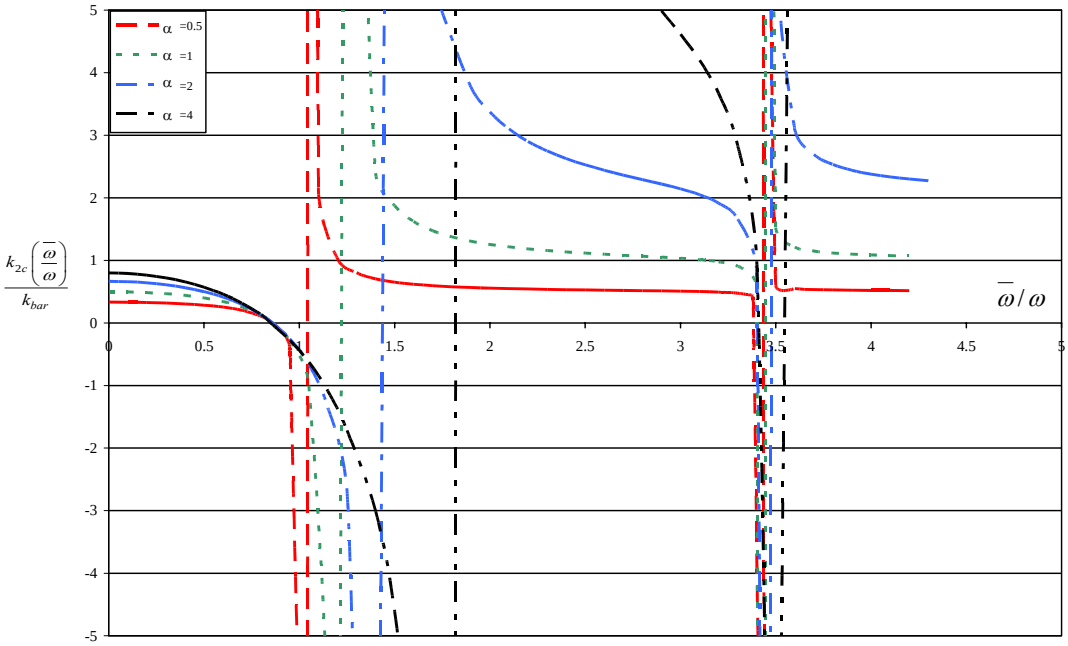

figure 27 dimensionless stiffness of the spring-mass-bar model (for $\zeta = 1$)

As in the corresponding discrete case for $\bar{\omega}/\omega = 0$ (static behaviour) the total stiffness is given by the stiffness of two springs in series; moreover an infinite number of resonance frequencies occurs, their values depending on ζ and α.

A mass-spring-bar system (figure 28) is now considered in which a spring (representing as an example rubber wrapping of the sleepers) is added under the bar, the spring stiffness given by:

$$k_{wra} = \beta \cdot \frac{EA}{l} = \beta \cdot k_{bar} \quad \text{with} \quad \beta \geq 0 \tag{6.249}$$

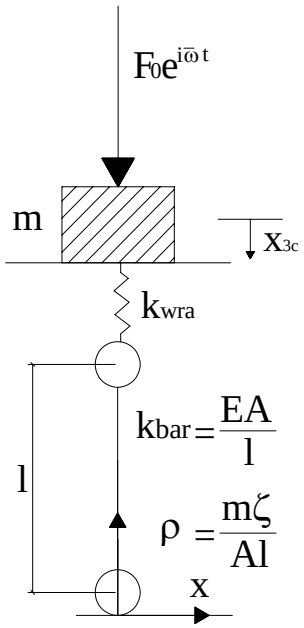

figure 28 mass-spring-bar model

This system can be easily studied considering the bar and the spring as two springs placed in series with the total stiffness:

$$k_{tot} = \frac{f_1\left(\frac{\bar{\omega}}{\omega}, \zeta\right) \cdot \beta k_{bar}}{\beta + f_1\left(\frac{\bar{\omega}}{\omega}, \zeta\right)} = f_3\left(\frac{\bar{\omega}}{\omega}, \zeta, \beta\right) \cdot k_{bar} \tag{6.250}$$

where:

$$f_3\left(\frac{\overline{\omega}}{\omega},\zeta,\beta\right)=\frac{f_1\left(\frac{\overline{\omega}}{\omega},\zeta\right)\cdot\beta}{\beta+f_1\left(\frac{\overline{\omega}}{\omega},\zeta\right)}\cdot k_{bar} \tag{6.251}$$

The relation (6.238) is applied with the proper expression of the total spring stiffness:

$$m\ddot{x}_{3c}+k_{bar}\cdot f_3\left(\frac{\overline{\omega}}{\omega},\zeta,\beta\right)\cdot x_{3c}=F_0e^{i\overline{\omega}t} \tag{6.252}$$

Solving the equation as in previous systems the solution is obtained:

$$x_{3c}=x_{st}\cdot\frac{1}{f_3\left(\overline{\omega}/\omega,\zeta,\beta\right)-\left(\frac{\overline{\omega}}{\omega}\right)^2} \tag{6.253}$$

Therefore flexibility and stiffness are given by:

$$d_{3c}\left(\overline{\omega}/\omega\right)=\frac{x_{3c}}{F}=\frac{1}{k_{bar}}\cdot\left[f_3\left(\frac{\overline{\omega}}{\omega},\zeta,\beta\right)-\left(\frac{\overline{\omega}}{\omega}\right)^2\right]^{-1} \tag{6.254}$$

$$k_{3c}\left(\overline{\omega}/\omega\right)=k_{bar}\left[f_3\left(\frac{\overline{\omega}}{\omega},\zeta,\beta\right)-\left(\frac{\overline{\omega}}{\omega}\right)^2\right] \tag{6.255}$$

Dimensionless stiffness is represented in figure 29.

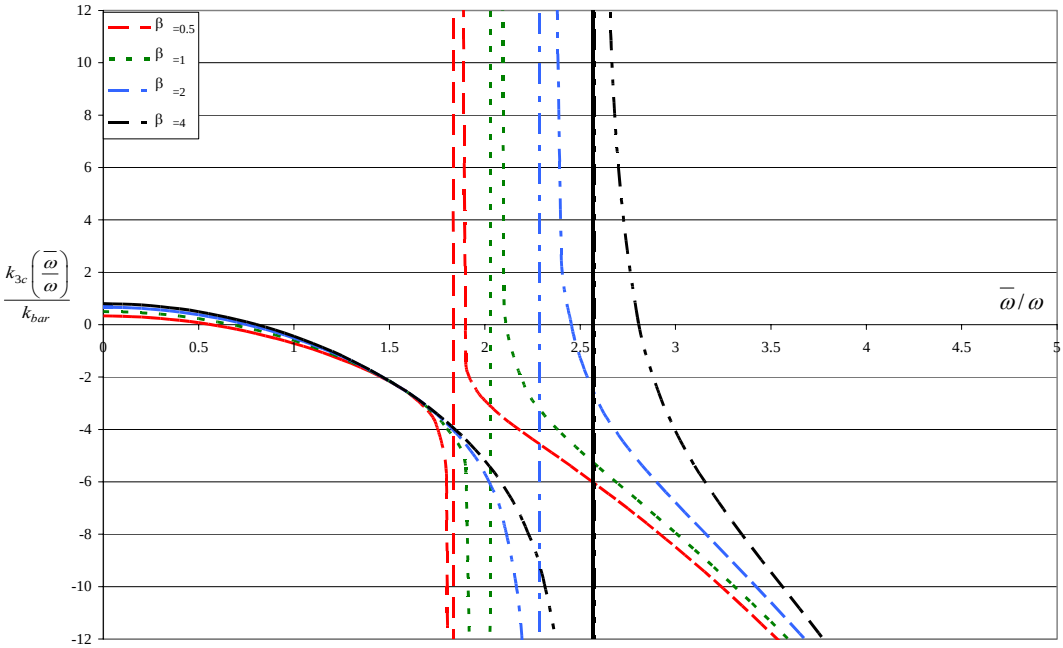

figure 29 dimensionless stiffness of the mass-spring-bar model (for $\zeta = 1$)

As in the corresponding discrete case, for $\overline{\omega}/\omega = 0$ (static behaviour) the total stiffness is given by the stiffness of the two springs in series; moreover an infinite number of resonance frequencies occurs, their values depending both ζ and β.

The following model consists of a mass-bar-spring system (figure 30) obtained adding a spring of stiffness $k_{mat} = \beta \cdot \frac{EA}{l} = \beta \cdot k_{bar}$ with $\beta \geq 0$.

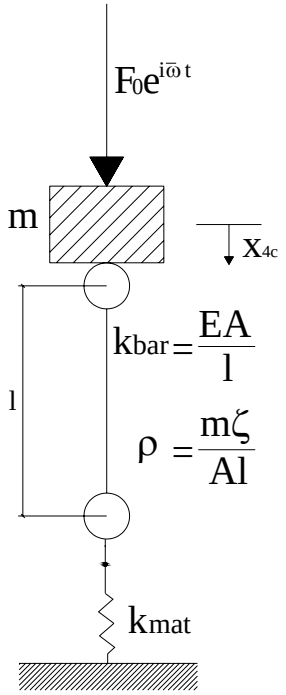

figure 30 mass-bar-spring model

It is considered the state stationary stiffness matrix of the bar (6.234) in which:

$$F_1 = F_0 e^{i\bar{\omega}\, t} \qquad y_2 = \frac{P_2}{k_{mat}} = \frac{P_2}{\beta \cdot k_{bar}} \tag{6.256}$$

Considering the bar parameters in (6.236), the global stiffness is obtained:

$$k_{tot} = k_{bar} \cdot \left[\frac{\frac{\bar{\omega}}{\omega} \cdot \sqrt{\zeta}}{\tan\left(\frac{\bar{\omega}}{\omega} \cdot \sqrt{\zeta}\right)} - \frac{\frac{\frac{\bar{\omega}}{\omega} \cdot \sqrt{\zeta}}{\sin\left(\frac{\bar{\omega}}{\omega} \cdot \sqrt{\zeta}\right)}}{\frac{\sin\left(\frac{\bar{\omega}}{\omega} \cdot \sqrt{\zeta}\right)}{\frac{\bar{\omega}}{\omega} \cdot \sqrt{\zeta}} \cdot \beta + \cos\left(\frac{\bar{\omega}}{\omega} \cdot \sqrt{\zeta}\right)} \right] = k_{bar} \cdot f_4\left(\frac{\bar{\omega}}{\omega}, \zeta, \beta\right) \tag{6.257}$$

The following equation is solved where the (6.257) is substituted:

$$m\ddot{x}_{1c} + k_{tot} x_{4c} = F_0 e^{i\bar{\omega}t} \tag{6.258}$$

Hence:

$$x_{4c} = x_{st} \cdot \frac{1}{f_4\left(\frac{\bar{\omega}}{\omega}, \zeta, \beta\right) - \left(\frac{\bar{\omega}^2}{\omega^2}\right)} \tag{6.259}$$

Therefore flexibility and stiffness are:

$$d_{4c}\left(\bar{\omega}/\omega\right) = \frac{x_{4c}}{F} = \frac{1}{k_{bar}} \cdot \left[f_4\left(\frac{\bar{\omega}}{\omega}, \zeta, \beta\right) - \left(\frac{\bar{\omega}}{\omega}\right)^2 \right]^{-1} \quad k_{4c}\left(\bar{\omega}/\omega\right) = k_{bar}\left[f_4\left(\frac{\bar{\omega}}{\omega}, \zeta, \beta\right) - \left(\frac{\bar{\omega}}{\omega}\right)^2 \right] \tag{6.260}$$

The dimensionless stiffness function is represented in figure 31.

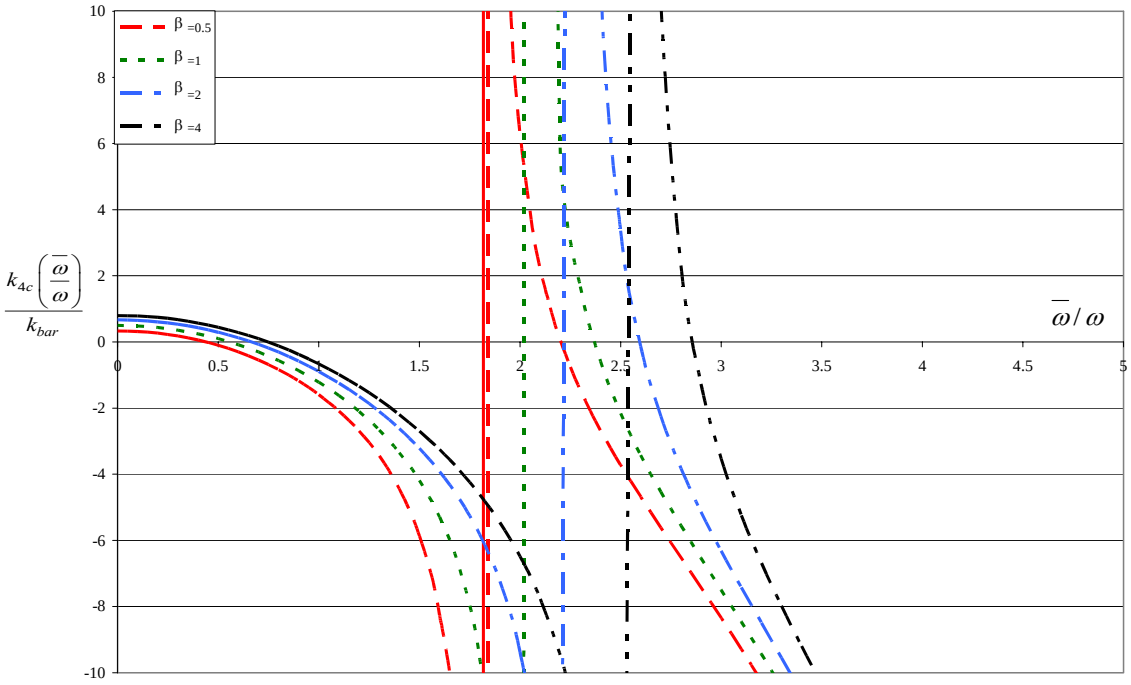

figure 31 dimensionless stiffness of the mass-bar-spring model (for $\zeta = 1$)

As in mass-spring-bar model for $\bar{\omega}/\omega = 0$ (static behaviour) the total stiffness is given by the stiffness of the two springs in series; the infinite number of resonance

frequencies still depends on ζ and β but they occur for lower frequencies because the total floating mass is greater.

The last system is a mass-spring-bar-spring model (figure 32) in which two springs are added: the first one of stiffness k_{mat} is in series to the bar and the other of stiffness k_{wra} is between the mass and the bar:

$$k_{mat} = \beta_1 \cdot k_{bar} = \beta_1 \cdot \frac{EA}{l} \qquad k_{wra} = \beta_2 \cdot k_{bar} = \beta_2 \cdot \frac{EA}{l} \tag{6.261}$$

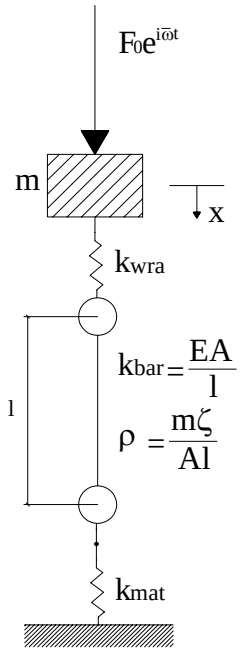

figure 32 mass-spring-bar-spring model

The problem is solved considering two springs in series, the first one of stiffness k_{wra}, the second one having a stiffness corresponding (according to (6.257)) to the bar and k_{mat} in series:

$$k_{bar}\cdot\left[\frac{\frac{\overline{\omega}}{\omega}\cdot\sqrt{\zeta}}{\tan\left(\frac{\overline{\omega}}{\omega}\cdot\sqrt{\zeta}\right)}-\frac{\frac{\frac{\overline{\omega}}{\omega}\cdot\sqrt{\zeta}}{\sin\left(\frac{\overline{\omega}}{\omega}\cdot\sqrt{\zeta}\right)}}{\frac{\sin\left(\frac{\overline{\omega}}{\omega}\cdot\sqrt{\zeta}\right)}{\frac{\overline{\omega}}{\omega}\cdot\sqrt{\zeta}}\cdot\beta_1+\cos\left(\frac{\overline{\omega}}{\omega}\cdot\sqrt{\zeta}\right)}\right]=k_{bar}\cdot f_4\left(\frac{\overline{\omega}}{\omega},\zeta,\beta_1\right)\qquad(6.262)$$

The total stiffness k_{tot} is then:

$$k_{tot}=\frac{1}{\frac{1}{k_{bar}\cdot f_4\left(\frac{\overline{\omega}}{\omega},\zeta,\beta_1\right)}+\frac{1}{\beta_2 k_{bar}}}=k_{bar}\cdot\frac{f_4\left(\frac{\overline{\omega}}{\omega},\zeta,\beta_1\right)\cdot\beta_2}{\beta_2+f_4\left(\frac{\overline{\omega}}{\omega},\zeta,\beta_1\right)}=k_{bar}\cdot f_5\left(\frac{\overline{\omega}}{\omega},\zeta,\beta_1,\beta_2\right)\qquad(6.263)$$

The solution is obtained:

$$x_{5c}=x_{st}\cdot\frac{1}{f_5\left(\overline{\omega}/\omega\right)-\left(\frac{\overline{\omega}^2}{\omega^2}\right)}\qquad(6.264)$$

Dimensionless flexibility and stiffness are derived (figure 33):

$$d_{5c}\left(\overline{\omega}/\omega\right)=\frac{x_{5c}}{F}=\frac{1}{k_{bar}}\cdot\left[f_5\left(\overline{\omega}/\omega\right)-\left(\frac{\overline{\omega}}{\omega}\right)^2\right]^{-1}\qquad k_{5c}\left(\overline{\omega}/\omega\right)=k_{bar}\left[f_5\left(\overline{\omega}/\omega\right)-\left(\frac{\overline{\omega}}{\omega}\right)^2\right]\qquad(6.265)$$

Again, in the static case $\left(\frac{\overline{\omega}}{\omega}=0\right)$ the total stiffness corresponds to the stiffness of the three springs in series and the infinite number of resonant frequencies now depends on the three parameters ζ,β_1 and β_2.

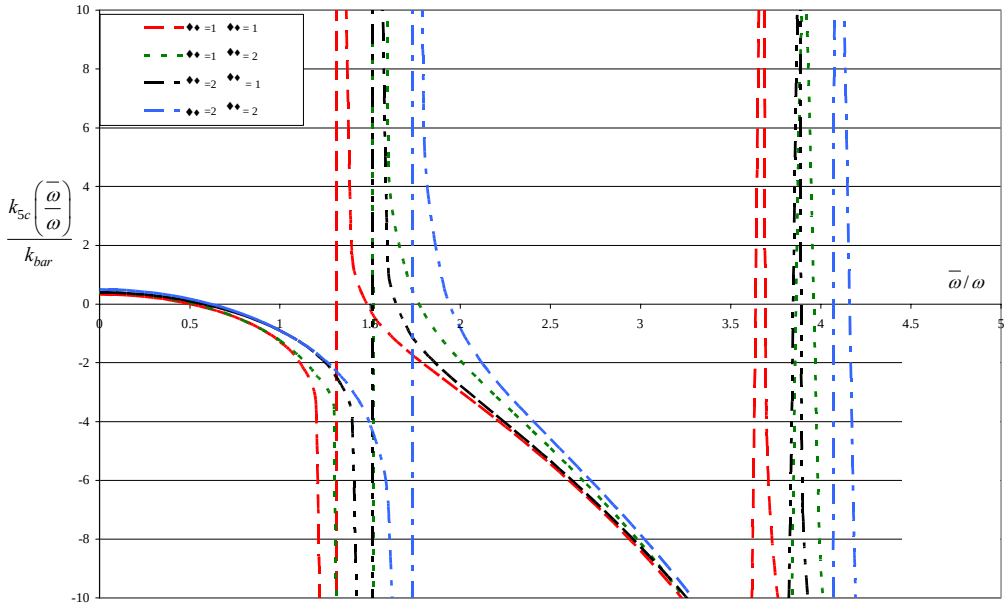

figure 33 dimensionless stiffness of the mass-spring-bar-spring model (for $\zeta = 1$)

CHAPTER 7

APPLICATION OF THE ANALYTICAL MODELS AND EXPERIMENTAL VALIDATION

Every model needs proper values for the elastic and massive elements that compose it, and it is important to make some experimental tests that can provide reliable values.

In the previous chapter analytical models cleared the main parameters that have to be defined to obtain good theoretical results comparable with the tests. It is necessary to know:

- the railway track typology is very important. In the case of a traditional ballasted system the problem is to model the ballast layer, in new innovative systems a concrete slab replaces the ballast layer and its modelling can be easier than the ballast one;
- the vertical stiffness of the elements that support the railway track;
- vertical damping of every element (rail, sleepers, etc);
- flexural and shear stiffness of rails, sleepers and slabs;

- load conditions and their combination taking into account the rail irregularities;
- vehicle parameters.

Analytical models have been applied to a traditional railway track and to four its variants (table 1); then theoretical results are compared with experimental tests performed on prototypes developed in a Pozzuoli where Research Centre of ISOLGOMMA is. They are on full scale and can help to find out the best solutions and provide a design procedure in the railway field.

table 1 brief description of prototypes

TRACK TYPE	MAIN CHARACTERISTICS
Traditional: **reference track type**	Rails connected to the sleepers with Vossloh fastenings. No elastic levels.
Innovative: **1st variant**	Addition of an underballast mat for exurban lines
Innovative: **2nd variant**	Addition of an underballast mat for urban lines
Innovative: **3rd variant**	Addition of an elastic wrapping of the sleepers
Innovative: **4th variant**	Addition of two elastic levels: an elastic wrapping of the sleepers and an underballast mat for urban lines

7.1 DESCRIPTION OF THE RAILWAY TRACK

The traditional railway track (figure 1) has been developed on a concrete basement (figure 2).

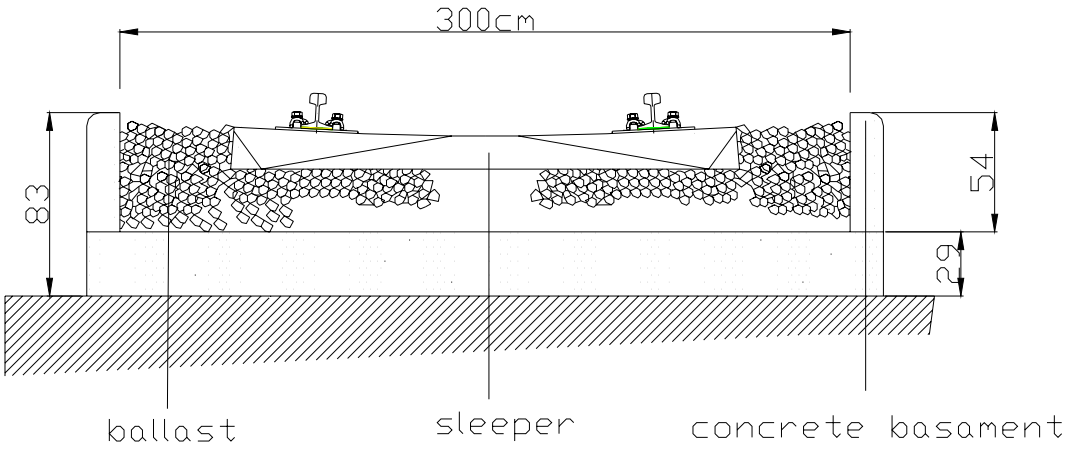

figure 1 transverse section of the traditional system: reference track type

figure 2 prototype on full scale of the reference track type

The system consists of UNI 60 rails (figure 3) and pre-stressed concrete single-block sleepers (figure 4). The rails are connected to the sleepers with Vossloh fastenings (figure 5). Longitudinal distance between sleepers is 0.60 m. The total length of the prototype is 10 m (in the following the choice of this length will be explained).

figure 3 UNI 60 rail

figure 4 concrete sleepers

figure 5 rigid and elastic fastenings

Innovative elastic elements at different levels are then added to the traditional track to verify their influence in the static and dynamic behaviour of the system. Four variants are considered. The elastic elements are derived by the material described in previous chapters.

The first one consists in the addition of an underballast mat for exurban lines (figure 6). The mat thickness is $s_{m1} = 17$ mm and it is composed by short fibres of SBR (50%) and big granules of grey EPDM (50%) obtaining a high density product $\left(\cong 900 \text{ kg/m}^3\right)$.

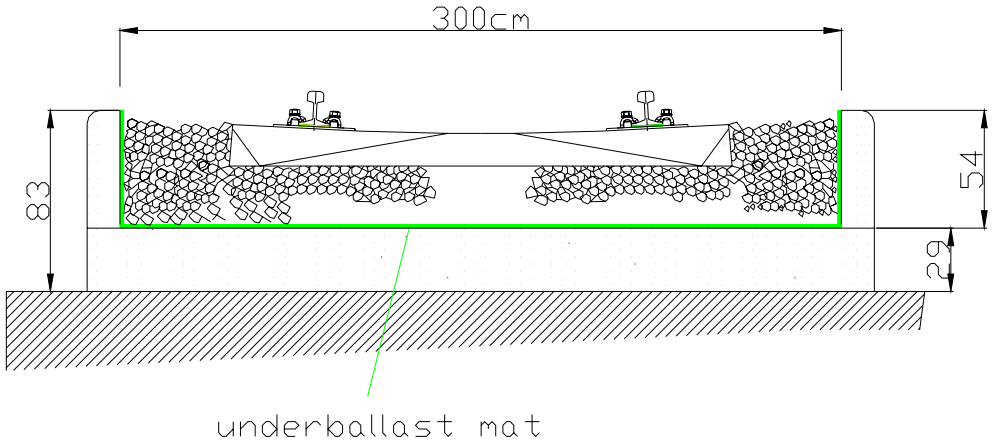

figure 6 transverse section of a traditional track with an exurban underballast mat: 1st variant

The second one is still developed with an underballast mat but conceived for urban lines with a greater thickness $\left(s_{m2} = 50 \text{ mm}\right)$ and with a smaller density $\left(\cong 500 \text{ kg/m}^3\right)$(figure 7). The components are still short fibres of SBR (90%) and small granules of grey EPDM (10%).

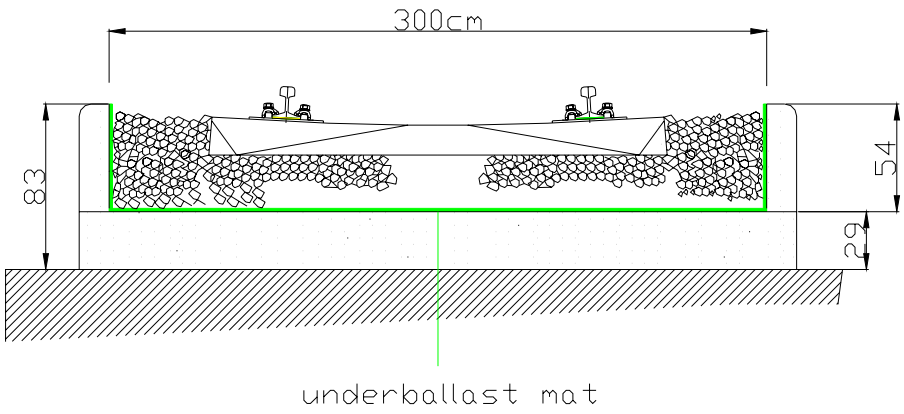

figure 7 transverse section of a traditional track with an urban underballast mat: 2nd variant

The third variant is carried out considering an elastic wrapping around the sleepers. The elastomeric element has thickness of $s_s = 20 \text{ mm}$ and its components are short

fibres of SBR (90%) and small granules of grey EPDM (10%) for a product with density of 700 kg/m^3 (figure 8).

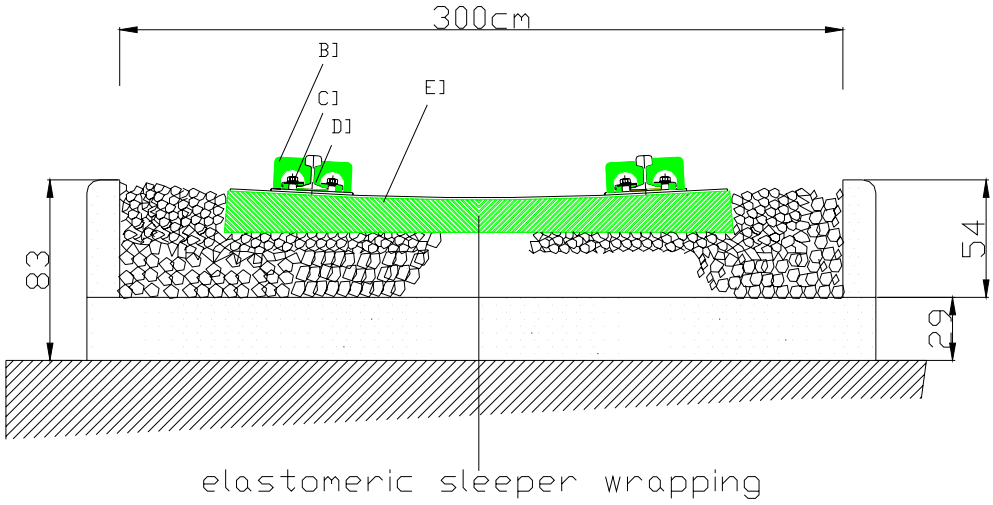

figure 8 transverse section of a traditional track with the sleepers wrapping: 3rd variant

Both elastic levels are in the forth variant obtained combined the underballast mat for urban lines and the elastic wrapping of sleepers (figure 9).

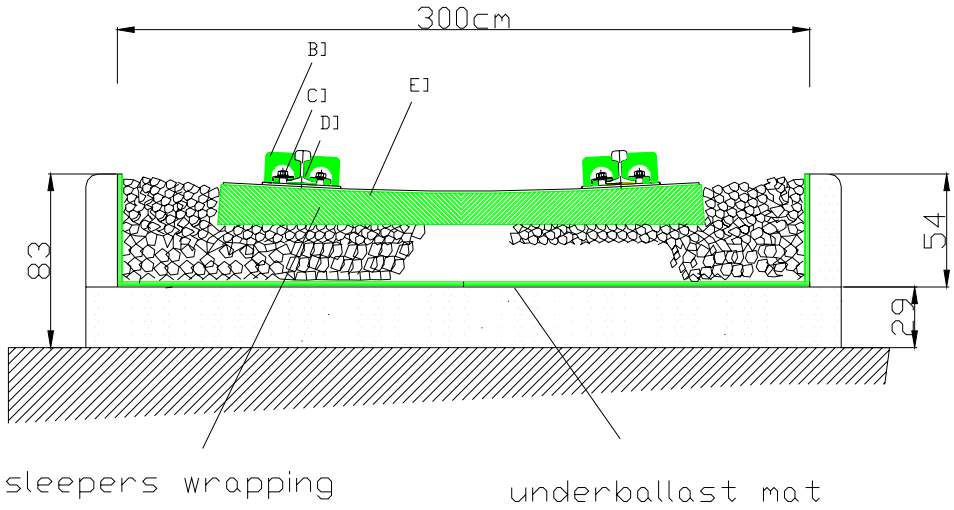

figure 9 transverse section of a traditional track with an urban underballast mat: 4th variant

7.2 PROTOTYPE MODELS

In the model of the traditional track system the rail is represented by an Euler beam characterized by its mass μ and flexural stiffness $E_r I_r$. The concrete sleepers are massive components modelled as concentrated masses m positioned at distance p to each other. The fastenings are an elastic elements taken into account in the model considering the spring above the mass. The ballast behaviour is quite difficult to determine; in the following it is modelled as a continuous bar with axial stiffness $E_b A_b$, length l and with a distributed mass $\rho_b A_b$.

The UNI 60 rail is characterized by:

$$I = 3055 \text{ cm}^4 = 3055 \cdot 10^{-8} \text{ m}^4 \qquad \mu = 60 \text{ kg/m} \tag{7.1}$$

In the model both of rails are considered and so the following data are obtained (E_r being the steel elastic modulus):

$$E_r I_r = 2 \cdot 210 \cdot 10^9 \cdot \frac{\text{N}}{\text{m}^2} \cdot 3055 \cdot 10^{-8} \text{m}^4 = 1.28 \cdot 10^7 \text{ Nm}^2 \tag{7.2}$$

$$\mu_r = 2 \cdot 60 \cdot \frac{\text{kg}}{\text{m}} = 120 \ \frac{\text{kg}}{\text{m}} \tag{7.3}$$

Fastenings are composed by two clips that push the rail foot on a rubber slab under the rail; this element transfers the vertical load deriving from rail on the sleepers. The horizontal (b_x) and vertical (h_y) dimensions of the under-rail slab in the track transverse section are (AFERIA, 2006): $b_x = 150$ mm; $h_y = 7$ mm In the railway track direction: $l_z = 200$ mm.

$m_a = 1000 \text{ kg/m}^3$; $\text{E} = 100 \text{ N/mm}^2$

The fastening can be modelled as a spring with constant stiffness K_a obtained in the following:

$$K_a = \frac{E_c A_{xz}}{h_y} \tag{7.4}$$

In which E_c is the confined elastic modulus given by:

$$E_c = 4GS^2 \tag{7.5}$$

S is the shape factor defined as the ratio between the loaded area and the free area, in the specific case:

$$S = \frac{\text{loaded area}}{\text{free area}} = \frac{l_z \cdot b_x}{2 \cdot l_z \cdot h_y + 2 \cdot b_x \cdot h_y} = \frac{150 \cdot 200}{(150 \cdot 7) \cdot 2 + (200 \cdot 7) \cdot 2} = \frac{30000}{4900} = 6.12 \tag{7.6}$$

It is known the elastic modulus and the shear one is calculated:

$$G = \frac{1}{3} \cdot E = \frac{1}{3} \cdot 100 \text{ N/mm}^2 \tag{7.7}$$

hence:

$$E_c = 4GS^2 = 4 \cdot 33.3 \cdot 6.12^2 = 4989 \text{ N/mm}^2 \tag{7.8}$$

Finally the constant stiffness of the spring is found:

$$K_a = \frac{E_c A_{xz}}{h_y} = 4989 \text{N/mm}^2 \cdot \frac{30000 \text{mm}^2}{7 \text{mm}} = 2.14 \cdot 10^7 \text{ N/mm} = 2.14 \cdot 10^{10} \text{ N/m} \tag{7.9}$$

It will be shown that the fastening stiffness is greater than the other elements and so its effect in the analytical modelling can be disregarded.

In figure 4 the concrete sleeper is showed. In the track transverse section sleeper dimensions are:

$l_x = 230$ cm; $b_z = 30$ cm

Its height is: $h_y = 18$ cm

If the sleeper is modelled as a spring and its stiffness can be calculated:

$$K_t = \frac{EA_{xz}}{h_y} = \frac{35 \cdot 10^9 \cdot 6900 \cdot 10^{-4}}{0.18} = 1.34 \cdot 10^{11} \text{N/m}$$

It is clear that the value is very great if it is compared with the fastening stiffness; for this reason in the model it is assumed that the sleeper is a massive component and its value is:

$$M = m_t \cdot b_z \cdot h_y \cdot l_x = 2500 \frac{\text{kg}}{\text{m}^3} \cdot (0.3 \cdot 2.3 \cdot 0.18)\,\text{m}^3 = 310.5\ \text{kg} \tag{7.10}$$

Bar parameters are assigned considering the ballast characteristics. Its length is the ballast height under the sleeper $(l = 30\ \text{cm})$. There are two areas on which the sleepers transfer railway loads, the value of these area (called A_{it}) is smaller than the total sleeper area and given by:

$$A_{it} = 2 \cdot 30 \cdot 80 = 4800\ \text{cm}^2 \tag{7.11}$$

The ballast mechanical characteristic are very hard to obtain, in the following is assumed (Pezzoli, 2005):

$$E_b = 1000\ \frac{\text{N}}{\text{cm}^2} \qquad \rho_b = 1800\ \frac{\text{kg}}{\text{m}^3} \tag{7.12}$$

The bar area is assumed:

$$A_b = 1.5 \cdot A_{it} = 7200\ \text{cm}^2 \tag{7.13}$$

Hence the other bar characteristics are derived:

$$E_b A_b = 7200\ \text{kN} \qquad k_b = \frac{EA}{l} = 2.40 \cdot 10^7\ \frac{\text{N}}{\text{m}} \tag{7.14}$$

The global model is in figure 10.

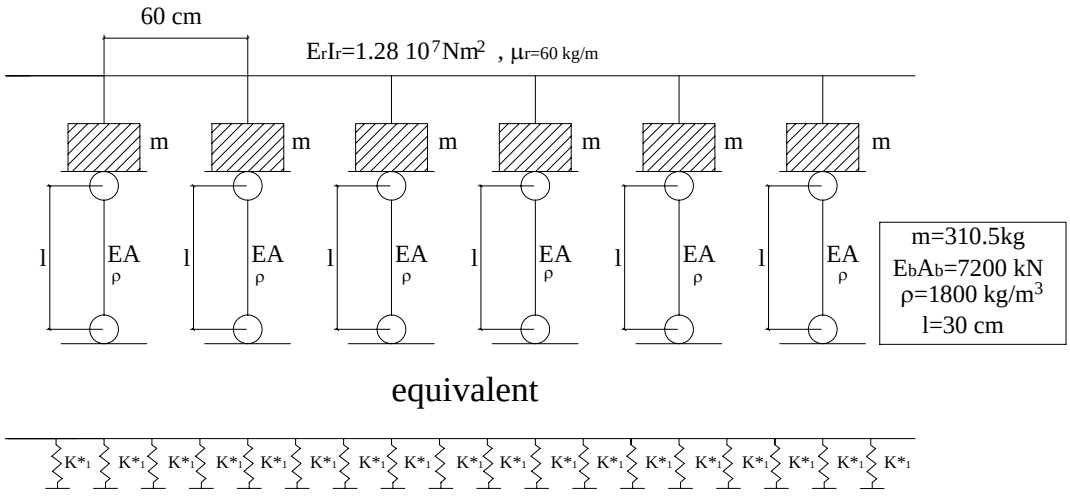

figure 10 model for the traditional track system

The stiffness expression for the mass-bar system is applied with the proper values of the massive and elastic elements obtaining $K_1(\bar{\omega})$ from which:

$$k_1^* = \frac{K_1}{p} - \mu\bar{\omega}^2 \tag{7.15}$$

The dimensionless parameters ζ is equal to:

$$\zeta = \frac{\mu_s Al}{m} = \frac{1800 \cdot 0.72 \cdot 0.3}{310.5} = 1.25 \tag{7.16}$$

Regarding the dynamic modelling the ballast can become stiffer and in the following it is assumed that its stiffness is three times greater than the static one:

$$k_{b,dyn} = 3 \cdot k_b = 3 \cdot 2.40 \cdot 10^7 \frac{\text{N}}{\text{m}} = 7.2 \cdot 10^7 \frac{\text{N}}{\text{m}} \tag{7.17}$$

Moreover a loss factor has to be assumed and it is set a loss factor $\nu_b = 0.15$.

7.2.1 Application of models for innovative railway tracks

Innovative elastic elements at different levels are then added to the traditional track to verify their influence in the static and dynamic behaviour of the system. Four variants of the traditional system are considered.

The first one consists in the addition of an underballast mat for exurban lines. The proper model is a mass-bar-spring system in which the mat is represented as a spring under the bar with stiffness k_{mat1}. This stiffness is derived from material tests (Chapter 5): $k_{mat1,stat} = 110$ N/cm^3.It is assumed that $k_{mat1,dyn} = k_{mat1,stat} = 110$ N/cm^3 and a loss factor $\nu_b = 0.2$.

Considering an influence area for the mat given by: $A_{mat1} = A_b = 1.5 \cdot A_{it} = 7200$ cm^2

The stiffness spring in the model is evaluated:

$$k_{mat1} = k_{d,mat1} = 110 \frac{\text{N}}{\text{cm}^3} \cdot 7200 \text{ cm}^2 = 7.92 \cdot 10^7 \text{ N/m} \tag{7.18}$$

And the non dimensional parameter β is:

$$\beta_1 = \beta_{d1} = \frac{k_{mat1}}{k_b} = \frac{7.92 \cdot 10^7}{2.40 \cdot 10^7} \tag{7.19}$$

The global model is in figure 11.

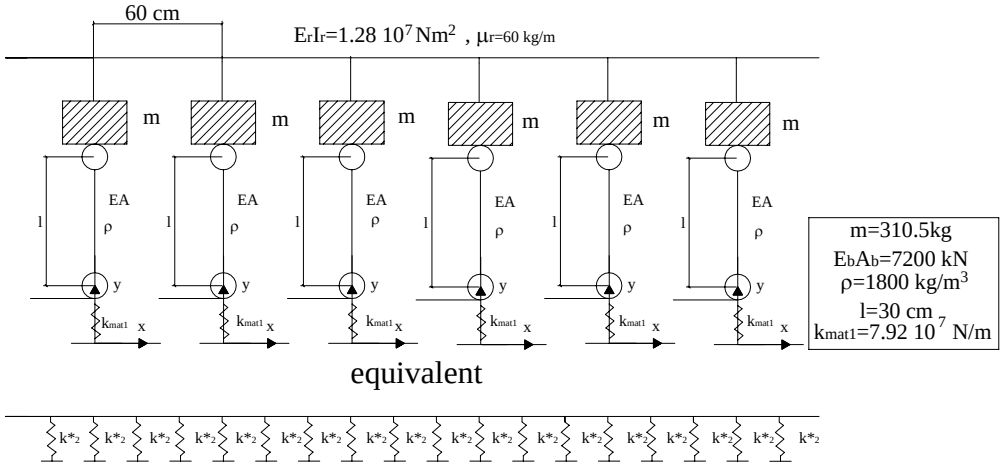

figure 11 model for the first variant

The second variant is equal to the first one but the underballast mat has different mechanical characteristics conceived for urban lines. The stiffness is obtained by static tests (chapter 5): $k_{mat2,stat} = 21\ \text{N/cm}^3$. In this case it is assumed a dynamic stiffening factor $R = 3$ and consequently $k_{mat2,dyn} = 63\ \text{N/cm}^3$. The loss factor is set $\nu_b = 0.2$. The influence area of the mat A_{mat2} has not changed $\left(A_{mat2} = A_{mat1} = 7200\ \text{cm}^2\right)$. The proper model is still a mass-bar-spring system in which the stiffness spring (representing the under-ballast mat) is given by:

$$k_{mat2} = 21\ \frac{\text{N}}{\text{cm}^3} \cdot 7200\ \text{cm}^2 = 1.5 \cdot 10^7\ \text{N/m} \tag{7.20}$$

and consequently:

$$k_{d,mat2} = 63\ \frac{\text{N}}{\text{cm}^3} \cdot 7200\ \text{cm}^2 = 4.54 \cdot 10^7\ \text{N/m} \tag{7.21}$$

the non dimensional parameter β in the static and dynamic case is given by:

$$\beta_2 = \frac{k_{mat2}}{k_b} = \frac{1.5 \cdot 10^7}{2.40 \cdot 10^7} = 0.63 \tag{7.22}$$

$$\beta_{d2} = \frac{k_{d,mat2}}{k_{b,}} = \frac{4.54 \cdot 10^7}{7.2 \cdot 10^7} = 0.63 \tag{7.23}$$

The global model is in figure 12.

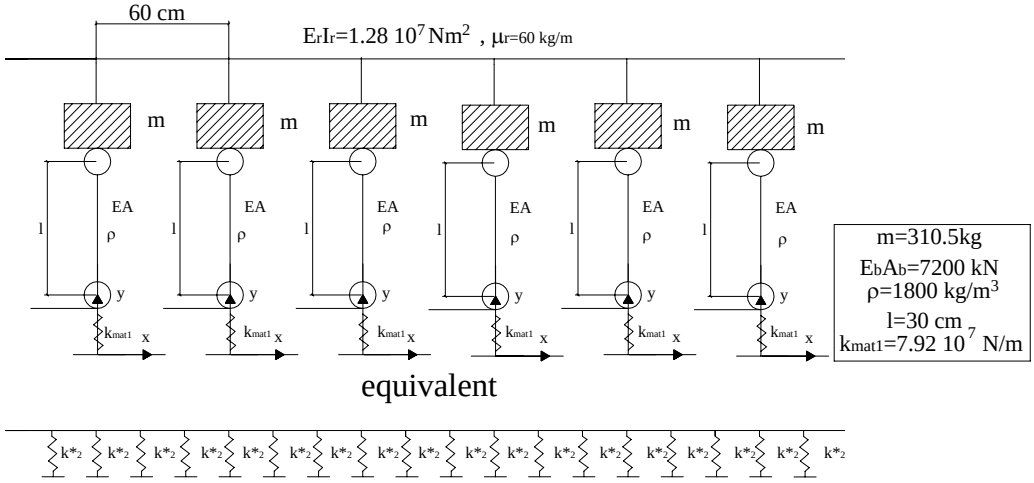

figure 12 model for the second variant

The third variant is carried out considering an elastic wrapping around the sleeper. A possible model is a mass-spring-bar system for which the wrapping is modelled as a spring between the mass and the bar. The stiffness for the wrapping is still derived from material tests (Chapter 5): $k_{wra,stat} = 75\ \text{N/cm}^3$. Assuming a dynamic stiffness factor $R = 1.5$, the dynamic stiffness is $k_{wra,dyn} = 112.5\ \text{N/cm}^3$. The loss factor is $\nu_b = 0.25$. The sleepers influence area is $A_{it} = 4800\ \text{cm}^2$. The stiffness spring in the model is:

$$k_{wra} = 75\ \frac{\text{N}}{\text{cm}^3} \cdot 4800\ \text{cm}^2 = 3.60 \cdot 10^7\ \text{N/m} \tag{7.24}$$

In the dynamic case:

$$k_{d,wra} = 112.5 \ \frac{\mathrm{N}}{\mathrm{cm}^3} \cdot 4800 \ \mathrm{cm}^2 = 8.1 \cdot 10^7 \ \mathrm{N/m} \tag{7.25}$$

And the non dimensional parameter β in the static and dynamic case is given by:

$$\beta_3 = \frac{k_{wra}}{k_b} = \frac{3.60 \cdot 10^7}{2.40 \cdot 10^7} = 1.5 \tag{7.26}$$

$$\beta_{d3} = \frac{k_{wra}}{k_b} = \frac{8.1 \cdot 10^7}{7.2 \cdot 10^7} = 1.13 \tag{7.27}$$

The global model is in figure 13.

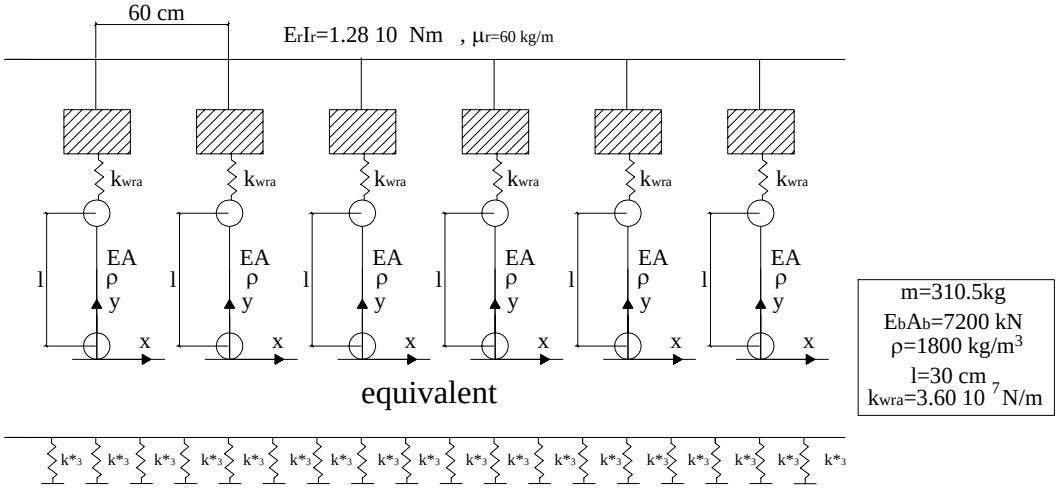

figure 13 model for the third variant

Both elastic levels are in the third variant; mass-spring-bar-spring system is applied in which the underballast mat is represented by a spring, in series to the bar, of stiffness k_{mat2} or $k_{d,mat2}$ and the wrapping is modelled as the spring between the mass and the bar of stiffness K_{wra} or $K_{d,wra}$ $\left(\beta_2 = 0.63, \beta_{d2} = 0.63;\ \beta_3 = 1.5, \beta_{d3} = 1.13\right)$. The global model is in figure 14.

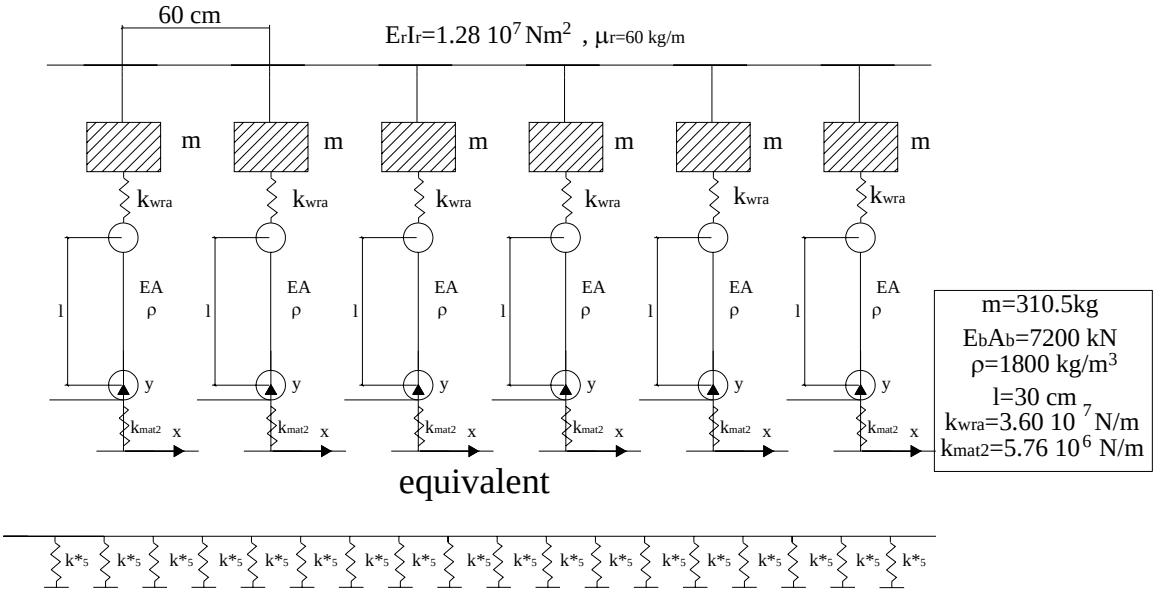

figure 14 model for the forth variant

Substituting proper values of elastic and massive elements global stiffness is obtained for each variant $K_i(\bar{\omega})$ and consequently:

$$k_i^* = \frac{K_i}{p} - \mu\bar{\omega}^2 \tag{7.28}$$

The theoretical transfer function in terms of acceleration is obtained for each variant:

$$H_a(\omega) = -\omega^2 \cdot H_w(\omega) = -\omega^2 \cdot \frac{w(0)}{F_0} = -\omega^2 \cdot \frac{1}{2L^* k^*} \tag{7.29}$$

in which L^* is given by (6.133).

7.3 DESCRIPTION OF THE STATIC TESTS

Tests want to evaluate the behaviour of the track system (represented by the prototype) for the effect of static railway loads.

The load is considered fixed on the track. It is applied on rail level by two hydraulic actuator that work between a lower cross-bar rest on the rail level and an upper one sustained by four bars anchored to the railway track basement. These bars go trough the prototype thanks to arranged holes but they do not interfere with the track behaviour. Displacements at rail level in assigned sections are monitored. The load is not constant but it starts to zero value and it slowly increases with a linear pattern until its maximum value (figure 15): three cycles are considered.

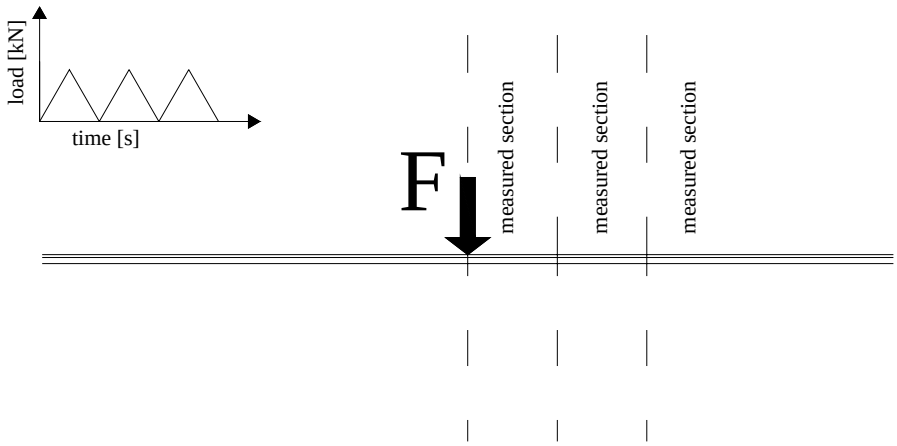

figure 15 procedure scheme for the static test

Two hydraulic actuator are used there are set in parallel and shown in figure 16.

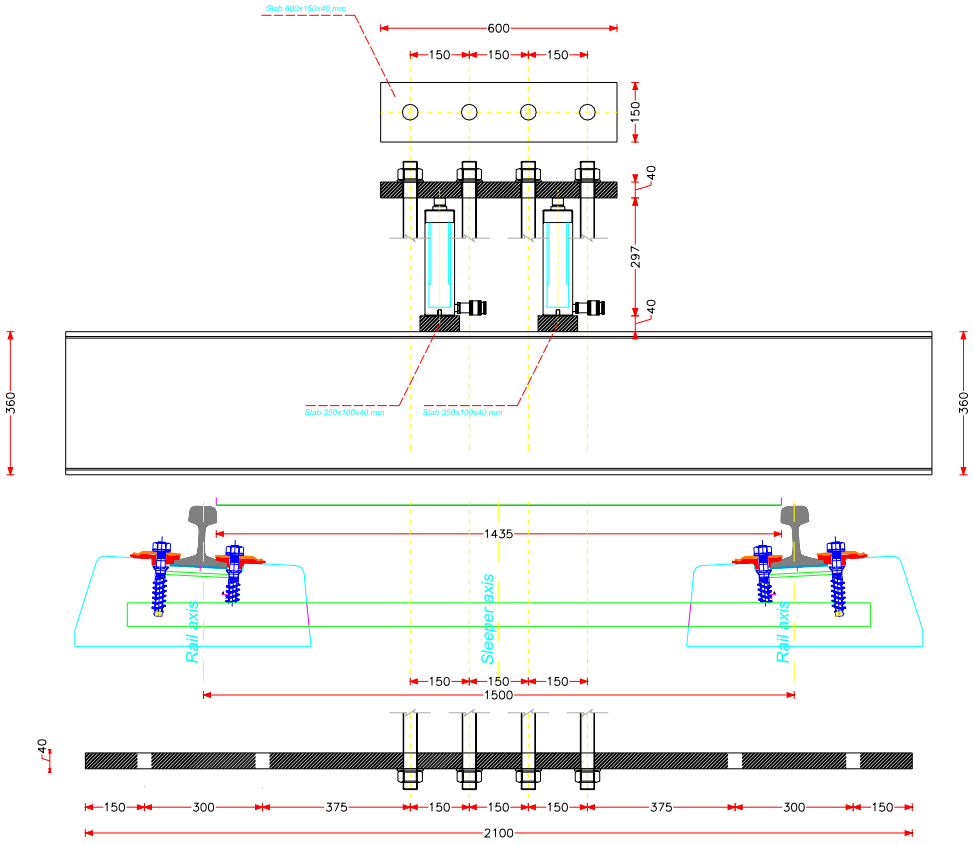

figure 16 hydraulic actuators for the static tests

They have the following characteristics:

- Builder: Larzep
- Type: SM01515
- Load: 15 t (150 kN)
- Limit: 155 mm
- Section size: 23.75 cm^2

Test loads depend on the type of the track system (see table2).

table 2 Test load for the static test

Type of line	Axle load	Test load	pressure
tramline	90kN/axle	120kN	260 atm
underground	120kN/axle	160kN	350 atm
railway	220kN/axle	290kN	630 atm

The load is monitored by a pressure cell HBM P3MB/1000BAR. Displacements on rail levels are measured using ten displacement transducers and their positions are shown in figure 17.

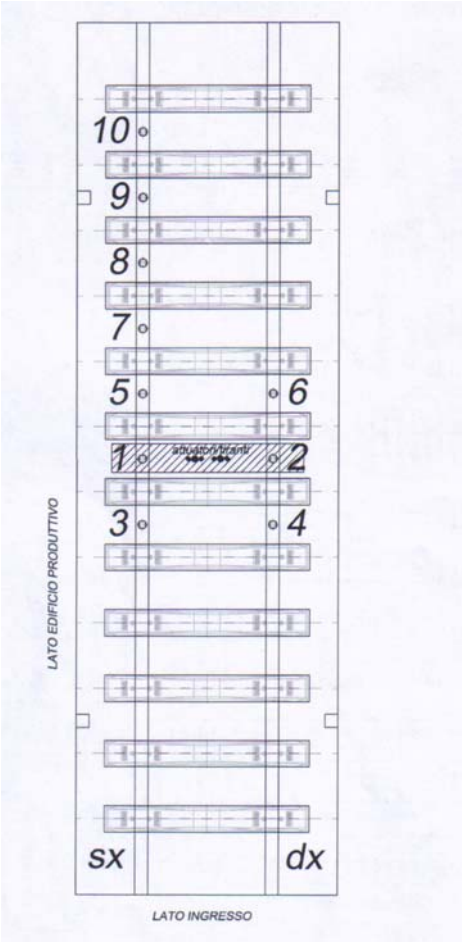

figure 17 position of displacement transducers on the prototype

figure 18 lay-out of the static tests

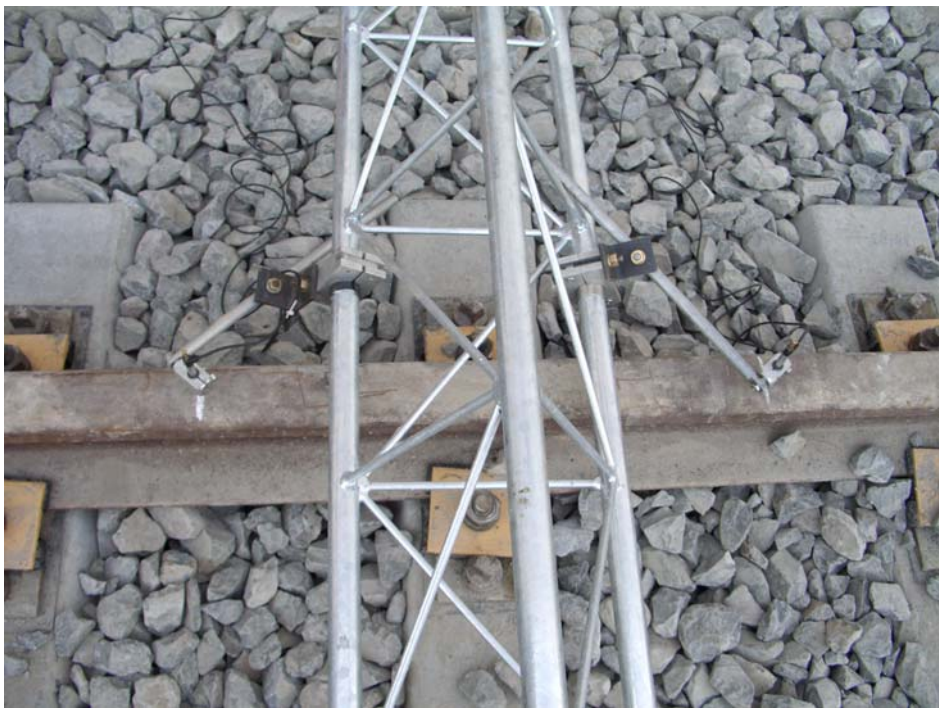

figure 19 details of the test equipment for the static tests

7.3.1 Static test results

Static tests are performed on the traditional track and on the four its variant, in the following the main results are shown.

First of all the traditional track system is built (figure 20). Its length will be sufficient to capture the main characteristics of its displacement path. The static test is performed following the previous procedure, the maximum value of the static load in performed tests is 290 kN (figure 21, 22).

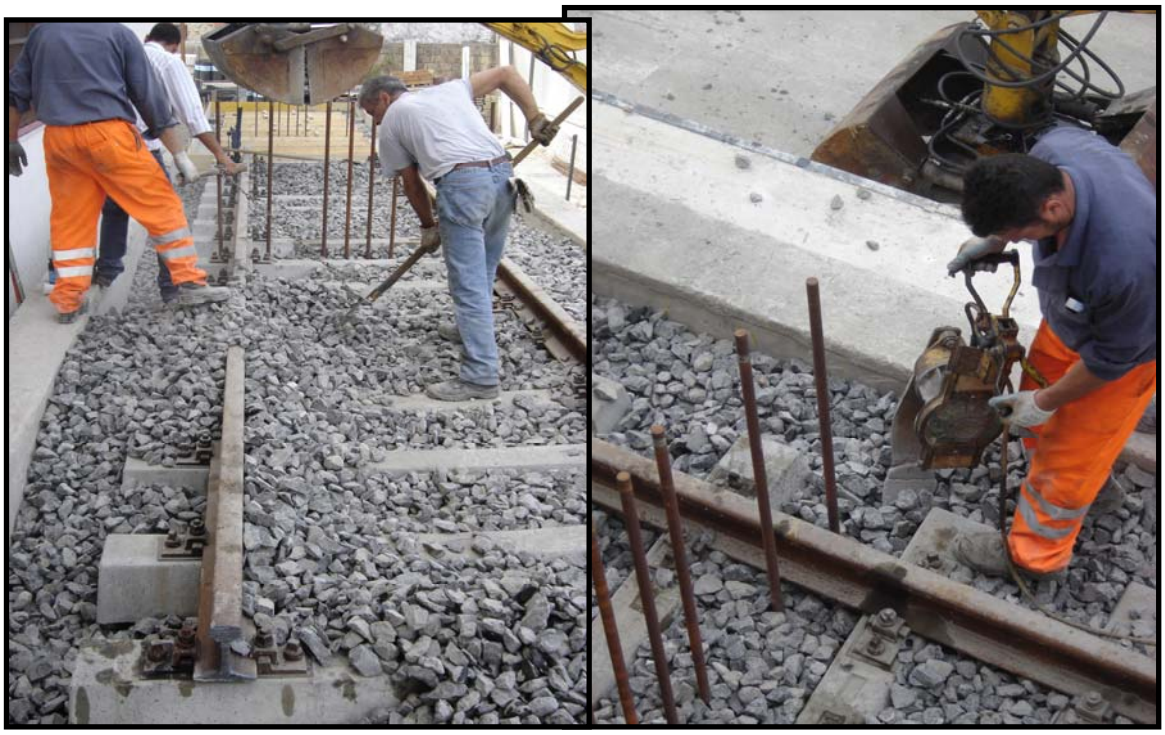

figure 20 phases of the railway track construction

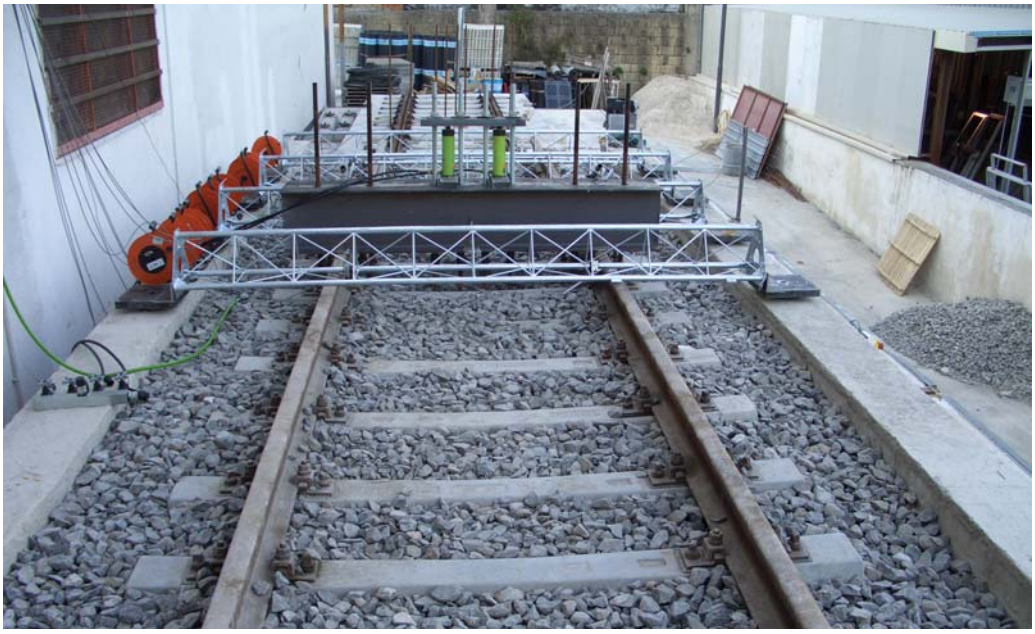

figure 21 static tests on the traditional track

figure 22 static tests on the traditional track (2)

The results are in terms of static displacements. The theoretical values are evaluated considering the models in the chapter 6. The experimental displacements are measured along the line considering the scheme in figure 17. In figure 23 static displacements for the maximum value of the test load are plotted and compared with the theoretical displacements.

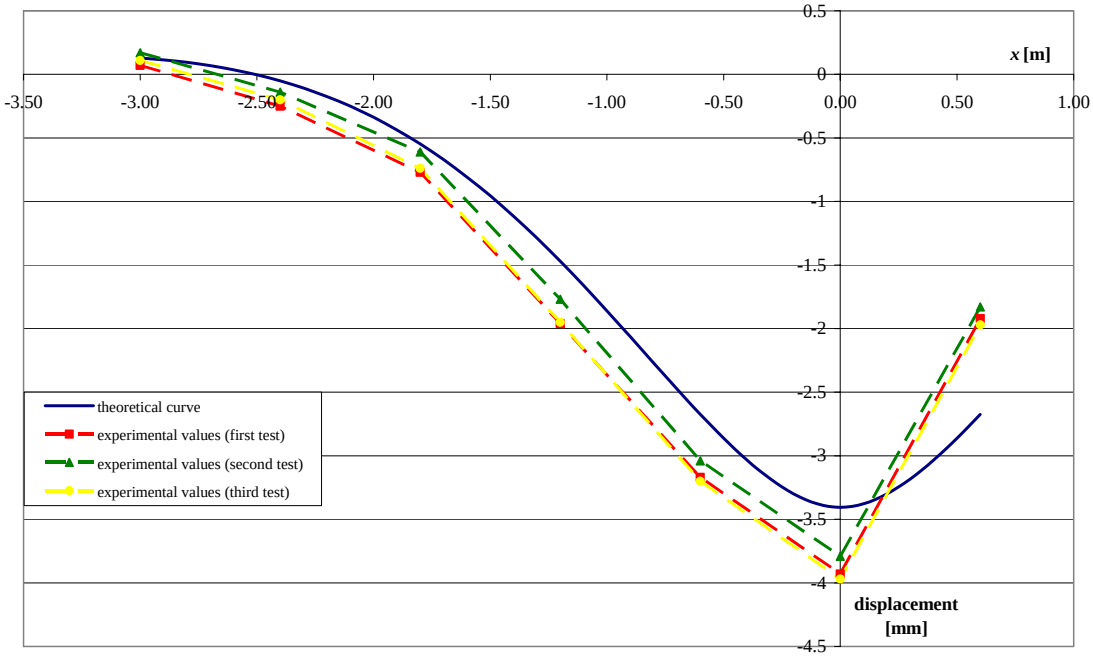

figure 23 static displacements for the reference track type

The first variant is obtained adding an under-ballast mat, so it is necessary to take away the ballast, sleepers and rail with their fastenings (figure 24) and place the mat; successively the track is replaced above the mat.

figure 24 concrete slab: the basement

The static test is performed (figure 25) and the results in terms displacements for the maximum load are in figure 26.

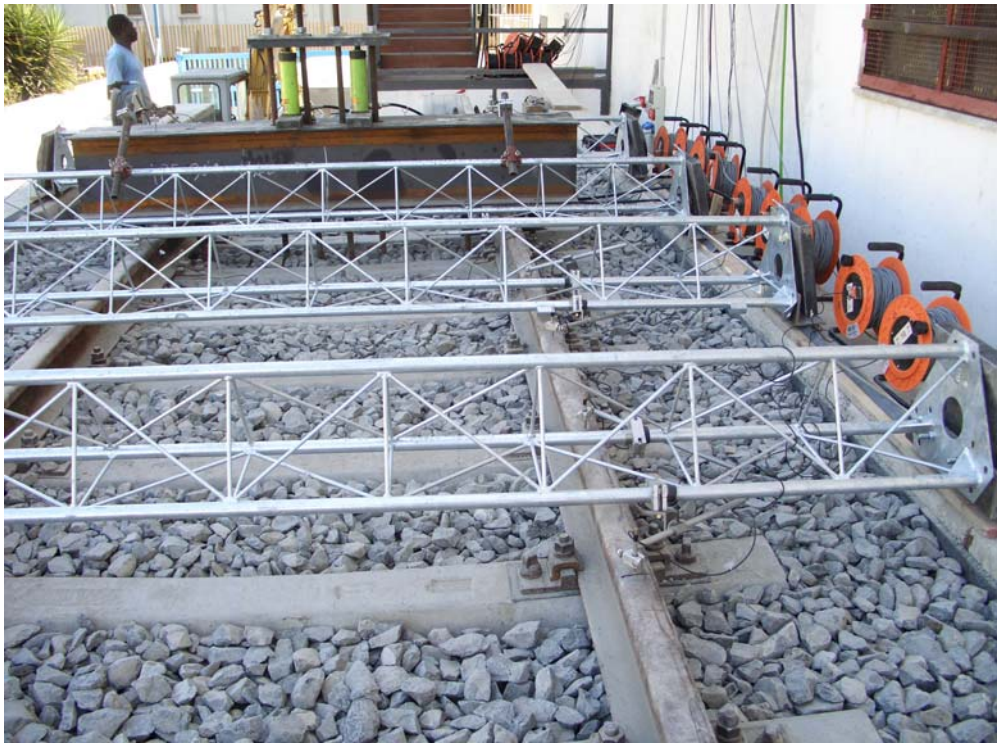

figure 25 static test on the first variant

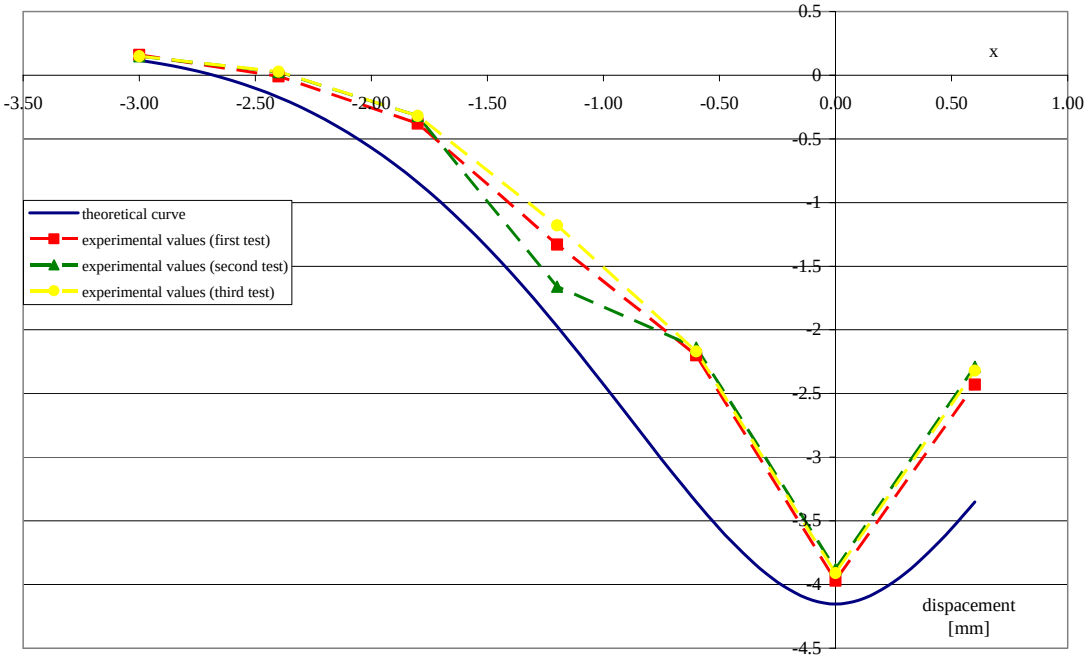

figure 26 static displacements for the first variant

The procedure is the same to obtain other different variants.

In figure 27 the static test for the second variant is shown and the elaboration of results are in figure 28.

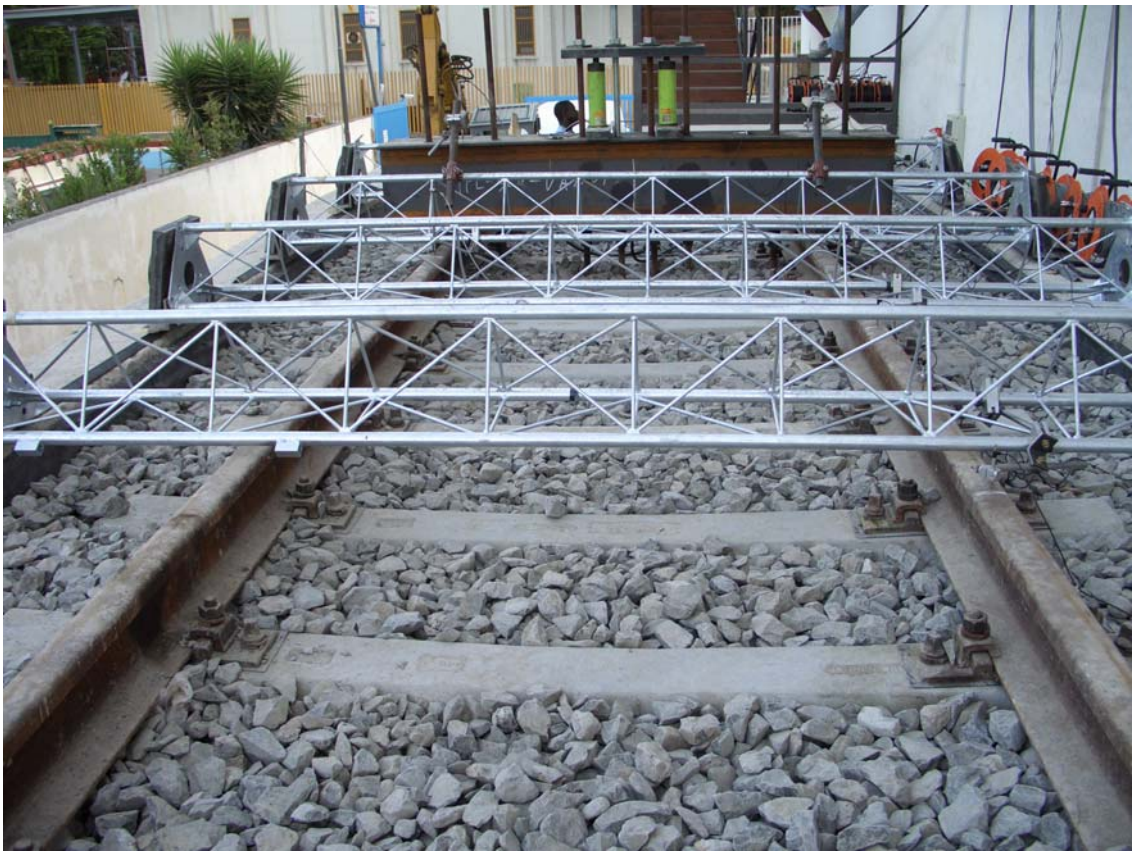

figure 27 static test on the second variant

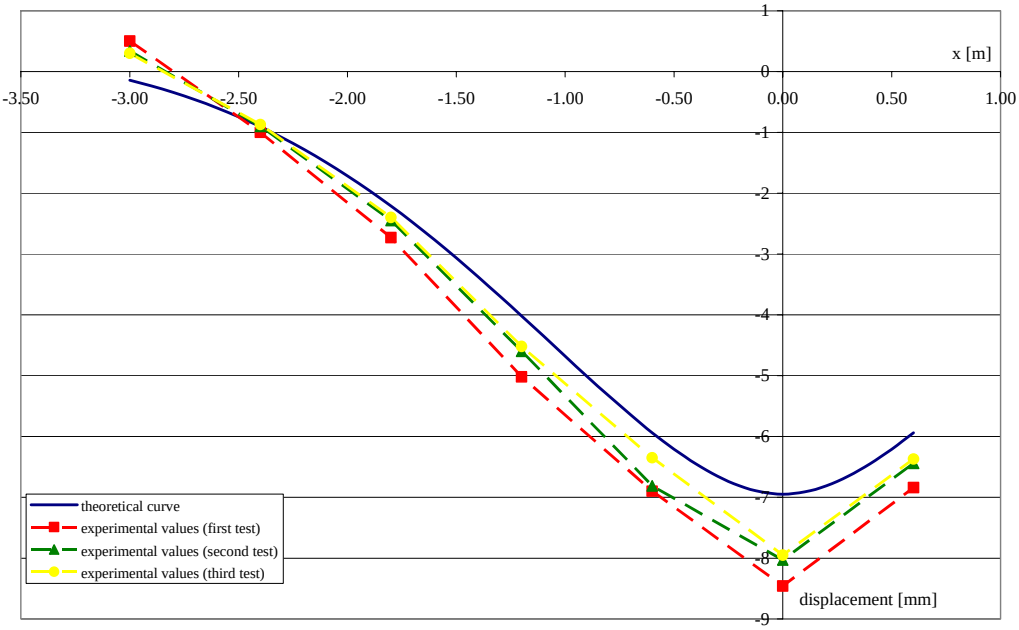

figure 28 static displacements for the second variant

In figure 29 the static test for the third variant is shown and the elaboration of results are in figure 30.

figure 29 static test on the third variant

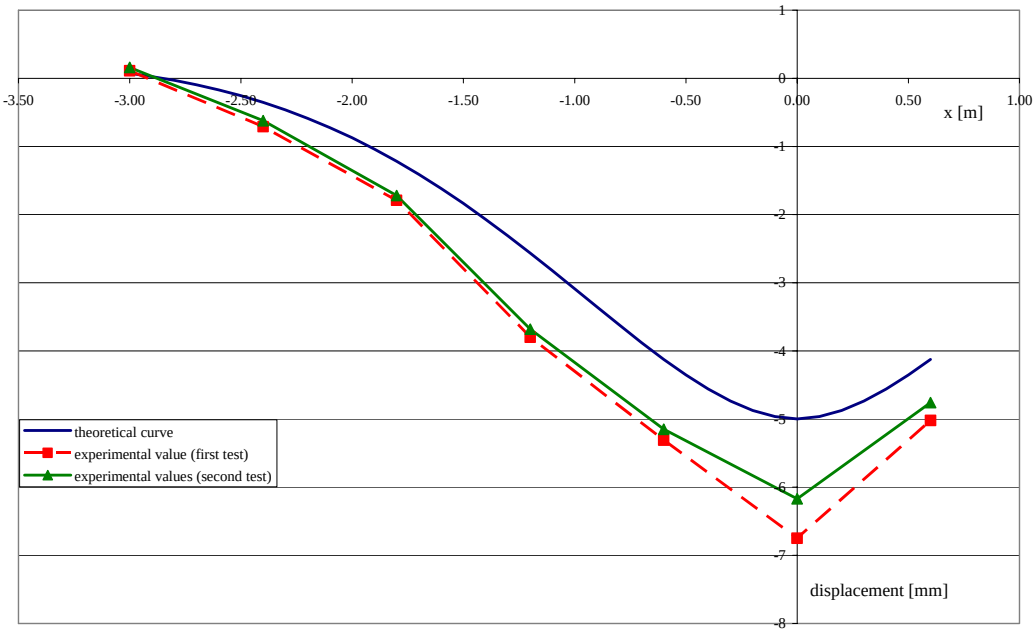

figure 30 static displacements for the third variant

Figure 31 represents the preparation of the forth variant in which both elastic levels are considered. The scheme of the static test is in figure 32 and in figure 33 the elaboration of the tests are discussed.

figure 31 preparation of the forth variant

figure 32 static test on the forth variant

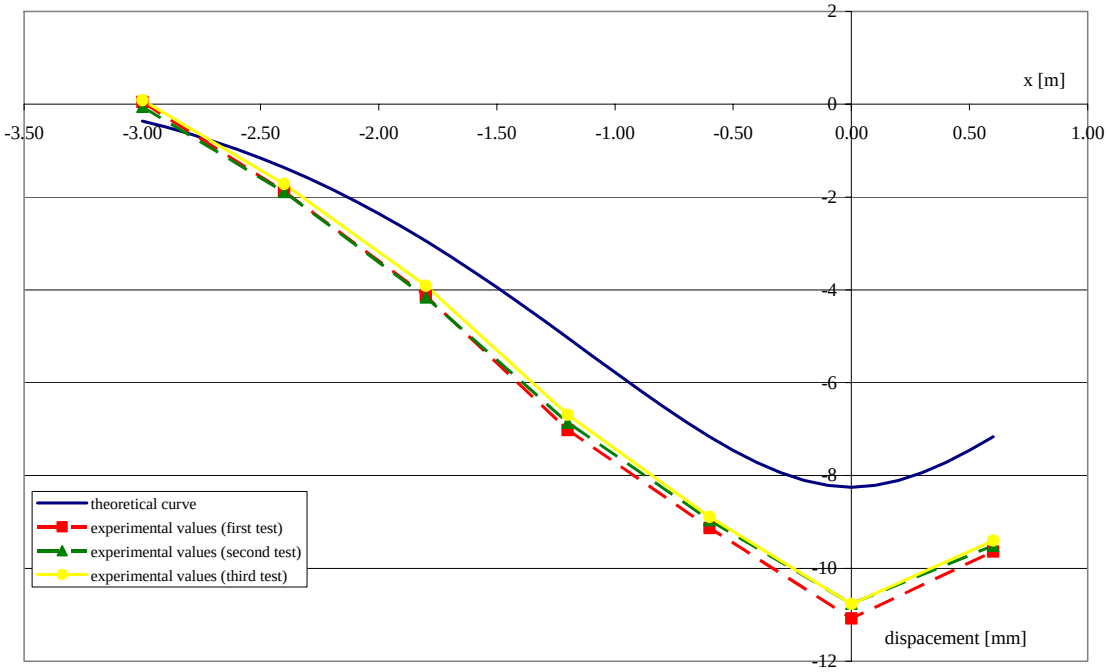

figure 33 static displacements for the forth variant

7.3.2 Elaboration of experimental results: static behaviour

Important considerations are derived from theoretical-experimental comparison. The real deformation form is well represented through the analytical curve, but the theoretical displacements often tend to be lower than the experimental values (see figure 23, 26, 28, 30 and 33); this aspect is also clear considering the table 3 where maximum static theoretical and experimental displacements are summarized. The table also show the per cent variation of the analytical values respect to the experimental displacements.

table 3 maximum displacements: theoretical values and experimental results

RAILWAY TRACK TYPE	THEORETICAL VALUES	TEST 1		TEST 2		TEST 3	
	[mm]	[mm]	[%]	[mm]	[%]	[mm]	[%]
reference track	-3.41	-3.93	-13.3	-3.79	-10.1	-3.97	-14.2
1st variant	-4.15	-3.97	4.6	-3.88	7.1	-3.91	6.2
2nd variant	-6.95	-8.46	-9.3	-8.03	-9.1	-7.95	-9.0
3rd variant	-5.00	-6.75	-25.6	-6.17	-19.0		
4th variant	-8.25	-11.25	-25.5	-11.08	-23.3	-10.8	23.4

Both theoretical curve and experimental results point out that new antivibration systems can involve an important increasing of the track deformability. Actually, the theoretical maximum displacement increases from -3.41 mm of the reference system up to -8.25 mm (2.5 times greater) of the 4th variant (most deformable system); while the experimental static displacement changes from about -4.00 mm of the reference track to -11.00 mm (almost 3 times greater) of the 4th variant. Deformability is an important aspect of the track design because a excessive displacements can create comfort problems or forbid the correct and safe operation of the railway line.

The prototype length is 10 m and it is sufficient to describe the track behaviour if their characteristic lengths are evaluated (table 4).

table 4 theoretical characteristic length of the reference track and of its four variants

RAILWAY TRACK TYPE	THEORETICAL VALUES	
	characteristic length [m]	**wave length** [m]
reference track	1.06	6.66
1st variant	1.14	7.16
2nd variant	1.35	8.48
3rd variant	1.21	7.60
4th variant	1.43	8.98

7.4 DESCRIPTION OF THE DYNAMIC TESTS

The main purpose is to determine the track behaviour under the effect of dynamic loads produced by the passage of vehicles. Dynamic loads are always applied together with static loads produced by trains: this aspect is clearly shown in figure 34.

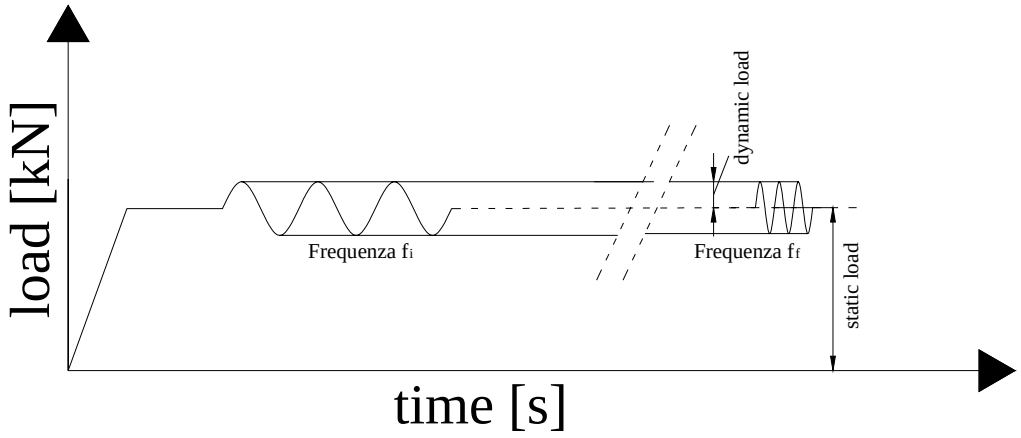

figure 34 dynamic load scheme

The static load is given by four big helicoidal lateral springs, while the dynamic one is produced through a vibrodyne (figure 35)

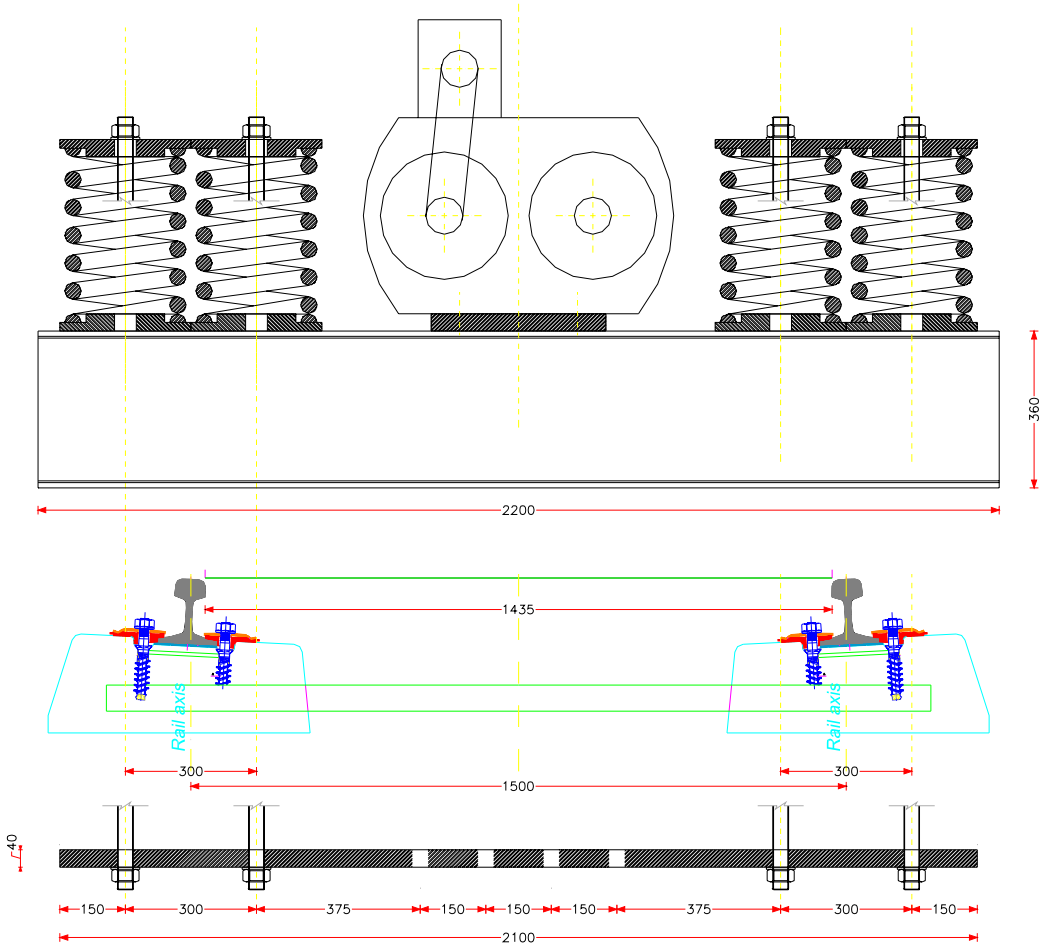

figure 35 scheme of the four helicoidal springs and of the vibrodyne

The four helicoidal springs (figure 36) has characterized by a very big elasticity (if compared with the elasticity of the railway track) and this fact makes the static load condition constant during the test. The static load produce by the helicoidal springs is 80 kN (20 kN/spring × 4 springs) They react through the four bars anchored in the basement.

Vibration acquisition is obtained by a network of accelerometers that monitor both vibration on the prototype both vibration near the prototype.

The following test equipment is used: vibrodyne VEM 20 kN 100Hz (figure) and a vibrotest system (digital system for the vibrodyne control and for the data acquisition and analysis) and the system configuration is in table 5.

figure 36 four helicoidal springs

figure 37 vibrodyne VEM 20 kN 100Hz

table 5 configuration of the system for dynamic tests

Lowest frequency	8Hz		
Biggest frequency	87.93Hz		
Constant of the vibrodyne	24.28 kN/Hz^2		
Number of cycles	5		
Delay	1s		
Angle α	176°	160°	52°
Mass angle 1 α_1	2°	10°	64°
Mass angle 2 α_2	178°	170°	116°

The position of accelerometers is in figure 38.

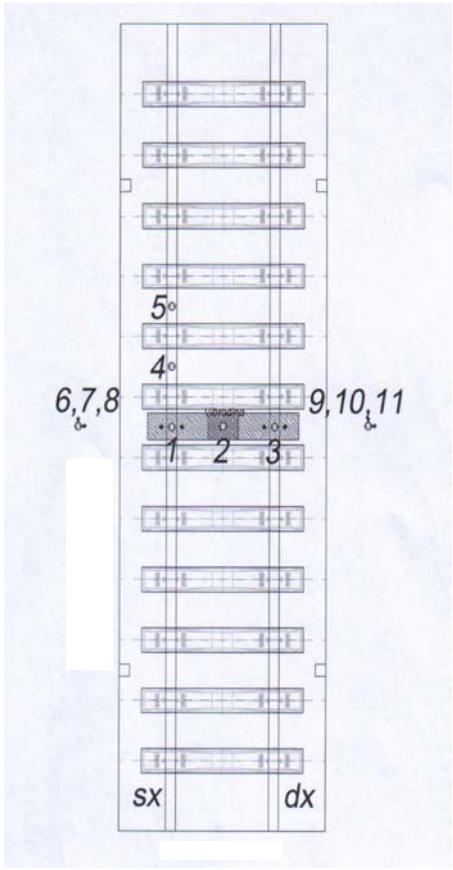

figure 38 position of accelerometers

Accelerometers on the railway track (pos $1 \div 5$) have vertical sensibility axis (figure 39), while set of three accelerometers (vertical, longitudinal and transverse sensibility axis) are on the basement for each side (pos $6 \div 8$ and pos $9 \div 11$) and shown in figure 40.

figure 39 accelerometers pos 1-5

figure 40 accelerometers pos 6-8 and pos 9-11

7.4.1 Dynamic tests and theoretical results comparison

Dynamic tests are performed on the reference track and on its four variants (previously described). Experimental results in terms of acceleration transfer functions are considered. They are compared with the theoretical transfer functions that are obtained considering prototype models (see figures 41-.

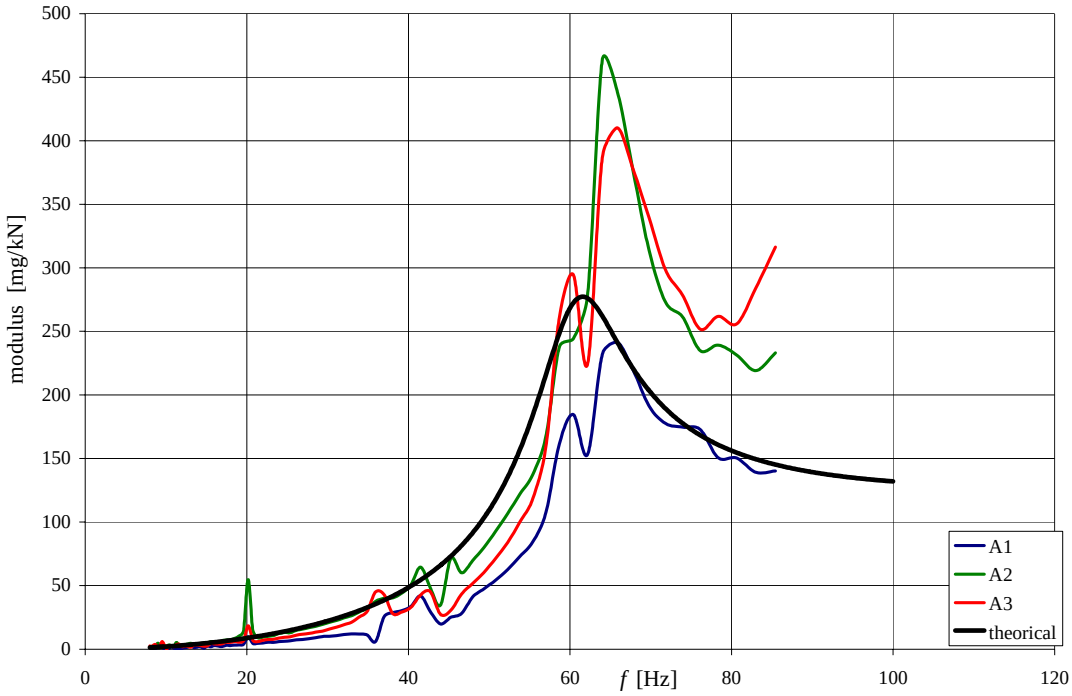

figure 41 theoretical and experimental modulus of the acceleration transfer function: reference track

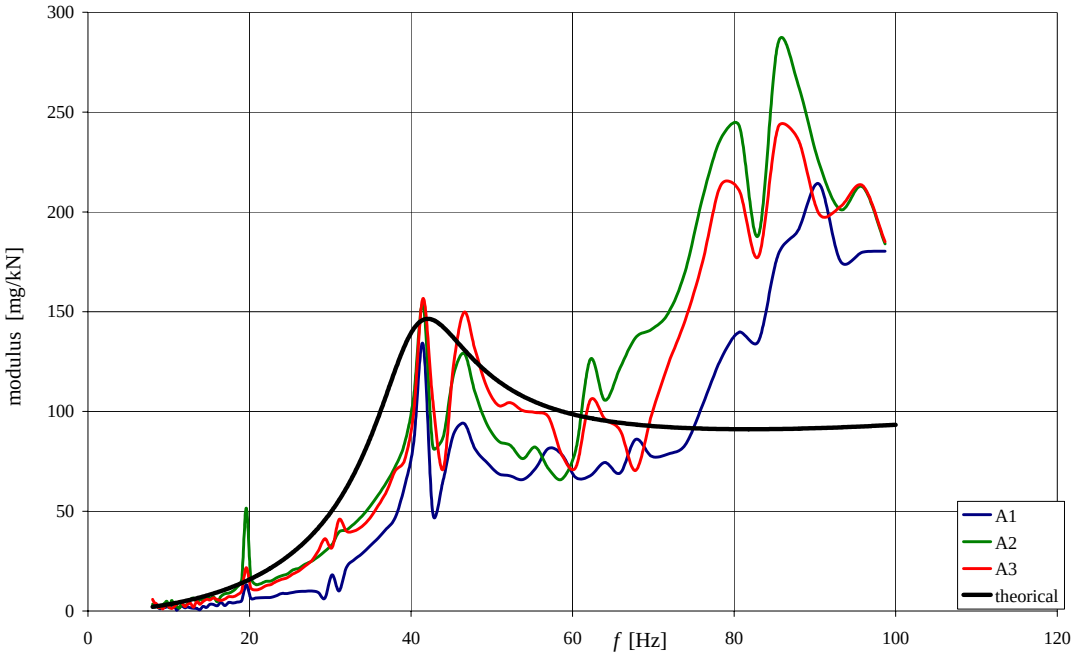

figure 42 theoretical and experimental modulus of the acceleration transfer function: 1st variant

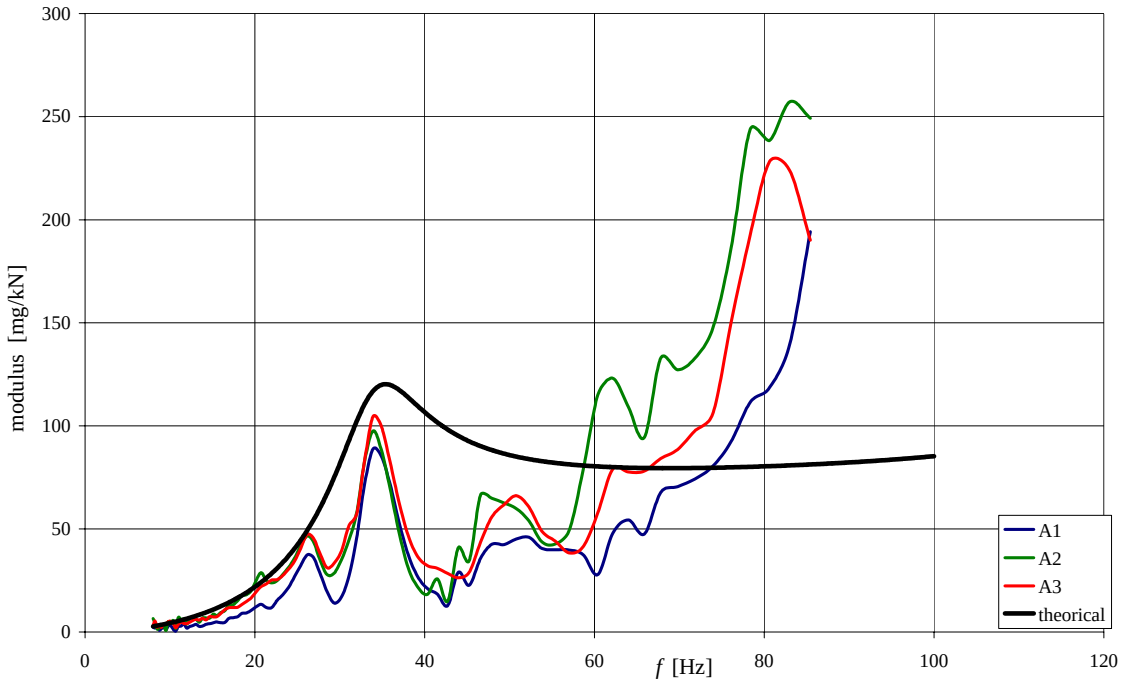

figure 43 theoretical and experimental modulus of the acceleration transfer function: 2nd variant

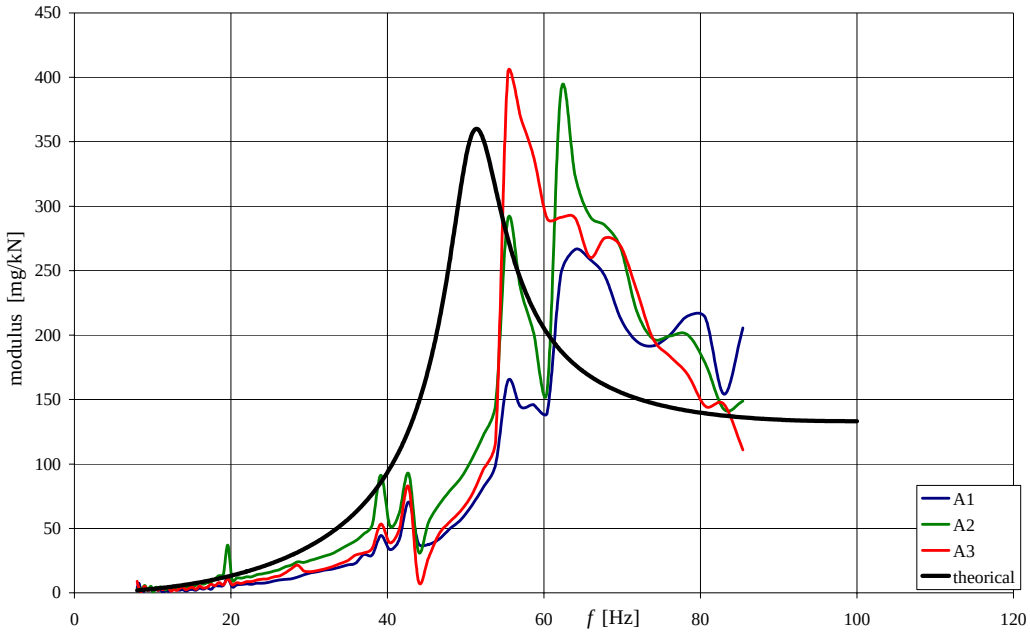

figure 44 theoretical and experimental modulus of the acceleration transfer function: 3rd variant

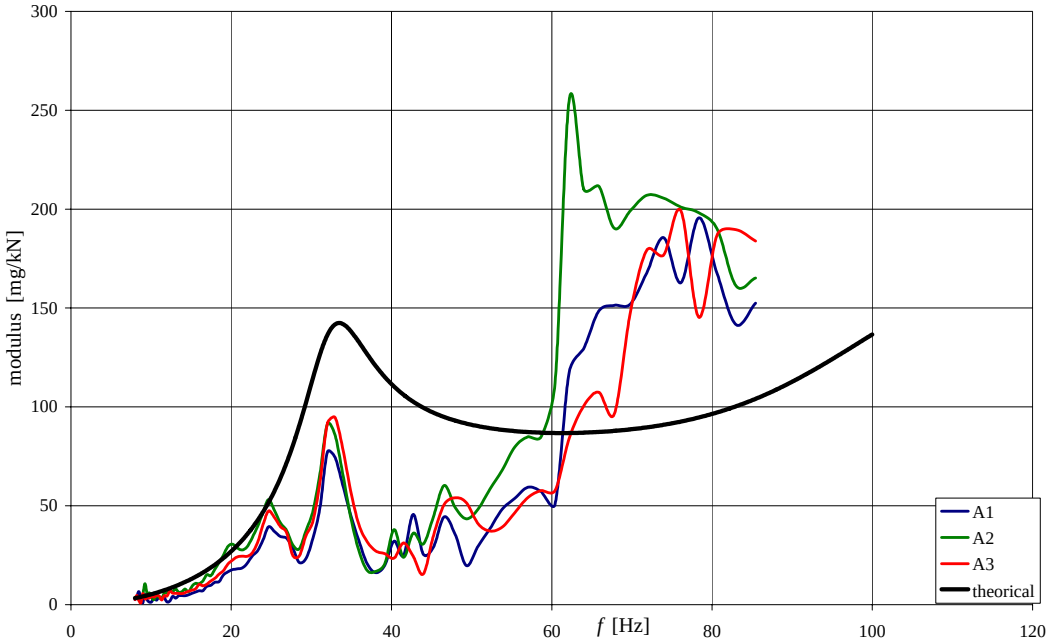

figure 45 theoretical and experimental modulus of the acceleration transfer function: 4th variant

The first frequency of a railway track is an important parameter to assess its dynamic behaviour and the effect in terms of vibration isolation. Fundamental frequencies for the reference system and its variants are summarized in table 6.

table 6 theoretical and experimental fundamental frequencies

TRACK TYPE	**theoretical fundamental frequency** [Hz]	**experimental fundamental frequency** [Hz]
reference track	62.2	64.5
1st variant	42.5	42.7
2nd variant	35.7	33.9
3rd variant	51.8	57.0
4th variant	33.5	32.0

CONCLUSIONS

The main scope of this thesis is to give a contribution in the determination of the best solution for reducing vibration in railway traffic. Moreover a new composite material has been proposed composed by recycled rubber that involves another important environmental aspect.

In the thesis there are two fundamental topics:

1. The theoretical and experimental study of the new composite material: recycled rubber and polyurethane.
2. The development of analytical modelling to design railway tracks conceiving for the vibration problem from the beginning. This part involves important experimental tests to validate theoretical results.

Regarding the material the aim is to make predictions of material behaviour from a theoretical point of view with the possibility to reduce the experimental costs, i.e. to obtain criteria to design a material with desired mechanical characteristics. Even though a very simplified model based on macromechanical theory is considered, which assumes the material as elastic and homogeneous, this study provides good values of the elastic modulus of the new composite material. The considered approach can lead to more refined models taking into account different properties of the material, and considering also dynamic and viscous behaviour.

The second part intends to be a contribution toward the understanding of the effect of added flexibilities and masses at different levels in the railway track. The theoretical models provide the following important conclusions:

- the introduction of a flexibility at fastenings level changes the static and but not the resonance frequency;
- an added flexibility at undersleeper or underballast level modifies both static behaviour and resonance frequency.

Static tests has been performed has been performed on the traditional track and on its four variants and they demonstrate that antivibration railway track can involve important displacements. The most deformable system (the 4th variant) can have displacements three times greater than the reference track and this aspect has to be considered. During the preliminary design the possibility to predict maximum displacement in a railway track can avoid problems. However there is a good correspondence between the theoretical predictions and experimental results.

Dynamic tests can give significant parameters to evaluate the effectiveness of a system in vibration reduction. One of these parameters (that has been taken into account in the thesis) is the fundamental frequency of the system. The traditional track gives lower performance in terms of vibration isolation and the most effective position of elastic element is at under-ballast level also considering the requirement to avoid excessive static displacements (so experimental measures confirmed theoretical considerations). In the specific case the lowest fundamental frequency is given by the forth variant that has two main elastic level (at sleeper and at underballast level).

Transfer functions in terms of acceleration demonstrate that there is also a good correspondence between analytical and dynamic experimental results in the considered frequency range.

This study provides a criteria to design innovative railway tracks during preliminary phase making predictions on static and dynamic behaviour.

ACKNOWLEDGEMENTS

I would like to express my deep and sincere gratitude to my Professor Giorgio Serino. His understanding, encouraging and personal guidance have provided a good basis for the present Ph.D thesis. His wide knowledge and his scientific rigour have given an important contribution to my growth.

Thank you to ISOLGOMMA for instruments and material resources that have provided to develop the experimental part of my thesis; in particular I want to thank Gianfranca and Simone Zannelli.

Thank you to Alessandra, Antonio, Franco, Mariacristina, Raffaello and Simona: we have spent nice moments together sharing smiles and tears. They have encouraged me to continue my research activity when doubts and fears could compromise my enthusiasm in my work.

Thank you to my mum because she have given me the possibility to continue my studies always offering her material and affective support.

Thank you to my sister Anita that knows and accepts my faults and in this three years she have helped me to overcome my difficult periods.

Thank you to my dad that I always feel near to me in spite of the distance.

Thank you to all persons that are in my heart and have lived with me this important experience.

REFERENCES

ABAQUS manual

Acquati M., Cavagna B., *Armamenti antivibranti:evoluzione storica e recenti esperienze di Metropolitana Milanese S.p.A.,* Impatto di Sistemi Elettrici per i trasporti sull'Ambiente Urbano, Milano, Italia (2003)

Acquati M., Cavagna B., *New Antivibration Track System for Subways,* Structure for High-Speed Railway Trasportation, IABSE Symposium, Anversa, Belgio (2003)

A.F.E.R.I.A., *materiali per i quattro sistemi di armamento del binario, appartenenti alle quattro linee di ricerca e relative varianti*, 2006

Castellani A., Kajon G., Panzeri P. & Pezzoli P. 1998, *Elastomeric materials used for vibration isolation of railway lines*, Journal of engineering mechanics Vol. 124 N°6 June pp 614-621.

Clough, Penzien, *Dynamics of Structures*, Wiley 1982

Crispino M., *Sovrastrutture ferroviarie per alta velocità:sviluppo di una metodologia di calcolo ed analisi teorico-sperimentale sul subballast per il miglioramento delle prestazioni*, tesi di dottorato in Ingegneria dei Trasporti, Napoli, Febbraio 1996

DIN 4150 Part 1, *Vibration in buildings: principles, predetermination and measurement of the amplitude of oscillation*, September 1975

DIN 4150 Part 2, *Structural vibration in buildings – effects on people in buildings*, 1979

DIN 4150 Part 3, *Structural vibration in buildings : effects on structures*, may 1986

Esveld C., *Recent developments in slab track*, European Railway Review Issue 2 (2003)

Esveld C., *Modern railway track*, Germany, 2001

Esveld C., *Track structures in an urban environment*, Symposium KU Leuven, 1997

Fryba L., *Vibration of solids and structures under moving loads,* Noordhoff International Publishing, Groningen Netherlands, 1999

Gent Alan N., *Engineering with Rubber: How to Design Rubber Components*, HANSER, Munich, 2001

INDAPRO, Resilient *Pad and Mat Testing Machine (RPMTM): user manual version 1.0* (in Italian), 2005

ISO 2631/1-1985, *Evaluation of human exposure to whole-body vibration-part 1:General requiriments.*

ISO 2631/2-1989, *Evaluation of human exposure to whole body vibration –part 2 : Continuos and shock-induced vibration in bildings(1 to 80 Hz).*

ISO 4866–1990, *Mechanical vibration and shock – vibration of buildings – Guidelines for the measurement of vibration and evaluation of their effects on buildings.*

Kreleven D.W.Van, *Properties of polymers*, Elsevier, 1990

Lei X., N.-A. Noda, *Analysis of dynamic response of vehicle and track coupling system with random irregularity of track vertical profile*, Journal of Sound and Vibration 258 (1), 147-165

Ludvigh E., *Elastic behaviuor of continuosly embedded rail system,* Periodica Polythecnica Ser.civ.eng. Vol 46 No.1 pp103-114 (2002)

Mathews P.M., *Vibrations of a beam on elastic foundation I,* Zeit. angew. Math. Mech., 38 (3/4) pp 105-115, 1958

Mathews P.M., *Vibrations of a beam on elastic foundation II*, Zeit. angew. Math. Mech., 39 1/2) pp 13-19, 1959

R.Panagin, *La dinamica del veicolo ferroviario,* Libreria Editrice Levrotto e Bella, Torino, aprile 1990

Pezzoli, P. 2005, Vibration investigations with forced excitation of a ballasted railway track without and with the underballast mat (in Italian), technical report

Pichler D., Zindler R.1999, *Development of artificial elastomers and application to vibration attenuating measures for modern railway superstructures*, Constitutive models for rubber Dorfmann & Muhr Rotterdam pp. 257-266

SN 640 312a, *Les ébranlements. Effet des ébranlements sur les constructions*, 1992

UNI 9614, *Misura delle vibrazioni negli edifici e criteri di valutazione del disturbo*, marzo 1990

UNI 9916, *Criteri di misura e valutazioni degli effetti delle vibrazioni sugli edifici*, novembre 1991

UNI 10570, *Prodotti per l'isolamento delle vibrazioni. Determinazione delle caratteristiche meccaniche di materassini e piastre*, giugno 1997

UNI 11059, *Elementi antivibranti. Materassini elastomerici per armamenti ferrotranviari. Indagini di qualifica e controllo delle caratteristiche meccaniche e delle prestazioni*, agosto 2003.

Ward I.M., Sweeney J., *An Introduction to the Mechanical Properties of Solid Polymers*, WILEY, 2004.